FINAL REPORT

MECHANISM OF COMBUSTION OF HETEROGENEOUS SOLID PROPELLANTS

By

E.W. Price, R.K. Sigman, S.R. Chakravarthy, H-J Chaing, S-T Lee, C.A. Beiter and K. Prasad

Prepared for

OFFICE OF NAVAL RESEARCH
ARLINGTON, VIRGINIA 22217

Under

Contract N00014-89-J-1293

September 1998

Approved for public release, distribution unlimited

GEORGIA INSTITUTE OF TECHNOLOGY
A UNIT OF THE UNIVERSITY SYSTEM OF GEORGIA
SCHOOL OF AEROSPACE ENGINEERING
ATLANTA, GEORGIA30332

Home of the 1996 Olympic Village
Georgia Institute of Technology

Office of Contract Administration
Contracting Support Division
Atlanta, Georgia 30332-0420 U.S.A.
PHONE 404·894·6944
FAX 404·894·5285

September 11, 1998

In reply refer to: **E-16-689**

Office of Naval Research
Program Officer, Richard S. Miller
Code 1132P
Ballston Centre Tower One
800 North Quincy Street
Arlington, VA 22217-5660

Subject: **Final Technical Report**
Project Director(s): E.W. Price/R.K Sigman
Telephone No.: (404)894-3022
Contract No.: **N00014-89-J-1293**
Prime No.: **N/A**
"AN EXPERIMENTAL INVESTIGATION OF THE LEADING EDGE OF DIFFUSION FLAMES"
Period Covered: 881015 through 951031

The subject report is forwarded in conformance with the contract/grant specifications.

Should you have any questions or comments regarding this report(s), please contact the Project Director or the undersigned at 404-894-4764.

/TW

Sincerely,

Wanda W. Simon /TW
Wanda W. Simon
Reports Coordinator

Distribution:
Addressee:**3 copies**
1 copy to: Director, Naval Research Laboratory
2 copies to: Defense Technical Information Center
Cc:ONR-RR

Acknowledgements

This research has been sponsored by the Mechanics Division of the Office of Naval Research, Arlington, Virginia, under Contract No. N00014-89-J-1293. Dr. Richard S. Miller and Dr. Judah Goldwasser served as the technical monitor and program manager for this contract. Their support of this research investigation is greatly appreciated.

Mechanism of Combustion of Heterogeneous Solid propellants

by

E.W. Price, R.K.Sigman, S.R. Chakravarthy, H-J. Chaing, S-T. Lee, C.A.Beiter, and K. Prasad

This report summarizes research conducted under ONR contract No. N00014-89-J-1293 from October 1988 to October 1995. The majority of the research is described in a survey paper that is used here as part of the text. More detailed reporting is contained in the Appendices.

Goal of the Research

The objective of the research is to establish the processes in solid propellant combustion that control steady and nonsteady combustion rate (composite propellants). The practical goal is to:

1. Tailor burning rate by variation of formulation (oxidizer particle size, ballistic modifiers, and choice of binders). This includes learning what processes lead to low or negative sensitivity of burning rate to pressure increase (plateau and mesa burning).
2. Determine steps in the combustion process that are most responsive to oscillatory flows (combustion instability).
3. Evaluate the combustion characteristics of new oxidizer and binder ingredients, and of propellants that include new ingredients (and compare results with those of AP oxidizer and AP/hydrocarbon binder propellants).
4. Develop a realistic qualitative model of the combustion process that would identify the requirements for formulation of realistic analytical models.

Approach

The first step in an approach to study of combustion of composite propellants is to recognize that the combustion is three dimensionally and chemically complex on a scale that is too small for direct observation of details. In the research described here, the strategy for circumvention of this barrier has been to :

1. Study the melting, decomposition, and self deflagration of individual ingredients.
2. Combine ingredients in geometrically simple forms for which the combustion is more amenable to direct observation and theoretical modeling (e.g., edge burning of laminate "sandwiches" of oxidizer and binder)
3. From systematic studies of the effects of dimensional variables, pressure, and ingredient variants, form postulates regarding rate controlling processes, and test the postulates by looking at the burning rate vs. pressure for specially formulated propellants.

This strategy has been pursued by this investigation team for many years prior to this contract, and it had led to a variety of observational methods and facilities, including:

1. Observation of sample burning in a window bomb (cinemicrophotography).

2. Quench burning by rapid depressurization, followed by examination of the macro and micro features of the quenched surface.

3. Thermal analysis studies (sample temperature and mass vs. time in the presence of external heating: also observation of sample melting and decomposition in a hot stage microscope).

4. T-burner testing (at NWC) on special formulations designed to distinguish the roles of different parts of the combustion zone in excitation of oscillatory burning.

5. Extensive use of systematic variation of ingredient combinations, particle size and proportions as probes to combustion zone processes.

A large part of the present research is built on earlier studies of "sandwich burning", i.e., edge burning of samples consisting of a binder lamina between two ammonium perchlorate laminae. In the present research, studies were made of:

1. Sandwiches in which the binder lamina was replaced by a matrix of fine AP and binder.

2. Sandwiches as in 1), but with iron-containing catalysts included in the matrix.

3. The same as 1) and 2) but using new oxidizer ingredients.

4. Two dimensional flames in a Wolfhard type gas burner simulating "sandwich flames" but at atmospheric pressure where detail of the flame could be measured.

5. A rigorous analytical-computational solution of the 2-D diffusion flame problem to further define the role of the "leading edge flame" portion of the oxidizer/fuel diffusion flame that had been found in 1) and 2) to dominate the heat feedback to the propellant surface and control burning rate.

The results of these and other studies are described briefly in the following sections and more fully in the Appendices.

Hot Stage Microscope Observations of the Response of Propellant Ingredients to Heating

A variety of propellant ingredients and combinations were viewed by video photography during heating at 1°C per second up to 600°C (Ref.1, Appendix A). Principal features were "melting temperature" and decomposition temperature. The results were edited into a summary video tape, which has been supplied to some fifteen investigators nationwide. The results for ingredients are shown in Table I. From the results it is evident that the physical aspects of the surface behavior of propellants will be radically different for different combinations of ingredients:

1) Typical combinations of AP and hydrocarbon binders decompose together at around 500 °C.

2) To the extent that binder melts affect combustion in 1), the binder melt layer would be much thicker with DDI-cured HTPB than with IPDI-cured HTPB or PBAN.

3) Oxidizers with low decomposition temperatures will decompose within the still-solid part of the surface layer with a high melting point binder like PBAN (with consequent surface disruption).

4) Binders with low decomposition temperatures like PEG and NMMO will decompose ahead of an oxidizer like AP, so the surface will be dominated by AP, some of which may leave the surface incompletely burned.

Current burning rate models are ill-suited to address the conditions in 2) - 4) above. For details of this work, see Appendix A.

Table 1.
Approximate Comparison of Ingredient Thermal Response and Energetics of Oxidizer/Fuel Flames

Ingredient	Melting Temperature [°C]	Vaporization (Decomposition) Temp. [°C]	Energetics of Decomposition	Energetics of O/F flame
PBAN binder	480	500	Endothermic	--
HTPB binder (DDI-cured)	260	500	Endothermic	--
NMMO binder	85	200	Mildly exothermic	--
AP oxidizer	~580*	rapidly above 400	Exothermic	--
AN oxidizer	145	245	Endothermic	--
KP oxidizer	--	400	Endothermic	--
HMX oxidizer	255	290	Exothermic	--
ADN oxidizer	90	165	Exothermic	--
CL-20 oxidizer	--	270	Exothermic	--
Aluminum	673	2493	Very exothermic	--
AP/PBAN	--	--	--	Very exothermic
AN/PBAN	--	--	--	Exothermic
HMX/PBAN	--	--	--	Nearly neutral
ADN/PBAN	--	--	--	Very exothermic

*Decomposes before melting except at heating rates> 10^5 °C/s

Combustion of AP/Hydrocarbon Binder Sandwiches

Earlier studies of 2-dimensional models of propellants had indicated the importance of the kinetically limited edge of the oxidizer-binder diffusion flamelets (Fig. 1) and had shown (Ref. 2) that ballistic modifiers like Fe_2O_3 acted by catalytic breakdown of primary binder vapors into more reactive fuel species, which in turn brought the leading edge flamelets closer to the burning surface and increased burning rate.

In the present studies, the sandwich burning approach was extended in two ways that involved closer approaches to combustion of conventional propellants, particularly propellants with bimodal AP particle size distributions (conditions that can lead to

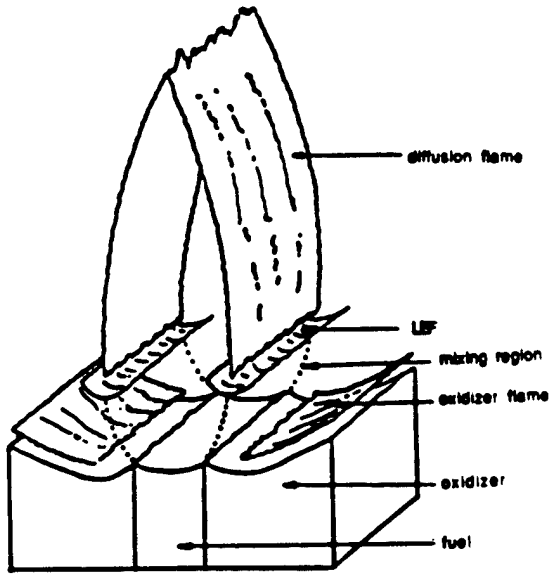

Fig. 1 Combustion zone structure or an AP/HC binder/AP sandwich.

"plateau burning"). The two studies were described in a recent survey paper (Appendix B, Ref. 3) which is excerpted here for the text of this report. More complete accounts are presented as further Appendices and References

Study #1. Sandwiches with fine AP included in the binder laminae (Appendix C, Ref. 4). This strategy allows study of the coupling of burning of large and small particles, and of the role of premixed flames (over surface areas consisting of only fine AP and binder, "matrix" surfaces). In this study the AP laminae play the role of coarse AP particles.

Study #2. Sandwiches with Fe_2O_3 added to the fine AP/binder laminae (Appendix D, Ref. 5). This strategy allows examination of the mechanism of burning rate catalysis in a mixture with high specific surface area of AP (in the fine AP matrix), and with very short diffusion distances for AP and binder vapor mixing and the opportunity for near-surface O/F reactions to contribute significantly to burning rate. In this study, ultra fine Fe_2O_3 was used to assure its availability to the surface and near surface reaction sites.

Sandwiches with AP-filled Binder Laminae

An investigation was made (Appendix C, and Ref. 4) of the burning of sandwiches in which the binder laminae was a matrix of PBAN binder and fine AP (10 or 35-μm) with AP contents of 50 and 70%. With such fine AP particles, the AP and fuel vapors can diffuse together before appreciable O/F reaction, giving a premixed flame if the mixture (e.g., 70% AP) is not too fuel rich to burn. At high pressure with 33.5-μm particles, there was evidence in quenched samples that LEFs and AP self-deflagration occurred on individual particles, (no such evidence for 10-μm particles, or for 33.5-μm particles at 300

psi). For 50/50 matrices this was evident only adjoining the lamina contact planes, indicating coupled behavior between lamina LEFs (LLEFs) and particle LEFs (PLEFs). The burning rates of the sandwiches with AP-filled binder laminae are shown in Fig. 2 (PBAN binder).

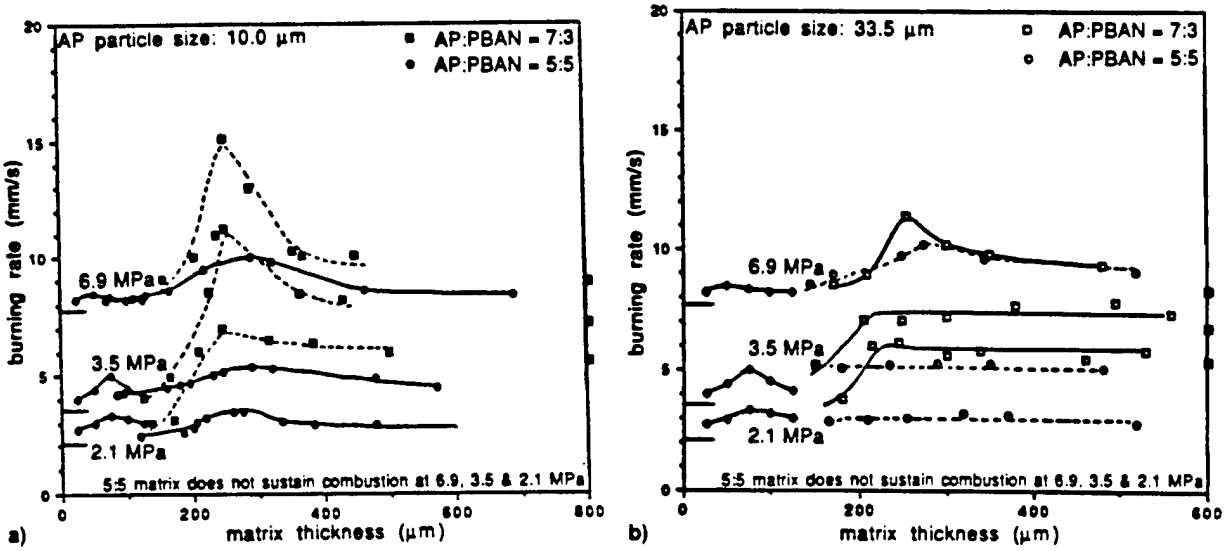

Fig.2. Dependence of sandwich burning rate on thickness of the binder lamina from binder laminae consisting of a matrix of PBAN and particles (from Ref. 4): a) 10- and 33.5-μm AP. AP burning rates are indicated on the left, and matrix burning rates are indicated on the right ordinate lines. Pure binder sandwich burning rate curves are shown in the thickness range 25-125 μm.

In interpreting the results in Fig. 2, it should be noted that the matrix mixtures are fuel-rich, even at a 70/30 ratio. The 50/50 mixture would not burn on its own, and quenched sandwiches showed matrix surfaces that were dominated by solidified binder melt (except as noted above). If one looks at the matrix as a "diluted fuel lamina" and repeats the argument about location of the interlamina mixing fan, stoichiometrc surface and LLEF, one would expect them to be shifted closer to the "extended" plane of the lamina contact surface (Fig. 3), reflecting the effect of a less concentrated fuel. One effect of this, evident in the quenched surfaces and combustion photography, is a reduction (and sometimes elimination) of the protrusion of AP adjoining the contact plane. The LLEF is located more favorably to heat this region than in the pure binder case, and also more favorably to reduce lateral heat loss to fuel lamina by supplying more LEF heat directly to the fuel lamina.

The premixed vapors in the "diluted" matrix outflow are, of course, more than a diluent. On the fuel rich side of the LLEF they are a combustible mixture, that extends the fuel rich side of the LLEF out over the matrix. This increases the total heat release in the LLEF, enabling the flame to stand closer to the surface and give a higher burning rate than resulted with pure binder laminae (Fig. 3), and higher than the matrix burning alone

Fig. 3. Shift in LLEFs when the binder is diluted with AP a) narrow LLEF over AP lamina. Heat flow from AP lamina to binder lamina, AP regression retarded at laminae contact plane; b) wider LLEF, stoichiometric point closer to the surface and shifted toward laminae contact plane. Less lateral heat flow in solid, less retardation of AP at contact plane. More conservative LLEF, closer to surface, correspondingly higher rate; and c) wider LLEF, stoichiometric point over outer edge of AP lamina. LLEF extends well over matrix lamina, probably minimal lateral heat flow in solid.

(indicated at the right in Fig 2). The thickness of matrix lamina for maximum burning rate is around 250-μm, as compared with 50-75 μm for pure binder lamina. This is consistent with the interpretation described for pure binder laminae if one allows for 1) the greater extent of the fuel-rich side of the LEFs that leads to attainment of LLEF coupling at greater thickness of the matrix laminae and 2) the fuel supply becomes deficient with decreasing lamina thickness at greater matrix thickness because the fuel is dilute.

The nature of the O/F flame complex for matrix sandwiches is sketched in Fig. 4, based on theoretical reasoning and experimental results. For a 70/30 mixture with 10-μm AP, the LLEFs act as flame holders for a premixed "canopy" flame over the matrix lamina (Figs. 4b and 4d). For a 50/50 matrix, the canopy is open (thick laminae) because the matrix does not support a flame alone (Figs. 4a and 4c). However, the fuel-rich side of the LLEF extends further than with pure binder, as noted earlier, because a flammable mixture is present. The burning rate of the samples with 70/30 matrices is higher than with 50/50 matrices at all matrix thicknesses except the lowest, suggesting that the size and location of the LLEFS (Fig. 4) are 1) closer to the surface and 2) more favorably located laterally to heat the matrix surface and minimize lateral heat loss in the condensed phase into the matrix lamina. The quenched samples indicate that the sandwich burning rate is determined by the LLEF-assisted regression of the AP lamina, as noted earlier for pure binder laminae.

The effect of particle size of the AP in the matrix gives important clues to the details of the O/F flamelets as follows:

1) Effect of particle size (i.e., 10 and 33.5-μm) is small for 50/50 matrix ratio and for 70/30 ratio at 300 psi. This suggests that under these conditions the matrix outflow is essentially premixed at the LLEF standoff height and premixed canopy flames (Figs. 4a and 4c) result.

2) Burning rates are higher with 10-μm AP than with 33.5-μm AP in the 70/30 matrix at 500 and 1000 psi, suggesting that mixing is not complete for the 33.5-μm AP (thereby limiting the contribution of the fuel-rich side of the LLEF to the rate).

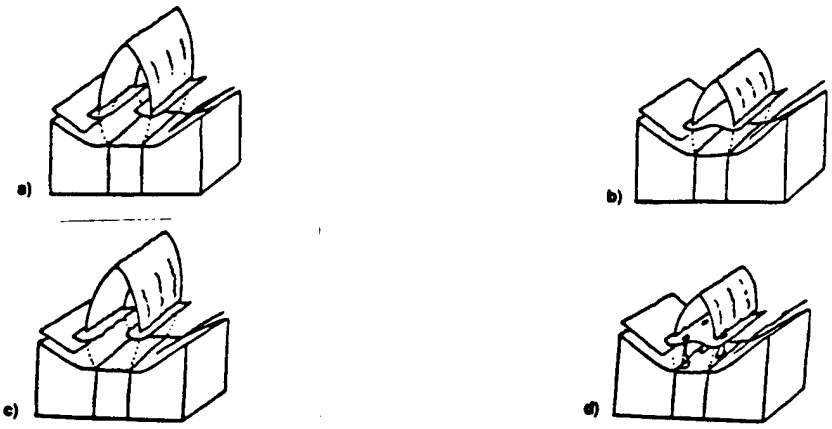

Figure 4. Flame complex for sandwiches with AP-filed binder laminae (300-μm matrix lamina, 500 psi, 3.45 MPa): a) 50/50 AP/PBAN matrix, 10-μm AP; b) 70/30 AP/PBAN matrix, 10-μm AP;c) 50/50 AP/PBAN matrix, 33.5-μm AP; and d) 70/30 AP/PBAN matrix, 33.5-μm AP. Refer to Fig. 1 for an explanation of general features.

3) A relatively strong maximum occurs in the rate vs. lamina thickness curves (70/30 matrix at 500 and 1000 psi), especially for 10-μm AP. This indicates that the matrix flame does not control the rate, but rather enhances it via augmentation of the LLEFs. Extra matrix (i.e., thick lamina) apparently acts to drain heat (and possibly oxidizer species) from the rate controlling region of the sandwich.

4) The weaker maximum of the rate curves in Fig. 2b with 33.5-μm AP presumably reflects the weaker contribution of the fuel-rich side of the LLEFs due to incomplete mixing of the matrix outflow.

5) The quenched 70/30 samples that were burned at 500 and 1000 psi showed evidence that the 33.5-μm particles adjoining the AP laminae were burning individually (i.e., with PLEFs and AP self-deflagration). This may have been a factor in the burning rate, but it is notable that the same behavior was not evident with 10-μm AP, which gave higher burning rate.

Taken collectively, the results indicate that, for the conditions tested, the LLEFs dominate the burning rate, and that AP in the binder lamina enhances the LLEF effect by shifting the LLEF position and extending the fuel-rich side (and, hence, increasing LLEF heat release). Fine AP is more effective because more complete mixing has occurred at the LLEF height. The optimum lamina thickness for rate enhancement is around 250 μm for the conditions tested. Under the conditions tested the individual particles of AP either did not establish their own flamelets, or when they did (33.5-μm, 70/30, 500 and 1000 psi) no major effect on burning rate was evident. This suggests that in a typical bimodal propellant, the fine AP/binder matrix does not control the burning rate directly, but rather that the matrix and peripheral regions of the coarse AP particles support each other by interacting in the LEF.. As the fine particle size and pressure increase, the fine particles burn more independently and enhance the coarse particle burning less (transition somewhere in the 500-1000-psi range for 33.5μm AP in a 70/30 matrix, above 1000 psi in a 50/50 matrix).

Effect of Pressure on Matrix Sandwich Burning Rate

In the foregoing summaries of sandwich burning, the goal was to understand flame structure, and the primary experimental variable was a structural one, i.e., matrix lamina thickness (Fig. 2-4 etc.). The effect of pressure on flame structure was inferred (Fig. 4) by testing at three different pressures. Toward the end of the project it was decided to look at pressure dependence of burning rate in greater detail (Ref. 5). The first step was to extend the pressure range for earlier (Fig. 2) AP/PBAN sandwich tests. The results are shown in Fig. 5. If one views this data in terms of dependence of burning rate on pressure, it is notable that there is low, and even negative dependence in the 1000 - 1500-psi region, but only for the lamina thickness domain for which the LLEFs are coupled, i.e., matrix thickness less than 325μm (and as a corollary, the matrix flame is strongly supported by the LLEFs). This point is probably relevant to the observations of other investigators that plateau burning occurs with bimodal propellants, but only for special proportions of coarse and fine AP (i.e., spacing between coarse particles).

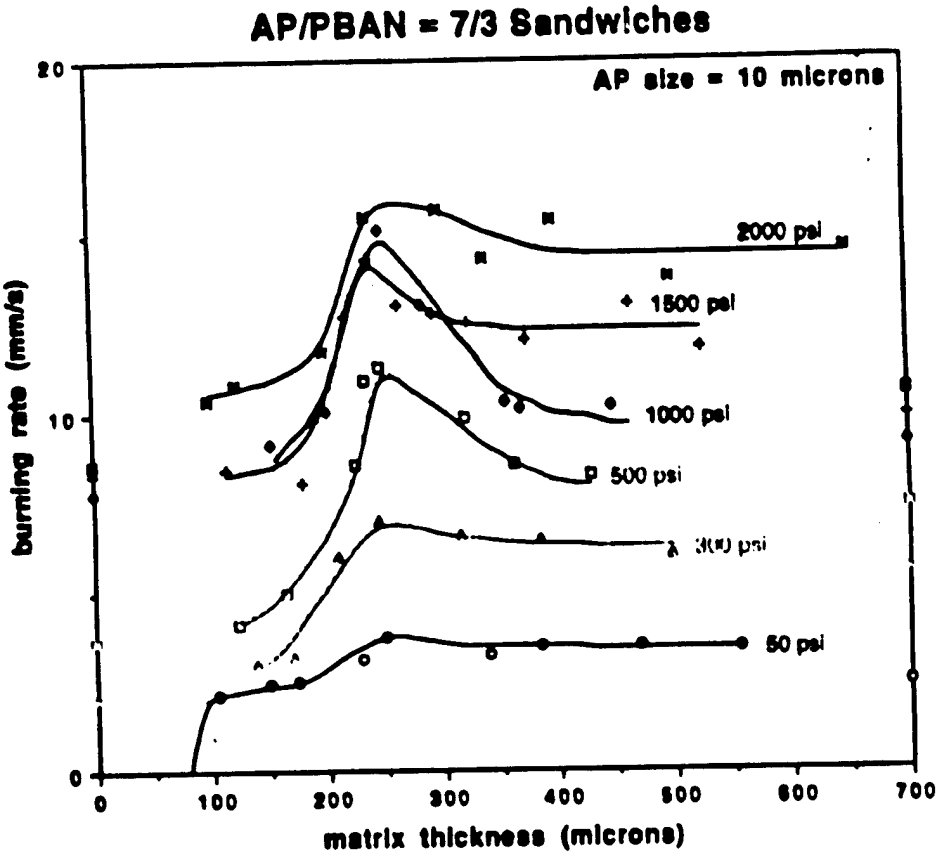

Fig. 5 Dependence of burning rate on matrix lamina thickness for sandwiches with AP(10-μm)/PBAN= 7/3 matrix at different pressures. The pressed AP self deflagration rates are indicated on the left ordinate line and the burning rates of the matrix alone are indicated on the right ordinate line.

Unfortunately, graphs like that in Fig. 5 are not available (or economically obtainable) for all the combinations of possible interest (O/F ratio, size of fine AP, and binder type). To look at the effect of these variables it was decided to use a lamina thickness of 250-275 μm, and look at the effect of fine AP particle size using IPDI-cured HTPB binder with matrixes with an O/F ratio of 65/35. The results (Ref. 5) are shown in Fig. 6. It is notable that:

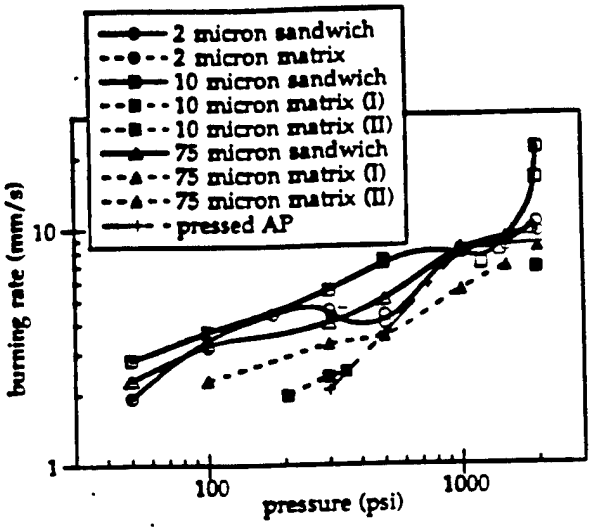

Fig. 6 Pressure dependence of burning rate for sandwiches with AP/IPDI-HTPB = 65/35 matrixes with lamina thickness ~ 250-275 μm, with different fine AP particles sizes. The 2-μm AP matrix does not sustain combustion in the pressure range 50-200 psi.

a) the matrix rates were lower with finer AP (the matrix with 2-μm AP did not burn at any pressure and the matrix with 10-μm AP did not burn in the mid-pressure range.

b) the sandwich rates were all higher than the corresponding matrix rates, and all exhibited some degree of plateau burning, with a particularly strong plateau (mesa) for the 2-μm case.

The effect of binder type is shown in Fig. 7 for sandwiches with 7/3 ratio of 10-μm AP to binder (Ref. 5). The results show that:

a) the matrix rate was higher for PBAN binder than for IPDI-cured HTPB, while the matrix with DDI-cured HTPB would not burn (the IPDI-HTPB matrix showed a plateau in the 100-3-- psi range).

b) the sandwiches with PBAN and IPDI-HTPB binders burned at about the same rate, appreciably faster than the corresponding matrixes.

c) the sandwiches with DDI-HTPB burned at lower rate and with a strong mesa in the 80-500 psi range.

In the case of (65/35 O/F ratio, IPDI-HTPB) the tendency toward plateau burning is associated with matrixes that don't burn well on their own, which in turn is associated

with finer AP particle size (again, corresponding to conditions where matrix burning is strongly coupled to the leading edge flames (LLEFs).

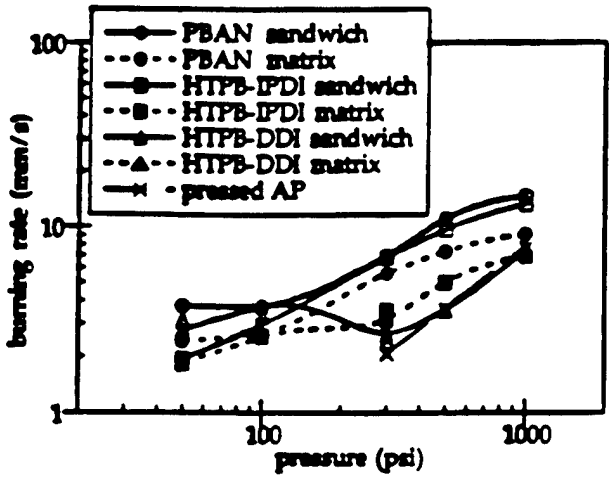

Fig. 7 Pressure dependence of burning rate of sandwiches and matrixes of 10-μm binder = 7/3 having different binder melt flow characteristics. Matrix lamina thickness in sandwiches is ~ 250-275 μm.

The foregoing set of tests was repeated, but with 1% of a very fine particle Fe_2O_3 catalyst added to the matrix (Ref. 5: see also Appendix D). This resulted (Fig. 8) in large increases in both matrix and sandwich rates with the sandwich rates only moderately higher than the matrix rates. While the binder effects on rate were small, they were highest with PBAN and lowest with DDI-HTPB. There were no burning rate plateaus with these fast burning matrixes.

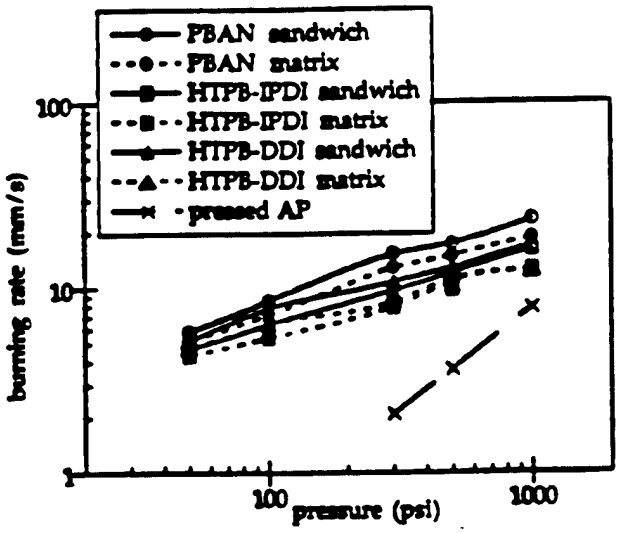

Fig. 8 Pressure dependence of burning rate of sandwiches and matrixes of 10-μm binder = 7/3 having different binder melt flow characteristics catalysed with 1% Pyrocat. Matrix lamina thickness in sandwiches is ~ 250-275 μm.

Combination of Fine AP and Fine Fe_2O_3 in the Binder Lamina

An extension of the "filled" binder lamina studies was initiated by adding Fe_2O_3 to the matrix. Initially, 10% of the 2-μm Fe_2O_3 used in the catalyzed binder lamina studies (described above and in Ref. 5) was attempted, using 10-μm AP and PBAN binder. Samples with 70/30 AP/PBAN ratio could not be processed, and samples with 50/50 ratio gave very erratic burning rates. A change was made to 1% of "Pyrocat" Fe2O3 (described by the manufacturer as 0.003-μm particles). Satisfactory results were obtained (Fig. 9, Ref. 5, Appendix D) with a major increase in the burning rate over similar samples without catalyst. Addition of the catalyst increased the burning rate over those of the 70/30 matrix by about 100% at all three pressures, and caused the burning of the 50/50 matrix to be self-sustaining (matrix rates shown at the right in Fig. 9). The burning rates of the sandwiches with 50/50 matrix were about double the rate of the matrix alone and insensitive to lamina thickness. The rates of the sandwiches with 70/30 catalyzed matrix were somewhat higher than the corresponding matrix, only mildly dependent on lamina thickness.

It was noted in earlier studies of the role of Fe_2O_3, that the catalyst concentrates on the binder surface, an effect that was argued in Ref. 2 to contribute to burning rate by providing a catalyst bed that served to break down the large primary binder vapor molecules into more easily oxidized fuel species (and hence shorter stand-off distance and higher burning rate). In this earlier work, the Fe_2O_3 particle size appeared to preclude any mechanism of catalysis without consideration of catalyst concentration on the surface, because of low collision probabilities anywhere in the combustion zone. In the present studies this reasoning was tested by incorporating iron in the sandwich matrix in four different ways (Ref. 5, Appendix D).

1. Use of ~1 μm Fe_2O_3.
2. Use of ultrafine Fe_2O_3 (Pyrocat).
3. Use of a liquid catocene catalyst.
4. Use of an HTPB binder in which iron atoms were incorporated in the polymer molecules.

The formulations were adjusted so that all had the same iron contest, IPDI-HTPB binder content, and 10 μm AP content. The burning rates of sandwiches (Fig. 10) with the four matrixes were similar, and to the extent that they differed, the difference did not correlate with the degree of dispersity of the catalyst. Somewhat surprisingly, all four methods of catalysis resulted in concentrations of Fe_2O_3 on the binder surface. These results suggest that catalysis does not act at the original sites of the catalyst, e.g., by catalyzing binder decomposition, or by catalysis of binder-oxidizer reactions at condensed phase contact surfaces. However, the large increase in burning rate in catalyzed matrix sandwiches suggests presence of a second mechanism in addition to the previous postulated catalytic breakdown of primary binder vapor molecules.

It was suspected that concentration of catalyst might play another role in the presence of very small AP particle size, in that diffusion of AP vapors to the catalyst concentrations would be possible in substantial amounts because of the increase in overall proximity with fine AP. This could lead to exothermic decomposition of $HClO_4$; in addition the resulting decomposition species are very powerful oxidizers of the fuel

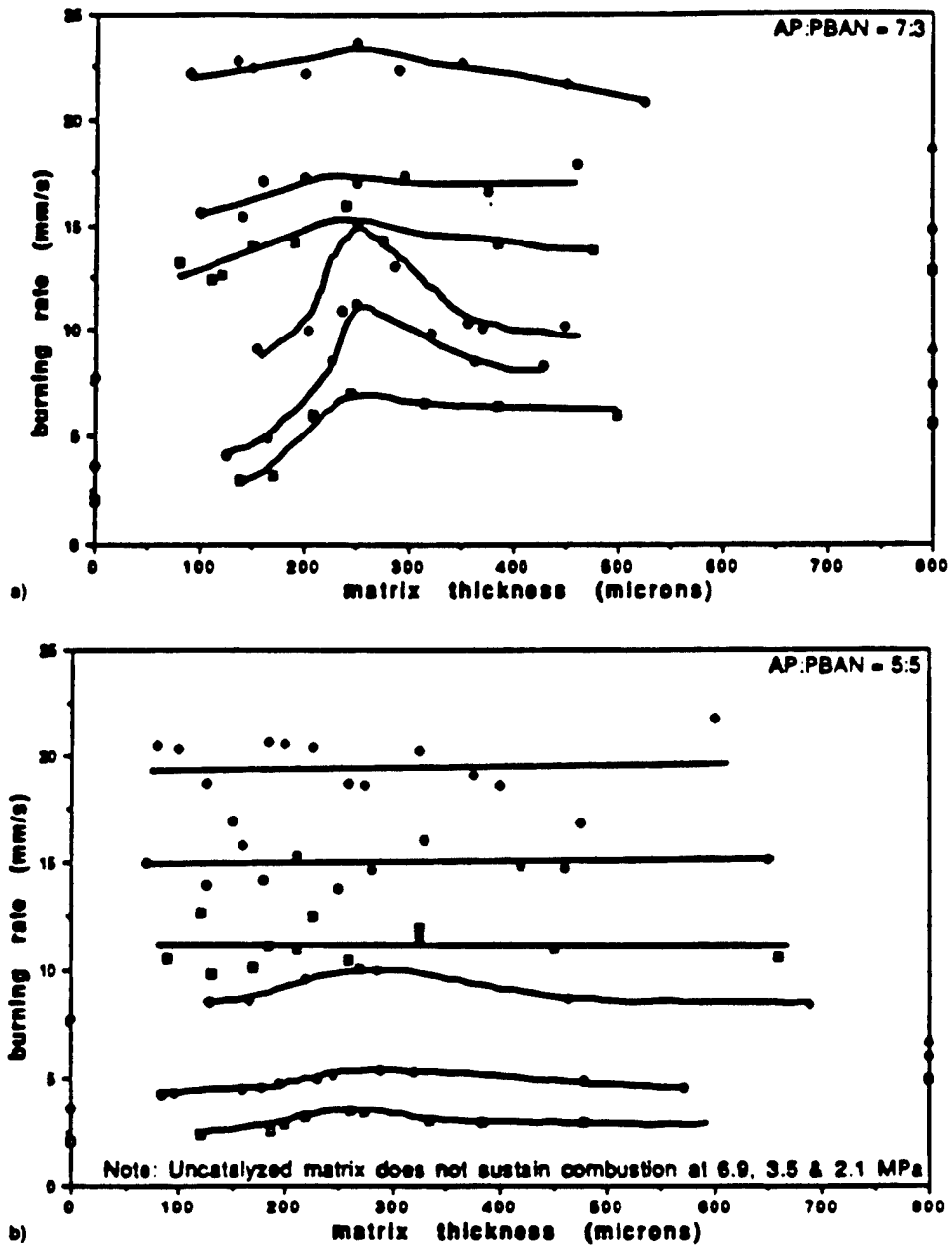

Legend:

- 2.1 MPa
- 3.5 MPa
- 6.9 MPa

Open symbols - uncatalyzed
Filled symbols - catalyzed
AP burning rates are indicated on the left hand ordinate line
Matrix burning rates are indicated on the right hand ordinate line

Fig. 9 Dependence of sandwich burning rate on thickness of the binder lamina for binder laminae consisting of a matrix of PBAN binder, fineAP (10μm) and 1% "Pyrocat" Fe_2O_3 catalyst: AP:PBAN = a) 7:3 and b) 5:5.

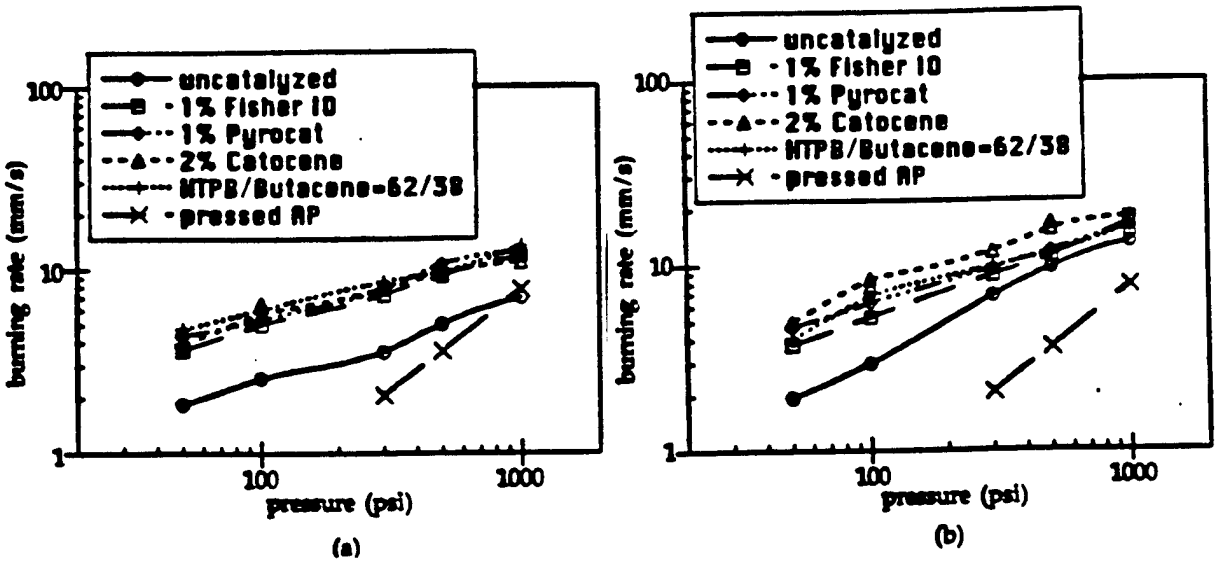

Fig. 10 Effect of dispersability of iron catalysts on the burning rate of 10-μm AP/IPDI-HTPB =7/3 samples: a) matrix, b) sandwich. Matrix lamina thickness in sandwiches is ~250-275 Mm.

species and even the binder surface. Such reactions very likely happen along AP/binder contact lines on the surface, and yet contribute little to burning rate except when these near-contact line surface areas constitute a major part of the total surface area. Following this reasoning, tests were run on sandwiches with Pyrocat-catalyzed 7/3 matrix using 2-μm AP instead of 10-μm AP. It was found (Fig. 11) that the enhancement of rate by addition of catalyst (rate with catalyst / rate without catalyst) was much larger with 2-μm AP than with 10-μm AP (as were the rates themselves) (Ref. 5).

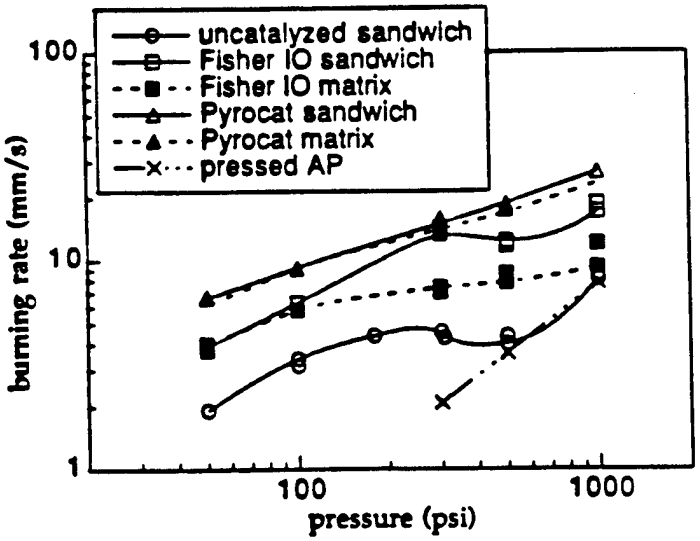

Fig. 11 Effect of particle size of ferric oxide on the burning rate of 2-μm AP/ HTPB-IPDI = 65/35 samples. Matrix lamina thickness in sandwiches is ~250-275 μm. The uncatalayzed matrix does not sustain combustioninthe pressure range 50-1000 psi.

It was concluded that such great rate enhancement for the 2-μm AP could not be explained by LLEF enhancement alone, and that catalytic decomposition of $HClO_4$ (and possibly exothermic near-surface reaction of the products with binder vapors and/or surface) provided a significant contribution to net surface heating. Such reactions are not thought to be important except with a substantial fraction of very fine AP. or at pressures lower than those common to rocket motor operation, On the other hand, Fe_2O_3 breakdown of primary binder vapors (and resulting LEF or premixed flame enhancement) is expected to increase rate under all conditions. In all cases, the tendency for Fe_2O_3 to concentrate on the burning surface is critical to the catalysis process.

Gas Burner and Numerical Modeling of Leading Edge Flames

The kinetically limited leading edge of the O/F diffusion flame (LEF) has emerged in these studies as the dominant part of the gas phase flame (dominant contribution to the burning rate). Unfortunately, it is also the most difficult to observe and to realistically describe analytically, a circumstance that frustrates propellant burning rate and combustion stability modeling. In fact the nature, importance and role of the LEFs had not been fully recognized because of the difficulty in studying them. In this program it was decided to study the LEF phenomenon by two further strategies described in this section.

Study #1: Construct a numerical model of the gas burner flame, based on the complete gas flow and chemical reaction equations, and run solutions on a Cray computer (Appendix E and Ref. 6).

Study #2: Construct and test an atmospheric pressure gas burner that simulates the two dimensional geometry of the sandwich flame, in which the LEFs would be large enough to be observed (Appendix F and Ref. 2).

Summaries of these two studies (excerpts from Ref. 1) are presented below:

Theoretical-Numerical Analysis of Leading-Edge Flames

Because of the emergence of LEFs as a critical factor in edge-burning of AP sandwiches and propellants, it was decided to attack the problem of rigorous modeling of two-dimensional diffusion flames. This effort was started because of the absence of direct observations of LEFs in propellant-sandwich combustion studies (because of inability to make such observations on microflamelets). In the modeling work the gases were assumed to emerge at the upstream boundary (Fig. 12) at specified velocity, density, and temperature (simulating a Wolfhard-type gas burner), and pressures near atmospheric were assumed (simulating a companion experimental study). Nonsteady laminar Navier-Stokes flow was assumed. Inlet gases were assumed to be $CH_4 + N_2$ in the center flow, and O_2 and N_2 in the outer flow. The chemistry was represented by a set of 48 elementary reactions involving 18 species. Temperature-dependent transport properties were used for each chemical specie. Details and computational methods are described in Ref. 6 and Appendix E. Some notable results about LEFs are discussed here.

Figure 13 shows plots of distribution of species concentration, heat release rate (per unit volume), pressure, and flow direction (streamlines). Fig. 13a shows the concentration of CHO, which is a short-lived intermediate product present only in the

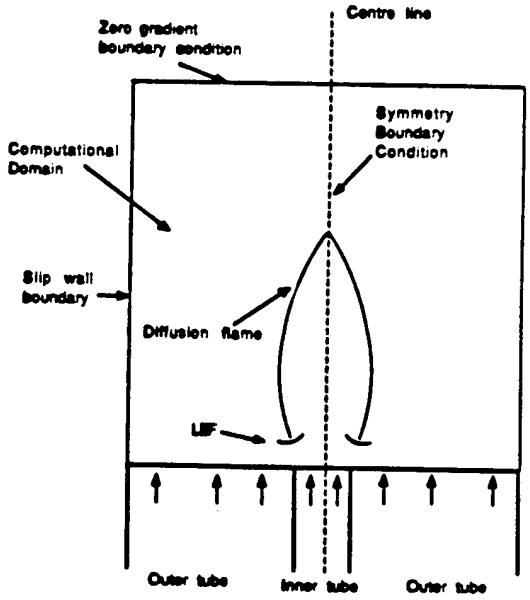

Fig. 12 Arrangement for a two-dimensional gas diffusion flame burner (numerical model and experiment.

flame. There are locally high concentrations at the LEF sites. Fig. 13b shows very high heat release rates at the same sites (high compared to the diffusion limited part of the flame further downstream), indicative of abrupt consumption of the reactants that have mixed upstream of this site. Fig. 13c shows that this concentrated reaction and the associated volume increase produce local pressure increases at the LEF sites, and Fig. 13d shows that this produces a divergence of the approach flow, as a result of which the vertical component of the velocity of the approach flow to the LEFs is reduced (i.e., does not increase as much as in a one-dimensional flame). These results support the idea of an intense leading-edge flame, and an extended, less intense diffusion limited "tent" flame (Fig. 1). These computed LEFs show little lateral extent, contrary to those suggested in earlier sketches and discussion here. This "narrowness" is a feature of LEFs produced by combinations of pure fuel and oxidizer flows (i.e., diluted only by relatively inert gas). In a following section on LEFs in gas burner flames, crescent LEFs resulted when some fuel was included in the oxidizer in-flow and some oxidizer in the fuel in-flow. In the sandwich burning tests, the products of AP pyrolysis are a mixture of fuel and oxidizer species (e.g., NH_3 and $HClO_4$); and most of the binders, and especially the AP/binder matrix laminae, have oxidizer species in the laminae outflow. Thus, the propellant LEFs have appreciable lateral extent as suggested earlier in the discussion of the effect of addition of AP to the binder lamina.

LEFs in Gas Burner Flames

To further verify the presence and nature of LEFs, a gas burner study was made using a rectangular atmospheric pressure burner with a fuel flow in the middle and oxidizer flows on the outside (analogous to sandwiches and to the numerical study. A methane-air combination was used, with N_2 and CO_2 used as diluents. Outflow velocities were matched, but varied together from 15-50 cm/s. The flames were viewed edge-on

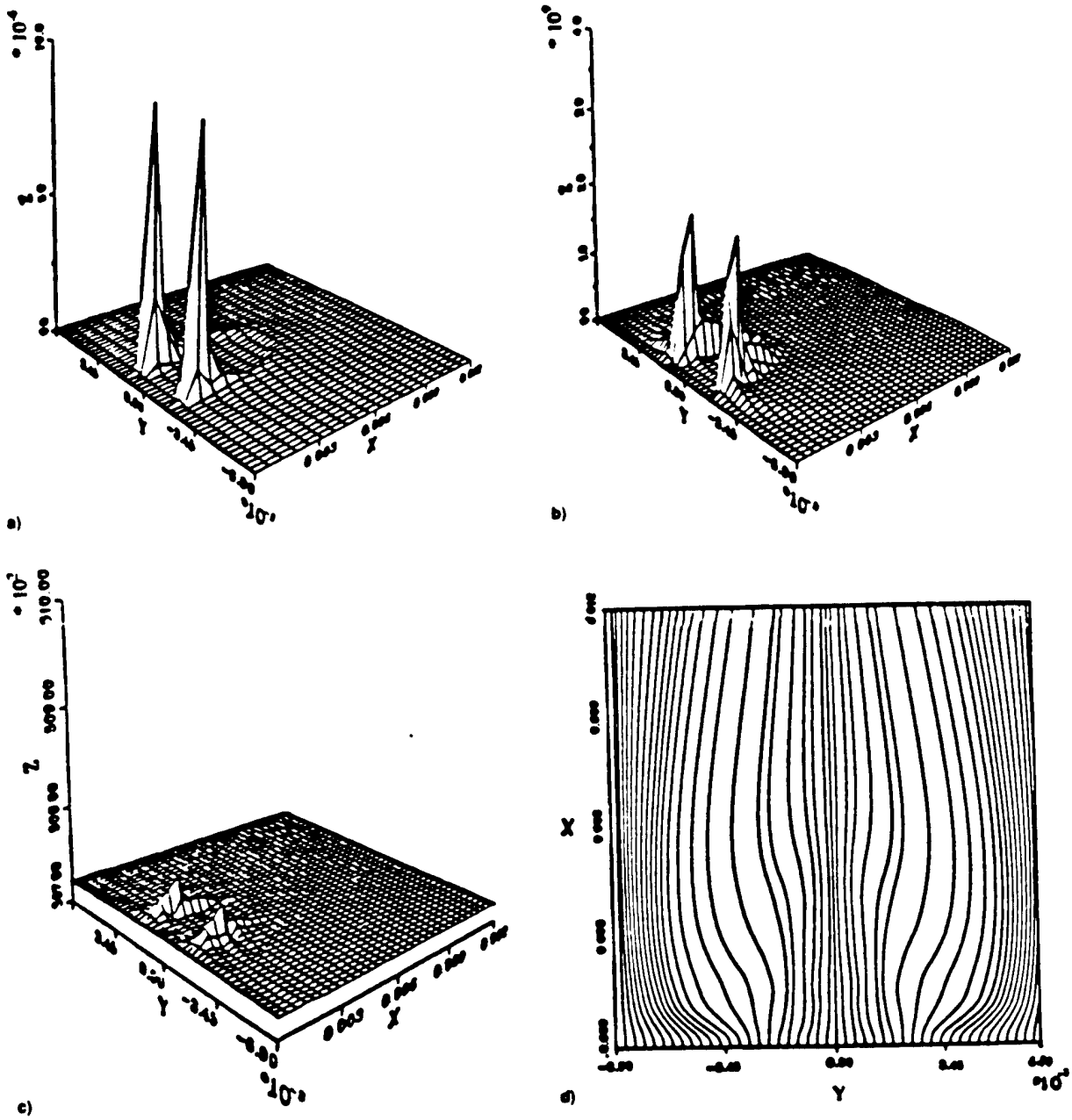

Fig. 13 Computed features of two-dimensional methane-air diffusion flame (N_2 diluted), burner configuration as in Fig. 12; X and Y dimensions are in meters; flow enters at the lower left: a), b) and c) and at the bottom in d): a) CHO concentration (mass fraction); b) volumetric heat release rate (J/m^3 s); c) pressure; and d)streamlines.

photographically, including viewing with a Mach-Zender interferometer that permitted determination of the temperature field (example in Fig. 14, where the interference fringes

correspond to exotherms). Temperatures were also measured with a transversing thermocouple. In addition, the flames were viewed side-on for intensity of CH radiation, a good indicator of heat release. The results of this study are detailed in Appendix F. Some highlights are summarized here.

1) An intense leading-edge region of the flame was indicated in the CH intensity and temperature measurements, and the flame standoff distance from the burner surface was measured from the photographs.

2) These LEFs were of limited lateral extent, consistent with results of the computational studies.

3) When fuel was added to the oxidizer flow and oxidizer added to the fuel flow, a crescent LEF resulted (Fig. 15).

4) The approach flow was deemed to be laminar, because the turbulence would smear out interference fringes, and effect that was not observed (Fig. 14).

5) The "effective flame speed" of the LEF was taken to be the flow velocity from the burner, and was compared with the flame speed of one-dimensional premixed

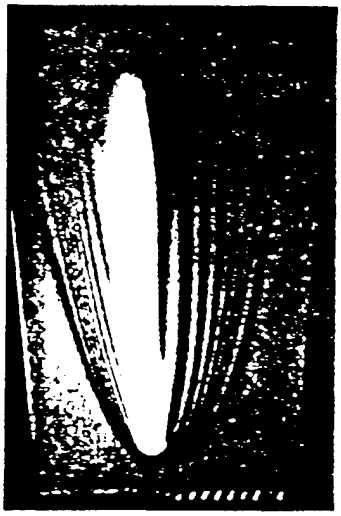

Fig. 14 Double exposure images of one of the two diffusion flames in the gas burner, viewed edge on. The bright central plume is the flame viewed by self-luminosity. The surrounding lines correspond to isotherms, produced by monohromatic light interference fringes (M-Z Interferometry.

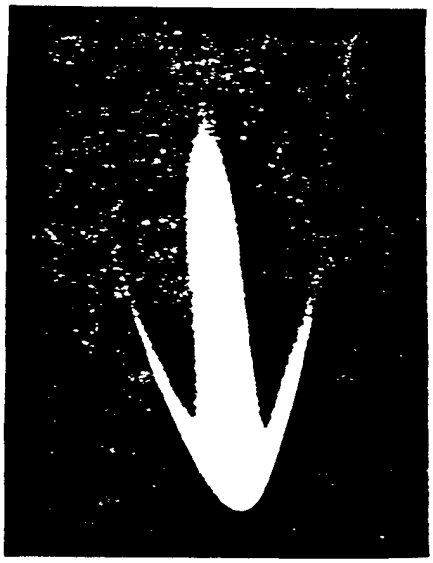

Fig.15 Leading-edge flame in the gas burner when O and F inflows were enriched with F and O (mixtures well below flammability limits: methane-airwith N_2 and CO_2 dilution, atmospheric pressure).

methane-air flames of the same temperature (Fig. 16). This effective flame speed was as much as 2.5 times the premixed flame speed.

In general, the experimental results were consistent with the numerical modeling results, indicating an intense, local LEF in the mixing fan, followed by a trailing diffusion limited flame with much lower heat release. The high effective flame speed is presumably due to divergence and retardation of the approach flow to the LEF due to the pressure "island" (Fig. 13c) at the site of the LEF. The crescent flame (Fig. 15) supports the interpretation of sandwich burning tests in which the fuel flow was enriched by inclusion of oxidizer in the binder lamina. Similar LEF behavior (crescent LEF and high flame speed) has been reported in stratified fuel-air mixtures in horizontal ducts. It may be worth re-emphasizing that this high effective flame speed is due to the high local heat release in the LEF, the resulting local pressure rise, and the resulting multidimensional convective flow in the neighborhood of the LEF. Not only is the upstream heat flow to the surface localized by the local nature of the heat source, but the location of the heat source is dependent on multidimensional aspects of both heat flow and gas flow.

To put the leading edge flame phenomenon simply, the mixing rates in the diffusion fans are extremely high near the surface because the lateral concentration

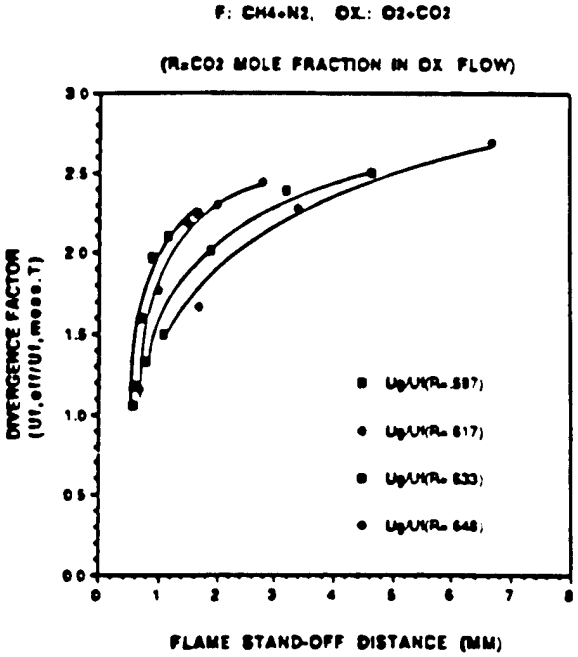

Fig. 16 Ratio of LEF speed to speed of methane-air flames of the same temperature (measured temperatures).

gradients of the reactants are extremely high. However, the O/F reaction rates are low because high temperatures cannot occur in the presence of "cold" incoming and adjoining flows. At some point in the mixing fan the amount of partially premixed O/F mixture becomes large enough to support a stationary leading edge flame, i.e., a flamelet that is hot enough in this high heat loss environment to give high chemical reaction rates. As seen in Fig. 13b, the volumetric heat release rate is very high in the LEF, indicative of the relatively large supply of O/F mixture at, and near to stoichiometric ratio. From the

computational results in Appendix E, it is evident that a major part of the O/F heat release can occur in the LEF. It is also notable that the resulting associated local pressure rise and approach flow divergence play an important role in location of the LEF. This also explains the high propagation velocities of LEFs observed in various earlier studies in gas burners and in experiments in horizontal stratified O/F mixtures (e.g., simulated mine tunnels).

New Ingredients

One goal of the present project was to explore the combustion behavior of propellants with new ingredients. Because of the very small amounts of ingredients required in the kinds of tests that were used, it was hoped that results could be provided early in the ingredient program to guide later, more costly development work. Unfortunately this goal was largely frustrated by difficulties in getting ingredient samples. However, some tests were made involving ADN, HNIW (CL-20) and HMX. These results are summarized in Appendix G. The most significant findings were that:

a) the self deflagration rate of ADN was much higher than the rate of AP, and relatively insensitive to pressure in the tested range of 100 to 1000 psi. Hot stage microscope test results suggest that exothermic decomposition of the melt is a factor in the high rate.

b) tests of sandwiches using ADN laminae yielded higher burning rates than ADN alone, implying that the O/F flame contributes to burning rate. This is contrary to conclusions reached by other investigators based on laser assisted tests at low pressure, and reminds us of our earlier findings with AP, that O/F diffusion flamelets (LEFs) do not get established at low pressures because reaction kinetics are too slow.

c) when ADN was used in the matrix lamina of AP/matrix/AP sandwiches, the burning rate with ADN matrix and AP laminae is substantially higher than the ADN matrix alone. Together these results indicate that the surface heat release of the ADN enhances rate, but the AP lamina/fuel flame (LLEF) is still important. The results with PBAN and IPDI-cured HTPB binder were alike.

d) when HNIW and HMX were used in the matrix of the AP/matrix/AP sandwiches, the burning rates were similar to those with ADN in the matrix, but less pressure sensitive (more like AP matrixes). It was notable that the burning rate of the HNIW matrix and the AP/matrix/AP sandwiches were essentially the same, suggesting that the matrix controlled the rate. In contrast, the rate of the HMX matrix alone was very low compared to the corresponding sandwich rate.

e) the sandwich rates with the different oxidizer matrixes were close enough to each other to justify a conclusion that all were dominated by the AP/binder lamina flame, and that the primary role of the matrix was to supply fuel for the lamina leading edge flamelets.

f. unfortunately the supplies of HNIW and HMX were too limited for self-deflagration tests or tests like those with ADN in which the ingredients could be used as the oxidizer laminae in the sandwiches.

Results with Propellants

The understanding of combustion of AP/HC binder sandwiches was applied in the present program to the granular AP propellant situation by two studies by Sambamurthi (Ref. 7,8). and Beiter (Ref. 9 and Appendix H). These investigations are summarized briefly here to demonstrate the role of the leading edge in propellant burning.

In view of the critical role of the LEF in precipitating the ignition and agglomeration of aluminum accumulations on the burning surface, it was proposed (Ref. 7 and 8) that this mechanism could be demonstrated by making and testing an aluminized propellant with bimodal oxidizer-particle-size distribution. In such propellants the burning surface consists of irregular arrays of coarse AP particles (400-μm mass mean diameter was used), with intervening areas consisting of a fuel-rich mixture of binder, fine AP, and aluminum. At low pressures, the fine AP particles will decompose without "attached" LEFs (analogous to the results of Lee noted earlier), and the accumulating aluminum on the surface will be ignited by the PLEFs on the coarse particles. The whole area of accumulation between coarse particles will then coalesce, to give large agglomerates. If test pressure is increased, a theshold will be reached where PLEFs will occur in the O/F mixing fans of the fine AP particles. This in turn will provide a large increase in number and proximity of sites for ignition of the accumulating aluminum, with a corresponding decrease in agglomerate size. This postulate was tested by Sambamurthi, who prepared bimodal propellants with four different AP particle sizes (400-μm coarse AP).
According to the mechanistic argument, the threshold pressure for onset of PLEFs on the "fine" AP particles would be lower for fine AP particles of larger size so the corresponding threshold for decreases in agglomerate size would be at lower pressures. Sambamurthi used combustion photography and agglomerate quench tests (Ref. 8) to determine agglomerate size. Figure 17 shows the trend of agglomerate size (mass average mean diameter) with pressure for the four sizes of fine AP used (17.5, 49, 82.5, and 196 μm). The results show an abrupt decrease in agglomerate size at a threshold pressure, as predicted in the foregoing scenario. The threshold pressure decreases with increases in AP particle size, as predicted. Keeping in mind that this rather singular trend in agglomerate size was forecast in advance on the basis of sandwich burning-based results and mechanistic arguments about leading edge flames and aluminum ignition, the results are a good validation of the mechanistic argument. The results provide a mechanistic basis for the empirical "pocket" model of agglomeration proposed originally by Crump (Ref. 10) and Price et al., (Ref. 11) and provide a more complete basis for the heuristic bimodal pocket model proposed by Cohen (Ref. 12).

The propellant study by Beiter has to do with the dynamic response of the combustion zone to pressure oscillations. In particular, the study considered the possibility that a large part of the dynamic response might result from the LEF behavior when the conditions are close to the threshold noted in the last paragraph. When the small particle LEFs are on the brink of detachment, their stability is marginal, and they may oscillate between an attached PLEF condition and a more remote premixed canopy flame configuration. It was proposed that, if a bimodal propellant with very narrow size

distribution of the fine AP were tested for pressure-coupled response function, a large portion of the fine AP particles would reach PLEF threshold conditions at the same pressure. Above that pressure, dynamic response would be typical of burning with the PLEF flame complex, and below it the response would be typical of coarse AP PLEFs with premixed canopy flames over the areas of fine AP-AL binder matrix. In between those two domains it seemed likely that a greatly increased response might occur due to the marginal stability of the fine particle LEFs. This postulate was tested by running a series of T-burner tests over the relevant pressure range. Figure 18 shows the response function vs. pressure for tests at 500 Hz with a propellant with 17.5-μm fine AP. While the data scatter in this type of test is rather appreciable, it seems clear that a peak in the response function curve occurred at 275 psi (1.91 MPa). Tests with the other sizes of fine AP were less decisive, apparently due to scatter in T-burner data and difficulty in achieving uniform particle size of the fine AP. The design of the experiment requires that the fine AP particles all experience threshold conditions for the PLEFs at the same pressure to produce a recognizable singularity in the collective dynamic response. In propellants with more conventional particle-size blends, the contribution to marginally stable LEFs is present to lesser degree over a wide pressure range, but is not distinguishable from other contributions to global dynamic response.

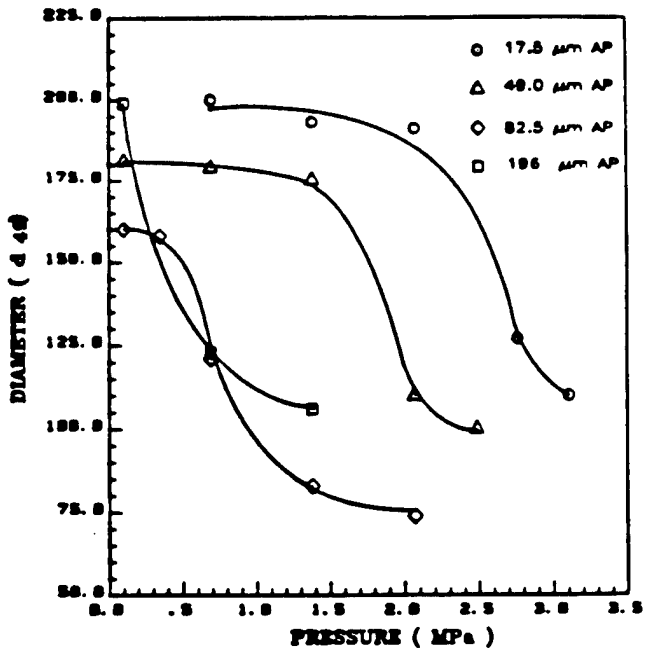

Fig. 17 Effect of pressure on mass average aluminum agglomerate size for propellants with coarse/fine AP in the ratio 8.2.

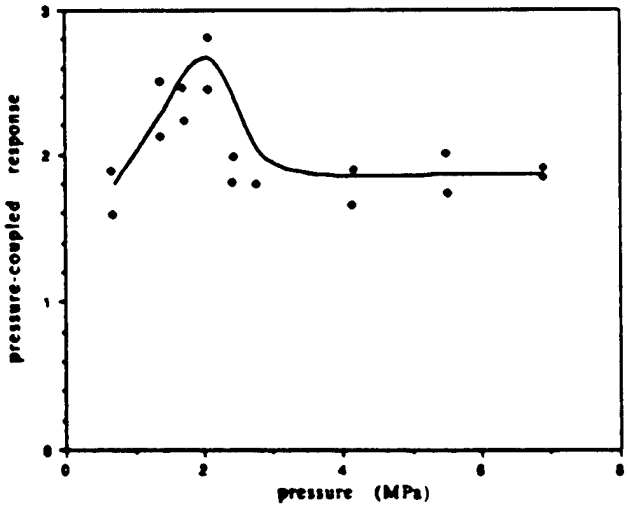

Fig. 18 Response function (vs. pressure) for an AP/PBAN propellant with bimodal AP size distribution, obtained from pulsed T-burner tests at a frequency of 500 Hz.

References

1. Price, E. W., Sigman, R. K., Chakravarthy, S. R. and Paulsen, P. D., "Hot Stage Microscope Studies of Decomposition of Propellant Ingredients," *Proceedings of the 30th JANNAF Combustion Meeting*, CPIA Publication 606, Vol. II, November 1993, pp. 289-296.

2. Chakravarthy, S. R., Price, E. W., and Sigman, R. K., "Mechanism of Burning Rate Enhancement of Composite Solid Propellants by Ferric Oxide," AIAA Paper 95-0601, 33rd Aerospace Sciences Meeting, Reno, NV, January 1995.

3. Price, E. W., "Effect of Multidimensional Flamelets in Composite Propellant Combustion," *Journal of Propulsion and Power*, Vol. 11, Number 4, July-August 1995, pp 717-728.

4. Lee, S-T., "Multidimensional Effects in Composite Propellant Combustion," Ph.D Dissertation, School of Aerospace Engineering, Georgia Institute of Technology, Atlanta, GA, March, 1991.

5. Chakravarthy, S. R., "The Role of Surface Layer Processes in Solid Propellant Combustion," Ph. D. Dissertation, School of Aerospace Engineering, Georgia Institute of Technology, Atlanta, GA, November, 1995.

6. Prasad, K., "Numerical Simulation of Reactive Flows through Two-Dimensional Burners," Ph. D. Dissertation , School of Aerospace Engineering, Georgia Institute of Technology, Atlanta, GA, December, 1990.

7.Sambamurthi, J.K. and Price, E.W., "Aluminum Agglomerationin Solid Propellant Rockets," *AIAA Journal*, Vol. 22, No. 8, 1984, pp. 1132-1138.

8. Sambamurthi, J. K., "Behavior of Aluminum on the Burning Surface of a Solid Propellant," Ph. D. Dissertation, School of Aerospace Engineering, Georgia Institute of Technology, Atlanta, GA, March 1983.

9. Beiter, C. A., "The Role of the Combustion Zone Microstructure in the Pressure-Coupled Response of Composite Propellants," Ph. D. Dissertation, School of Aerospace Engineering, Georgia Institute of Technology, Atlanta, GA, May 1991.

10. Crump,J. E., "Photographic Survey of Aluminum Combustion in Solid Rocket Propellants," *Proceedings of the Inter Agency Chemical Rocket Propulsion Group*, Vol. 1, CPIA Publ. 68, Jan. 1965, pp. 367-370.

11. Price, E. W., Kraeutle, K. J., Prentice, J. L., Boggs, T. L., Crump, J.E., and Zurn, D. E., "Behavior of Aluminum in Solid Propellant Combustion,"Naval Weapons Center TP 6120, China Lake, CA, March 1982.

12. Cohen, N. S., "A Pocket Model of Aluminum Agglomeration in Composite Propellants," *AIAA Journal*, Vol. 21, No. 5, 1983, pp. 720-725.

Appendix A

Hot Stage Microscope Studies of Decomposition of Propellant Ingredients

Proceedings of the 30th JANNAF Combustion Meeting
November 1993

CPIA Pub. No. 606, Vol. II, pp. 289 - 296.

HOT STAGE MICROSCOPE STUDIES OF DECOMPOSITION OF PROPELLANT INGREDIENTS

E. W. Price, R. K. Sigman, S. R. Chakravarthy and P. D. Paulsen
School of Aerospace Engineering
Georgia Institute of Technology
Atlanta, Georgia 30332

ABSTRACT

This report summarizes results of direct observation of ingredient decomposition using a hot stage microscope. Materials tested were PBAN and HTPB binders and their individual ingredients. Also tested were particles of several oxidizers, binders with oxidizer particles, and binders with Fe_2O_3 and TiO_2 additives.

INTRODUCTION

This study was motivated by increasing evidence that the physical behavior of binders in the surface layer of burning propellants plays a significant role in the burning rate. In this regard, the various hydrocarbon binders in common use are believed to each melt and decompose at rather different temperatures, but there is little direct or quantitative evidence. The hot stage microscope is a convenient means for obtaining such information. While such slow heating experiments may not accurately simulate the behavior in fast pyrolysis, they are a good starting point, easy to use, and qualitatively in agreement with combustion experiments.

EXPERIMENTAL METHOD AND MATERIALS

Experiments were conducted in a Leitz microscope with Leitz hot stage. Then samples are heated on a sapphire surface in an argon atmosphere. The sapphire is heated by an electrical heater, and the surface temperature is monitored by a thermocouple. Typical heating tests run to about 500° C in 10-20 minutes. Most tests were monitored visually, and progress of sample discoloration, "smoking," melting, bubbling and residue formation were noted vs temperature manually. Late in the study, the capability for video pictures and recording with time and temperature read-out became available.

Materials tested were binder ingredients (liquid), cured binders (PBAN, DDI-cured HTPB, IPPI-cured HTPB), oxidizer particles (AP, AN, CL-20, ADN), cured binder with isolated oxidizer particles, cured binders with additives (Fe_2O_3, TiO_2), and DDI-cured HTPB loaded 50/50 and 65/35 with 2 μm AP.

RESULTS

Observations from the tests are summarized in the accompanying charts, as descriptions of physical behavior or state vs temperature (scale on the vertical "coordinate" at the left). In the case of binders with variants (addition of DOA plasticizer, Fe_2O_3 or TiO_2), the pure binder is in the left-hand column and additives are identified by further entries at the column heading.

The principal observations about sample behavior were

1. HTPB binders melted at around 230° C, and decomposed vigorously around 475°.

---

* This work was performed under Contract No. N00014-89-J-1293 from the Office of Naval Research, Arlington, Virginia.

2. PBAN binder didn't become fully melted until around 450° C, and decomposed vigorously at around 475° C.

3. The presence of DOA, Fe_2O_3 or TiO_2 delayed the onset of visible melting of HTPB slightly, and had little effect on the onset of boiling decomposition (possibly a small lowering of gassing temperature in HTPB with Fe_2O_3).

4. TiO_2 (submicron) caused reduced fluidity of the HTPB binder melt, and a coagulation into wet clumps with some surrounding liquid.

5. AP particles (250 μm) start gassifying at lower temperature than do the binders (around 420° C), and cause discoloration of the contacting HTPB binder melt prior to vigorous gassification (i.e., below 420° C). After the binder melt is decomposed, residual crusts remain around the sites of the AP particles (all binders).

6. Fe_2O_3 caused progressive discoloration and some gassing at intermediate temperatures in some (but not all) binder-AP combinations.

7. TiO_2 had little effect other than that noted in 4, except for a tendency for binder darkening around the AP particles at intermediate temperature (320-380° C).

8. The samples with 65% 2 μm AP (DDI cured HTPB) ignited at about 350° C.

CONCLUSIONS

The hot stage testing shows a conspicuous difference in melt behavior of PBAN and HTPB binder, which is consistent with conclusions reached in sandwich burning tests and various propellant tests, with HTPB showing extensive melts. Fe_2O_3 in the binder did not change visual evidence of binder melting or decomposition much, an observation consistent with conclusions reach in many, but not all, combustion tests. Some Fe_2O_3 activity was evident around AP particles, with residue patterns suggestive of AP-binder reactions. The observation that AP particles decomposed before (i.e., at lower temperature) than the binders is not consistent with conclusions reached in sandwich and propellant combustion tests, but suggests that binder melt (HTPB) present in excess could flow over the AP surfaces in burning propellants and interfere with AP deflagration. The occurrence of ignition events in the samples with a large fraction of 2 μm AP is significant in that it shows that interfacial reactions can become important when sufficient contact surface is present (but a results that might be dependent on heating rate).

Future efforts will include videotaping critical tests for better presentation of results, and testing of a wide variety of binders.

ACKNOWLDGEMENT

The authors would like to express their appreciation to ONR and Dr. R. S. Miller for support of these studies, and to thank Mr. John Guimont (CSD), Dr. Russel Reed (NAWS) and Dr. Carol Hinshaw (Thiokol) for providing ingredients for this study.

OXIDIZERS

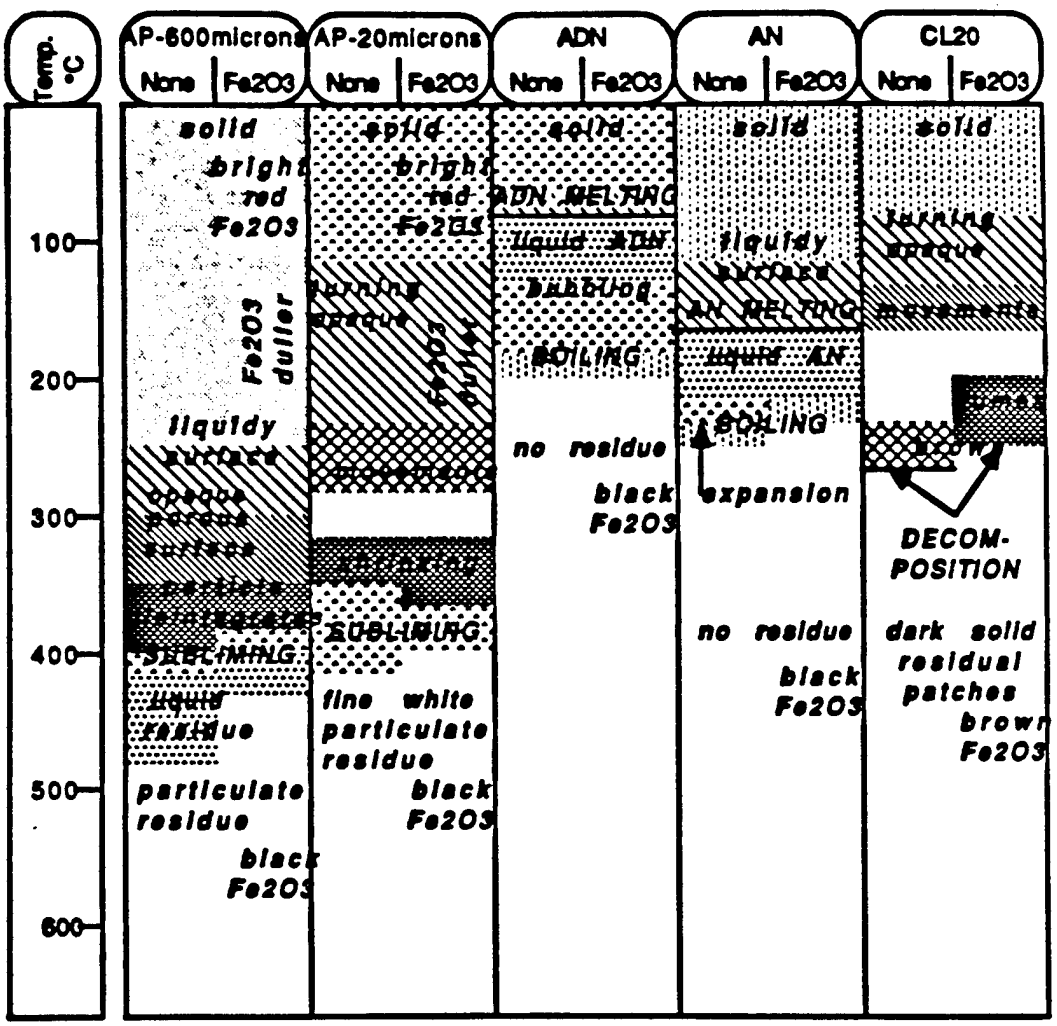
Temp. °C
AP-600microns
None
Fe2O3
AP-20microns
None
Fe2O3
ADN
None
Fe2O3
AN
None
Fe2O3
CL20
None
Fe2O3
100
200
300
400
500
600
solid
bright red Fe2O3
Fe2O3 duller
liquidy surface
opaque porous surface
particle agglomerate
SUBLIMING
liquid residue
particulate residue
black Fe2O3
solid
bright red Fe2O3
burning opaque
Fe2O3 duller
SUBLIMING
fine white particulate residue
black Fe2O3
solid
ADN MELTING
liquid ADN
BOILING
no residue
black Fe2O3
solid
liquidy surface
AN MELTING
liquid AN
BOILING
expansion
no residue
black Fe2O3
solid
burning opaque
movements
DECOM-
POSITION
dark solid residual patches
brown Fe2O3

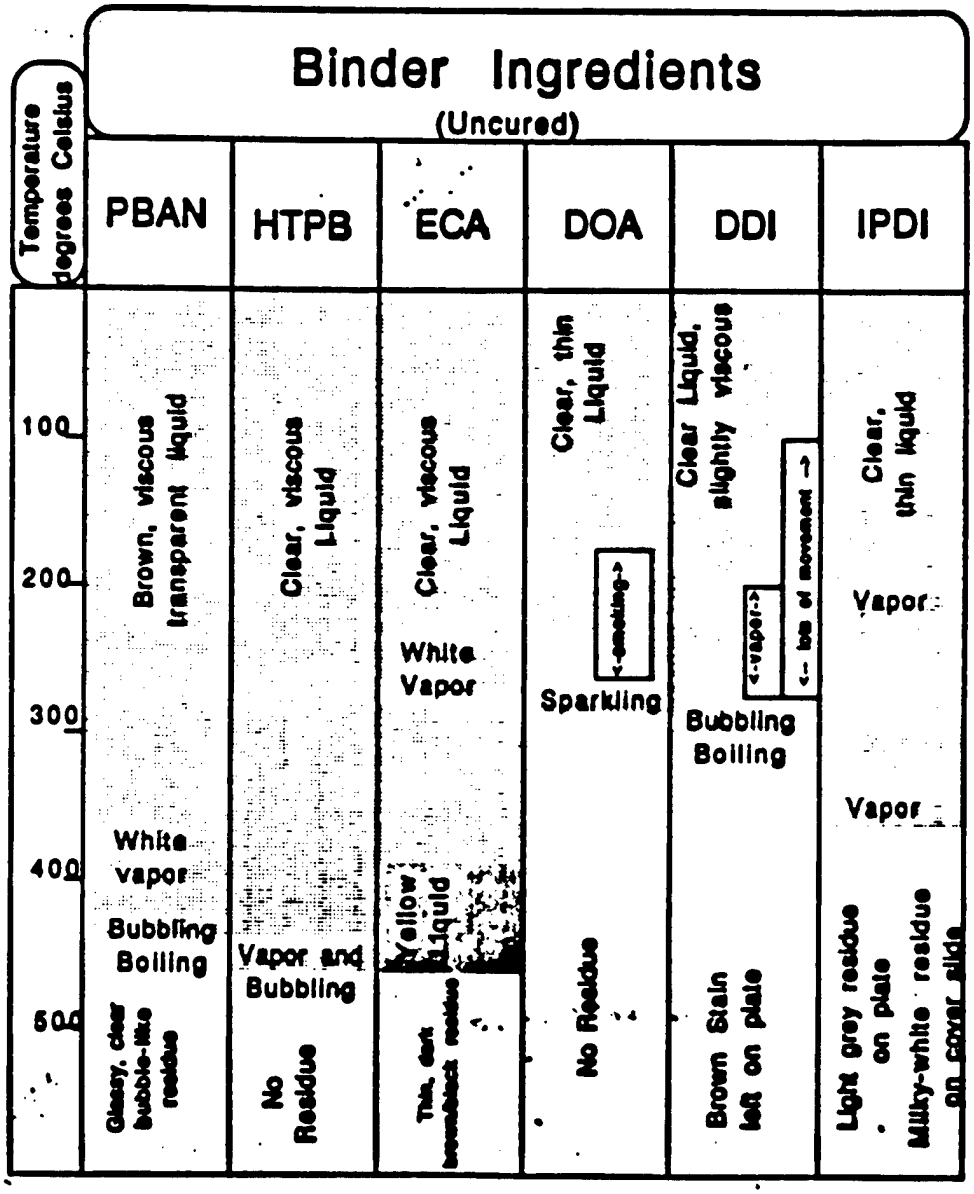
Binder Ingredients
(Uncured)
Temperature degrees Celsius
PBAN
HTPB
ECA
DOA
DDI
IPDI
100
200
300
400
500
Brown, viscous transparent liquid
White vapor
Bubbling Boiling
Glassy, clear bubble-like residue
Clear, viscous Liquid
Vapor and Bubbling
No Residue
Clear, viscous Liquid
White Vapor
Yellow Liquid
Thin, dark brown/black residue
Clear, thin Liquid
<-melting->
Sparkling
No Residue
Clear Liquid, slightly viscous
<-vapor->
<-- loss of movement -->
Bubbling Boiling
Brown Stain left on plate
Clear, thin liquid
Vapor
Vapor
Light grey residue on plate
Milky-white residue on cover slide

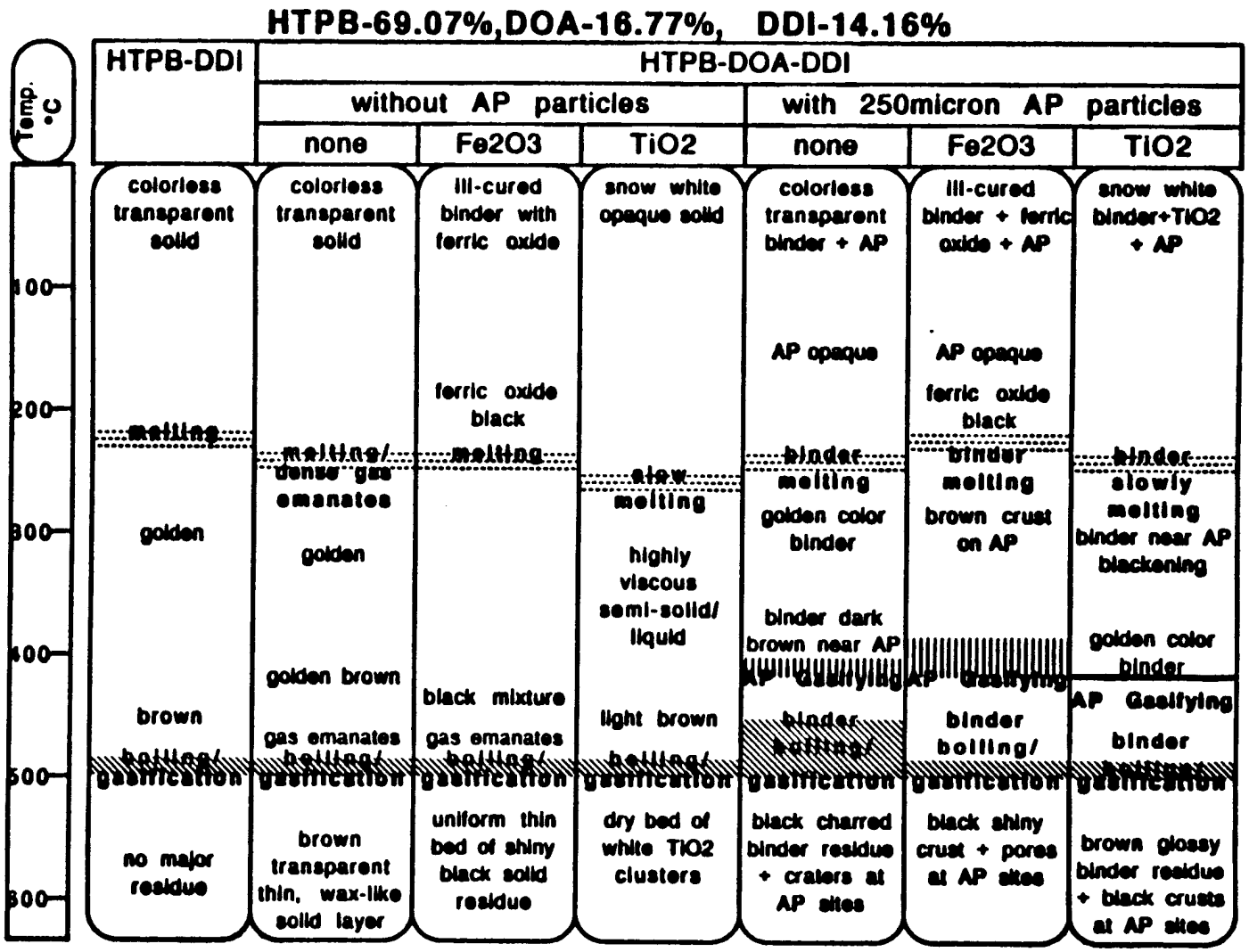
HTPB-69.07%,DOA-16.77%, DDI-14.16%
Temp. °C
HTPB-DDI
HTPB-DOA-DDI
without AP particles
with 250micron AP particles
none
Fe2O3
TiO2
none
Fe2O3
TiO2
colorless transparent solid
melting
golden
brown
boiling/ gasification
no major residue
colorless transparent solid
melting/ dense gas emanates
golden
golden brown
gas emanates boiling/ gasification
brown transparent thin, wax-like solid layer
ill-cured binder with ferric oxide
ferric oxide black
melting
black mixture
gas emanates boiling/ gasification
uniform thin bed of shiny black solid residue
snow white opaque solid
slow melting
highly viscous semi-solid/ liquid
light brown
boiling/ gasification
dry bed of white TiO2 clusters
colorless transparent binder + AP
AP opaque
binder melting
golden color binder
binder dark brown near AP
AP Gasifying
binder boiling/ gasification
black charred binder residue + craters at AP sites
ill-cured binder + ferric oxide + AP
AP opaque
ferric oxide black
binder melting
brown crust on AP
AP Gasifying
binder boiling/ gasification
black shiny crust + pores at AP sites
snow white binder+TiO2 + AP
binder
slowly melting
binder near AP blackening
golden color binder
AP Gasifying
binder boiling/ gasification
brown glossy binder residue + black crusts at AP sites
100
200
300
400
500
600

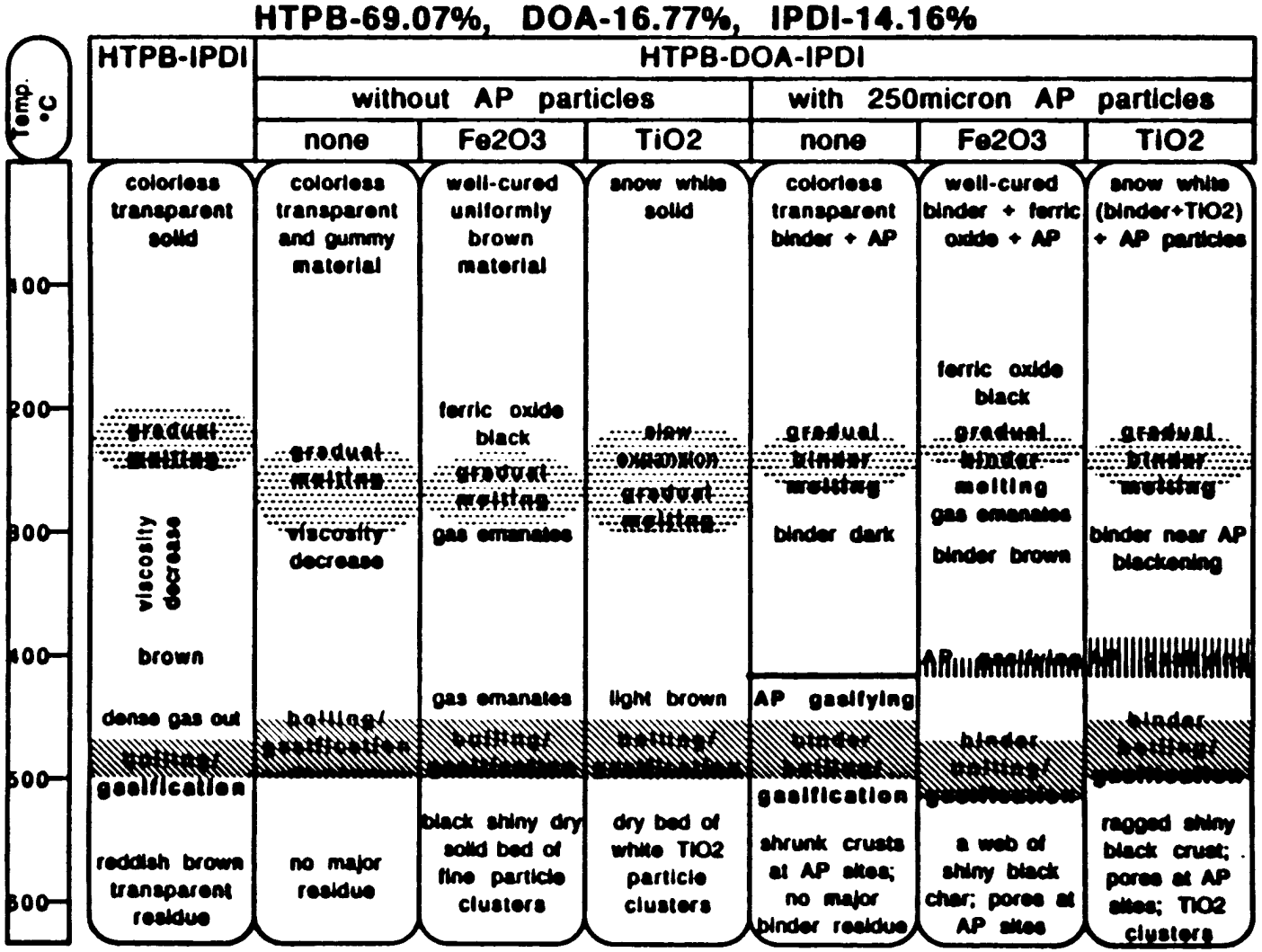
HTPB-69.07%, DOA-16.77%, IPDI-14.16%
Temp. °C
HTPB-IPDI
HTPB-DOA-IPDI
without AP particles
with 250micron AP particles
none
Fe2O3
TiO2
none
Fe2O3
TiO2
colorless transparent solid
colorless transparent and gummy material
well-cured uniformly brown material
snow white solid
colorless transparent binder + AP
well-cured binder + ferric oxide + AP
snow white (binder+TiO2) + AP particles
100
200
300
400
500
600
gradual melting
viscosity decrease
brown
dense gas out
melting/ gasification
reddish brown transparent residue
gradual melting
viscosity decrease
boiling/ gasification
no major residue
ferric oxide black
gradual melting
gas emanates
boiling/ gasification
black shiny dry solid bed of fine particle clusters
slow oxidation
gradual melting
gas emanates
light brown
melting/ gasification
dry bed of white TiO2 particle clusters
gradual binder melting
binder dark
AP gasifying
binder melting/ gasification
shrunk crusts at AP sites; no major binder residue
ferric oxide black
gradual binder melting
gas emanates
binder brown
AP gasifying
binder melting/ gasification
a web of shiny black char; pores at AP sites
gradual binder melting
binder near AP blackening
binder melting/ gasification
ragged shiny black crust; pores at AP sites; TiO2 clusters

PBAN-64.14%,DOA-15.00%,ECA-20.86%

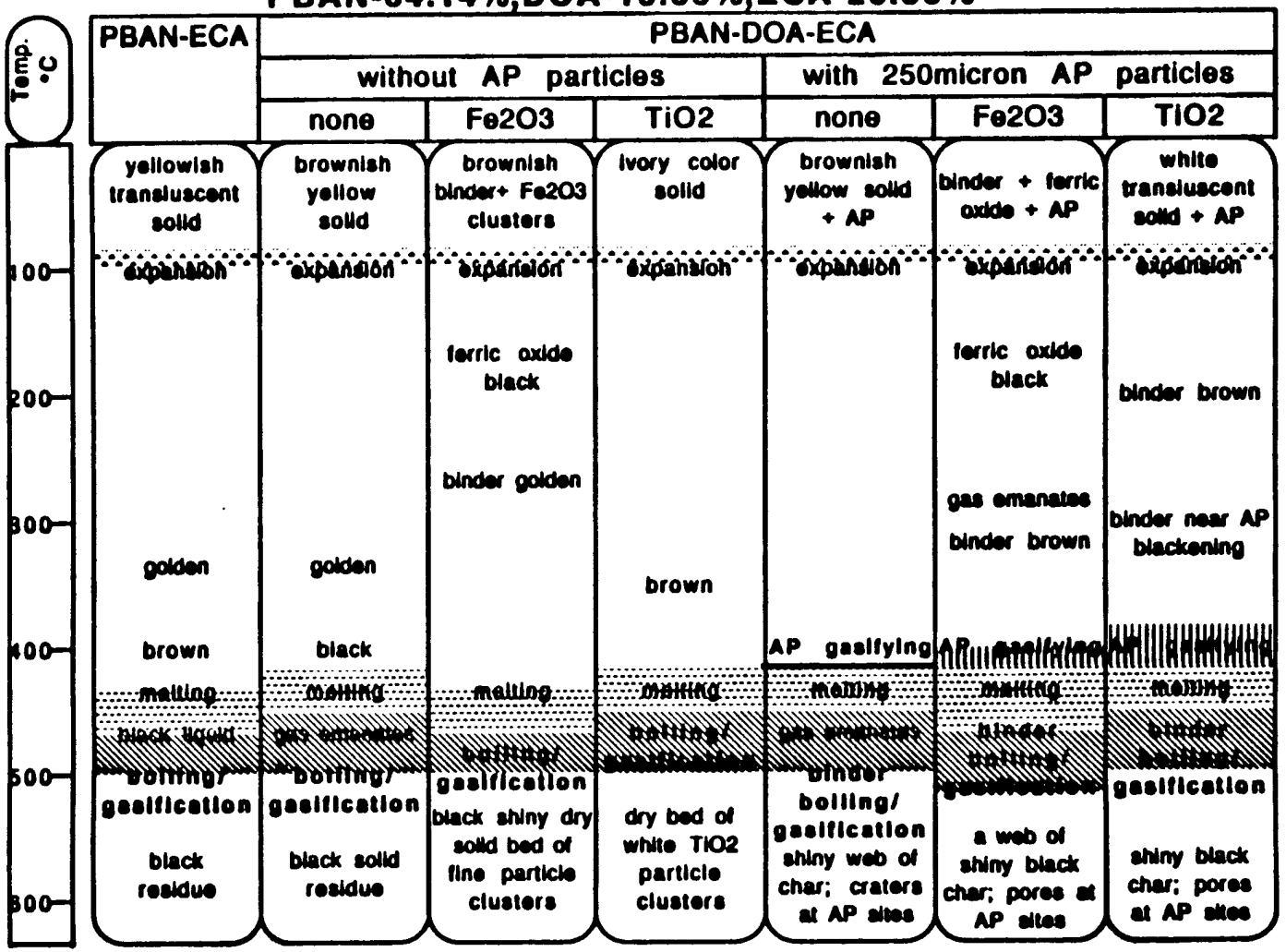

HTPB Binder with 2 micron AP

Temperature degrees Celsius

	Uncured		DDI Cured		IPDI Cured	
	Thin Mix	Thick Mix	Thin Mix	Thick Mix	Thin Mix	Thick Mix
100	Clear, but cloudy liquid	Light Pink,waxy solid	Cloudy, soft solid	Waxy, white, soft solid	Hard, rubbery solid	Waxy, white, soft solid
		Clear Liquid				Slow Melting
200	Sample darkens	<-browning-> Pinprick popping	<-browning-> Clears up	<-browning-> Pinprick popping	Slow Melting <-browning->	<-browning-> Pinprick popping
300	Black	Black	Black	Black	Liquid Black	Black
		Ignition	Tiny white pinholes	Ignition	Possible Ignition	Ignition
400	small bubbling	Residue is a silvery brown/black sand	small bubbling	Black, charred cratered ash	small bubbling	No residue except for a very small amount of brown/black sand with silver specks
500	Cracked, black, sandy, brittle residue		Cracked, black, sandy, brittle residue		Cracked, black, sandy, brittle residue	

Appendix B

Effect of Multidimensional Flamelets in Composite Propellant Combustion

Journal of Propulsion and Power

Volume 11, Number 4, July-August 1995, pp. 717-728

JOURNAL OF PROPULSION AND POWER
Vol. 11, No. 4, July-August 1995

Effect of Multidimensional Flamelets in Composite Propellant Combustion

Edward W. Price*
Georgia Institute of Technology, Atlanta, Georgia 30332-0150

This article reviews the results of a series of studies involving two-dimensional models of combustion of solid propellants. The results presented are selected to illustrate the role of the kinetically limited leading-edge portion of the oxidizer/fuel "diffusion" flamelets in controlling burning rate and aluminum agglomeration. Included are results from "sandwich burning," gas burner, numerical modeling of the two-dimensional flame, and tests on propellants to validate the applicability to propellants.

Introduction

THE mechanistic features of combustion of composite solid propellants differ conspicuously according to the kind of ingredients, scale of heterogeneity, and pressure. All propellants burn by decomposition, combustion, heat release, and heat return to the burning solid to sustain decomposition. Most analytical models are based on this "one-dimensional" view of burning. In this view of burning, the progress of chemical reactions is distributed in one dimension. It is recognized that heat release may occur at several locations, e.g., condensed-phase, surface, and gas-phase reactions. Problems arise in analytical modeling when the scale of heterogeneity of the propellant (e.g., particle size of oxidizer) is large enough for significant lateral temperature gradients in the microstructure, and for long enough mixing times of decomposition products (in surface liquid layers and gas phase) to limit reaction rates. The modeling problems are greatly aggravated when the melting and decomposition temperatures of the ingredients are markedly different. This is clarified by examples in Table 1. Another factor important to this article is the exothermicity of the oxidizer/fuel (O/F) flame (comparisons in Table 1). This article is concerned with propellant systems in which the oxidizer and binder decompose at comparable temperatures and in which the gas phase oxidizer/binder flame is strongly exothermic. These features are typical of combustion of most ammonium perchlorate/hydrocarbon (AP/HC) binder propellants. For such propellants a major part of the heat release can occur in an array of hot microflamelets standing in the mixing O/F flows ("mixing fans") formed above the oxidizer/binder contact lines on the burning surface. This is illustrated in idealized form in Fig. 1, using a two-dimensional microstructure for simplicity.

Modeling of AP/HC binder propellants[1,2] has sought to accommodate the deviations from one dimensionality in a variety of approximations involving the determination of some kind of average heat release and standoff distance of the AP flame and parts of the O/F flame. The averaging process is necessitated by the presence of a range of particle sizes, but usually ends up with some form of one dimensionalization that decouples the individual flamelets from the surface sites that feed the flamelet reactions. Considering the complexity of a rigorous model for a chaotic propellant structure, it is easy to understand why such approximations are used in models, and why the combustion details are often studied in simpler two-dimensional experiments as pictured in Fig. 1. The goal of this article is to look at the local details and nature of the O/F flamelets and see how they couple to the burning surface. The discussion will rely extensively on the experiments and analyses of two-dimensional models of propellants.

Before embarking on a discussion of O/F flamelets, it is appropriate for the sake of perspective to consider further the conditions under which such flamelets are present and are important. Under some conditions, such as those for which diffusion rates are high compared to O/F reaction rates, the O/F flame is premixed and approximately one dimensional (e.g., very fine AP or low pressure, or both). At very low pressure (i.e., low for rocket motor applications), all gas-phase reactions become so slow that little if any heat is returned to the burning surface and burning may be sustained by reactions in the condensed phase that are usually relatively unimportant at motor pressures (1000 psi). In heterogeneous propellants such low-pressure (subatmospheric) burning ordinarily occurs only if fine AP and/or catalysts are used in the propellant to enhance O/F reactions. The following observations are for typical AP/HC binder propellants in the pressure range 100–2000 psi:

1) The O/F reaction occurs in three-dimensional flamelets anchored in the mixing "fans" of oxidizer and fuel vapors that are in turn anchored at the contact lines of oxidizer and fuel on the surface.[3]

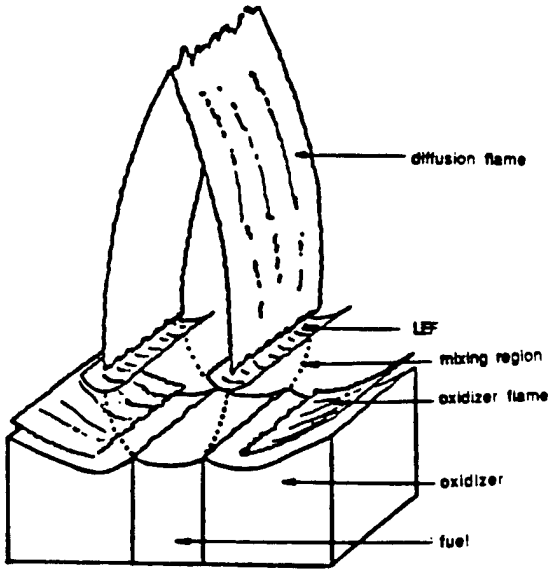

Fig. 1 Combustion zone structure for an AP/HC binders/AP sandwich.

Received Sept. 10, 1994; revision received Nov. 30, 1994; accepted for publication Dec. 2, 1994.

*Regents' Professor Emeritus, School of Aerospace Engineering. Fellow AIAA.

On theoretical grounds, one can argue that the stoichiometric surface in the mixing fan above each contact plane extends out over the AP surface because the oxidizer is relatively dilute compared to the binder. It can also be argued that the LEF will be centered on the stoichiometric surface, while the curvature of the AP surface profiles indicate that the LEF is close to the surface (e.g., 50 μm or so). As shown in Fig. 1, there is one LEF for each contact plane. Because the overall stoichiometry of the sandwiches discussed here are usually oxidizer-rich (i.e., thin binder laminae), the trailing diffusion flamelets "close" over the binder as in the sketch (Fig. 1). However, under propellant-like conditions, the sandwich binder lamina is usually very thin, the sandwich LEFs are close together, and the diffusion flame "tent" is very short. The LEFs are so close together that they may be coupled, consuming most of the fuel, leaving little for the diffusion limited parts of the flame tent (Fig. 3). The effect of this trend is evident in the dependence of sandwich burning rate on thickness of the binder lamina (Fig. 4). For binder thicknesses greater than 125 μm, the rate is relatively independent of thickness, indicating that burning is proceeding as two uncoupled burning fronts (with protruding binder in-between). A maximum burning rate occurs for thickness in the 50–75-μm range, a result that is explained[5] as optimum for LEF sharing of the fuel supply while minimizing heat "loss" through lateral heat flow to excess fuel that flows out between the LEFs without local exothermic reaction. For thinner fuel laminas the burning rate is lower because of insufficient fuel for the LEFs, so that the burning rate tends towards the AP self-deflagration rate as the thickness of the binder lamina approaches zero. These observations, described in more detail in Ref. 3, give an idea of the role of LEFs in sandwich burning, of the relevant dimensional scales, and of how they depend on pressure and lamina thickness. The relation to burning of a fuel-rich system with propellant-like microstructure is not too difficult to visualize (Fig. 5), except for the details of particle burnout, etc. The results are consistent with modern computational models in which it is found that LEFs are the primary source of heat to drive the combustion wave at intermediate pressures, with AP self-deflagration becoming more important above 1000 psi. There is direct evidence that condensed-phase or surface O/F interactions are not important in the >300-psi range in burning of AP/HC binder/AP sandwiches.[5]

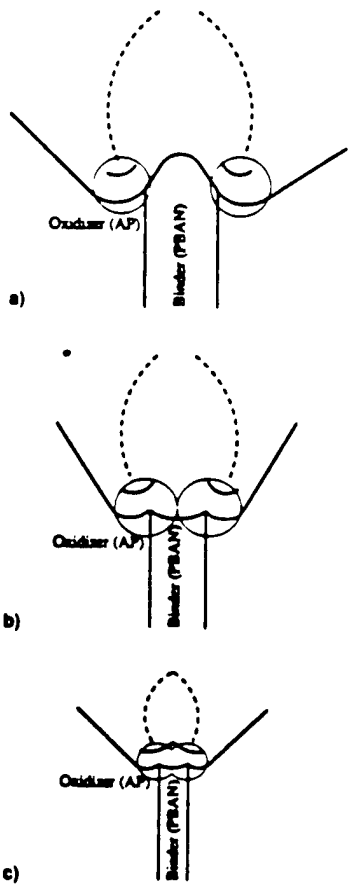

Fig. 3 Dependence of flame complex on thickness of binder lamina. Circles around LEFs indicate their domain of influence: a) thick binder lamina, b) 70–100 μm, and c) ~50 μm.

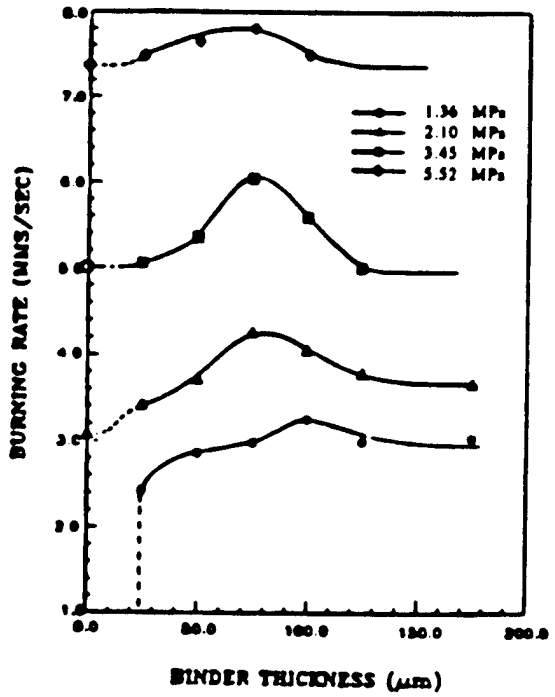

Fig. 4 Dependence of sandwich burning rate on thickness of the binder lamina.

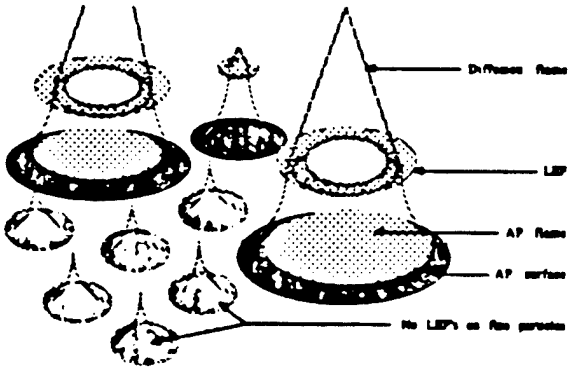

Fig. 5 Sketch of flame complex for a propellant with particulate AP.

As noted in Ref. 5, the results of sandwich burning studies by different investigators do not all agree. The disagreement appears to be due to the differences in binder and the failure to examine the effect of thickness of binder laminas (and widespread use of large thicknesses).

The results presented here are for polybutadiene acrylonitrile acrylic acid (PBAN) binder laminas of low thickness compared to most other sandwich-burning studies (for relevance to propellants). Tests with other binders showed some differences (example in Fig. 6) that appear to be related to tendency of some binders to form a melt layer that flows onto the AP surface. This is uneven and nonsteady along the edge of the laminas, causing a loss of two dimensionality of the combustion, including sometimes faster burning down one

Table 1 Approximate comparison of ingredient thermal response and energetics of oxidizer/fuel flames

Ingredient	Melting temperature, °C	Vaporization (decomposition) temperature, °C	Energetics of decomposition	Energetics of O/F flame
PBAN binder	480	500	Endothermic	—
HTPB binder (DDI-cured)	260	500	Endothermic	—
NMMO binder	85	200	Mildly endothermic	—
AP oxidizer	~580[a]	Rapidly above 400	Exothermic	—
AN oxidizer	145	245	Endothermic	—
KP oxidizer	—	400	Endothermic	—
HMX oxidizer	255	290	Exothermic	—
ADN oxidizer	90	165	Exothermic	—
CL-20 oxidizer	—	270	Exothermic	—
Aluminum	673	2493	Very endothermic	—
AP/PBAN	—	—	—	Very exothermic
AN/PBAN	—	—	—	Exothermic
HMX/PBAN	—	—	—	Nearly neutral
ADN/PBAN	—	—	—	Very exothermic

[a]Decomposes before melting except at heating rates $>10^5$ °C/s.

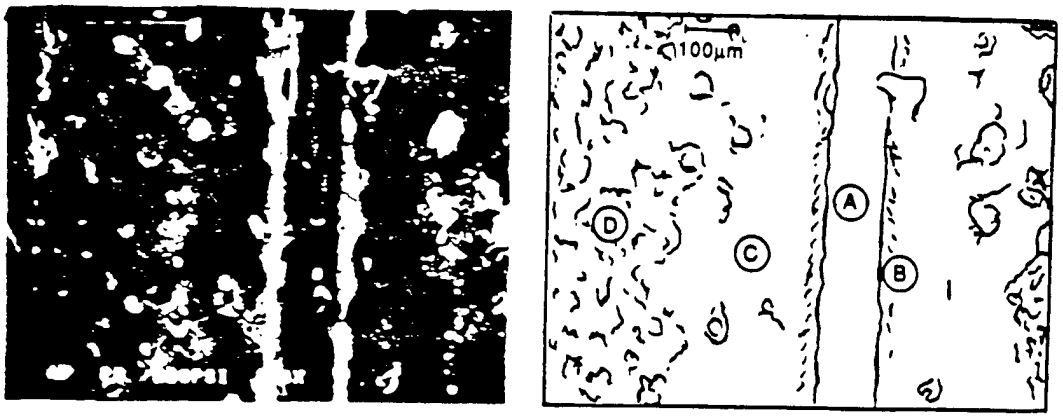

Fig 2 Details of an AP/PBAN/AP sandwich quenched by rapid depressurization from 500 psi (3.46 MPa): Ⓐ surface of the binder lamina, Ⓑ AP protruding along the laminas contact plane, Ⓒ location in a band of smooth surface (AP), concave upward. The leading edge of the burning front is located here, and Ⓓ frothy inclined surface typical of AP self-deflagration.

2) These flamelets are the principal site of heat release, coupled locally to the surface structure via the mixing fans.[3]

3) The part of each flamelet that is closest to the surface is most favorably located for returning heat to the surface, and is particularly intense because it consumes the accumulation of mixed O/F vapors prepared upstream of the "ignition point."

4) While the overall nature of the flamelet array is controlled by the rate of diffusion in the mixing fans, the location of the critical leading edge of each flamelet is also dependent on chemical kinetic rates in the mixing fans.

Modern combustion models for AP/HC binder propellants all incorporate these features (except the latter part of item 2) in one form or another.[4,5] The purpose of this article is to present and discuss studies aimed at determining the nature and role of the O/F flamelets more fully. These studies include edge burning of oxidizer-binder sandwiches, a gas burner study aimed at clarifying the nature of the leading-edge portion of the O/F flame, a numerical simulation of this leading-edge flame (LEF), and investigations aimed at determining the role of LEFs in ignition of aluminum. These studies used two-dimensional simulation of propellants to facilitate the observation, modeling, and interpretation of results. In this regard it should be understood that the critical features of the combustion zone occur on a dimensional scale of less than 100 μm (at motor pressures), below the spatial resolution of direct real-time experimental measurement. As a result, conclusions concerning experimental results are based on a variety of experimental data such as burning rate vs pressure and lamina thickness, observations of surfaces of quenched samples, and dependence of surface profiles on test variables. The gas burner studies were conducted at atmospheric pressure to facilitate detailed measurements.

Results from Combustion of AP/HC Binder Sandwiches

Studies of edge burning of laminates made up of alternate layers of oxidizer and fuel have been conducted by several investigators over the last 30 years; most of these studies are described in Ref. 5. For those studies that simulate propellant combustion, the features of the combustion zone are similar to those in the sketch in Fig. 1. The AP laminas are thick enough so that most of the edge surface of each self-deflagrates independently of the O/F flame, with an inclination that is determined by the relative burning rate of the sandwich and the AP (Fig. 1). The sketch shows the AP self-deflagration flame [which probably includes exothermic reactions in a surface froth (Fig. 2)]. The curvature of the AP surface profile closer to the lamina contact plane is an indication of heat flux from the O/F flame, with the point of maximum regression being the site of maximum net heat flux, and the rate-determining point (maximum heat in, minus heat loss by lateral heat flow). There is usually a region immediately adjacent to the binder lamina where the AP regression is retarded due to lateral heat loss to the (endothermic) binder lamina.[3] As can be seen in Fig. 2, the surface quality of the AP is different in the region that is heated by the O/F flame.

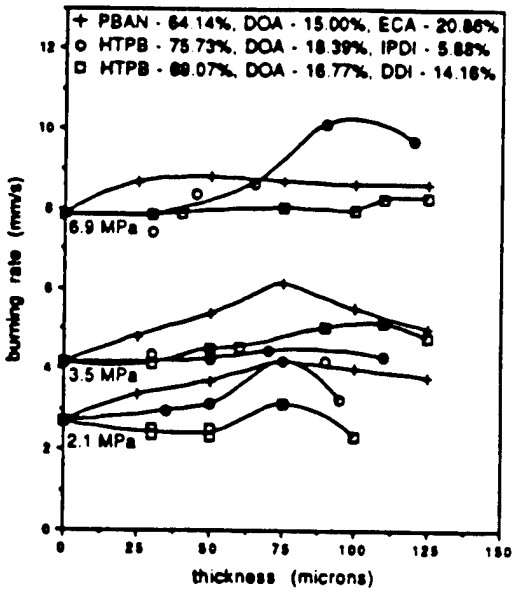

Fig. 6 Comparison of sandwich burning rates for different binders: burning rate vs binder lamina thickness.

interface than the other. The test results are simpler and easier to interpret when melt flow effects are minimized as with PBAN binder, but more attention to melt flow effects is needed because widely used binders such as dimeryl diisocyanate (DDI)-cured hydroxyl-terminated polybutadiene (HTPB) are prone to melt effects, evident even in sandwich burning rates (Fig. 6). It is not yet clear what O/F flamelet arrays result when binder melts encroach on the oxidizer surface, and it seems unlikely that all past sandwich burning studies (or propellant burning studies) can be reconciled without learning more about how the melt flow proceeds, and about the corresponding effects on surface pyrolysis and flamelet arrays. Melt flow is minimal with the PBAN binder used in most of the studies reported here.

Effect of Burning Rate Catalysts in AP/HC Binder/AP Sandwiches

A number of investigators have added catalysts to the AP laminas, binder lamina, or contact planes, with various proposed catalytic mechanisms.[5] In the present studies, catalysts were added to the binder lamina, in order to simulate propellants.[6,7] An example of test results is shown in Fig. 7. In interpreting the results the following was noted:

1) There is only limited exposure of the catalyst to the AP decomposition region or to the AP-binder interface (because the catalyst particles are in the binder), suggesting that rate enhancement involves the binder decomposition or the LEF, or both.[7]

2) Simple catalysis of decomposition of the binder would not in itself affect burning rate much because the effect would primarily be to cause the binder surface to be recessed a little more.[8]

3) The presence of particulate catalyst in the mixing fan and LEFs would not have much catalytic effect because of limited collision rate with catalyst.

4) The effective catalysts were observed to concentrate on the binder surface, where preliminary binder-decomposition fragments have high collision probabilities in passing through the "catalyst bed"; even the Catocene catalyst produced iron oxide concentration on the binder surface.

5) The catalysts are known to be effective in "cracking" heavy hydrocarbons.

6) Flames with heavy hydrocarbons are known to form only where the hydrocarbons have pyrolyzed to more reactive light species.

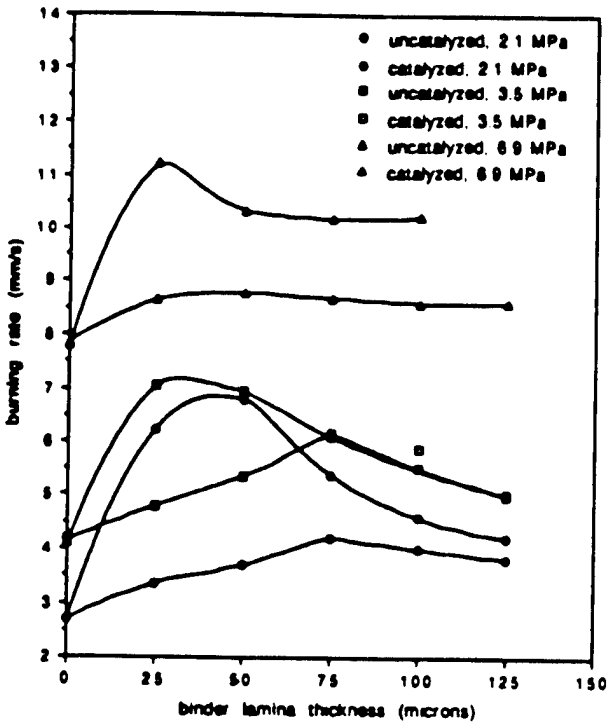

Fig. 7 Effect of Fe_2O_3 catalyst (10%, 2 μm, in the binder lamina) on the burning rate of AP/PBAN/AP sandwiches (from Ref. 6).

From these observations it was concluded[6,7] that in these tests the catalyst acted by supplying more reactive fuel fragments to the LEFs, allowing the LEFs to locate closer to the surface with correspondingly higher heat flux to the surface. This interpretation is supported by the fact that the burning rate and surface profiles showed dependence on thickness of the binder lamina and on pressure similar to that observed with uncatalyzed sandwiches. Thus, the catalysts effectively catalyze the LEF, but actually act at the binder surface by decomposing the heavy binder-vapor fragments. In this regard, it is emphasized that the response of the LEF is responsible for the burning rate increase. It will be seen in a later section that the catalyst may act in a different way when higher contact area of AP, binder, and catalyst exists.

Conditions for Presence of LEFs, and LEF Coupling

An investigation was made[9-12] of the burning of sandwiches in which the "binder" lamina was a matrix of PBAN binder and fine AP (10 or 33.5 μm) with AP contents of 50 and 70%. With such fine AP particles, the AP and fuel vapors can diffuse together before appreciable O/F reaction, giving a premixed flame if the mixture (e.g., 70% AP) is not too fuel rich to burn. At high pressure with 33.5-μm particles, there was evidence in quenched samples that LEFs and AP self-deflagration occurred on individual particles, (no such evidence for 10-μm particles, or for 33.5-μm particles at 300 psi). For 50/50 matrices this was evident only adjoining the lamina contact planes, indicating coupled behavior between lamina LEFs (LLEFs) and particle LEFs (PLEFs). The burning rates of the sandwiches with AP-filled binder laminae are shown in Fig. 8 (PBAN binder).

In interpreting the results in Fig. 8, it should be noted that the matrix mixtures are fuel-rich, even at a 70/30 ratio. The 50/50 mixture would not burn on its own, and quenched sandwiches showed matrix surfaces that were dominated by solidified binder melt (except as noted above). If one looks at the matrix as a "diluted fuel lamina" and repeats the argument about location of the interlamina mixing fan, stoichiometric surface and LLEF, one would expect them to be shifted closer to the "extended" plane of the lamina contact surface (Fig. 9), reflecting the effect of a less concentrated fuel. One effect

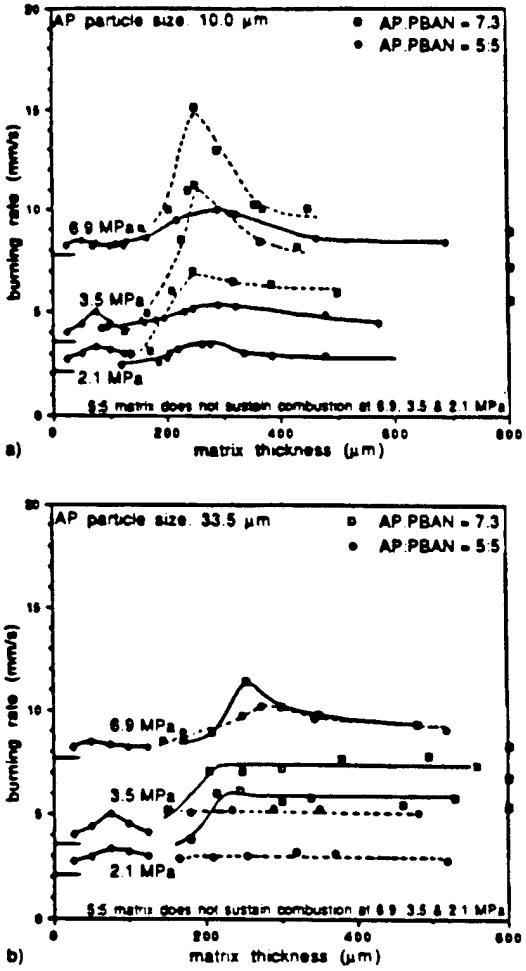

Fig. 8 Dependence of sandwich burning rate on thickness of the binder lamina from binder laminas consisting of a matrix of PBAN and particles (from Ref. 9): a) 10- and b) 33.5-μm AP. AP burning rates are indicated on the left, and matrix burning rates are indicated on the right ordinate lines. Pure binder sandwich burning rate curves are shown in the thickness range 25–125 μm.

of this, evident in the quenched surfaces and combustion photography, is a reduction (and sometimes elimination) of the protrusion of AP adjoining the contact plane. The LLEF is located more favorably to heat this region than in the pure binder case, and also more favorably to reduce lateral heat loss to the fuel lamina by supplying more LEF heat directly to the fuel lamina.

The premixed AP vapors in the "diluted" matrix outflow are, of course, more than a diluent. On the fuel-rich side of the LLEF they are a combustible mixture, that extends the fuel rich side of the LLEF out over the matrix. This increases the total heat release in the LLEF, enabling the flame to stand closer to the surface and give a higher burning rate than resulted with pure binder laminas (Fig. 3), and higher than the matrix burning alone (indicated at the right in Fig. 8). The thickness of matrix lamina for maximum burning rate is around 250 μm, as compared with 50–75 μm for pure binder lamina. This is consistent with the interpretation described for pure binder laminas if one allows for 1) the greater extent of the fuel-rich side of the LEFs that leads to attainment of LLEF coupling at greater thickness of the matrix laminas and 2) the fuel supply becomes deficient with decreasing lamina thickness at greater matrix thickness because the fuel is dilute.

The nature of the O/F flame complex for matrix sandwiches is sketched in Fig. 10, based on theoretical reasoning and experimental results. For a 70/30 mixture with 10-μm AP, the LLEFs act as flameholders for a premixed "canopy" flame over the matrix lamina (Figs. 10b and 10d). For a 50/50 matrix

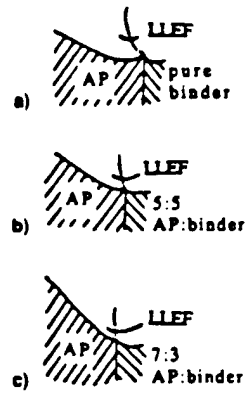

Fig. 9 Shift in LLEFs when the binder is "diluted" with AP a) narrow LLEF, over AP lamina. Heat flow from AP lamina to binder lamina, AP regression retarded at laminas contact plane; b) wider LLEF, stoichiometric point closer to surface and shifted toward laminas contact plane. Less lateral heat flow in solid, less retardation of AP at contact plane. More conservative LLEF, closer to surface, correspondingly higher rate; and c) wider LLEF, stoichiometric point over outer edge of AP lamina. LLEF extends well over matrix lamina, probably minimal lateral heat flow in solid.

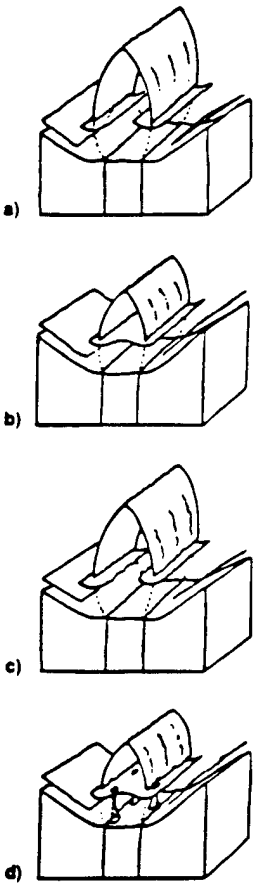

Fig. 10 Flame complex for sandwiches with AP-filled binder laminae (300-μm matrix lamina, 500 psi, 3.45 MPa): a) 50/50 AP/PBAN matrix, 10-μm AP; b) 70/30 AP/PBAN matrix, 10-μm AP; c) 50/50 AP/PBAN matrix, 33.5-μm AP; and d) 70/30 AP/PBAN matrix, 33.5-μm AP. Refer to Fig. 1 for an explanation of general features.

the canopy is open (thick laminas) because the matrix does not support a flame alone (Figs. 10a and 10c). However, the fuel-rich side of the LLEF extends further than with pure binder, as noted earlier, because a flammable mixture is present. The burning rate of the samples with 70/30 matrices is higher than with 50/50 matrices at all matrix thicknesses except the lowest, suggesting that the size and location of the LLEFs (Fig. 10) are 1) closer to the surface and 2) more favorably

located laterally to heat the matrix surface and minimize lateral heat loss in the condensed phase into the matrix lamina. The quenched samples indicate that the sandwich burning rate is determined by LLEF-assisted regression of the AP lamina, as noted earlier for pure binder laminae.

The effect of particle size of the AP in the matrix gives important clues to the details of the O/F flamelets, as follows:

1) Effect of particle size (i.e., 10 and 33.5 μm) is small for 50/50 matrix ratio, and for 70/30 ratio at 300 psi. This suggests that under these conditions the matrix outflow is essentially premixed at the LLEF standoff height and premixed canopy flames (Figs. 10a and 10c) result.

2) Burning rates are higher with 10-μm AP than with 33.5-μm AP in the 70/30 matrix at 500 and 1000 psi, suggesting that mixing is not complete for the 33.5-μm AP (thereby limiting the contribution of the fuel-rich side of the LLEF to the rate).

3) A relatively strong maximum occurs in the rate vs lamina thickness curves (70/30 matrix at 500 and 1000 psi), especially for 10-μm AP. This indicates that the matrix flame does not

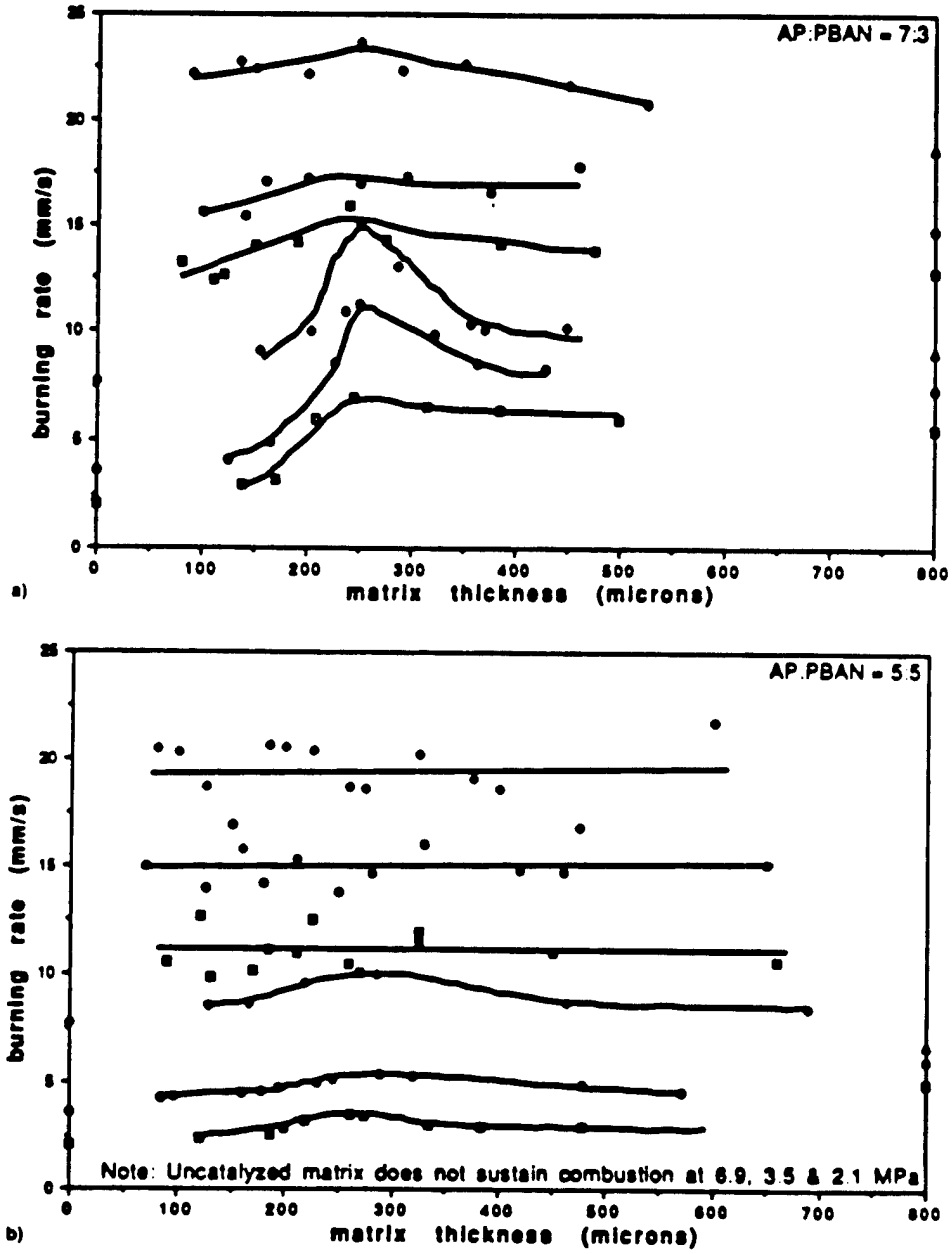

Fig. 11 Dependence of sandwich burning rate on thickness of the binder lamina for binder laminas consisting of a matrix of PBAN binder, fine AP (10 μm and 1% "Pyrocat" Fe_2O_3 catalyst: AP:PBAN = a) 7:3 and b) 5:5 (from Ref. 13).

control the rate, but rather enhances it via augmentation of the LLEFs. Extra matrix (i.e., thick lamina) apparently acts to drain heat (and possibly oxidizer species) from the rate controlling region of the sandwich.

4) The weaker maximum of the rate curves in 3 with 33.5-μm AP presumably reflects the weaker contribution of the fuel-rich side of the LLEFs due to incomplete mixing of the matrix outflow.

5) The quenched 70/30 samples that were burned at 500 and 1000 psi showed evidence that the 33.5-μm particles adjoining the AP laminae were burning individually (i.e., with PLEFs and AP self-deflagration). This may have been a factor in the burning rate, but it is notable that the same behavior was not evident with 10-μm AP, which gave higher burning rate.

Taken collectively, the results indicate that, for the conditions tested, the LLEFs dominate the burning rate, and that AP in the binder lamina enhances the LLEF effect by shifting the LEFF position and extending the fuel-rich side (and, hence, increasing LLEF heat release). Fine AP is more effective because more complete mixing has occurred at the LLEF height. The optimum lamina thickness for rate enhancement is around 250 μm for the conditions tested. Under the conditions tested the individual particles of AP either did not establish their own flamelets, or when they did (33.5 μm, 70/30, 500, and 1000 psi) no major effect on burning rate was evident. This suggests that in a typical bimodal propellant, the fine AP/binder matrix does not control the burning rate directly, but rather enhances the burning rate of the coarse AP particles. As the fine particle size and pressure increase, the fine particles burn more independently and enhance the coarse particle burning less (transition somewhere in the 500–1000-psi range for 33.5-μm AP in a 70/30 matrix, above 1000 psi in a 50/50 matrix).

Combination of Fine AP and Fine Fe_2O_3 in the Binder Lamina

An extension of the "filled" binder lamina studies was initiated by adding Fe_2O_3 to the matrix. Initially 10% of the 2-μm Fe_2O_3 used in the catalyzed binder lamina studies (described above and in Refs. 7 and 8) was attempted, using 10-μm AP and PBAN binder. Samples with 70/30 AP/PBAN ratio could not be processed, and samples with 50/50 ratio gave very erratic burning rates. A change was made to 1% of "Pyrocat" Fe_2O_3 (described by the manufacturer as 0.003-μm particles). Satisfactory results were obtained (Fig. 11, Ref. 13) with a major increase in the burning rate over similar samples without catalyst (Fig. 8). Addition of the catalyst increased the burning rate of the 70/30 matrix by about 100% at all three pressures, and caused the burning of the 50/50 matrix to be self-sustaining (matrix rates shown at the right in Fig. 11). The burning rates of the sandwiches with 50/50 matrix were about double the rate of the matrix alone and insensitive to lamina thickness. The rates of the sandwiches with 70/30 matrix were somewhat higher than the corresponding matrix, only mildly dependent on lamina thickness. The features of quenched samples are not yet completely available, but limited results show only a narrow portion of the AP laminas with the smooth surface quality, a narrow ledge that is no longer clearly "horizontal" (i.e., compared to the vertical laminas contact plane). As a preliminary conclusion, it appears that the LLEF plays a less important role in the burning rate in the catalyzed matrix sandwiches (some role is indicated by the fact that the sandwiches burn faster than the matrix alone). Many authors have argued that Fe_2O_3 acts by catalysis of reactions at the oxidizer/binder contact surfaces, an argument that is supported most strongly by burning tests of propellants at pressures near 1 atm. The evidence described in a preceding section for catalyzed binder laminas supported a contrary argument, but the situation is very different in the AP-filled binder laminas, because the amount of AP-binder contact area is enormously increased, and the very fine Fe_2O_3 has far greater surface area, more uniformly available in the solid. Thus, it seems plausible to assume that catalyzed contact-surface reactions contribute significantly or predominantly to the heat flow that determines burning rate in the catalyzed matrix sandwiches (the reactions may involve gas phase in microscopic interface crevises at contact surfaces). If LLEF heating were the primary factor in rate, one would expect a greater dependence of rate on lamina thickness than is evident in Fig. 11. It is possible that catalytic cracking of binder vapors also contributes to burning rate enhancement by bringing the LLEFs and the premixed matrix flame closer to the matrix surface in the manner argued earlier for the LLEFs in the case of sandwiches with catalyzed binder. Further study is needed.

Role of LLEFs in Behavior of Aluminum in the Combustion Zone

When powdered aluminum is used in AP propellants, the aluminum is observed to concentrate on the burning surface and depart as large agglomerates, a condition that can pose problems with combustion efficiency, slag formation, and prediction of combustor stability. A critical factor in agglomerate formation is the inflammation of the accumulating aluminum, which leads abruptly to the formation of a burning droplet that is too hot to remain on the burning surface. Several studies[14,15] suggested that inflammation of accumulating aluminum did not occur until exposed to the high temperatures of the O/F flamelets. This issue was examined by the introduction of aluminum powder in the binder laminae of AP/PBAN/AP sandwiches (binder laminae around 70 μm thick, pressure 500–1000 psi). Combustion photography and quenched samples showed sintered accumulations of aluminum, with inflammation always starting at locations nearest to the contact planes. Aluminum leaving the surface near the center of the binder lamina did not ignite near the surface (no oxidizer vapors). Sandwiches were then tested in which the aluminum was mixed with the AP before dry pressing (i.e., the AP laminae contained the aluminum). During burning, the AP surface became covered with a layer of sintered aluminum. This accumulation ignited only at the edge adjoining the contact plane where LLEF heating was present. Once ignited locally, the inflammation spread rapidly along the contact plane, and more slowly outward over the covered AP surface, forming one or more large burning agglomerates. Tests were

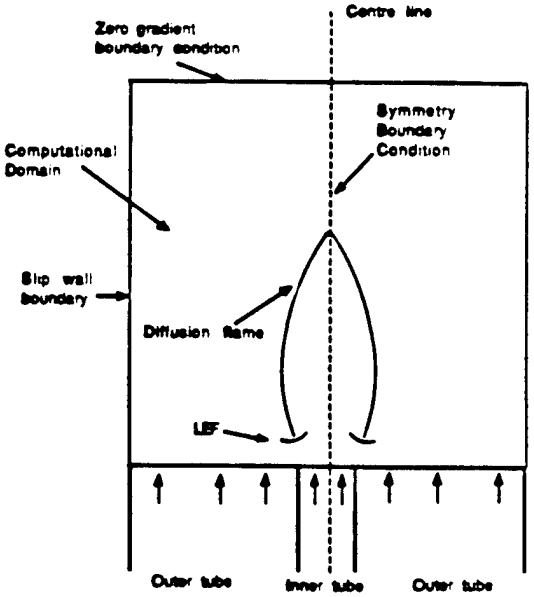

Fig. 12 Arrangement for a two-dimensional gas diffusion flame burner (numerical model and experiment).

also run on aluminized AP laminae alone (no binder lamina). The aluminum was observed to concentrate on the burning surface and leave the surface as large sintered accumulations with ignition and agglomeration being only occasional and apparently starting at sites where the sintered accumulations experienced break up. These results showed the critical role of the O/F flame in igniting surface aluminum accumulations, thereby limiting agglomerate size.

Theoretical-Numerical Analysis of Leading-Edge Flames

Because of the emergence of LEFs as a critical factor in edge-burning of AP sandwiches and propellants, it was decided to attack the problem of rigorous modeling of two-dimensional diffusion flames.[12,16,17] This effort was started because of the absence of direct observations of LEFs in propellant-sandwich combustion studies (because of inability to make such observations on microflamelets). In the modeling work the gases were assumed to emerge at the upstream boundary (Fig. 12) at specified velocity, density, and temperature (simulating a Wolfhard-type gas burner), and pressures near atmospheric were assumed (simulating a companion experimental study). Nonsteady laminar Navier–Stokes flow was assumed. Inlet gases were assumed to be $CH_4 + N_2$ in the center flow, and $O_2 + N_2$ in the outer flow. The chemistry was represented by a set of 48 elementary reactions involving 18 species. Temperature-dependent transport properties were used for each chemical specie. Details and computational methods are described in Ref. 16. Some notable results about LEFs are discussed here.

Figure 13 shows plots of distribution of species concentration, heat release rate (per unit volume), pressure, and flow direction (streamlines). Figure 13a shows the concentration of CHO, which is a short-lived intermediate product present only in the flame. There are locally high concentrations at the LEF sites. Figure 13b shows very high heat release rates at the same sites (high rates compared to the diffusion limited part of the flame further downstream), indicative of abrupt

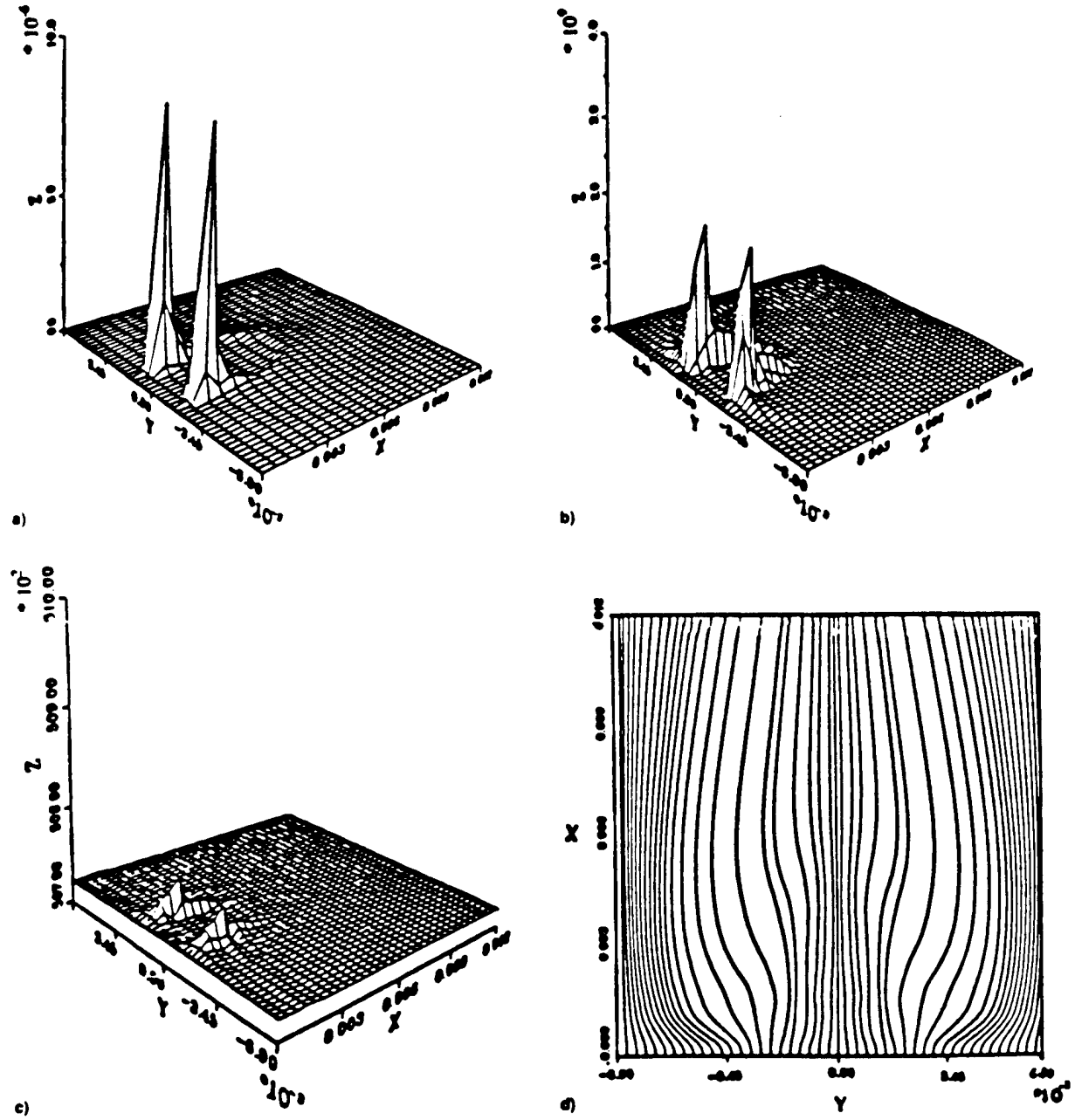

Fig. 13 Computed features of two-dimensional methane-air diffusion flame (N_2 diluted), burner configuration as in Fig. 12; X and Y dimensions are in meters; flow enters at lower left: a), b) and c), and at the bottom in d): a) CHO concentration (mass fraction); b) volumetric heat release rate ($J/m^3 s$); c) pressure [N/m^2]; and d) streamlines (Ref. 16).

consumption of the reactants that have mixed upstream of this site. Figure 13c shows that this concentrated reaction and the associated volume increase produce local pressure increases at the LEF sites, and Fig. 13d shows that this produces a divergence of the approach flow, as a result of which the vertical component of the velocity of the approach flow to the LEFs is reduced (i.e., does not increase as much as in a one-dimensional flame). These results support the idea of an intense leading-edge flame, an extended, less intense diffusion limited "tent" flame (Fig. 1). These computed LEFs show little lateral extent, contrary to those suggested in earlier sketches and discussion here. This "narrowness" is a feature of LEFs produced by combinations of pure fuel and oxidizer flows (i.e., diluted only by relatively inert gas). In a following section on LEFs in gas burner flames, crescent LEFs resulted when some fuel was included in the oxidizer inflow and some oxidizer in the fuel inflow. In the sandwich burning tests, the products of AP pyrolysis are a mixture of fuel and oxidizer species (e.g., NH_3 and $HClO_4$); and most of the binders, and especially the AP/binder matrix laminae, have oxidizer species in the laminae outflow. Thus, the propellant LEFs probably have appreciable lateral extent as suggested earlier in the discussion of the effect of addition of AP to the binder lamina.

Fig. 14 Double exposure images of one of the two diffusion flames in the gas burner, viewed edge-on. The bright central plume is the flame viewed by self-luminosity. The surrounding lines correspond to isotherms, produced by monochromatic light interference fringes (M-Z interferometry) (Ref. 18).

LEFs in Gas Burner Flames

To further verify the presence and nature of LEFs, a gas burner study was made[12,18] using a rectangular atmospheric pressure burner with a fuel flow in the middle and oxidizer flows on the outside (analogous to sandwiches and to the numerical study). A methane-air combination was used, with N_2 and CO_2 used as diluents. Outflow velocities were matched, but varied together from 15–50 cm/s. The flames were viewed edge-on photographically, including viewing with a Mach–Zehnder interferometer that permitted determination of the temperature field (example in Fig. 14). Temperatures were also measured with a traversing thermocouple. In addition, the flames were viewed side-on for intensity of CH radiation, a good indicator of heat release rate. The results of this study are detailed in Ref. 18. Some highlights are summarized here.

1) An intense leading-edge region of the flame was indicated in the CH intensity and temperature measurements, and the flame standoff distance from the burner surface was measured from photographs.

2) These LEFs were of limited lateral extent, consistent with results of the computational studies.

3) When fuel was added to the oxidizer flow and oxidizer added to the fuel flow, a crescent LEF resulted (Fig. 15).

4) The approach flow was deemed to be laminar, because turbulence would smear out interference fringes, an effect that was not observed (Fig. 14).

5) The "effective flame speed" of the LEF was taken to be the flow velocity from the burner, and was compared with the flame speed of one-dimensional premixed methane-air flames of the same temperature (Fig. 16). This effective flame speed was as much as 2.5 times the premixed flame speed.

In general, the experimental results were consistent with the numerical modeling results, indicating an intense, local LEF in the mixing fan, followed by a trailing diffusion limited flame with much lower heat release rate. The high effective

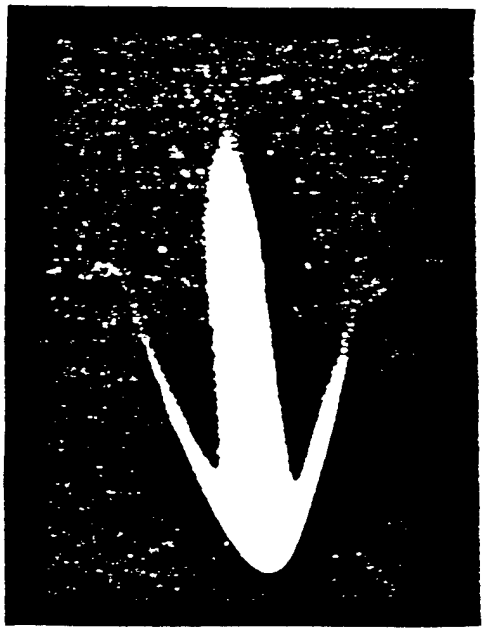

Fig. 15 Leading-edge flame in the gas burner when O and F inflows were enriched with F and O (mixtures well below flammability limits: methane-air with N_2 and CO_2 dilution, atmospheric pressure).

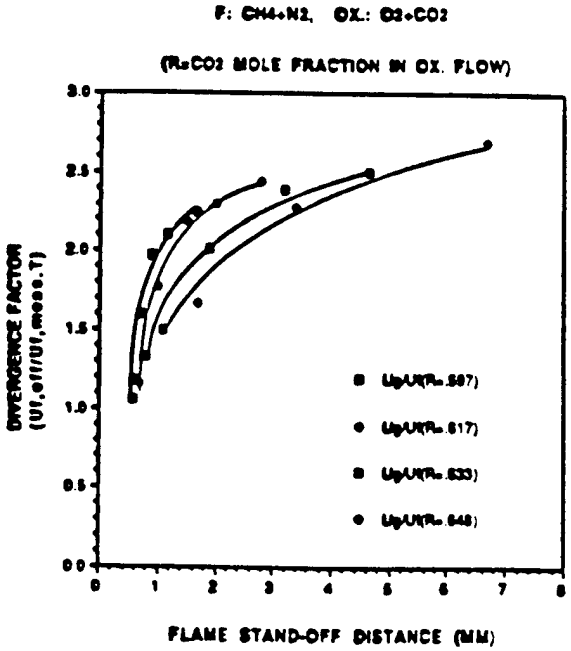

Fig. 16 Ratio of LEF speed to speed of methane-air flames of the same flame temperature (measured temperatures) (Ref. 18).

flame speed is presumably due to divergence and retardation of the approach flow to the LEF due to the pressure "island" (Fig. 13c) at the site of the LEF. The crescent flame (Fig 15) supports the interpretation of sandwich burning tests in which the fuel flow was enriched by inclusion of oxidizer in the binder lamina. Similar LEF behavior (crescent LEF and high flame speed) has been reported[19,20] in stratified fuel-air mixtures in horizontal ducts. It may be worth re-emphasizing that this high effective flame speed is due to the high local heat release rate in the LEF, the resulting local pressure rise, and the resulting multidimensional convective flow in the neighborhood of the LEF. Not only is the upstream heat flow to the surface localized by the local nature of the heat source, but the location of the heat source is dependent on multidimensional aspects of both heat flow and gas flow.

Results with Propellants

The understanding of combustion of AP/HC binder sandwiches was applied in the present program to the granular AP propellant situation by two studies by Sambamurthi[21,22] and Beiter.[23,24] These investigations are summarized briefly here to demonstrate the role of the leading-edge flame in propellant burning.

In view of the critical role of the LEF in precipitating the ignition and agglomeration of aluminum accumulations on the burning surface, it was proposed[21,22] that this mechanism could be demonstrated by making and testing an aluminized propellant with bimodal oxidizer-particle-size distribution. In such propellants the burning surface consists of irregular arrays of coarse AP particles (400-μm mass mean diameter was used), with intervening areas consisting of a fuel-rich mixture of binder, fine AP, and aluminum. At low pressures the fine AP particles will decompose without "attached" LEFs (analogous to the results of Lee noted earlier), and the accumulating aluminum on the surface will be ignited by the PLEFs on the coarse particles. The whole area of accumulation between coarse particles will then coalesce, to give large agglomerates. If test pressure is increased, a threshold will be reached where PLEFs will occur in the O/F mixing fans of the fine AP particles. This in turn will provide a large increase in number and proximity of sites for ignition of the accumulating aluminum, with a corresponding decrease in agglomerate size. This postulate was tested by Sambamurthi, who prepared bimodal propellants with four different fine AP particle sizes. According to the mechanistic argument, the threshold pressure for onset of PLEFs on the "fine" AP particles would be lower for fine particles of larger size, so the corresponding threshold for decreases in agglomerate size would be at lower pressures. Sambamurthi used combustion photography and agglomerate quench tests[22] to determine agglomerate size. Figure 17 shows the trend of agglomerate size (mass average mean diameter) with pressure for the four sizes of fine AP used (17.5, 49, 82.5, and 196 μm). The results show an abrupt decrease in agglomerate size at a threshold pressure, as predicted in the foregoing scenario. The threshold pressure decreases with increases in AP particle size, as predicted. Keeping in mind that this rather singular trend in agglomerate size was forecast in advance on the basis of sandwich burning-based results and mechanistic arguments about leading-edge flames and aluminum ignition, the results are a good validation of the mechanistic argument. The results provide a mechanistic basis for the empirical "pocket" model of agglomeration proposed originally by Crump[25] and Price et al.,[26] and provide a more complete basis for the heuristic bimodal pocket model proposed by Cohen.[27]

The propellant study by Beiter has to do with the dynamic response of the combustion zone to pressure oscillations. In particular, the study considered the possibility that a large part of the dynamic response might result from the LEF behavior when the conditions are close to the threshold noted in the last paragraph. When the small particle LEFs are on

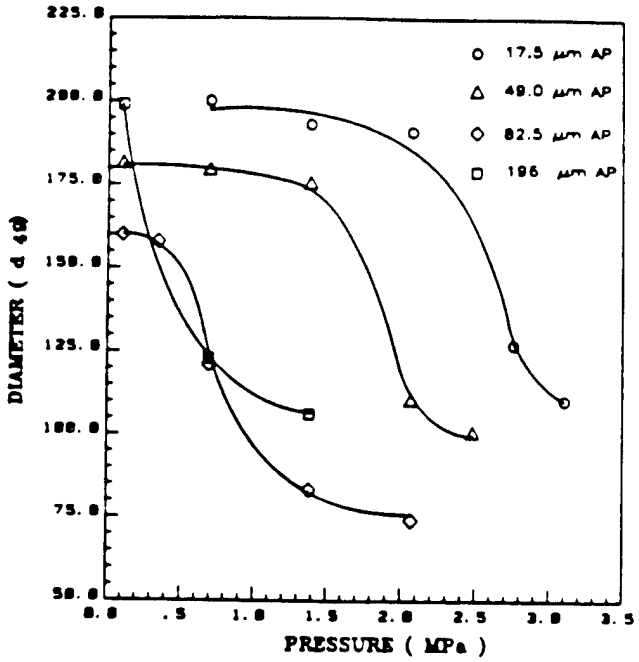

Fig. 17 Effect of pressure on mass average aluminum agglomerate size for propellants with coarse/fine AP in the ratio 8:2 (Ref. 22).

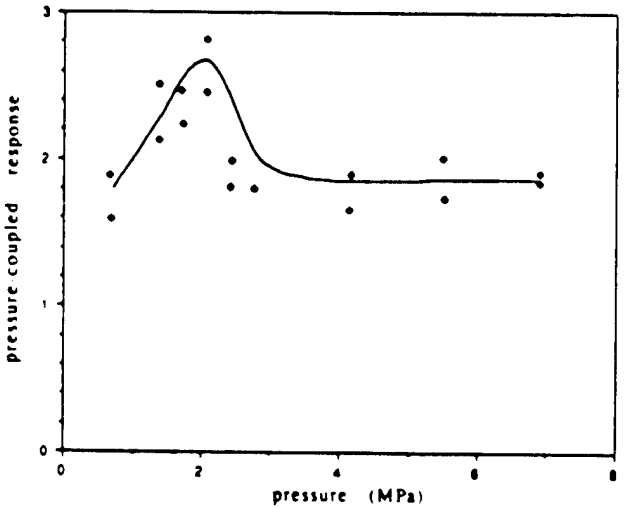

Fig. 18 Response function (vs pressure) for an AP/PBAN propellant with bimodal AP size distribution, obtained from pulsed T-burner tests at a frequency of 500 Hz (Ref. 24).

the brink of detachment, their stability is marginal, and they may oscillate between an attached PLEF condition and a more remote premixed canopy flame configuration. It was proposed that, if a bimodal propellant with very narrow size distribution of the fine AP were tested for pressure-coupled response function, a large portion of the fine AP particles would reach PLEF threshold conditions at the same pressure. Above that pressure, dynamic response would be typical of burning with the PLEF flame complex, and below it the response would be typical of coarse AP PLEFS with premixed canopy flames over the areas of fine AP-Al-binder matrix. In-between those two domains it seemed likely that a greatly increased response might occur due to the marginal stability of the fine particle LEFs. This postulate was tested by running a series of T-burner tests over the relevant pressure range.[23,24] Figure 18 shows the response function vs pressure for tests at 500 Hz with a propellant with 17.5-μm fine AP. While the data scatter in this type of test is rather appreciable, it seems clear that a peak in the response function curve occurred at 275 psi (1.91 MPa). Tests with the other sizes of fine AP were less decisive.

apparently due to scatter in T-burner data and difficulty in achieving uniform particle size of the fine AP. The design of the experiment requires that the fine AP particles all experience threshold conditions for PLEFs at the same pressure to produce a recognizable singularity in the collective dynamic response. In propellants with more conventional particle-size blends, the contribution of marginally stable LEFs is present to lesser degree over a wide pressure range, but is not distinguishable from other contributions to global dynamic response.

Summary

Studies of the edge-burning of laminates of oxidizer and binder layers ("sandwiches") have been conducted for some 30–35 years as a means to observe the combustion of heterogeneous solid propellants without the chaotic field of three-dimensional flamelets typical of AP propellants. The accumulating results of the sandwich burning tests led to increased attention to the leading-edge portion of the oxidizer/fuel diffusion flamelets. This portion of the flamelet (referred to variously as the "flame root," "phalanx flame," "primary flame," and "LEF") was not well-understood or modeled analytically, primarily because it is too small to observe experimentally, is not one dimensional, and cannot be modeled realistically without realistic description of species reaction and diffusion rates. However, it has been clear that this portion of the O/F flamelets is important to the propellant combustion because it is the part of the hot O/F diffusion flame that is closest to the propellant surface.

This article summarizes studies that clarify the nature of LEFs (gas burner and numerical modeling) and shows them to be local sites of high heat release rate, so high that they produce a local pressure peak and divergence in the approach flow, a result consistent with the interpretations of the sandwich-burning test results. This leads to close local coupling between the LEF and the surface regions close to the oxidizer contact lines (coupling via the O/F mixing fans). Tests on AP/PBAN/AP sandwiches with Fe_2O_3 burning rate catalyst in the binder lamina indicate that the catalyst acts by accelerating the breakdown of heavy binder product molecules to more reactive fragments, enabling the LEF to stand closer to the burning surface and thus increase burning rate.

Sandwich-burning tests on sandwich samples with AP-filled binder lamina matrix indicate that the AP in the matrix acted as a source of a reactive diluent in the fuel vapor, that caused a shift in position and size of the LLEF in a manner that enhanced burning rate. The results indicated that the sandwich burning rate was controlled by regression of the AP lamina under the influence of the LLEF. With the finer AP (10 μm), the mixing of the AP and binder vapors was apparently near complete before it reached the LLEF standoff distance (without appreciable exothermic reaction). With the coarser AP (33.5 μm), mixing was apparently less complete, resulting in less enhancement of the rate-controlling lamina LEF, and correspondingly less enhancement of burning rate. At higher pressure, PLEFs were apparently established on the individual particles (1000 psi, 70% 33.5-μm AP). However, the sandwich rate does not seem to have been enhanced by this condition, since the rate remained lower than for 10 μm AP, for which particle LEFs were not indicated. The collected results localize a boundary between two long recognized domains of burning of the matrix of fine oxidizer and binder. In one domain (fine AP, low AP content, low pressure) AP vapors mix and yield a premixed flame. In the other domain mixing is incomplete at lamina LEF height. At high enough pressure, PLEFs may be present in association with the larger exposed (fine) oxidizer particle surfaces. In all cases the sandwich burning rate is controlled by the lamina LEF-assisted regression of the AP laminas, indicating a complex coupling of the nature and pyrolysis of the matrix lamina with the lamina LEFs and the rate-controlling AP lamina regression.

Some preliminary results were presented of tests on sandwiches with both fine AP and fine Fe_2O_3 in the PBAN lamina. This combination resulted in very high burning rates. Details of the results indicate that the catalyst does more than break down heavy fuel molecules for easier reaction in the lamina LEF. There appears to be exothermic O/F reaction in the surface layer of the matrix. It seems likely that the high AP/binder surface contact area, in combination with very fine catalyst particle size, allows significant interfacial reactions at or very near the surface that are not manifested in results with simpler sandwiches.

Sandwich burning tests with aluminum powder in the PBAN lamina showed concentration of the aluminum on the binder surface, and showed that ignition-agglomeration of the aluminum initiated only in the region exposed to the hot LEF. Tests on single laminas of AP/aluminum mixture burned with aluminum concentration on the surface, but showed detachment from the surface with minimal ignition and agglomeration. These results indicate that LEFs provide the source of high temperature needed to break down the oxide coating on the sintered aluminum concentrations. In propellants this role of LEFs is the event that terminates accumulation and, hence, limits agglomerate size.

The tests on propellants were designed to test the importance of LEFs in two important aspects of propellant combustion: 1) aluminum agglomeration and 2) dynamic response to pressure oscillations. The propellants were designed to test the mechanistic arguments convincingly on the basis of qualitative trends in results, and results were consistent with the sandwich burning-derived mechanistic arguments.

At issue were possible effects of the transition (for propellants with bimodal AP) from a condition of attached PLEFs to a region where there are attached PLEFs on coarse particles only. The results indicated a strong transition in aluminum agglomerate size and a peak in response function associated with the flame transition. The 400/17.5-μm AP particle combination was used in both studies, with the indicated transition pressure being comparable (1.91 MPa for peak response function, 2.43 MPa for agglomerate size distribution). The moderate difference may be due to the large mass fraction of aluminum and to lower AP/binder ratio in the fine AP/binder matrix of the aluminized formulation.

It is important to note that the studies reported here were designed to study (and clarify) aspects of combustion that are not well-encompassed in current models of propellant combustion, aspects such as the following:

1) The nature and role of LEFs.

2) The localized coupling of each LEF with the specific site of the solid surface that is the source of the mixing O/F flow that feeds the LEF.

3) The nature of and conditions for interaction of adjoining LEFs, associated lateral heat flow (and species flow in the gas phase), and dependence of effect on LEF spacing (scale of heterogeneity).

4) The nature of the transition from LEF-controlled burning to premixed O/F flame-controlled burning.

5) The special contribution to pressure-coupled combustion response that is made by particle burning in the transition region noted in 4.

6) The critical role of PLEFs in limiting aluminum concentration (by initiating its burning) and the corresponding effect of AP particle size and pressure on agglomerate droplet size.

7) The consequences of combination of large and small particle sizes (AP laminas and matrix laminas), and the relation to difficulties in model correlation of burning rates of bimodal AP propellants with wide mode separation.

Acknowledgments

The author would like to thank several sponsors: principal sponsor, U.S. Office of Naval Research (R. S. Miller); U.S. Air Force Office of Scientific Research (L. Caveny), for sup-

port of aluminum combustion research; and for support of computational modeling of diffusion flames by the Thiokol Corporation (D. Flanigan). The contents of this report are drawn from research with several graduate students and the Ph.D. Dissertation of J. K. Sambamurthi, Christos Markou, S.-T. Lee, C. A. Beiter, H.-J. Chiang, and K. Prasad, and the current research of S. R. Chakravarthy. The author would like to thank R. K. Sigman for able support of all these studies as Combustion Lab Director.

References

[1]Beckstead, M. W., Derr, R. L., and Price, C. F., "A Model of Composite Solid Propellant Combustion Based on Multiple Flames," *AIAA Journal*, Vol. 8, No. 12, 1970, pp. 2200–2207.

[2]Glick, R. L., and Condon, J. A., "Statistical Analysis of Polydisperse Heterogeneous Propellant Combustion: Steady State," *Proceedings of the 13th JANNAF Combustion Meeting*, Vol. II, CPIA Publ. 281, 1976, pp. 313–345.

[3]Price, E. W., Sambamurthi, J. K., Sigman, R. K., and Panyam, R. R., "Combustion of Ammonium Perchlorate-Polymer Sandwiches," *Combustion and Flame*, Vol. 63, No. 1986, 1986, pp. 381–413.

[4]Cohen, N. S., "Review of Composite Propellant Burning Rate Models," *AIAA Journal*, Vol. 18, No. 3, 1980, pp. 277–293.

[5]Price, E. W., "Review of Sandwich Burning," *Proceedings of the 30th JANNAF Combustion Meeting*, Vol. 2, CPIA Publ. 606, 1993, pp. 259–279.

[6]Markou, C., "Effect of Different Binders and Additives on Sandwich Burning," Ph.D. Dissertation, Georgia Inst. of Technology, Atlanta, GA, 1988.

[7]Price, E. W., Sambamurthi, J. K., and Sigman, R. K., "Further Results on the Combustion Behavior of AP Polymer Sandwiches with Additives," *Proceedings of the 22nd JANNAF Combustion Meeting*, Vol. I, CPIA, Publ. 432, Oct. 1985, pp. 41–54.

[8]Deur, J. M., and Price, E. W., "Steady State One-Dimensional Pyrolysis of Oxidizer-Binder Laminates," AIAA Paper 88-2938, June 1988.

[9]Lee, S.-T., "Multidimensional Effects in Composite Propellant Combustion," Ph.D. Dissertation, Georgia Inst. of Technology, Atlanta, GA, 1991.

[10]Lee, S.-T., Price, E. W., and Sigman, R. K., "Effect of Multidimensional Flamelets in Composite Propellant Combustion," *Journal of Propulsion and Power*, Vol. 10, No. 6, 1994, pp. 761–768.

[11]Price, E. W., et al., "Role of the Leading Edge of Diffusion Flames in Combustion of Solid Propellants," *Proceedings of the 27th JANNAF Combustion Meeting*, Vol. III, CPIA, Publ. 557, 1990, pp. 257–263.

[12]Price, E. W., Lee, S.-T., and Sigman, R. T., "Role of the Leading Edge of Diffusion Flames in Combustion of Solid-Propellants," *Proceedings of the 28th JANNAF Combustion Meeting*, Vol. 2, CPIA, Publ. 573, 1991, pp. 257–263.

[13]Chakravarthy, S. R., private communication, School of AE, Georgia Inst. of Technology, Atlanta, GA, Feb. 1994.

[14]Price, E. W., Sambamurthi, J. K., Sigman, R. K., and Sheshadri, T. S., "Conditions for Inflammation of Accumulated Aluminum in the Propellant Combustion Zone," *Proceedings of the 20th JANNAF Combustion Meeting*, Vol. 1, CPIA, Publ. 383, Oct. 1983, pp. 333–341.

[15]Price, E. W., "Combustion of Metalized Propellants," *Fundamentals of Solid-Propellant Combustion*, Vol. 90, Progress in Astronautics and Aeronautics, AIAA, New York, 1984, pp. 479–513.

[16]Prasad, K., "Numerical Simulation of Reactive Flows Through Two-Dimensional Burners," Ph.D. Dissertation, Georgia Inst. of Technology, Atlanta, GA, 1990.

[17]Prasad, K., and Price, E. W., "A Numerical Study of the Leading Edge of Laminar Diffusion Flames," *Combustion and Flame*, Vol. 90, No. 1992, 1992, pp. 155–173.

[18]Chiang, H.-J., "An Experimental Investigation of the Leading Edge of Diffusion Flames," Ph.D. Dissertation, Georgia Inst. of Technology, Atlanta, GA, 1990.

[19]Phillips, H., "Flame in a Buoyant Methane Layer," *Proceedings of the Tenth Symposium (International) on Combustion*, The Combustion Inst., Pittsburgh, PA, 1965, p. 1277.

[20]Feng, C. C., Lam, S. H., and Glassman, I., "Flame Propagation Through Layered Fuel-Air Mixtures," *Combustion Science and Technology*, Vol. 1, No. 1970, 1975, p. 59.

[21]Sambamurthi, J. K., and Price, E. W., "Aluminum Agglomeration in Solid Propellant Combustion," *AIAA Journal*, Vol. 22, No. 8, 1984, pp. 1132–1138.

[22]Sambamurthi, J. K., "Behavior of Aluminum on the Burning Surface of a Solid Propellant," Ph.D. Dissertation, Georgia Inst. of Technology, Atlanta, GA, 1983.

[23]Beiter, C. A., and Price, E. W., "The Role of Detachment of the Leading Edge of the Diffusion Flame in the Pressure-Coupled Response of Composite Propellants," *Journal of Propulsion and Power* (to be published).

[24]Beiter, C. A., "The Role of Combustion Zone Microstructure in the Pressure-Coupled Response of Composite Propellants," Ph.D. Dissertation, Georgia Inst. of Technology, Atlanta, GA, 1991.

[25]Crump, J. E., "Photographic Survey of Aluminum Combustion in Solid Propellants," *Proceedings of the Inter Agency Chemical Rocket Propulsion Group*, Vol. 1, CPIA Publ. 68, Jan. 1965, pp. 367–370.

[26]Price, E. W., Kraeutle, K. J., Prentice, J. L., Boggs, T. L., Crump, J. E., and Zurn, D. E., "Behavior of Aluminum in Solid Propellant Combustion," Naval Weapons Center TP 6120, China Lake, CA, March 1982.

[27]Cohen, N. S., "A Pocket Model of Aluminum Agglomeration in Composite Propellants," *AIAA Journal*, Vol. 21, No. 5, 1983, pp. 720–725.

Appendix C

Effect of Multidimensional Flamelets in Composite Propellant Combustion

Journal of Propulsion and Power

Volume 10, Number 4, November-December 1994, pp 761-768

JOURNAL OF PROPULSION AND POWER
Vol. 10, No. 6, Nov.-Dec. 1994

Effect of Multidimensional Flamelets in Composite Propellant Combustion

Sung-Taick Lee,* Edward W. Price,† and Robert K. Sigman‡
Georgia Institute of Technology, Atlanta, Georgia 30332

Studies of edge burning of oxidizer-fuel laminae were extended by inclusion of different sizes of fine ammonium perchlorate (AP) into the binder lamina to study the combustion zone microstructure in composite-propellant combustion. Different modes of burning in heterogeneous systems resulting from pressure effects, AP particle-size effects, lamina thickness, and AP/binder mix ratios were determined. Results are interpreted in terms of the effects on flame structure and multidimensional processes in the combustion zone.

Introduction

THE detailed processes of composite-propellant combustion are complicated by the microscopic scale of the combustion zone, the hostility of the high-temperature and high-pressure environment, and the microscopically complex and chaotic structure of the propellants. The complexities imposed by combustion microstructure can be reduced or alleviated by the use of laminate propellants, in which the microgeometry and combustion zone are two dimensional. Edge burning of sandwiches, consisting of two laminae of ammonium perchlorate (AP) oxidizer with a layer of polymeric binder in between, has been studied extensively to understand combustion processes of composite propellants.[1-6] Studies have been made of the effect of inclusion of ballistic modifiers in the binder lamina,[3,4] and the effect of different binders.[4] The present study consists of a detailed examination of the effect of the inclusion of granular AP in the binder lamina to make what is referred to as AP-filled sandwiches.

Figure 1 is a sketch showing the principal features of the combustion zone, in which the oxidizer-fuel flames consist of a leading-edge flame (LEF) that stands in the mixing region of the oxidizer and fuel vapors, and a diffusion flame that trails from the LEF up to a point where the fuel vapor is all consumed. The LEF is a region of very high heat release as compared to the rest of the diffusion flame, and contributes most of the heat transfer back to the propellant surface.[7] Considerable insight has been acquired regarding the nature and role of LEFs from the earlier sandwich burning experiments.[1-7] This flame complex of AP-binder-AP sandwiches is also applicable to propellant burning, and the most conspicuous differences between the composite propellants and the sandwiches are the following features: in the propellants—typically fuel-rich—the stoichiometric tip closes over the oxidizer particles, and the stoichiometric tip height is related primarily to oxidizer particle size. The role of the LEF is similar to that with sandwiches except that the flame closure is linked to the oxidizer dimensions (i.e., AP particle sizes) instead of binder lamina thickness, and the nature of the flame complex on each AP particle would differ depending on the size of AP exposed surface and the width of the adjoining binder.

Referring to the flame complex in Fig. 1, the questions addressed here are, how is the flame complex changed by the presence of oxidizer particles in the binder, what is the resulting effect on sample burning rate, and what do the results suggest about the burning of a propellant with multimodal oxidizer size distribution? In a qualitative way, the vapors from very fine AP particles in the binder might diffuse into the binder vapors so quickly that normal self-deflagration would not occur on the particle. If there are many fine AP particles, the lamina may then burn on its own with premixed flame, with a burning rate that may, or may not exceed that of AP laminae. If the particles are large enough, they may burn as individual particles, with normal AP self-deflagration and a surrounding diffusion flame analogous to the one in Fig. 1. If there are enough of these AP particles in the binder, the lamina may burn on its own, with a myriad of flames like the ones in Fig. 2. When particles are near enough to each

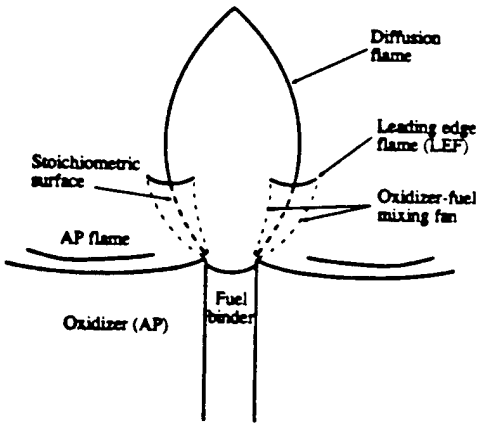

Fig. 1 Flame complex for an AP-binder-AP sandwich.

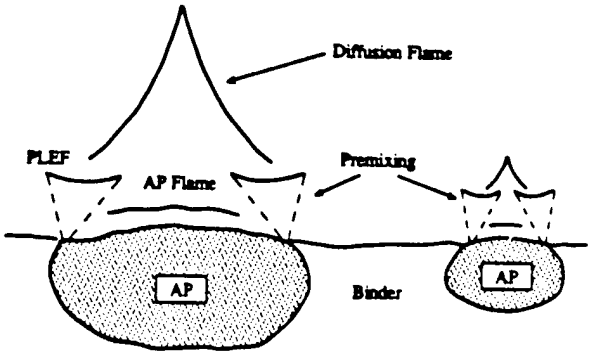

Fig. 2 Flames over AP particles in the matrix.

Received Jan. 25, 1993; revision received Nov. 17, 1993; accepted for publication Feb. 11, 1994.

*Currently Senior Research Engineer, Han Wha Co., Republic of Korea. Senior Member AIAA.
†Regents' Professor, School of Aerospace Engineering. Fellow AIAA.
‡Senior Research Engineer, School of Aerospace Engineering.

other or to the AP lamina, interactive behavior will occur, both through multidimensional heat flow in the condensed phase, and heat and species diffusion in the gas phase.

The AP-filled sandwich samples—laminates of AP-filled binder between two AP laminae—were prepared to investigate these features, using combustion photography, burning rate measurement, and microscopic study of quenched samples. The effects of binder thickness, pressure, percentage of the AP in the binder lamina, and particle size of the AP in the binder lamina were measured and interpreted in terms of qualitative theory of LEF behavior and thermal coupling with the heterogeneous surface.

Experimental Methods

Experimental methods in the present work are mostly routine and detailed elsewhere.[1-5] The principal difference is the inclusion of particulate AP in the binder, by simply hand mixing the mixture before making the sandwich. Sandwiches were made by bonding two AP laminae together with the AP-filled binder. Thickness of the AP-filled binder lamina (matrix lamina) was controlled with spacer shims. The AP laminae was prepared by compacting polycrystalline AP into disks and cutting to shape. The AP was propellant-grade 99.7% purity, low-alkali Kerr-McGee AP size graded at 200 μm. The polycrystalline AP disks were prepared by weighing approximately 1.73 g of ground AP, and pressing at 220 MPa for 2 hr. For the matrix lamina, a nominal size of 10 μm (the 10-μm AP was supplied by K. Kraeutle of the U.S. Naval Weapon Center, China Lake, California) was chosen as the fine matrix-oxidizer, and 33.5 μm was chosen as the coarse matrix-oxidizer. The 33.5 μm was a nominal designation for a screening fraction of ground 200-μm material that passed a 37-μm sieve and was retained in a 30-μm sieve. The polybutadiene acrylonitrile acrylic acid (PBAN) binder was prepared by mixing PBAN prepolymer with epoxy curing agent (Epon 828) and its plasticizer (DOA) in proportions 64.14, 20.86, and 15%.

The amounts and particle size of AP used in the matrix laminae have a significant effect on the rheological properties of the sandwiches. Fractions higher than 70% of AP in the mixture make mixing and handling during sandwich fabrication too difficult. In the present study, the ratios of ingredients were chosen to ensure that the matrix surface area would be fuel-rich (thus ensuring the flamelet closure over the AP particles and fuel-rich conditions above the stoichiometric tips of AP particles in the matrix). The mass-mixture ratios of AP and PBAN binder were chosen as 5:5 and 7:3 (a few samples were made with 8:2 mixtures). Matrix thicknesses were chosen between 125–600 μm, the lower limit being determined by difficulty in sandwich fabrication, and the upper limit by the expectation of no useful results for greater thickness.

Several test samples were cast from the excess matrix mixture for measurement of the matrix burning rate. These propellant-type of samples (matrix samples) were prepared using the same matrix mixtures used in the sandwiches. After the mixture was vacuumed, it was then transferred to rectangular molds of dimensions 20.7 × 11.2 × 2.3 mm, and hand pressed by tapping the mixture with a 1-cm-diam cylindrical Teflon® rod.

All samples (sandwich and matrix) were cured in an oven at 72°C for 7 days. After curing, the matrix samples were cut into rectangular shapes (11.2 × 5.5 × 2.3 mm) and the sandwich samples were sanded down on the edge to form a parallelepiped of the desired dimensions (10 × 7 × 3.0 mm) for burning-rate tests. Equivalent sandwiches without AP in the binder were also made to compare with previously obtained results,[3] and to address the resulting effects of AP particles in the binder.

The principal experimental facilities used here are comprised of a nitrogen-flushed high-pressure combustion chamber with quartz windows for combustion photography, a nitrogen-flushed high-pressure chamber with a burst disk for quenched burning, a video camera-monitor-recorder system, an optical microscope, and a scanning electron microscope. The video camera recorded 32 frames/s, each with an imaging time of 1/2000 s. Combustion photography was employed for measuring the burning rate. Burning rates of both sandwiches and propellant-type samples were taken after a steady-state profile had been developed. The tests were run at pressures of 2.07, 3.45, and 6.89 MPa. The test plan was to have at least two experiments yielding two independent measurements for each test condition. The burning rate was determined by the data collected in the form of position vs time from the video pictures (minimum 5 points), and a least-square linear fit was used to decide the burning rate. The average burning rate of these two (or more) experiments was calculated to obtain a data point corresponding to a particular matrix thickness at a specific pressure. In cases of poor reproducibility, three (or more) tests were sometimes run.

Table 1 Summary of experimental conditions

Combustion photography for burning rate
- Pure binder sandwiches
- AP-filled sandwiches with 10-μm AP in the binder
- AP-filled sandwiches with 33.5-μm AP in the binder

1) Range of matrix thickness 125–600 μm
2) AP-binder matrix material
   - Mass ratios of AP:PBAN binder = 5:5 and 7:3
   - AP particle size: 10 and 33.5 μm
3) Test pressure: 2.07, 3.45, 6.89 MPa

Quench burning, SEM of the samples
1) All pressure-matrix conditions notes above
2) Matrix lamina thickness chosen to correspond to thin, thick, and one or two intermediate thickness near maxima of burning rate vs matrix thickness curve

Interruption of burning by rapid depressurization permits better resolution of the burning surface details than is possible in the combustion photography. Results from the combustion photography tests were used to choose appropriate delay times after ignition to assure quench after a steady-state surface profile was reached. The quench was accomplished by venting the test chamber with a burst diaphragm. The quenched surface was examined to collect information on surface profile, the oxidizer-fuel laminae interface region, and AP particles in matrix laminae, using an optical microscope and a scanning electron microscope. The matrix thicknesses that were used in quench tests were chosen to correspond to points on the burning-rate curves that seemed most important (see Table 1).

Experimental Results

The results of burning-rate tests are shown in Figs. 3 and 4. Figure 3 is for 5:5 matrix materials. This very fuel-rich material would not sustain burning when tested as propellant-type samples. Figure 4 is for 7:3 matrix material. The burning rate of the material when burned on its own is marked by lines on the right-y axis. In each of these figures the burning rates are shown as functions of matrix lamina thickness, for each particle size and three pressures. Marks on the left-y axis show the AP self-deflagration rate.

Figure 5 shows the surface profiles of the sandwiches under selected conditions indicated in the figure. The differences in profiles under different conditions are used to help reconstruct the corresponding flame structures and identify the part of the flame that dominates the sandwich burning rates. The profile has an overall concave shape if the sandwich burning rate is higher than the AP self-deflagration rate (typical of low pressure). If the matrix burned very fast on its own, the matrix surface would be expected to get progressively further ahead of the rest of the surface. This did not happen for the conditions tested here.

Scanning electron micrograms of selected quenched sandwiches are shown in Figs. 6–12.

1) The surface of the AP laminae had the same froth, depressions, and ripples on the AP surface (typical of AP self-

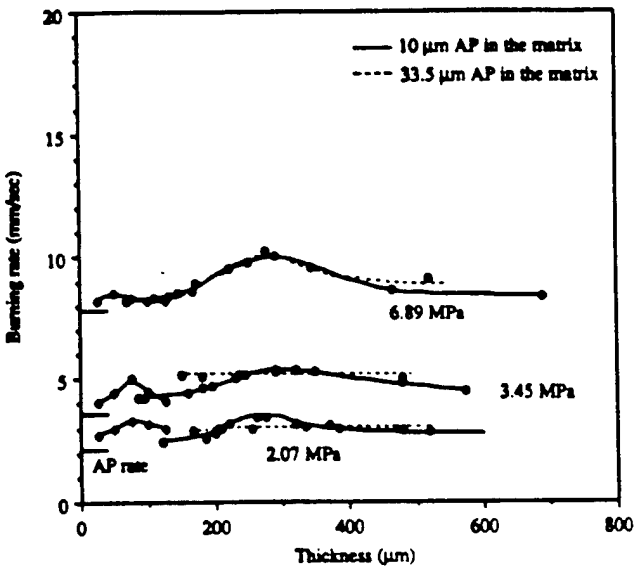

Fig. 3 Burning rate of 5:5 sandwiches.

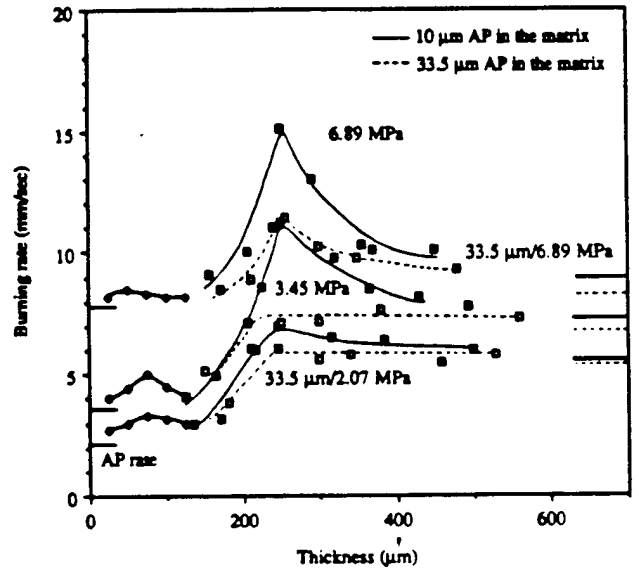

Fig. 4 Burning rate of 7:3 sandwiches.

deflagration) as in other sandwich burning tests with pure binder laminae (without AP in the binder).[1-4]

2) AP surface areas along the AP-binder contact interface exhibited a smooth surface. This region almost always "protrudes," in the sense that the leading point of the AP profile occurs 25–50 μm out from the AP laminae-matrix contact plane similar to sandwiches with pure binder laminae (Figs. 5 and 9).[1-4]

3) The "smooth band" extends out approximately to the leading-edge point (Figs. 5 and 6). The band was very irregular with the coarse AP matrix at higher pressures (Fig. 7), with the irregularities often relatable to the proximity of adjoining matrix particles.

4) Conditions that gave the highest burning rates resulted in narrow smooth bands with little "protrusion" of AP at the interface plane (Figs. 5 and 8).

5) The matrix surfaces were usually recessed slightly relative to the AP laminae, and appeared to have been dominated by a binder melt (especially with 5:5 mass ratio). The fine-AP particles appeared to be covered by binder, although many were revealed as smooth "bumps" (Fig. 9).

6) Coarse AP particles in the matrix were often visible (especially at higher pressure and/or 7:3 mass ratio), usually recessed in surface depressions (in 6.89-MPa tests). The ma-

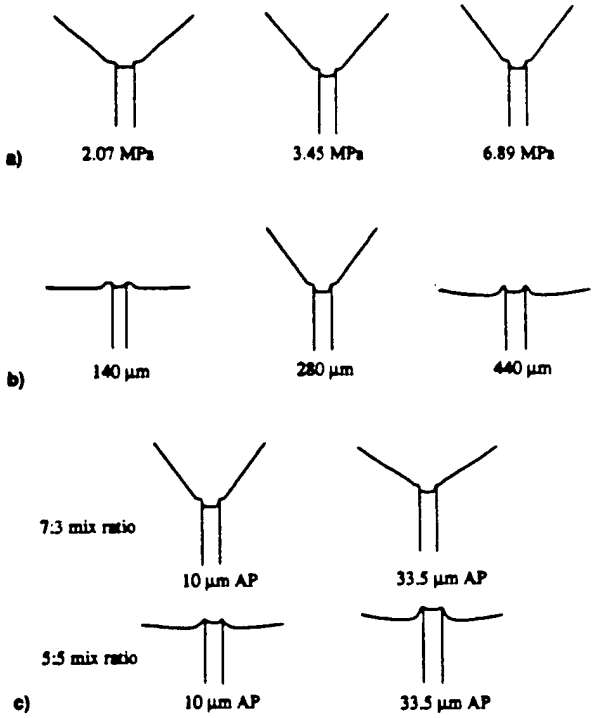

Fig. 5 Examples of burning surface profiles: a) profiles at maxima of burning rate vs matrix thickness, b) profiles at different matrix thickness at 6.89 MPa (10 μm and 7:3 mix), and c) profiles at maxima of burning rate vs matrix thickness curves at 6.89 MPa.

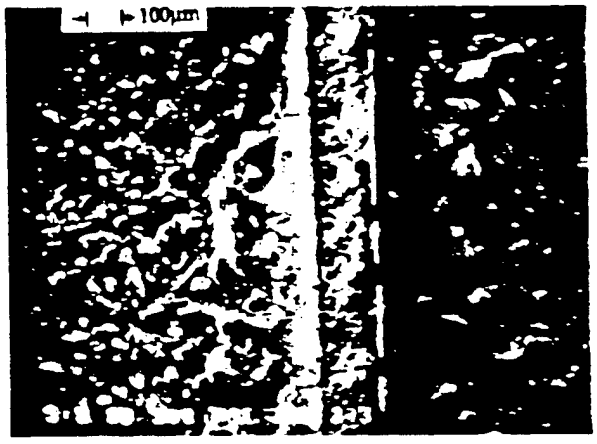

Fig. 6 Quench surface of a 5:5 (10 μm) AP-filled sandwich at 3.45 MPa.

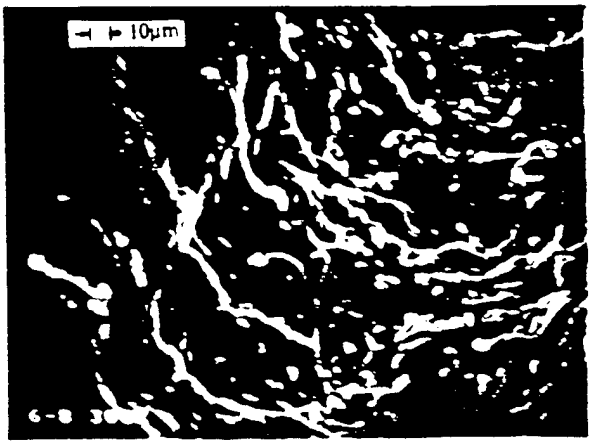

Fig. 7 Quench surface of a 7:3 (33.5 μm) AP-filled sandwich at 6.89 MPa.

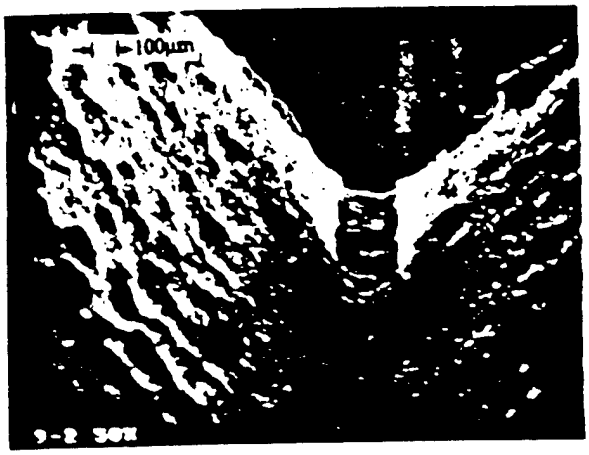

Fig. 8 Quench surface of a 7:3 (10 μm) AP-filled sandwich at 2.07 MPa.

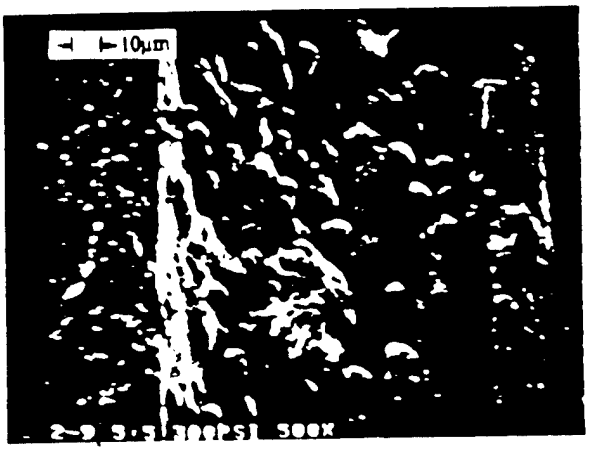

Fig. 9 Quench surface of a 5:5 (10 μm) AP-filled sandwich at 2.07 MPa.

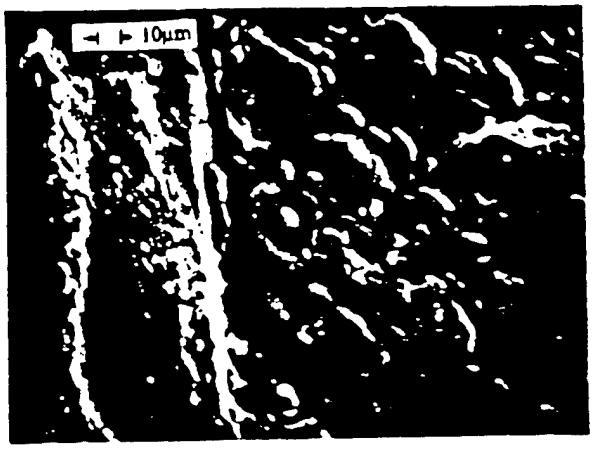

Fig. 10 Quench surface of a 8:2 (33.5 μm) AP-filled sandwich at 6.89 MPa.

trix surfaces had a cellular quality with AP particles visible in the bottom of cells. Some depressions were empty, apparently left by burned out AP particles (Figs. 10 and 11).

7) Under conditions where some AP particles are exposed (and appear to have been burning independently), such particles were more numerous in the part of the surface immediately adjoining the AP laminae (Fig. 12).

8) The quench tests on sandwiches with 8:2 ratio in the matrix laminae showed a somewhat drier surface, but otherwise looked like the corresponding results with 7:3 matrix (Fig. 10).

Considerations Involved in Discussion of Results

For sandwiches with pure binder laminae, the flame complex consists of an AP self-deflagration flame over most of the AP laminae, except at pressures below the AP self-deflagration limit.[2,7] The oxidizer-fuel diffusion flame originates in the AP-binder vapor mixing region above each AP-binder contact line on the surface. The LEFs stand off from the surface at sites where heat losses and heat release are in balance, to give a local flame with flame speed sufficient to be stationary in the outflowing gas (Fig. 1). The size and location of LEF is dependent on the accumulation of premixed reactants, chemical reaction rates, and hence on pressure or presence of diluents. Beyond the LEF, the diffusion flame extends outward in the flow until one or both reactants are consumed, usually at a closure between the two diffusion-flame sheets over the matrix lamina, because the sandwiches are oxidizer rich. It is important to note that the LEF is an intense premixed flame, close to the surface, with characteristics very different from the outer diffusion flame.[7] In this article these LEFs will be called lamina leading-edge flames or "LLEFs," to distinguish them from similar flames that occur above the AP particles when conditions permit (larger particles and/or higher pressures). The particle LEFs will be referred to here as "PLEFs." In Fig. 13, the two LLEFs burn independently of each other in sandwiches with pure binder laminae that were thick, while their interaction becomes important when they are close together (thin binder). The effect of binder lamina thickness on burning rate is due primarily to this LLEF interaction, indicating the importance of the local nature of the action of LLEFs and the importance of interactive behavior.[2,5-7] In this article, this interpretation must be extended to the presence of PLEFs and the possible interaction of PLEFs with other PLEFs and with adjoining LLEFs. The interactions occur when the flamelets are effectively competing for the same reactant and heat supplies through multidimensional diffusion of heat and reactants.

AP particles used in the matrix in this study may have fully developed flame complexes of their own (Fig. 2), but the earlier sandwich-burning studies[2] suggested that conditions for such flames would not be satisfied for the samples used here except with the larger particles at high matrix loading (i.e., 7:3), at high pressure. The reasoning is as follows: the LEF centers on the stoichiometric surface of the mixing fan that develops above the AP/binder contact line on the surface. The particles are in a locally fuel-rich environment, so that the stoichiometric surface closes at a "tip" above the AP particle (Fig. 2). At low pressure, the LEF stands far out on this stoichiometric "tent." If the particle is small (short tent) or the pressure is low (large PLEF standoff), the PLEF may be clear out at the tip. Further decreases in particle size or pressure tend to force the PLEF to a location beyond the tip. However, in this region there is no stoichiometric point; conditions are fuel-rich, and increasingly so at further distances from the surface. This situation is not conducive to a stable PLEF because the flame temperature decreases when the PLEF moves outward to find a stable heat-loss, heat release condition. In pure binder sandwiches these conditions led to quenching of the LEFs,[2] and it is expected that this will happen to PLEFs also when the exposed AP area is small, the pressure is low, and/or the local mixture ratio is more fuel-rich. This argument is supported not only by qualitative theory, but also by sandwich burning results,[2] and by the combustion behavior of bimodal AP propellants.[8] In the presence of still-attached LEFs on neighboring larger particles or AP laminae, the areas of fine particles on the surface continue to pyrolyze, and it is postulated that the resulting AP/binder vapor mixture forms a premixed "canopy" flame further from the surface (Fig. 14), probably piloted by the attached LEFs still present on the larger particles or laminae. In a limiting case of very fine AP particles, the AP vapors produce a mixture that behaves in the lamina mixing fan as a diluted fuel, but behaves

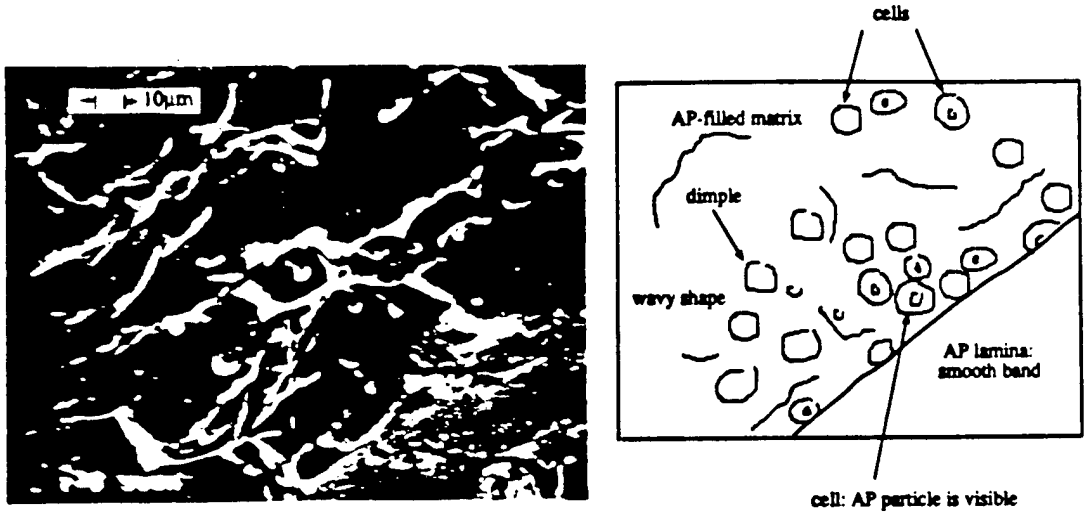

Fig. 11 Quench surface of a 5:5 (33.5 μm) AP-filled sandwich at 6.89 MPa.

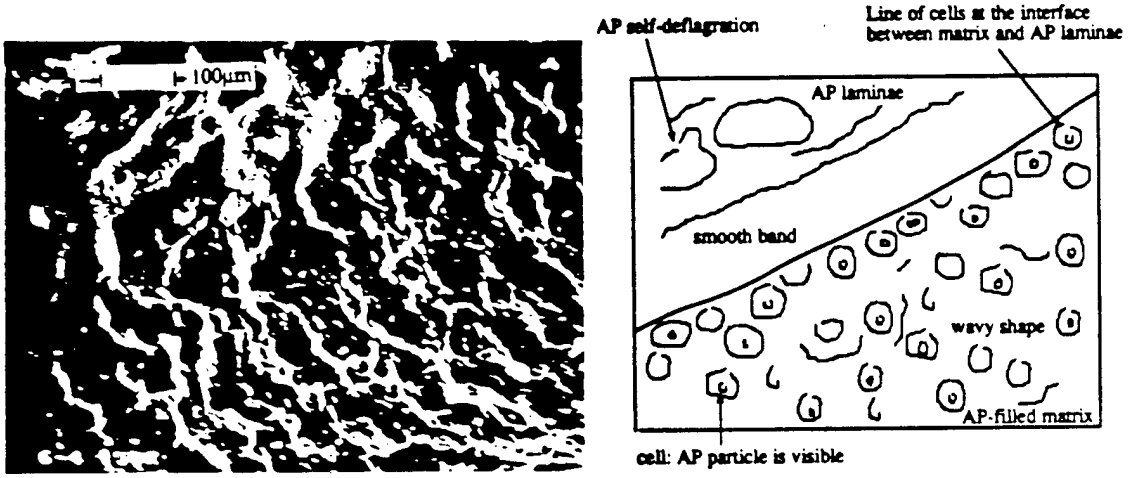

Fig. 12 Quench surface of a 7:3 (33.5 μm) AP-filled sandwich at 6.89 MPa.

as a premixed O/F system when the LLEF is reached. This behavior is enlarged upon in the following section.

Discussion of Results

The discussion of results is shown below as a series of statements about the combustion zone structure and processes. The first five statements were developed in studies of combustion of sandwiches with pure binder laminae,[1-4] but are applicable to the present results with AP-filled matrix laminae as well. The subsequent statements pertain to further observations and interpretation pertinent to AP-filled matrix laminae (in the range of variables studied).

1) The burning rate of the sandwiches is determined by the regression rate at the leading point of the AP surface, and hence by the heat flow to, and heat loss from that location. This generalization results from the fact that the AP contributes its own exothermic reactions to the heat balance, and the fact that the LLEF is usually centered over the AP surface because the stoichiometric surface in the mixing fan is located there due to the relatively dilute oxidizer species concentrations in the AP vapors and products (Figs. 1 and 14b).

2) With thick binder laminae, the two LLEFs do not interact, and vapors from the center part of the matrix flow away between the LLEFs without near-surface exothermic reaction. The lateral heat flow to this "excess" fuel in the solid and gas phase represent a heat drain from the rate controlling site in the AP surface (Fig. 13a). The binder lamina protrudes in the middle where heat sources are relatively distant.

3) With intermediate binder lamina thickness, the LLEFs interact to form one flame (the entire species and heat diffusion fields interact). The loss effect in 2 is minimized, leading to higher flame temperatures, reduced standoff distance from the condensed surface, and correspondingly higher burning rate at the leading edge site (Fig. 13b).

4) For still thinner binder laminae, the coupled LLEFs are fuel-deficient, so that the overall heat release is low. The lateral heat loss from the leading-edge sites to the rest of the AP lamina(e) becomes increasingly important because of the decreased net heat flux, and the burning rate is lower. In the limit as the binder thickness approaches zero, the burning rate falls to the AP self-deflagration rate (Fig. 13c).

5) A phenomenon described here as "LLEF detachment" occurs at some finite low binder thickness for which the LLEFs are no longer stable in the mixing flow, because there is no location where heat release can match the needs for a flame with speed equal to the outflow speed. The sandwich rate is presumably equal to the AP rate below this limit, but is not well verified because test samples of good quality are difficult to fabricate at these low binder thicknesses (this condition would determine the approach of the burning-rate curves to the AP rate at the left in Figs. 3 and 4).

To interpret the effects of granular AP in the binder lamina, the following arguments will be added to the above list.

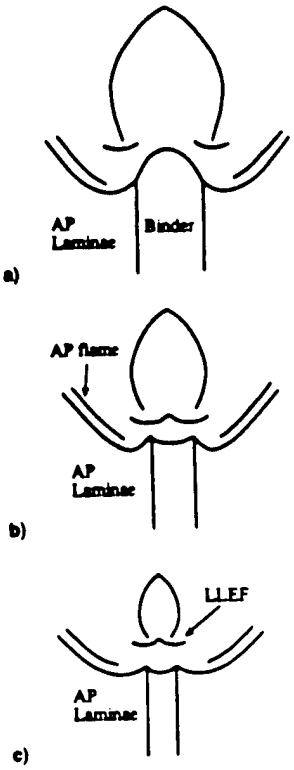

Fig. 13 Dependence of flame complex for AP-binder-AP sandwich on binder lamina thickness: a) thick binder (>125 μm), b) intermediate binder, and c) thin binder.

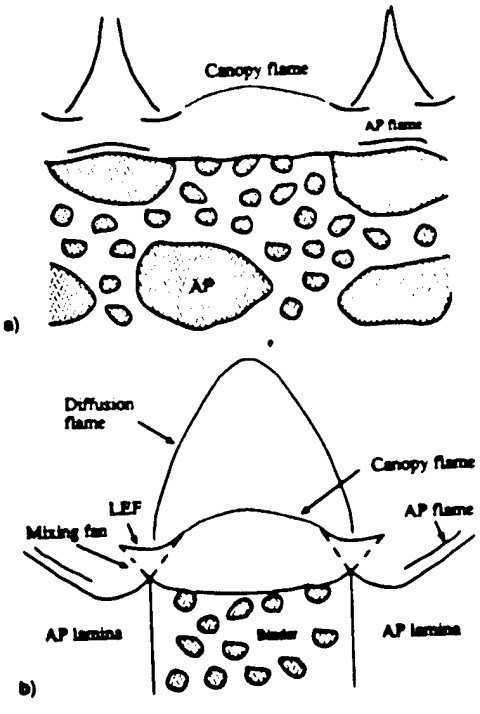

Fig. 14 Flame complex in systems with bimodal AP size distribution not supporting attached flames on individual particles: a) propellant with coarse and fine AP and b) sandwich with fine AP in the binder lamina.

6) One effect of AP in the binder is dilution of the fuel, which will shift the stoichiometric surface and leading edge of the LLEF toward the matrix lamina (Fig. 15).

7) A second effect of AP in the binder is to extend the fuel-rich side of the LLEF further toward and over the binder lamina because of the presence of oxidizer enrichment there (Fig. 15).

8) A third effect of AP relates to the extent of mixing of the AP particle vapors with the fuel vapors by the time they

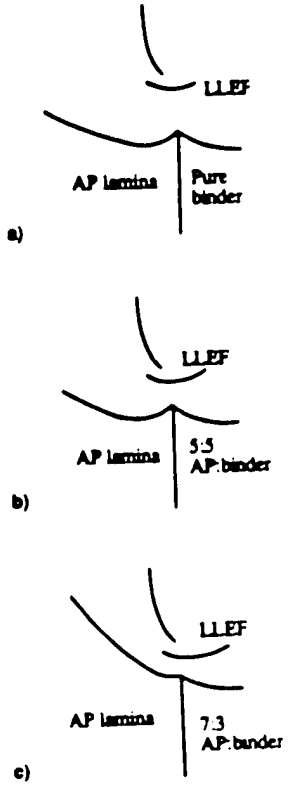

Fig. 15 Effect of fine AP to the binder lamina: a) narrow LLEF over AP lamina; b) wider LLEF, stoichiometric point close to the surface and shifted toward lamina contact plane; and c) wider LLEF, stoichiometric point over outer edge of AP lamina, LLEF extends well over matrix lamina.

reach the LLEF locations. With fine AP particles or large LLEF standoff (low pressure), mixing can be complete. With coarser AP, the mixing may be incomplete, with mixing fans around larger exposed particle surfaces, extending out to and beyond the LLEF standoff distance.

9) The larger AP particles may have their own attached particle LEFs (PLEFs), particularly at high pressures.

In order to make an interpretation of results, attention will be focused on the burning-rate trends, and the surface profiles and surface details will be used to test or complete the mechanistic arguments. The strategy will be to compare the burning rate curves with different amounts of AP, different size particles, and different pressures, and construct arguments to explain the differences based on the nine contributing effects listed above. When these arguments, qualitative theory, and the secondary evidence are all reconciled, a fairly detailed picture of the combustion behavior emerges. At the outset it is helpful to note some features that were common to all or most of the results.

1) The sandwich rates were all higher than the AP self-deflagration rates, but decreased toward the AP rate at the low end of the lamina thickness range. This positive slope region of the rate vs thickness curves occurred over a larger lamina thickness range with AP in the matrix. Recalling item 4 above, this presumably reflects the effect of a more dilute fuel (item 6), which extends the fuel-deficient region to greater lamina thickness.

2) The sandwich profiles were all more or less "V" shaped, to a degree consistent with the ratio of the sandwich rate to AP self-deflagration rate, establishing that the rate is controlled by the local flame complex involving the lamina interface region. Some protrusion of the AP/binder matrix lamina at its center occurred with thick 5:5 matrix laminae (i.e., the matrix does not control the rate). Nearly flat AP profiles occurred in some tests at high pressure, indicating that the AP rate is almost rate-controlling at higher pressure. There was no evidence of interfacial burning between laminae.

3) Under nearly all conditions the detailed profile of the AP lamina in the region near the lamina contact plane was concave upwards, with a leading edge at some tens of micrometers from the contact planes, and with a region of retarded AP regression and smooth surface closer to the contact plane. As in the interpretation of results with pure binder laminae,[3] this supports the interpretation in no. 2, and indicates that heat loss by conduction from the AP to the matrix lamina is occurring, and the LLEF is still centered over the AP. A possible exception was with test conditions that gave the highest burning rate, with the 7:3/10-μm matrix, where the leading edge of the AP was a ledge at the interface plane (Figs. 5a and 8).

4) The matrix laminae were recessed relative to the adjoining part of the AP laminae, with slight protrusion in the middle of some thick laminae. This is similar to results with pure binder laminae,[3] and is believed to result from the lower pyrolysis temperature of the binder (compared to the AP). Protrusion in the center (no. 2 above) is an indication that the matrix burning does not control the sandwich burning rate, and that interlamina heat transfer and/or the LLEFs contribute to pyrolysis of the matrix surface nearest to the AP laminae.

Turning now to comparisons of burning rate vs matrix thickness curves, the addition of AP shifted the maximum of the rate curves to a higher lamina thickness, an effect of fuel dilution (no. 6 above). It also gave higher burning rate (except in the fuel-deficient thin binder domain), an effect (no. 7 above) of greater width of the LLEFs because of premixed AP vapor in the fuel flow (and hence, less lateral heat loss, higher LLEF temperature). In the case of the 7:3 mixture, the asymptote at high matrix thickness is particularly high because the matrix burning rate is considerably higher than the AP rate. However, it is important to note that 1) the rate is higher than matrix rate under most conditions, indicating cooperative interactions of the LLEF and the matrix "canopy" flame (Fig. 14); 2) the matrix lamina never runs on ahead of the AP, indicating that the matrix-assisted LLEFs control the rate via the leading edge in the AP; and 3) the rate peaks at intermediate lamina thickness, further supporting the interpretation in 2) that it is the LLEF that controls rate, and the matrix exerts a rate depressing effect as a heat sink for heat flow from the rate controlling site in the AP lamina (this heat drain is reduced at lower lamina thickness, allowing higher rate until the fuel deficient domain is reached).

In summary, the mechanistic effect of addition of AP to the binder lamina is to give a more dilute fuel flow that extends the fuel deficient thin-lamina region to higher lamina thickness, and shifts the stoichiometric surface of the lamina mixing fan (and hence the leading edge of the LLEF) toward the lamina contact plane. At the same time, the presence of the AP vapor mixed with the fuel from the matrix surface extends the fuel-rich side of the LLEF, yielding more net LLEF heat release (except in the fuel deficient thin binder domain), with increased heat flow directly to the interface region and matrix lamina. In the domain of parameters tested, the maximum burning rate is higher with more AP addition, consistent with the above interpretation.

Comparing the burning rate curves for 10- and 33.5-μm particles, the rate is higher for 10-μm particles under almost all conditions. This is consistent with the thesis that the premixed vapors are more fully reacted in the LLEF, supporting heat flow to the rate controlling site, and probably reducing lateral heat drain from that site by more effective direct heating of the matrix lamina. This is supported by the observation that the rate of the 7:3 matrix alone is higher for 10-μm AP than for 33.5-μm AP.

It is notable that the peak in the burning rate curve with 7:3 matrix (Fig. 4) is more conspicuous with fine AP than with coarse AP, further supporting the interpretation that more complete mixing at the level of the LLEF gives greater extension of the LLEF on the fuel-rich side, and greater shift of the stoichiometric surface. The AP/binder vapors appear to be almost completely premixed at the LLEF height with 10-μm AP, whereas the 33.5-μm particles probably have stoichiometric tips near the LLEF height (higher than LLEF height at 6.89 MPa, less than LLEF height at 2.07 MPa). The large particles appear to have PLEFs at 6.89 MPa, and to a limited extent at 3.45 MPa, presumably partially compensating for the incomplete mixing to give a peak in the rate curve. The presence of PLEFs is also indicated by the quenched samples, which show exposed AP surfaces in the matrix (Figs. 7, 10, and 12). The number of such particles is higher along the contact plane, indicating cooperative support by the LLEF, and oxidizer enrichment by diffusion from the AP lamina outflow (a complex three-dimensional diffusion field). This coupled behavior between the lamina burning and the particle burning is indicated by the irregular edge of the AP lamina that was manifested only under these conditions (7:3, 33.5 μm, 6.89 MPa, Figs. 7 and 12) and absent under other conditions.

The mechanistic effect of particle size on burning rate is alluded to above, but merits focused comment. Fine particles appear to vaporize endothermally (presumably by dissociative sublimation to NH_3 and $HClO_4$), and the vapors diffuse into the surrounding flow of fuel vapor (fuel rich) before appreciable heat release. A premixed flame can then occur, which would give the observed matrix rate (zero in 5:5 mixtures, higher than the pure AP rate with 7:3 mixtures, see Fig. 4). However, the sandwich rate is higher than the matrix rate under most conditions, indicating a cooperative effect between AP self-deflagration and matrix burning that has been described above as governed by matrix vapor enhancement of the LLEF and resulting enhancement of the heat balance at the leading edge of the AP lamina profile. When coarser AP particles are used in the matrix, the matrix rate is reduced because the oxidizer/fuel (O/F) mixing takes longer (i.e., is not complete at LLEF height). The sandwich rate is reduced for the same reason. However, the nature of the matrix flame changes to a particle flame complex as pressure and particle size increase, a flame complex that is an array of three-dimensional particle flames is analogous to the two-dimensional sandwich flame. For the coarser AP particles used here, this change was apparently 1) fully developed only at 6.89 MPa and 2) significantly aided locally adjoining the AP lamina where additional oxidizer vapors and lateral heat flow were available. However, this enhancement of PLEFs did not enhance the sandwich burning rate as much as the premixed O/F flow to the LLEF provided by the fine AP matrices.

The mechanistic effect of pressure is primarily facilitation of a faster gas phase reaction rate at higher pressure, resulting in establishment of LLEFs and PLEFs and canopy flames closer to the surface. This effect is included in almost all combustion models, but the present results indicate the effect in a much more complicated framework because it involves all three kinds of flamelets, acting locally and interactively, and with the possibility of absence or presence of the canopy flames and PLEFs depending on pressure, particle size, and AP/binder ratio in the matrix. In propellants with multimodal AP size these local effects may, under some circumstances, average out in time, allowing the conventional one-dimensional form of the energy equation. However, the conditions for applicability of that assumption need to be re-examined, and provisions are needed for including the pressure-dependence, i.e., of PLEFs and canopy flames. The one-dimensionalization of the energy equation seems to be particularly inapplicable for modeling oscillatory response of combustion.

Summary

It has long been understood that the combustion zone of a composite propellant consists of three-dimensionally complex microscopic structures.[9,10,12,13] In order to develop useful an-

alytical models that are mathematically tractable, it is necessary to determine what features of this complex process dominate the steady and nonsteady burning. Since the dominant processes differ over the range of particle sizes, pressure and mixture ratio, one must either tailor the model to limited conditions or be sure that it is complete enough to reflect the dominant processes and correctly reflect the range of conditions of interest, while excluding unnecessary detail that burdens the model and computational requirements. The present studies provide many mechanistic insights needed for realistic phenomenological modeling, and has motivated more rigorous modeling of the oxidizer-fuel flames.[7-11] Some of these insights were suggested from earlier sandwich burning studies and propellant combustion models,[1-13] and are simply validated by the present study. But the study does more. It starts the job of sorting out what mechanisms are important under what conditions. It identifies conditions under which premixing of oxidizer and binder vapors gives a premixed "canopy" O/F flame, and conditions under which the flame structure is not premixed and is three-dimensionally complex. It shows that these extremes of behavior can both be present at different sites on the same burning surface, and that coupling behavior between such sites can be a significant factor in burning rate. It shows details of the process by which, as proposed by Summerfield,[12] the control of burning is "handed over" from kinetic control at low pressure to diffusion control at high pressure, and shows that, as proposed by Beckstead et al.[9] and Cohen,[10] control is never fully handed over to diffusion control because of the persistent importance of a kinetically limited leading edge of the diffusion flame at high pressure. Coupling of adjoining flamelets, proposed in some propellant combustion models,[13] is shown to be real, and details of the process are proposed based on high resolution studies of quenched samples and interpretation of sandwich burning rates.

While extension of the enhanced understanding of the combustion details to practical application was beyond the scope of this study, there is obvious potential for application to tailoring burning characteristics, and for improvement of modern burning rate and combustion response models.

Acknowledgments

Facilities and support of the authors were provided by the Thiokol Corporation, Brigham City, Utah, the U.S. Office of Naval Research, Arlington, Virginia, and the Georgia Institute of Technology, Atlanta, Georgia.

References

[1]Hightower, J. D., and Price, E. W., "Experimental Studies Relating to the Combustion Mechanism of Composite Propellants," *Astronautica Acta*, Vol. 14, No. 1, 1968, pp. 11-21.

[2]Price, E. W., Handley, J. C., Panyam, R. R., Sigman, R. K., and Ghosh, A., "Combustion of Ammonium Perchlorate-Polymer Sandwiches," *AIAA Journal*, Vol. 19, No. 3, 1981, pp. 380-386.

[3]Price, E. W., Sambamurthi, J. K., Sigman, R. K., and Panyam, R. R., "Combustion of Ammonium Perchlorate-Polymer Sandwiches," *Combustion and Flame*, Vol. 63, No. 3, 1986, pp. 381-413.

[4]Price, E. W., Sambamurthi, J. K., and Sigman, R. K., "Further Results on the Combustion Behavior of AP/Polymer Sandwiches with Additives," *Proceedings of the 22nd JANNAF Combustion Meeting* (Pasadena, CA), Vol. 1, 1985, pp. 41-54 (CPIA 432).

[5]Markou, C. P., "Effect of Different Binder and Additives on Sandwich Burning," Ph.D. Dissertation, Georgia Inst. of Technology, Atlanta, GA, 1988.

[6]Lee, S. T., "Multidimensional Effects in Composite Propellant Combustion," Ph.D. Dissertation, Georgia Inst. of Technology, Atlanta, GA, 1991.

[7]Price, E. W., Sigman, R. K., Beiter, C., Lee, S. T., Markou, C., Chiang, H. J., and Prasad, K., "Role of the Leading Edge of the Diffusion Flame in Combustion of Solid Propellants," *Proceedings of the 27th JANNAF Combustion Meeting* (Cheyenne, WY), Vol. III, 1990, pp. 31-56 (CPIA 557).

[8]Cohen, N. S., and Hightower, J. O., "An Explanation for Anomalies in Behavior in Composite Propellants," *Proceedings of the 29th JANNAF Combustion Meeting* (Hampton, VA), Vol. IV, 1992, pp. 253-273 (CPIA 593).

[9]Beckstead, M. W., Derr, R. L., and Price, C. F., "A Model of Composite Solid Propellant Combustion Based on Multiple Flames," *AIAA Journal*, Vol. 8, No. 12, 1970, pp. 2200-2207.

[10]Cohen, N. S., "Review of Composite Propellant Burn Rate Modeling," *AIAA Journal*, Vol. 18, No. 3, 1980, pp. 277-293.

[11]Prasad, K., and Price, E. W., "A Numerical Study of the Leading Edge of Laminar Diffusion Flames," *Combustion and Flame*, Vol. 90, No. 2, 1992, pp. 155-173.

[12]Summerfield, M., Sutherland, G. S., Webb, M. J., Taback, H. J., and Hall, K. P., "Burning Mechanism of Ammonium Perchlorate Propellants," *Solid Propellant Rocket Research*, Vol. 1, Progress in Astronautics and Rocketry Series, Academic Press, New York, 1960, pp. 141-182.

[13]Cohen, N. S., and Strand, L. D., "An Improved Model for the Combustion of AP Composite Propellants," *AIAA Journal*, Vol. 20, No. 12, 1982, pp. 1739-1746.

Appendix D

Mechanism of Burning Rate Enhancement of Composite Solid Propellants by Ferric Oxide

Journal of Propulsion and Power

Volume 13, Number 4, July-August 1997, pp 471-480

JOURNAL OF PROPULSION AND POWER
Vol. 13, No. 4, July–August 1997

Mechanism of Burning Rate Enhancement of Composite Solid Propellants by Ferric Oxide

Satyanarayanan R. Chakravarthy,* Edward W. Price,† and Robert K. Sigman‡
Georgia Institute of Technology, Atlanta, Georgia 30332-0150

This paper reports a series of experimental studies performed on sandwich propellants, wherein a matrix lamina of particulate oxidizer and polymeric binder is sandwiched between two ammonium perchlorate (AP) laminae. The catalyst (ferric oxide) is incorporated in the matrix lamina. The variables are pressure (0.345–6.9 MPa), matrix lamina thickness, catalyst concentration, matrix mixture ratio, types of oxidizer and binder, and the dispersion ability of the catalyst. The combined results indicate that, under the conditions tested, near-surface reactions associated with the particulate AP/binder contact lines on the burning surface assume significance in the presence of the catalyst. These reactions are further augmented by the presence of the leading-edge portion of the diffusion flame above the interface of the matrix and AP laminae.

I. Introduction

THE burning rates of ammonium perchlorate (AP) composite solid rocket propellants are routinely adjusted by the addition of small amounts of ballistic modifiers to the propellant formulation. For increasing the burning rate, the most common catalyst is iron oxide (IO, Fe_2O_3). The rate-controlling steps in the combustion of composite propellants have been debated for 40 years, and the mode of action of ballistic modifiers remains uncertain because of the remaining debate about the rate controlling steps.

Kishore and Sunitha[1] have made a nearly comprehensive survey of the literature on burning rate catalysis spanning roughly two decades up to the late 1970s. They observe that a wide variety of sites and mechanisms of action of the catalysts are proposed by the numerous studies. Subsequent studies, steadily decreasing in number, have done little to alleviate this situation.

The diverse and fragmentary nature of the literature pertaining to the problem makes it difficult to summarize the different viewpoints presented therein. Reported studies include effects of catalysts on the combustion and thermal decomposition of AP, condensed mixtures, model propellants, and regular propellants. Although this study is concerned mainly with the effect of iron oxide (IO), it seems natural to consider it as part of a broader class of transition metal oxides from a chemical point of view, and, hence, studies with other such additives cannot be ignored.

Proposed mechanisms include 1) physical effect of IO accumulated on the surface getting heated up from the flame and aiding binder regression by direct contact[2]; 2) effect on binder melt flow behavior, physically or chemically[3]; 3) catalysis of binder thermal degradation at the urethane linkages in the condensed phase at low pressures (2–7 MPa)[4,5]; 4) enhanced near-surface breakdown of heavy fuel molecules,[6–10] better with finer AP particles,[9] supplying more reactive fuel species to the O/F flame,[6,7] thereby bringing it closer to the surface and increasing the burning rate[6,7,11]; 5) action in the gas phase by a) modification of gas phase reactions by chloride derivatives of the catalyst,[9] b) exothermic breakdown of the catalyst by reactions with other species,[11] c) catalysis of the O/F flame,[12,13] and/ or d) catalysis of $HClO_4$ decomposition[14] (heterogeneous surface reactions not excluded[10]); 6) heterogeneous gas phase exothermic reactions between catalyst particles and $HClO_4$ (Ref. 15); 7) gas phase and/or heterogeneous reactions in crevices between fuel and AP[12]; 8) catalysis of some process in the vicinity of the AP/binder interface[16]; 9) catalysis of AP deflagration,[12,17] or decomposition[13] (by proton transfer[10] or electron transfer[18]); 10) action in the condensed phase: a) at the AP/binder interfacial surfaces,[8,9,19] b) by altering the decomposition products of AP and binder,[10,11] or c) by catalyzing $HClO_4$ decomposition, the products of which eventually enhance binder degradation,[20] or by catalyzing the oxidative polymer degradation by $HClO_4$ (Ref. 21); and 11) formation of thermally unstable metal perchlorates[10,18] or metal perchlorate amines.[22]

In spite of the diverse views on the problem, some general impressions are gained and are noteworthy. It appears that copper chromite (CC) and IO are most effective among the class of transition metal oxide additives.[1,6,7] CC acts better on AP,[17] whereas IO acts better when both AP and binder are involved.[12,16,21] CC is a better catalyst at high pressure, and IO at low pressure.[19]

Many investigators have proposed multiple mechanisms. In some cases, the results do not allow resolution among these mechanisms, and in some others, the investigators believe that a single mechanism cannot exclusively account for the net catalytic effect.[1] Many of these investigations have been carried out under various conditions that are not directly related to rocket operating conditions, and as such, their inferences are restricted in applicability to specific domains of propellant burning. It would be desirable to delineate domains of test conditions (pressure, particle size, etc.), in which the different mechanisms predominate over the others in controlling the burning rate of the propellant.

The present study is part of a larger investigation on the combustion mechanisms of solid propellants using the sandwich-burning method. This method provides relative ease of preparation and variation of test samples, and observation and characterization of the combustion behavior. This method also provides a rich background of previous studies for comparison with new results. Earlier results are available for sandwiches of AP-binder–AP laminae, in which the binder lamina consisted of 1) pure binder,[23] 2) catalyzed binder,[6,7,24] and 3) particulate AP-filled binder.[25,26] The present study concerns combustion with various iron catalysts and oxidizers (primarily

Received Feb. 20, 1996; revision received Feb. 19, 1997; accepted for publication April 8, 1997.

*Post Doctoral Fellow, School of Aerospace Engineering.
†Regents' Professor Emeritus, School of Aerospace Engineering. Fellow AIAA.

Considering the complex nature of the problem, the goal of this study would be accomplished if evidence were obtained that indicated the possible sites of predominant action of the Fe_2O_3 for the given initial geometry of ingredients. Attempts at resolving the exact chemistry are beyond the scope of this work, although plausible mechanisms may be proposed.

II. Background

Sandwiches with AP-filled binder laminae can be thought of as a two-dimensionalized simulation of the microscopic region included by adjacent coarse AP particles in a typical propellant with bimodal AP size distribution.

In the case of pure binder sandwiches, the leading edges of the oxidizer/fuel (O/F) diffusion flames (LEFs) are the sites of major near-surface heat release[12,16,27,28] and, hence, behave as rate controlling.[13,23,29] For thin nonmelting binder lamina, e.g., polybutadiene acrylonitrile acrylic acid (PBAN), the LEFs are multidimensionally coupled (in terms of heat feedback to the surface), and this is reflected in a maximum in the burning rate at a binder lamina thickness ~50–75 μm (Fig. 1). When ferric oxide is present in the binder lamina,[6,7,24] it accumulates on the binder surface, facilitating breakdown of heavy fuel molecules into lighter, more reactive species. This enables the LEFs to be located closer to the surface, resulting in an increase in the burning rate.

The mechanics of AP-filled sandwiches have been elucidated in detail recently.[25-27] It is briefly revisited here to establish some terminology used in this study, and also to serve as a comparison with the situation when the catalyst is present. With AP-filled binder laminae, the previous LEFs are designated as lamina leading-edge flames (LLEFs), to distinguish them from smaller LEFs that could exist above the fine AP particles, particle leading-edge flames (PLEFs), in the AP/binder matrix lamina. The mutual interaction of the LLEFs again results in a peak in the burning rate vs lamina thickness curve, but at a matrix lamina thickness ~225–275 μm (Fig. 1). The larger thickness is because of the diluting effect of the AP particles; but they do not act as just a diluent:

1) The matrix is less fuel rich than the pure binder, and, hence, the stoichiometric surface above the lamina interface shifts inward.

2) The lateral extent of the fuel side of the LLEFs is increased.

3) The total heat release in the LLEFs is increased, enabling the flame to stand closer to the surface.

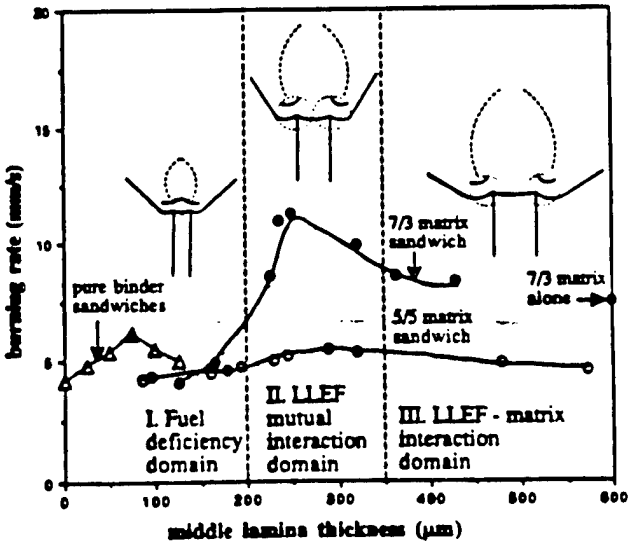

Fig. 1 Typical dependence of uncatalyzed sandwich burning behavior on matrix lamina thickness for pure PBAN binder, and

These effects are favorable for direct heating of the matrix lamina, and so condensed phase lateral heat transfer from the AP lamina across the lamina interface plane is reduced. This is reflected in 1) reduced width of the smooth band[23] on the AP surface adjoining the lamina interface and 2) reduced extent of AP retardation in that region. When the matrix mixture is adequately less fuel rich, so that the premixing matrix gases can sustain combustion (as in AP/PBAN = 7/3), and when the thermal wave thickness >> fine AP particle size (small particles, low pressure), a premixed canopy flame exists above the matrix lamina, connecting the fuel-rich sides of the LLEFs; when the thermal wave thickness ~ fine AP particle size (large particles, high pressure), LEFs are attached to the individual fine particles, resulting in PLEFs.

The matrix flame does not control the rate, but augments the mutual interaction of the LLEFs (Fig. 1).[27] For large matrix thickness, the LLEFs are uncoupled, but the rate is still slightly higher than that of the matrix alone. This indicates a domain of LLEF-matrix interaction, where the interaction between a single LLEF and processes associated with the matrix (either in the gas phase, condensed phase, or heterogeneous) are rate controlling. It will be seen in this paper that this domain assumes importance in the presence of the catalyst.

III. Experimental

A. Experimental Techniques

Three principal techniques were employed in this study: 1) combustion videography, 2) examination of quenched samples in the scanning electron microscope (SEM), and 3) hot-stage (optical) microscopy (HSM) of ingredients. These techniques are rather routine and are detailed elsewhere.[24,25] Besides serving as a tool for macroscopic flame structure and surface profile studies, the video pictures were also used for burning rate measurements. Flame front positions in successive frames (typically 10–40 points, more for lower rates) were fitted with a straight line in the least-square sense, with a correlation ≥99.9%. The slope of this line gave the burning rate. Approximately 50% of the data points, selected at random, were checked by repeated tests for reproducibility within 5% variation. In the combustion experiments, the samples were coated with a very thin layer of high vacuum grease to inhibit burning down the sides, and were burned in a nitrogen atmosphere. The heating rate in the hot-stage experiments was ~3°C/s, and they were performed at atmospheric pressure in an argon atmosphere.

B. Samples

Fabrication of sandwiches is also detailed elsewhere.[25] The catalyst was thoroughly mixed in the binder first, before adding the oxidizer particles. All of the ingredients for the matrix were weighed within an error of 0.5%. The position of the samples in the oven was inverted periodically during the curing period to prevent the oxidizer particles in the matrix from settling on to one side of the sandwich as a result of gravity. Different size levels of AP particles were used, with appropriate designations: the 2-μm AP was a mixture of AP particles of that size and hydroxyl-terminated polybutadiene (HTPB) prepolymer; the 10-μm AP is from the same batch as used in previous studies[26]; the 33-μm AP and 75-μm AP are those that remained between sieves of mesh sizes 37 and 30 μm, and 90 and 75 μm, respectively. The particle sizes of ammonium dinitramide (ADN), hexanitro hexaazaisowurtzitane (HNIW), and cyclotetramethylene tetranitramine (HMX) were nominally 40, 10, and 10 μm, respectively. The potassium perchlorate (KP) nominal size was about 30 μm. No attempt was made to quantitatively characterize the size distributions of these oxidizer particles beyond ascertaining on the optical and/or SEM that samples of these ingredients did not contain particles of significantly different sizes than just specified. It is considered that such a qualitative approach is sufficient for the purposes of this study. The form of availability of the 2-μm

Table 1 Binder compositions

No.	Binder	Prepolymer, %	Plasticizer, % (DOA)	Curing agent Type	Curing agent Amount, %
1	PBAN	64.14	15.00	ECA	20.86
2	HTPB-DDI	69.07	16.77	DDI	14.16
3	HTPB-IPDI	75.73	18.39	IPDI	5.88

up to a common maximum ratio of AP/binder = 65/35 with the different curing agents. Three different binder types were employed, and their compositions are given in Table 1. Throughout the text, the designations HTPB–IPDI and HTPB–DDI are used to denote HTPB cured by isophorone diisocyanate (IPDI) and dimeryl diisocyanate (DDI), respectively. 1–2 μl of a cure catalyst, dibutyl tin dilaurate (T-12) was usually added to 5 g of a HTPB-based matrix mixture. This enabled curing of HTPB samples in a day, instead of a week. [T-12 acts on diisocyanate curing agents and could not be used with PBAN/ECA (epoxy curing agent) binder.] The addition of T-12 does not seem to significantly alter the physical behavior of HTPB binder, as observed on the hot stage. The Fe_2O_3 used in this study, unless stated otherwise, is called Pyrocat (manufacturer's specifications: Nanocat™ SF1O catalyst, lot 3-1-125, α-type, particle size 0.003 μm, specific surface area 270 m^2/g, density 0.05 g/cc).

IV. Results

This section is a listing of results with detailed specifications of the test conditions. The implications of the results are discussed in Sec. V.

A. Effects of Matrix Lamina Thickness, Catalyst Concentration, and Matrix Mixture Ratio

Figure 2 shows the dependence of the sandwich burning rate on matrix lamina thickness for 0.2 and 1% Pyrocat in a matrix of AP/PBAN = 7/3 (Fig. 2a) and AP/PBAN = 5/5 (Fig. 2b) at 2.1, 3.5, and 6.9 MPa. The 10-μm AP was used in these tests. The burning rate vs matrix thickness trend for the corresponding uncatalyzed sandwiches (taken from Ref. 25) are presented for comparison. In general, the scatter in the data is slightly-to-considerably more when the catalyst is present; more at the 1% level than at the 0.2% level, and more for a mixture ratio of 5/5 than for 7/3. The AP/PBAN = 5/5, 1% Pyrocat sandwich data are highly scattered, but do not indicate any conspicuous dependence of the burning rate on the matrix lamina thickness. The scatter is not unexpected because the 5/5 mixture is in the region of flammability limits; the uncatalyzed 5/5 matrix alone does not sustain combustion, whereas the catalyzed ones barely burn, at very low rates. However, the following broad features are noted:

1) The 0.2 and 1% catalyzed AP-filled sandwich burning rates are several times higher (≥100%) than corresponding uncatalyzed sandwich rates, compared to a relatively marginal (~30%) increase in the burning rate of pure PBAN binder sandwiches with 10% catalyst.[24] (The corresponding curves are not shown for comparison in Fig. 2 in the interest of clarity.)

2) The 5/5 matrix alone begins to sustain combustion in the presence of as low a catalyst level as 0.2%, and the 7/3 matrix displays a major increase in the burning rate when catalyzed.

3) The catalyzed 5/5 matrix rates are very low, and the samples burn in a smoldering fashion, without a conspicuous visible flame; the pressure dependence of their burning rates is very weak.

4) The burning rates of the catalyzed 5/5 sandwiches are several times higher than their corresponding matrix rates. On the other hand, the 7/3 sandwiches burn only slightly faster than their corresponding matrices.

5) It must be remembered that no matter how high the catalyzed sandwich rates are, they should logically tend to the AP rate shown on the left ordinate line in Figs. 2a and 2b, in the limit of zero matrix lamina thickness. (This cannot be effectively tested because AP-filled sandwiches with very thin matrix laminae cannot be fabricated practically.) The curves show that even a thin lamina of matrix is sufficient for major catalytic action; it is greater for higher AP loading and catalyst concentration in the matrix.

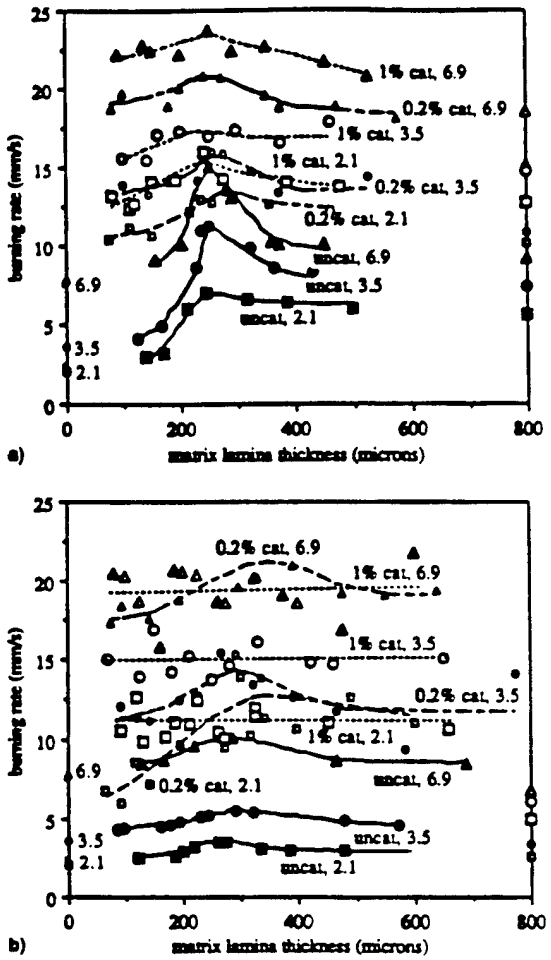

Fig. 2 Dependence of burning rate on matrix lamina thickness for uncatalyzed and catalyzed AP-filled sandwiches at different pressure levels (noted in MPa). Burning rates of pressed AP are shown on the left ordinate, and those of matrix burning alone on the right ordinate lines. AP/PBAN = a) 7/3 matrix and b) 5/5 matrix.

6) The effect of catalyst concentration (0.2 vs 1%) is slight in the case of the 7/3 samples and the 5/5 matrix; it is nearly negligible for the 5/5 sandwiches, except perhaps in the thin matrix lamina limit. Weak dependence of catalytic effect on the catalyst concentration is also reported in the literature.[4,9,15]

7) Except for the case of the 5/5, 0.2% catalyst sandwiches in the thin matrix lamina limit again, and the dependence of sandwich burning rates on the matrix lamina thickness is weakened in the presence of the catalyst.

B. Surface Profile and Features

Sandwiches of the type in item Sec. IV.A in the previous text were quenched by rapid depressurization while burning, and their quenched surfaces were examined in the SEM. The matrix and the lamina AP in the immediate vicinity of the lamina interface burn down so fast, compared to the outer region of the AP laminae, that the surface profile assumes an almost V shape. This makes SEM observations difficult. No remarkable differences are seen between the various quenched samples in an overall sense. A typical quenched surface is

Fig. 3 Quenched surface of a typical catalyzed AP-filled sandwich: ● matrix surface, ● dry band in the AP lamina, ● frothy surface of the AP lamina (not in focus).

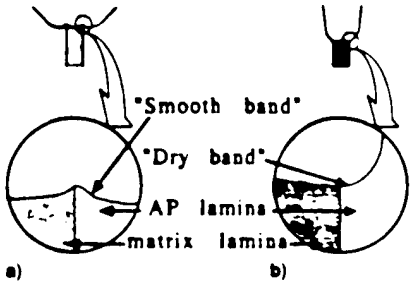

Fig. 4 Typical burning surface profile for AP-filled PBAN sandwiches: a) uncatalyzed and b) catalyzed by Pyrocat.

presented in Fig. 3. Figure 4 shows a typical sketch of the surface profile of these sandwiches in comparison to that of the uncatalyzed case. The following features are noted:

1) There is no retardation in the regression of the AP lamina in the immediate vicinity of the lamina interface in the case of catalyzed sandwiches, as against such a protrusion in uncatalyzed sandwiches.[26] The AP lamina surface in that region has a curvature that is concave upward.

2) The AP surface in the immediate vicinity of the interface has a dry and parched appearance (dry band), as against a smooth and soft surface region (smooth band) in the uncatalyzed sandwiches. The dry bandwidth is much smaller than the corresponding smooth bandwidth.

3) Accumulation of catalyst particles can be observed as sporadic thin white filigrees (size >> catalyst particle size), randomly distributed on the surface of the matrix lamina. The extent of accumulation is lower at the 0.2% catalyst level when compared to the 1% level. Considering the high oxidizer loading, low catalyst content, very fine size of the catalyst, and the fact that the catalyst is in the binder, accumulation of the catalyst cannot be expected to be as high as in earlier work, with sandwiches having 10% IO in pure binder lamina.[6,7,24] Catalyst accumulation in propellants is also reported in the literature.[2,6]

C. Combustion Videography of Very Thick Sandwiches

Video pictures of burning of sandwiches with 10-μm AP/PBAN = 7/3 and 5/5, 1% Pyrocat matrices of lamina thickness > 1000 μm (much larger than typical values) were taken. Figure 5 shows frames from such video pictures for the two mixture ratios. The pictures show some protrusion of the matrix lamina for the 5/5 matrix (Fig. 5a), whereas no such protrusion is found in the case of the 7/3 matrix (Fig. 5b). The burning rates of these sandwiches agree very well with the burning rates of sandwiches in the thick limit of matrix lamina shown in Fig. 2.

D. Effect of Oxidizer Type

Five different oxidizers, AP, KP, ADN, HNIW, and HMX, were tested in conjunction with PBAN (oxidizer/PBAN = 7/3), with and without 1% Pyrocat. Attempts to study ammonium nitrate (AN) did not succeed because of the lack of

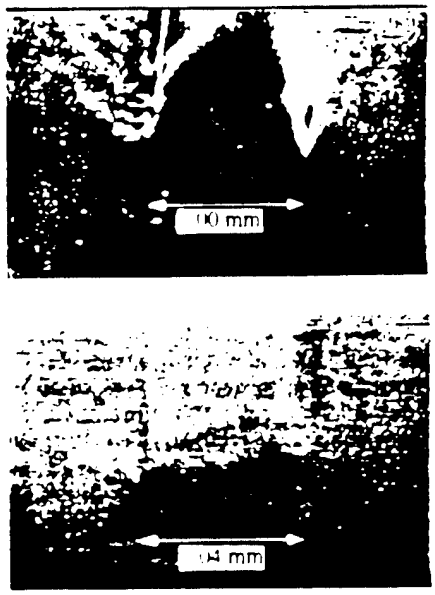

Fig. 5 Video pictures of the combustion of sandwiches with a very thick lamina of 10-μm AP/PBAN, 1% Pyrocat matrix at 3.5 MPa. AP/PBAN = a) 5/5 and b) 7/3.

proper wetting properties between that oxidizer and PBAN. In all cases, the oxidizer/PBAN matrix was sandwiched between two AP laminae.

The rationale behind sandwiching these matrices by AP laminae is to see how the matrix burning responds to the presence of a pair of LLEFs. Ideally, it would be desirable to test sandwiches with the same oxidizer in the matrix and oxidizer laminae, but this could not be done because 1) some of the materials (notably ADN and HNIW) were available only in very small quantities, and 2) safety concerns about pressing pellets of these materials persist. However, the matrix lamina thickness in all of these sandwiches was designed to be ~375–400 μm, to be out in the LLEF–matrix interaction domain rather than the LLEF mutual interaction domain (see Fig. 1).

It was difficult to obtain these different oxidizer particles in the same size range. Also, the particle size effects of these oxidizers are either unknown or mostly different from each other. In any case, the available supplies seem to fall into two size ranges: 10–20 μm for HMX and HNIW, and 30–40 μm for KP and ADN. For effective comparison, the 10-μm AP was used in connection with the first range, and the 33-μm AP was used for the second range.

The ratios of the burning rates of catalyzed and uncatalyzed samples (both sandwiches and matrices) are shown in Fig. 6. This parameter helps reduce the number of curves by half, but inevitably conceals the actual burning rate information. However, it would suffice for the present purpose to note that the burning rates of all samples at a given pressure are comparable on an order of magnitude basis (1.5–8 mm/s at 0.69 MPa; 9–25 mm/s at 6.9 MPa), except HMX matrices, which are lower by one order at every pressure level (0.6 mm/s at 0.69 MPa; 2 mm/s at 6.9 MPa). It is seen clearly from Fig. 6 that the burning rate increase is markedly the highest for AP (≥100%), with the curves corresponding to the other oxidizers lying around a burning rate ratio of unity or slightly more (marginal catalytic effect). Tests on propellants with different oxidizers found in the literature also support the choice of AP for maximum catalysis.[14,15]

E. Effect of Susceptibility of the Binder to Melt Flow

The susceptibility of HTPB binders to melt before vaporization is significantly altered by the choice of different diisocyanate curing agents, which in turn is different from that of PBAN cured by ECA. Aspects related to binder melt flow,

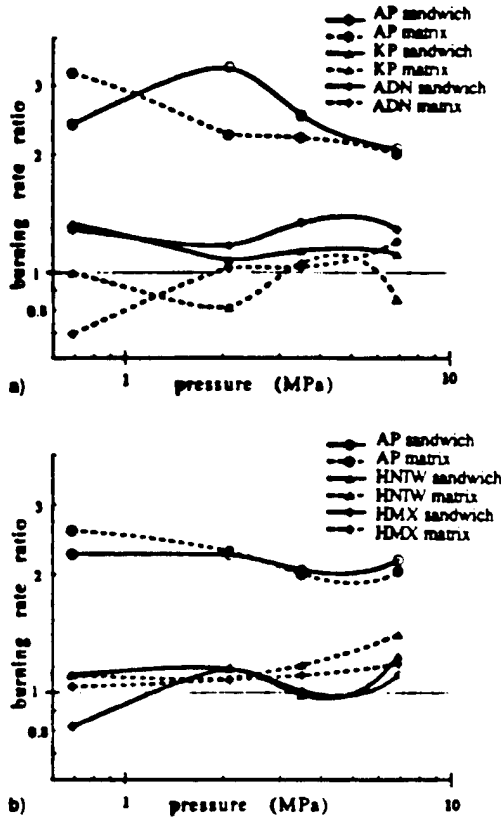

Fig. 6 Ratio of burning rate of catalyzed to uncatalyzed samples with oxidizer-filled PBAN matrices (oxidizer/PBAN = 7/3) in two oxidizer particle size categories: a) 30–40 and b) 10–15 μm.

such as plateau burning behavior of propellants, are addressed in detail in a separate paper.[30] It would suffice here to point out that, as observed in the hot-stage microscope, PBAN melts above 450°C, HTPB–IPDI melts slowly between 300–360°C, whereas HTPB–DDI melts rather abruptly at 230°C. All of these binders vaporize vigorously at 500°C, a value not too different from the decomposition temperature of AP. The hot-stage microscope experiments,[31] and various other combustion tests with pure binder as well as AP-filled sandwiches, have indicated that a qualitative order of increasing susceptibility for melt flow of the binders considered in this work is PBAN < HTPB–IPDI < HTPB–DDI. It should be recorded here that the addition of Pyrocat to the HTPB samples seems to retard the curing process, and advances the onset of melting (conspicuously noticeable in HTPB–DDI) to a lower temperature. The implications of this has been reported in the literature.[6,5,32]

Tests on sandwiches and matrices with and without 1% Pyrocat in a mixture of these binders and the 10-μm AP in the ratio AP/binder = 7/3 resulted in Fig. 7. The sandwiches have a matrix lamina thickness of ~250–275 μm, corresponding to maximum burning rates in Fig. 2. Figure 7a shows burning rates vs pressure for the uncatalyzed samples. In the case of PBAN, the sandwich and matrix curves are more or less parallel to each other. The HTPB–IPDI matrix curve exhibits a plateau in the pressure range 0.7–2 MPa, an effect suspected to be caused by the binder melt flow. The corresponding sandwich burning rate increases steadily with pressure in the entire pressure range tested. The HTPB–DDI matrix does not sustain combustion in the entire pressure range tested; however, it tends to burn, but self-quenches soon after ignition in the low-pressure range 0.35–0.7 MPa. The corresponding sandwich burning rate increases in that pressure range, but subsequently falls back to the AP rate at higher pressures. Above 2.1 MPa, when the AP begins to self-deflagrate, the AP laminae lead the sandwich burning surface (as can also be seen in the video pictures).

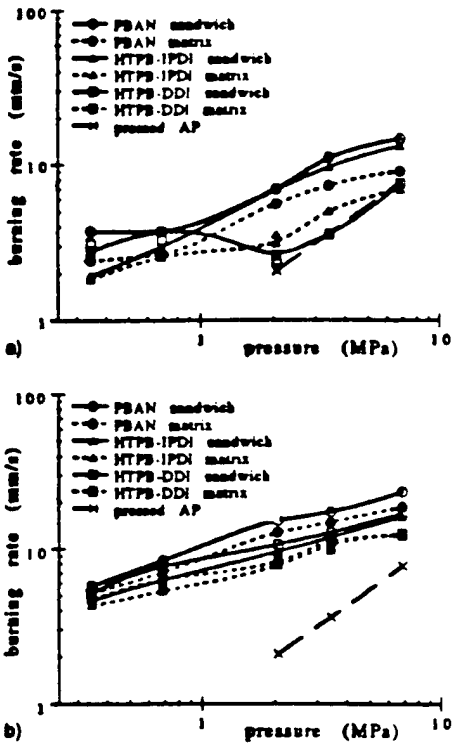

Fig. 7 Effect of binder melt flow characteristics on the burning rate of sandwiches and matrices of 10-μm AP/binder = 7/3: a) uncatalyzed and b) catalyzed by 1% Pyrocat.

Figure 7b shows the burning-rate curves for the catalyzed samples. The overall rates for all of the binders are substantially higher than for their corresponding uncatalyzed samples. Also, in all of the cases, the corresponding matrix and sandwich curves are almost parallel to each other. In fact, the differences in the curves for HTPB–IPDI and HTPB–DDI are slight. The PBAN rates are slightly higher than those of the HTPB-based samples. The effects caused by binder melt flow witnessed in the uncatalyzed situation are considerably washed out when the catalyst is present.

F. Effect of AP Particle Size

This subsection reports a systematic variation of the size of fine AP particles in a wide range of sizes (approaching different orders of magnitude). Three ranges of AP size were employed: the 2, 10, and the 75-μm AP. Since the 2-μm AP was available only with HTPB, and in a mixture ratio of AP/binder = 65/35, for reasons explained earlier, all of the other test samples in this subsection also conform to these stipulations. The HTPB is cured with IPDI, which has reduced melt flow effects compared to DDI, the other diisocyanate curing agent studied in this work. 1% Pyrocat was used in the catalyzed samples. The matrix lamina thickness in the sandwiches is again ~250–275 μm, as in Sec. IV.E. The burning rates for matrix and sandwich are shown separately in Figs. 8a and 8b for the sake of clarity.

The uncatalyzed 2-μm AP matrix does not burn in the entire pressure range tested. Other uncatalyzed matrices burn only in the pressure ranges indicated in Fig. 8a. Note that the particle size effect on the uncatalyzed matrix is the reverse of the conventional trend of increasing burning rate with decreasing particle size. The 2- and 10-μm AP uncatalyzed sandwiches exhibit a mesa in the 1.04–3.5 MPa range, and a plateau in the 3.5–6.9 MPa range, and higher (not shown here), respectively (Fig. 8b). The uncatalyzed 75-μm AP sandwich curve also exhibits a relatively low exponent in the midpressure range (0.69–2.1 MPa). Such effects, explained as related to the relative length scales of lateral binder melt flow and fine AP particle size in the matrix [30] are smeared by the presence of

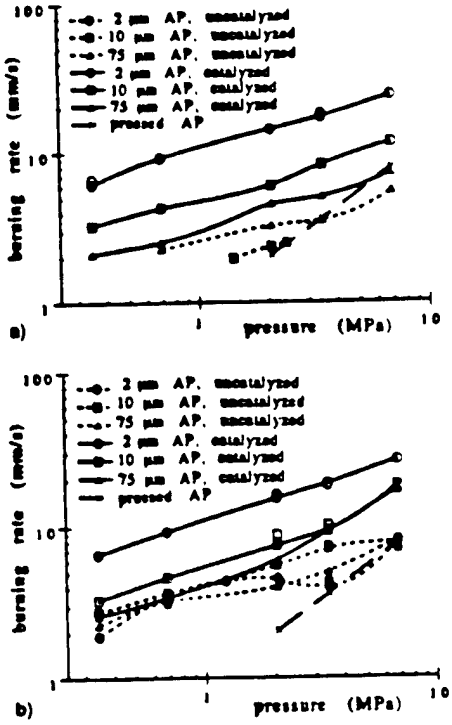

Fig. 8 Effect of fine AP particle size on the catalytic effect of 1% Pyrocat on samples with a matrix of AP/HTPB-IPDI = 65/35: a) matrix and b) sandwich burning rates.

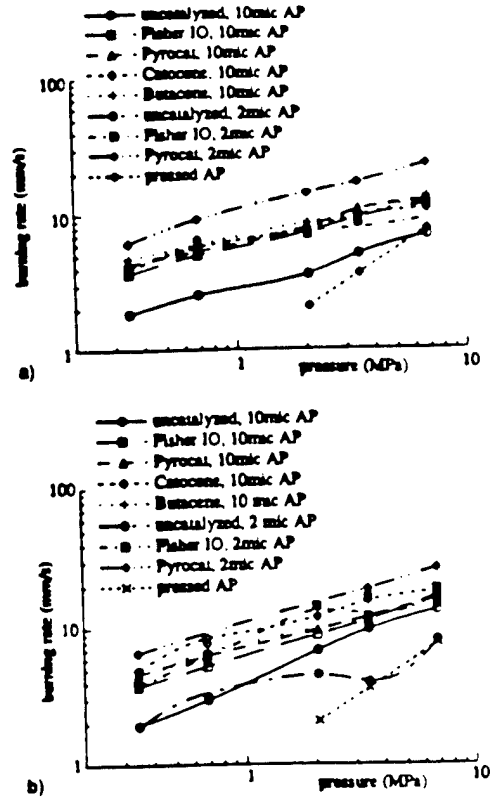

Fig. 9 Effect of dispersion ability of iron catalysts on the burning rate catalysis of AP/HTPB-IPDI samples: a) matrix and b) sandwich.

the catalyst. As for the effect of AP particle size on the catalysis, the 2-μm AP samples clearly register the highest catalytic effect, followed by the 10- and 75-μm AP samples. The effect is clearer in matrices than in sandwiches; the differences in the particle-size dependence of the catalytic effect in the sandwiches is diminished, particularly between that of the 10- and 75-μm AP sandwiches and at higher pressures. Similar AP particle size effects on catalysis are also reported in the literature.[9] Also, the conventional trend of increasing burning rate with decreasing particle size is restored in the presence of the catalyst.[7]

G. Effect of Dispersibility of the Catalyst

Four different iron-containing catalysts were chosen to investigate the effect of the degree and scale of dispersion of the catalyst in the binder: 1) Fisher Fe_2O_3, particle size $\sim$1 μm (larger than Pyrocat); 2) Pyrocat; 3) Catocene, a liquid catalyst; and 4) Butacene®, a specialty resin, produced by SNPE, France, in which a ferrocenic silane group is grafted to the backbone of the HTPB molecule.[32]

1. HSM Observations

Both Fisher and Pyrocat IO are rust colored and turn black at $\sim$200°C; no further changes are observed up to $\sim$900°C. Catocene vaporizes at $\sim$360°C, leaving a fine bed of black particulate residue. Butacene (uncured) vaporizes between 470–500°C, just as HTPB prepolymer would, leaving a residue similar to that left by Catocene. A blend of HTPB:Butacene = 62:38 cured by IPDI behaves similarly to HTPB binder without Butacene; it slowly melts at $\sim$300–360°C, and boils at 480–500°C, but leaves a residue characteristic of uncured Butacene, as opposed to no significant residue for HTPB with no catalyst.[31]

2. Burning Rate Measurements

Two sets of tests were performed. In the first set, all the four iron catalysts were used in combination with 10-μm AP in the matrix. The IO particulate catalysts were added at

propellants, twice as much Catocene is generally used as the amount of IO to roughly equalize the iron content[24] (the exact equivalent amount is slightly more than 2% in an AP/binder = 7/3 mixture). Butacene has an average iron content of approximately 7.8% by weight. A blend of HTPB:Butacene = 62:38 was used to obtain an iron content that is equivalent to the other catalyzed mixtures. For the sake of compatibility with the Butacene tests, HTPB was chosen as binder in the other tests where the catalyst was externally added. Again, IPDI was chosen as the curative to have reduced binder melt flow effects. The matrix is a mixture of 10-μm AP and HTPB-IPDI in the ratio of 7/3. Matrix lamina thickness in all sandwiches is $\sim$250–275 μm, corresponding to maximum burning rates in Fig. 2, as in Secs. IV.E and IV.F.

The results are presented as part of Figs. 9a and 9b, as matrix and sandwich burning rates vs pressure, respectively. The sandwich rates are always slightly higher than the corresponding matrix rates, except for the Butacene samples at 0.345 MPa. Curves for the different catalysts are clustered in the case of matrix (similar results are reported in the literature[2,11]), and slightly spread out in the case of sandwich rates. In either case, the arrangement of the curves does not directly correlate to the extent of dispersion of the catalyst in the binder.

The second set of tests is on a smaller scale. Here, the Fisher IO was used at the 1% level in combination with the 2-μm AP in a matrix of AP/HTPB-IPDI = 65/35. The remaining parameters are the same as in the first case. This situation corresponds to comparable orders of magnitude for the particle sizes of the catalyst and the oxidizer. These results are also shown in Fig. 9. The Fisher IO matrix burns in the entire pressure range 0.345–6.9 MPa, in contrast to no deflagration by the uncatalyzed 2-μm AP matrix. The Fisher IO sandwich rates have a greater overall burning rate, but preserve the mesa exhibited by the corresponding uncatalyzed sandwich burning rate curve; this is in contrast with washout of plateau and mesa

sandwich, the burning rates of the Fisher IO samples are significantly lower than those of Pyrocat samples at all of the pressures tested, registering a definite effect of the dispersibility of the catalyst when in combination with the 2-μm AP.

3. SEM Observations

Sandwiches, in Sec. IV.G.2, were quenched while burning by rapid depressurization, and the quenched surfaces were examined in the SEM. The relevant pictures are not presented here in the interests of economy of space, and because they are not too different from Fig. 3. In all of the cases, accumulation of the catalyst on the surface is evident. Qualitatively, the extent of accumulation varies from dense but sporadic clusters in the case of Fisher IO, to a more uniform web of thin filigrees in the case of Butacene. The overall matrix surface does not indicate any undulations at the locations of these clusters. Even in the case of the Fisher IO, the dense clusters are smaller than the fine AP particle size, so that any such undulations in the surface caused by them are smaller in length scale than those caused by the AP particles and, therefore, may go unnoticed.

V. Discussion

A. Perspective Based on Previous Studies

Earlier studies in the present project involved tests on sandwiches with outer AP laminae and either pure binder,[23] catalyzed binder,[6,7,24] or AP-filled binder[25,26] as the middle laminae. In these studies it was concluded that the exothermic reactions that controlled the sandwich burning rate were in the gas phase flames (LEFs), and that high burning rate resulted from close proximity of those flames to the burning surface. In the case of sandwiches with catalyzed binder, it was concluded that the catalyst acted at the binder surface by the breakdown of heavy fuel molecules into more reactive species, but that the dominant rate enhancement resulted from greater proximity of the O/F flames to the surface because of the more reactive fuel species. In the case of sandwiches with fine AP added to the binder, it was recognized that the contact area of AP and binder in the solid was enormously increased, posing the possibility of a significant increase in heat release in condensed phase, interfacial, and heterogeneous surface reactions, if any. However, the results suggested that gas phase flames (LLEFs and PLEFs/canopy premixed flames) still controlled the burning rate. In the present study, a catalyst was added to the AP-filled binder, providing greater opportunities for exothermic reactions associated with the greater proximity of the catalyst to O/F interfaces, oxidizer, and all vapors at the surface.

B. Opportunity for Catalytic Action at Different Sites in the Combustion Zone and Its Implications

When discussing the mechanism of catalytic enhancement of the burning rate in the present case, it is important to remember several physical aspects of the test samples and propellants in general, aspects often overlooked in past studies on burning rate catalysis. Items 1–5, shown next, roughly pertain to the condensed phase, items 6–10 pertain to the surface layer, and items 11 and 12 pertain to the gas phase of the propellant combustion zone (Fig. 10).

1) The catalyst is present in test samples only in the binder, poorly situated to directly catalyze the oxidizer in the condensed phase.

2) The catalyst has the opportunity to affect the oxidizer in the condensed phase only at the oxidizer/binder interfacial surfaces.

3) The catalyst may be able to directly act on the binder in the condensed phase within the thermal wave.

4) Catalytic action in the condensed phase, on the binder, and/or at the interfacial surfaces, might a) be exothermic, b) accelerate the condensed phase decomposition of the ingredients, and/or c) alter the decomposition vapors, probably into a more reactive species. As for item a, catalytic action on conventional hydrocarbon binders is expected not to be exothermic, but catalyzed interfacial surface reactions might be. Exothermicity in the condensed phase is effective in terms of heat feedback and rate enhancement. An additional implication of such a mechanism is a relatively higher catalytic effectiveness at low pressures, and vice versa.[33] Item b would merely allow the surface of the ingredient that pyrolyzes faster to be recessed more,[34] without considerably affecting the burning rate. Item c is a potential mechanism because it would facilitate the gas phase flames being held closer to the burning surface, and thereby increase the burning rate.

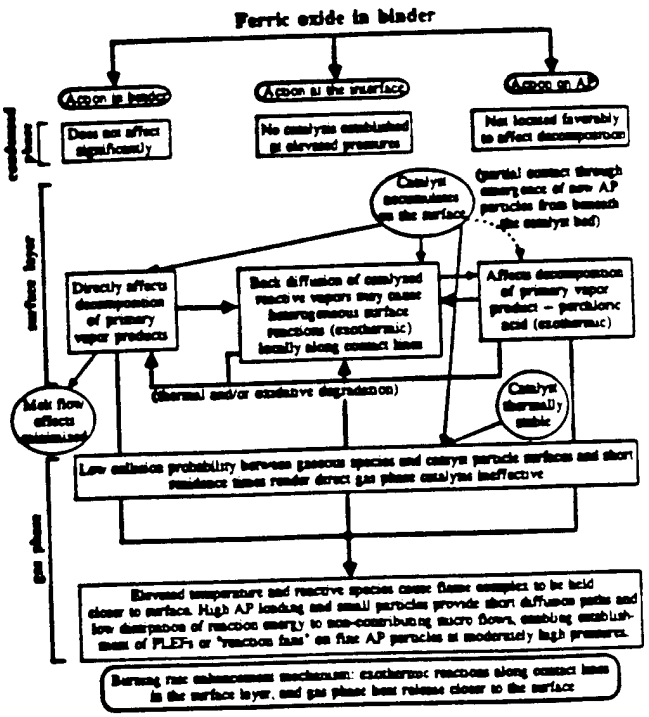

Fig. 10 Overview schematic of the mechanistic arguments for the action of ferric oxide in the combustion of AP composite propellants.

5) In considering factors that influence the burning rate, it is important not only to note sites of exothermic heat release, but also regions (usually) adjacent to those sites that are receptors of heat, but not contributors to local heat release. With fine oxidizer particles, the increase in the interfacial area facilitates enhanced thermal diffusion between oxidizer particles and adjacent binder layers, so that the heat generated at interfacial surfaces can be readily distributed uniformly into parts of the solid that do not directly participate in the local exothermic reactions.

6) The catalyst has been observed in the past,[2,6] and the present studies to concentrate on the binder surface, providing an enhanced opportunity for the breakdown of primary fuel decomposition products into more reactive vapor species.

7) With very small oxidizer particle size, the catalyst concentration may be encountered by some of the primary oxidizer vapors, raising the possibility of a catalyzed near-surface breakdown of some of those primary oxidizer product vapors. With AP oxidizer, it is quite likely that the catalyzed decomposition of $HClO_4$ is accompanied by exothermic heat release,[10] and more reactive oxidizer species.

8) With a very fine oxidizer, the diffusion distances for heterogeneous surface reactions are short, i.e., all oxidizer vapor is near fuel surfaces, and all fuel vapor is near oxidizer surfaces, increasing the possible role of vapor–surface O/F reactions. The presence of the catalyst can further enhance such reactions.

9) Besides the possibility noted in item 8, the opportunity exists for catalytic decomposition vapors of fuel and oxidizer to undergo gas phase (exothermic) reactions in the mixing region along the oxidizer/binder contact lines while diffusing to each other's surfaces.

10) Remarks about thermal diffusion in the solid made in item 5 are also pertinent to near-surface and heterogeneous reactions noted in items 6–9.

11) Fe_2O_3 is thermally stable up to ~1000°C (Ref. 9). Therefore, it would remain in condensed form in most of the combustion zone, except possibly as it enters the gas phase flame. Considering the low initial concentration of the catalyst in the propellant, and the fact that it accumulates on the surface, catalyst particles may, at best, be sporadically distributed in the gas phase at any instant of time. Thus, the catalyst does not have much opportunity to catalyze the LEF reactions directly because such flames are thin, and the opportunity for catalysis is small because of low collision probability with catalyst particles in the thin O/F flamelets. To the extent that direct flame catalysis might be present, one would expect the effect to be proportional to concentration used in the propellant, a corollary contrary to the test results (Fig. 2).[15] Thus, it seems that catalysis in the gas phase has a minimal role in influencing burning rate.

12) On the other hand, if the inclusion of the catalyst can result in exothermic heat release at or below the surface, and/or release more reactive fuel and oxidizer species into the gas phase, it can cause the gas phase flame complex to stand closer to the surface, and increase the burning rate correspondingly. It appears that this could potentially change the gas phase flame structure, the implications of which will be addressed later.

C. Present Results

The new results described in the last section indicate that the use of iron catalysts in the fine AP/binder matrix lamina produced a much larger enhancement in sandwich rates than did the addition of either catalyst[6,7,24] or AP alone[25,26] to the binder lamina. The catalyst also enhanced the rate of the matrix burning alone (Fig. 2a), and led to matrix burning under conditions for which the uncatalyzed matrix would not burn alone [binder melt + fine AP (Figs. 7 and 8), and more fuel-rich mixtures (Fig. 2b)]. The burning rates of sandwiches with catalyzed matrices were relatively insensitive to matrix lamina thickness (Fig. 2). All of these effects are indicative of an enhanced role for the matrix in determining the burning rate when the iron catalyst is present. The extent of the enhanced role for the catalyzed matrix appears to be dependent on the AP/binder mixture fraction and the size of the AP particles, but not on the dispersibility of the catalyst in the binder or the susceptibility of the binder to melt. The implications of these dependencies will be discussed next.

1. *Effect of Dispersibility of the Catalyst*

The different iron catalysts (dispersed differently in the binder) retain differences in their structural identity only beneath the surface, but all emerge as a fine bed of black particles accumulated on the surface (see Secs. IV.G.1 and IV.G.2). However, the dependence of the burning rate on the difference in the way the iron catalysts are dispersed beneath the surface is negligible (Fig. 9).[2,11] Iron atoms are contained in Fe_2O_3 when particulate catalysts are used, and in ferrocenic structures in Catocene and Butacene, with the latter being attached to binder molecules. Considering that catalytic effectiveness depends upon contact with AP oxidizer (discussed next), and assuming that the chemical mechanism of action of all these catalysts is fundamentally the same, it is unlikely that the different catalysts would have the same opportunity for action in the condensed phase. Furthermore, the pressure dependence of the matrix burning rate is preserved, even with the inclusion of the catalyst (e.g., Fig. 9a); in other words, there is an overall increase in burning rate with the catalyst present, without particular preference to any pressure level in the 0.69–6.9 MPa pressure range. To the contrary, any exothermicity in the condensed phase caused by the catalyst would result in a lower pressure exponent of the catalyzed matrix rate than the uncatalyzed matrix rate, i.e., more catalytic effectiveness at low pressure. These considerations indicate that the condensed phase is not the location of prominent action of the catalyst in the 0.69–6.9 MPa range. The catalytic effectiveness of the sandwich burning rates (Fig. 9b) weakens with an increase in pressure because of the increased predominance of the LLEFs in the uncatalyzed sandwiches at higher pressures. This indicates that catalysis of the LLEFs (by way of more reactive species) is probably not the primary mechanism controlling the burning rate of the catalyzed AP-filled binder sandwiches.

2. *Effect of Oxidizer Type*

The relatively weak (or negative) effect of the iron catalysts on burning rate with non-AP oxidizers (Fig. 6) indicates that either 1) the oxidizer–fuel reactions are not important contributors to heat flow to the surface, or 2) the non-AP oxidizer reactions are not catalyzed by iron catalysts. For instance, HMX/PBAN reactions are not considered as important, but KP/PBAN reactions are considered adequately exothermic to influence burning rate. The noneffect of Fe_2O_3 on KP-based samples (Fig. 6)[14,15] lends support to the view in 2. Among the oxidizers that were tested, AP was unique in that one of its two primary decomposition products is $HClO_4$. This gives rise to the possibility of a variety of heterogeneous and vapor phase reactions involving Fe_2O_3, some exothermic, such as 1) catalyzed decomposition of $HClO_4$ (Refs. 10, 13–15) (products of which may, in turn, accelerate binder destruction),[20] 2) catalysis of $HClO_4$ + binder → products,[21] and/or 3) the formation of thermally unstable intermediates such as iron perchlorate amines (with associated heat release).[10,18,22] With item 1, indeed, lighter fuel fragments are reported with finer AP particles.[9]

But recall that the catalyst is primarily in the binder. With fine AP particles, the opportunity for the catalyst concentration on the surface to come in contact with AP primary decomposition vapors along the AP/binder contact lines is enormous. Furthermore, the finer the dispersion of the catalyst in the binder, the more uniform the web of concentrated catalyst on the surface, allowing for the possibility of direct contact between the catalyst and new AP particles emerging on the surface from beneath the web. An immediate implication of such a scenario is that the catalyst may not be very effective if it is of comparable particle size to the oxidizer particles. This is indeed attested to by the results of this study (see Sec. IV.G.2, third paragraph).

3. *Effect of Fine AP Size*

Figure 8 clearly shows that the effect of Fe_2O_3 increases with a decrease in fine AP particle size. Since direct action of the catalyst in the condensed phase or gas phase is unlikely, as discussed previously, the remaining plausible scenarios that can explain this effect are: 1) increased catalytic action, gas phase and heterogeneous, along the contact lines between AP particles and the binder in the surface layer that are increased by decreasing particle size; and 2) attachment of gas phase PLEFs in the mixing fans arising from the contact lines of the AP particles, which may increase in number as a result of a decrease in particle size. Considering that Pyrocat is much finer than the smallest AP size tested (the 2-μm AP), the results in Fig. 8 strongly support the possibility in 1, as also suggested in the last paragraph. The possibility suggested in 2 is not mutually exclusive to that in 1; in other words, they can happen simultaneously. This will be addressed in some detail later. However, since the mixing distances in the gas phase would be very short for the 2-μm AP particles, it is unlikely that PLEFs can be attached before complete mixing takes

place. But the catalytic effect is maximum with the 2-μm AP particles (Fig. 8). The possibility in 2 is speculative in view of this aspect.

4. Effect of Binder Melt Flow

The presence of binder melt flows 1) significantly affects the flammability of fuel-rich mixtures such as the matrices tested in this study, 2) reverses the trend of AP particle size effect on burning rate, and 3) is also strongly associated with the plateau and mesa burning behavior of sandwiches.[10] It is notable that the presence of iron catalysts tends to support combustion of fuel-rich mixtures, independent of the degree of susceptibility of the binder to melt (Fig. 7), re-establishes the particle size effect trend (Fig. 8), and eliminates the plateau-burning features attributed to melt flow (Figs. 7 and 8). The effect of binder melt flows can be better explained when the importance of the microscopic regions along fine AP/binder contact lines in the matrix is considered because this is the region where the melt flow is most intrusive on the adjacent AP particles. The present results suggest that the catalyst may initiate or catalyze exothermic reactions at sites aligned with the contact lines that accelerate the decomposition of binder melts that would otherwise flow onto AP surfaces and cause the anomalous effects listed earlier. Unfortunately, these three-dimensional microscopic details (e.g., of the 1-μm scale) are not resolvable in photography, and surface details appear to be obscured in quench tests by binder melt flow during or after flame quench (even for binders that are less susceptible to melt, e.g., PBAN).

The amount of heat release from these reactions may not be large because of the limitation on the availability of reactants at the reaction sites, but such reactions may be important because of the abundance of such reaction sites with the inclusion of fine AP particles, and their strategic location along contact lines close to or at the surface.

5. Interpretation of Surface Features

The catalytic exothermic reactions at the O/F contact lines would furnish hotter and more reactive vapor species for reaction at the gas phase flame (premixed or LEF). This is conducive to greater proximity of the flame complex to the surface than in the absence of the catalyst. The quenched surface features of catalyzed sandwiches (Figs. 3 and 4) may be explained based on the previous scenario. The enormity of interfacial contact in the fine AP/binder matrix lamina affords a net heat release sufficient to pyrolyze the matrix without having to cause lateral heat drain from the adjoining AP laminae, preventing retarded regression of the lamina AP immediately adjacent to the interface. The external heating of the lamina AP self-deflagration in the immediate vicinity of the interface edge by the LLEFs is speculated to cause the thin liquid layer on the deflagrating AP surface to dry up, resulting in a parched appearance of the surface in that region. (The smooth quality of the AP lamina in the corresponding region of an uncatalyzed sandwich is speculated to be caused by the dissociative sublimation of AP, owing to lateral heat loss to the binder/matrix lamina.[23]) The greater proximity of the LLEFs to the lamina interface edges (compared to the case of uncatalyzed sandwich) explains the smaller width of the dry band (when compared to the smooth band of the uncatalyzed sandwich).

D. Implications on the Gas Phase Flame Structure

The closer location of the overall flame complex would increase the temperature gradient in the gas phase and provide increased heat feedback to the surface, thereby causing the burning rate to increase. However, the details of how the gas phase flame above the fine AP/binder matrix lamina responds to exothermic reactions along the contact lines in the presence of the catalyst is not clear (because of the lack of direct observation). It appears that the catalyzed breakdown of both the binder and oxidizer primary decomposition products (the latter accompanied by heat release), would produce hotter and more reactive species (than without the catalyst) in the micro O/F mixing fans above the AP/binder contact lines, as mentioned earlier. It is not hard to visualize, then, the possibility of a buildup of subsequent exothermic O/F reactions along these mixing fans in a diffusion limited fashion. The limitations on such reactions are 1) the diffusion length scales dictated by AP particle size, the thickness of adjacent binder layers (governed by matrix mixture fraction), and the extent of peripheral contact between the oxidizer particles and the catalyst; and 2) upstream–lateral thermal diffusion from the mixing fans to adjacent nonparticipating species both in the gas phase and particularly in the condensed phase that needs to be pyrolyzed, again dictated by the same geometric factors as in 1. Such a three-dimensional mass and energy balance applied locally to these microscopic sites would, in reality, yield fairly low temperatures for reactions in the mixing fans in the immediate vicinity of the AP/binder contact lines on the surface. For this reason, such reaction fans attached to AP particles (if present) would not behave like conventional diffusion (Burke–Schumann) flames, but with an axially increasing temperature and reactivity (greatest along the stoichiometric contours in the mixing fans) in the immediate vicinity of the surface. If the catalytic action is less, or the upstream heat loss is greater, then reactivity near the surface would be less, and the reaction fans may be replaced by PLEFs. Under favorable conditions of high AP fraction and optimum (explained shortly) particle size in the matrix, it is quite possible that such reaction fans or PLEFs are established in the presence of the catalyst, whereas the corresponding uncatalyzed matrix may burn with a premixed canopy flame considerably far away from the surface. The reason for the optimum size stipulation is as follows: the finer the AP size, the greater the contact line density, the greater the total catalytic heat release at the contact lines, and the lesser the thermal burden on the reaction fans. Finer AP size also implies shorter diffusion distances, which means the reactants may mix completely before appreciable heat release above the contact lines, and burn in a premixed flame slightly farther away (still much closer than in the uncatalyzed case). Note that the optimum size stipulation is for the existence of reaction fans or PLEFs and is not to imply higher burning rates as being associated with reaction fans or PLEFs as opposed to a premixed flame. The following subsection is aimed at further clarifying the gas phase details.

In the case of an AP (10-μm)/PBAN = 5/5 matrix, the uncatalyzed matrix does not burn, whereas the catalyzed matrix sustains combustion in a smoldering fashion with low burning rates that exhibit negligible pressure dependence. In such a case, it is very likely that the heat loss to the excess binder precludes establishment of reaction fans or PLEFs, and the pyrolysis is barely sustained by the catalytic reactions along the AP/binder contact lines. When such a matrix is sandwiched between AP laminae, significant assistance is obtained by these surface-layer reactions from the LLEFs in the vicinity of the lamina interface edge, probably by way of an increased temperature at which to react. The result is a tremendous jump in the burning rate for the sandwiches when compared to the matrix burning alone (Fig. 2b). The sandwich surface profile also exhibits a conspicuous protrusion of the central portion of a very thick matrix lamina (Fig. 5a), commensurate with such a hypothesis.

In the case of the sandwiches with catalyzed 10-μm AP/PBAN = 7/3 matrix, there is no protrusion of the matrix lamina (Fig. 5b). In such a situation, it is not clear whether the matrix burning proceeds with a premixed flame or with PLEFs/reaction fans; the AP loading and particle sizes are not unfavorable for the establishment of PLEFs or reaction fans. Recall that the uncatalyzed 7/3 matrix is expected to burn with a premixed flame at the pressures tested.[26] However, since the PLEFs or reaction fans in the catalyzed matrix would be closer to the surface than the LLEFs above the lamina interface edges (owing to the catalytic action), it is likely that a matrix (alone) with PLEFs or reaction

fans burns just as fast as, or faster than, its corresponding sandwich. The results of this study are contrary to such an expectation, i.e., the sandwich rates are almost always greater than the corresponding matrix rates for the present test variables. Therefore, the matrix lamina in these tests most probably burns with a premixed flame, held closer to the surface (along with the LLEFs) than in the uncatalyzed case. The LLEFs do not directly control the burning rate as in the uncatalyzed case, but do so in interaction with the catalytic reactions and the matrix gas phase flame (premixed or PLEF/reaction fan array). For this reason, the interaction between adjacent LLEFs is weakened relative to the matrix processes, and this is borne out by the weaker peaks in the burning rate vs matrix lamina thickness curves of the catalyzed sandwiches when compared to the corresponding uncatalyzed sandwich curves (Fig. 2).

VI. Conclusions

The results of the present study indicate that the Fe_2O_3 catalyst in AP/hydrocarbon binder propellants can act by multiple paths to increase the burning rate. As reported earlier,[6,7,24] the catalyst is located in the binder and concentrates on the surface, and is best suited to alter the fuel decomposition products. However, the present results with fine particulate oxidizer-filled matrices indicate that the catalyst enhances exothermic reactions at, and/or very close to the surface along the oxidizer-binder contact lines on the surface. These reactions become an increasingly important source of heat release and reactive fuel and oxidizer species as the density of contact lines increases with decreasing AP particle size and increasing proportion of AP in the AP/binder matrix.

Acknowledgments

This work was performed under Contract N00014-89-J-1293 with the U.S. Office of Naval Research, with Richard S. Miller as the Technical Monitor. Useful guidance was offered by Russell Reed, U.S. Naval Air Warfare Center, China Lake, California. Some ingredients used in this study were supplied by Woodward Waesche, Science Applications International Corp.; Carol Hinshaw and Robert Wardle, Thiokol Corporation; John Murphy, Elf Atochem North America, Inc.; and Elizabeth Katres, Hüls America, Inc.

References

[1]Kishore, K., and Sunitha, M. R., "Effect of Transition Metal Oxides on Decomposition and Deflagration of Composite Solid Propellant Systems: A Survey," *AIAA Journal*, Vol. 17, No. 10, 1979, pp. 1118–1125.

[2]Lengellé, G., Brulard, J., and Moutet, H., "Combustion Mechanisms of Composite Solid Propellants," *Proceedings of the 16th Symposium (International) on Combustion*, The Combustion Inst., Pittsburgh, PA, 1976, pp. 1257–1269.

[3]Handley, J. C., and Strahle, W. C., "Behavior of Several Catalysts in the Combustion of Solid Propellant Sandwiches," *AIAA Journal*, Vol. 13, No. 1, 1975, pp. 5, 6.

[4]Fong, C. W., and Hamshere, B. L., "The Mechanism of Burning Rate Catalysis in Composite HTPB—AP Propellant Combustion," *Combustion and Flame*, Vol. 65, 1986, pp. 61–69.

[5]Fong, C. W., and Hamshere, B. L., "The Mechanism of Burning Rate Catalysis in Composite Propellants by Transition Metal Complexes," *Combustion and Flame*, Vol. 65, 1986, pp. 71–78.

[6]Price, E. W., and Sambamurthi, J. K., "Mechanism of Burning Rate Enhancement by Ferric Oxide," *Proceedings of the 21st JANNAF Combustion Meeting*, Chemical Propulsion Information Agency, Publ. 412, Vol. 1, 1984.

[7]Price, E. W., Sambamurthi, J. K., and Sigman, R. K., "Further Results on the Combustion of AP/Polymer Sandwiches with Additives," *Proceedings of the 22nd JANNAF Combustion Meeting*, Chemical Propulsion Information Agency, Publ. 432, Vol. 1, 1985.

[8]Krishnan, S., and Jeenu, R., "Subatmospheric Burning Characteristics of AP/CTPB Composite Propellants with Burning Rate Modifiers," *Combustion and Flame*, Vol. 80, 1990, pp. 1–6.

[9]Krishnan, S., and Jeenu, R., "Combustion Characteristics of AP/HTPB Propellants with Burning Rate Modifiers," *Journal of Propulsion and Power*, Vol. 8, No. 4, 1992, pp. 748–755.

[10]Pearson, G. S., "The Role of Catalysts in the Ignition and Combustion of Solid Propellants," *Combustion Science and Technology*, Vol. 3, 1971, pp. 155–163.

[11]Bobolev, V. K., Gen, M. Y., Mal'tsev, V. M., Melesov, G. P., Pokhil, P. F., Seleznev, V. A., Stasenko, A. N., and Chuiko, S. V., "Mechanism of Action of Iron Catalysts on the Combustion of Composite Systems," *Fizika Goreniya i Vzryva*, Vol. 7, No. 3, 1971, pp. 366–375.

[12]Jones, H. E., and Strahle, W. C., "Effects of Copper Chromite and Iron Oxide Catalysts on AP/CTPB Sandwiches," *Proceedings of the 14th Symposium (International) on Combustion*, The Combustion Inst., Pittsburgh, PA, 1973, pp. 1287–1295.

[13]Ermolaev, B. S., Korotkov, A. I., and Frolov, Y. V., "Study of the Action of Catalysts Using Layered Systems," *Fizika Goreniya i Vzryva*, Vol. 5, No. 2, 1969, pp. 286–289.

[14]Pittman, C. U., Jr., "Location of Action of Burning-Rate Catalysts in Composite Propellant Combustion," *AIAA Journal*, Vol. 7, No. 2, 1969, pp. 328–334.

[15]Bakhman, N. N., Nikiforov, V. S., Avdyunin, V. I., Fogelzang, A. E., and Kichin, Y. S., "Catalytic Effect of Ferrous Oxide on Burning Rate of Condensed Mixtures," *Combustion and Flame*, Vol. 22, 1974, pp. 77–87.

[16]Strahle, W. C., Handley, J. C., and Milkie, T. T., "Catalytic Effects in the Combustion of AP-HTPB Sandwiches to 3200 PSIA," *Combustion Science and Technology*, Vol. 8, 1974, pp. 297–304.

[17]Boggs, T. L., Zurn, D. E., Cordes, H. F., and Covino, J., "Combustion of Ammonium Perchlorate with Various Inorganic Additives," *Journal of Propulsion and Power*, Vol. 4, No. 1, 1988, pp. 27–40.

[18]Kishore, K., and Sunitha, M. R., "Mechanism of Catalytic Activity of Transition Metal Oxides on Solid Propellant Burning Rate," *Combustion and Flame*, Vol. 33, 1978, pp. 311–314.

[19]Krishnan, S., and Periasamy, C., "Low-Pressure Burning of Catalyzed Composite Propellants," *AIAA Journal*, Vol. 24, No. 10, 1986, pp. 1670–1675.

[20]Korobeinichev, O. P., Anisiforov, G. I., and Tereschenko, A. G., "High-Temperature Decomposition of Ammonium Perchlorate-Polystyrene-Catalyst Mixtures," *AIAA Journal*, Vol. 13, No. 5, 1975, pp. 628–633.

[21]Korobeinichev, O. P., Kovalenko, K. K., and Lesnikovich, A. I., "Investigation of Effect of Oxide and Organometallic Catalysts on Thermal Decomposition and Combustion of a Model Ammonium Perchlorate-Polymer System," Plenum, New York, 1978.

[22]Kishore, K., Pai Verneker, V. R., and Sunitha, M. R., "Action of Transition Metal Oxides on Composite Solid Propellants," *AIAA Journal*, Vol. 18, No. 11, 1980, pp. 1404, 1405.

[23]Price, E. W., Sambamurthi, J. K., Sigman, R. K., and Panyam, R. R., "Combustion of Ammonium Perchlorate-Polymer Sandwiches," *Combustion and Flame*, Vol. 63, 1986, pp. 381–413.

[24]Markou, C. P., "Effect of Different Binders and Additives on Sandwich Burning," Ph.D. Dissertation, Georgia Inst. of Technology, Atlanta, GA, May 1988.

[25]Lee, S.-T., "Multidimensional Effects in Composite Propellant Combustion," Ph.D. Dissertation, Georgia Inst. of Technology, Atlanta, GA, May 1991.

[26]Lee, S.-T., Price, E. W., and Sigman, R. K., "Effect of Multidimensional Flamelets in Composite Propellant Combustion," *Journal of Propulsion and Power*, Vol. 10, No. 6, 1994, pp. 761–768.

[27]Price, E. W., "Effect of Multidimensional Flamelets in Composite Propellant Combustion," *Journal of Propulsion and Power*, Vol. 11, No. 4, 1995, pp. 717–728.

[28]Prasad, K., and Price, E. W., "A Numerical Study of the Leading Edge of Laminar Diffusion Flames," *Combustion and Flame*, Vol. 90, 1992, pp. 155–173.

[29]Fenn, J. B., "A Phalanx Flame Model for the Combustion of Composite Solid Propellants," *Combustion and Flame*, Vol. 12, June 1968, pp. 201–216.

[30]Chakravarthy, S. R., Price, E. W., and Sigman, R. K., "Binder Melt Flow Effects in the Combustion of AP-HC Composite Solid Propellants," AIAA Paper 95-2710, July 1995.

[31]Price, E. W., Chakravarthy, S. R., Zachary, E. K., and Sigman, R. K., "Ingredient Response and Interaction During Heating on a Hot Stage Microscope," *Proceedings of the 31st JANNAF Combustion Meeting*, Chemical Propulsion Information Agency, Publ. 620, Oct. 1994.

[32]Chen, J. K., Cheng, S. S., and Chou, S. C., "DSC, TG and Infrared Spectroscopic Studies of HTPB and Butacene Propellant Polymers," AIAA Paper 94-3176, June 1994.

[33]Krishnan, S., and Jeenu, R., "A Surface Reaction Model for Catalyzed Composite Propellants," *AIAA Journal*, Vol. 30, No. 11, 1992, pp. 2788–2791.

[34]Deur, J. M., and Price, E. W., "Steady State One-Dimensional Pyrolysis of Oxidizer-Binder Laminates," AIAA Paper 86-1446, June 1986.

Appendix E

Prasad paper

Appendix E

A Numerical Study of the Leading Edge Laminar Diffusion Flames

Combustion and Flame

Volume 90, Number 2, August 1992, pp 155-173

COMBUSTION AND FLAME 90: 155–173 (1992)

A Numerical Study of the Leading Edge of Laminar Diffusion Flames

K. PRASAD* and E. W. PRICE
School of Aerospace Engineering, Georgia Institute of Technology, Atlanta, GA 30332

This study deals with a fundamental numerical investigation of chemically reacting fluid flows through two-dimensional burners. We make use of a detailed set of finite chemical kinetic rate equations to numerically simulate a laminar diffusion flame. The code has been constructed to consider the viscous effects in a mixing layer, heat conduction, the multicomponent diffusion and convection of important species, the finite rate reactions of these species, and the resulting interactions between the fluid mechanics and the chemistry. The numerical model has been used to obtain a detailed description of the leading edge of laminar diffusion flames obtained above two-dimensional methane/air burners. It is shown that the leading edge flame, a flame holding point for the rest of the diffusion flame, is dominated by the kinetic aspects of the fuel/oxidizer species and is mainly responsible for heat transfer to any upstream boundary surface.

INTRODUCTION

Most practical combustion systems involve flames in regions of mixing oxidizer and fuel vapors as in gas turbines, rocket engines, and commercial furnaces. The overall combustion is governed by a complex interplay of chemical reactions, transport, and gas dynamic processes that are strongly dependent on physical boundary conditions and type of chemical system. The ability to predict the coupled effects of various complex transport processes and chemical kinetics in these systems is critical in predicting flammability limits, stability criteria, and extinction limits. The studies described here were originally motivated by conditions pertinent to combustion of heterogeneous solid rocket propellants, but are descriptive of the flames in burners commonly referred to as "Wolfhard" burners, which are often used for laboratory scale studies of diffusion flames, combustion kinetics, and pollutant formation.

A numerical model was constructed for the purpose of understanding the interplay of diffusion, convection, and chemical reactions, and the resulting flame complex when a laminar mixing flow undergoes exothermic chemical reactions. Figure 1 provides a schematic diagram of the burner geometry and the computational domain in which the solution is desired. The classical description of a diffusion controlled flame in such a configuration pictures a thin flame in the mixing region that extends all the way to the burner surface. In the present study there was particular concern with that region of the flame near the burner surface, where heat loss from the reaction region to surrounding flow limits the temperature rise and thus limits reaction rates. In this region close to the initial point of fuel–oxidizer contact the assumption of diffusion limited flames are inapplicable, and detailed consideration of coupled thermal and species diffusion and chemical reaction rates is required for a realistic description of the flame complex.

Near the burner surface, the concentration gradients of primary reactants are high, and mixing rates correspondingly high. Chemical reaction rates are low because of the relatively low temperatures, so that a small region of partially premixed reactants develops, which is increasingly heated as it moves outwards towards a flame that stabilizes in the mixing region. The leading edge of this flame (referred to here as the "leading edge flame" or "LEF") differs from the trailing diffusion limited flame in that it stands in a region of premixed gases that are continuously premixed

* Corresponding author. Present address: Department of Theoretical and Applied Mechanics, UIUC, Urbana, IL 61801.

Published by Elsevier Science Publishing Co., Inc.

0010-2180/92/$5.00

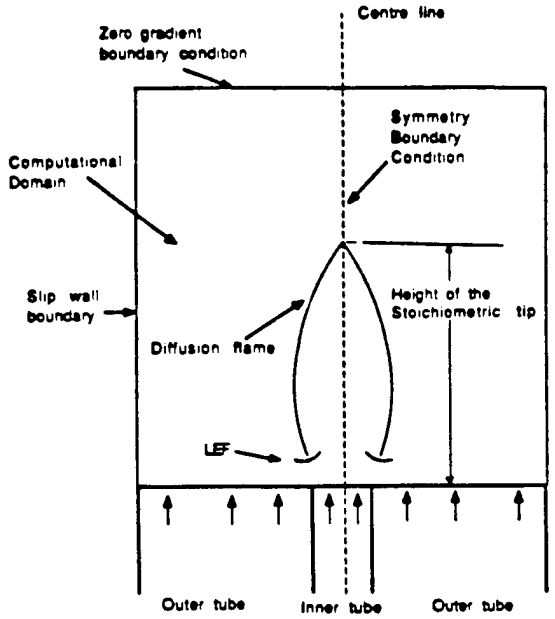

Fig. 1. Schematic diagram of burner geometry and computational domain.

in the approach flow and lead to very concentrated reaction because of the premixing. The flame cannot move upstream all the way to the burner surface, and must stabilize at some location where the temperature-dependent reaction rate can provide heat release rate consistent with multidimensional heat outflow. The details of this complex flame region are not well known because it is usually very small, and difficult to observe experimentally. It is equally difficult to describe analytically because of the necessity to consider coupled convective flow, species diffusion, heat transfer, and reaction processes in at least two space dimensions.

The numerical model examines the leading edge portion of the diffusion flame. It is shown that the leading edge portion of the diffusion flame has the maximum rate of heat release per unit volume and is dominated by the kinetic aspects of the fuel-oxidizer species. This complicated type of flame arrangement has been observed experimentally by Phillips [1], Liebman et al. [2], and Ishikawa [3]. Price et al. [4] performed a series of experimental studies of edge burning sandwiches of binder (fuel) between two solid AP oxidizer laminas, and the results were used to develop a detailed qualitative model for the combustion zone microstructure. Wichman [5] has constructed a mathematical model of the leading edge portion of a diffusion flame formed over two initially separated co-flowing streams of fuel and oxidizer. The temperature field was analyzed in the pure diffusion flame region, in the premixed flame region, in the pure quenching region, and in the "triple point region" where all of the separate zones meet. Dold [6] has developed a low heat-release model for triple flame structure and have shown that triple-flame propagation speed depend on the transverse mixture fraction gradient and is bounded above by the maximum adiabatic laminar flame speed of the system.

Most of the computationally oriented combustion studies that have appeared in the literature that use detailed chemistry have focused on steady, one-dimensional flames, that is, freely propagating or burner stabilized premixed flames [7] and counterflow premixed [8] or diffusion flames [9]. A comprehensive survey of the numerical techniques currently employed in detail combustion modeling have been provided by Oran and Boris [10, 11].

McMurtry et al. [12] studied the effect of chemical heat release on a subsonic, temporally developing mixing layer. They solved both the compressible form of the governing equations as well as a more computationally efficient form of the equations valid for low Mach numbers. Reactions were modeled with a binary, single-step irreversible reaction. Drummond and Hussaini [13] used a detailed hydrogen kinetic scheme to develop an implicit procedure for studying a reacting mixing layer. Bussing and Murman [14] developed a finite volume method for calculation of compressible chemically reacting flows. The techniques include the implicit treatment of the chemical source term, point implicit multiple grid accelerator and a constant CFL condition. Eklund et al. [15] used both Runge Kutta and Adams predictor corrector method for computations involving reaction rate terms.

Smooke et al. [16] used a detailed chemistry transport combustion model for studying axisymmetric laminar diffusion flames in which a cylindrical fuel stream is surrounded by a co-flowing oxidizer jet. They used vorticity and stream function to eliminate pressure as one of

the dependent variables. The diffusion velocities were obtained using a modified Fick's law. They also utilized a thin, infinitely fast, global reaction model as a starting point for the determination of good initial solution estimates for their finite rate axisymmetric model.

In this research a numerical model has been constructed for the study of two-dimensional multicomponent chemically reacting fluid flows with detailed kinetics, variable transport, and thermodynamic properties. The model is used to obtain a detailed description of the leading edge portion of laminar diffusion flames.

MATHEMATICAL FORMULATION

Modeling gas-phase reactive flows is based on a generally accepted set of time-dependent, coupled partial differential equations maintaining conservation of total density, momentum, total energy, and individual species density. These equations describe the convective motion of the fluid, the chemical reactions among the constituent species, and the diffusive transport processes such as thermal conduction and molecular diffusion.

Governing Equations

A strong conservation form of the two-dimensional, unsteady, compressible Navier–Stokes equations, used to describe gas-phase reactive flows for a system containing N species undergoing M elementary chemical reactions [17] can be written as follows:

$$\partial_t \vec{q} + \partial_x \vec{E} + \partial_y \vec{F} = \partial_x \vec{R} + \partial_y \vec{S} + \vec{K}, \tag{1}$$

where $\vec{q}$, $\vec{E}$, $\vec{F}$, $\vec{R}$, $\vec{S}$, and $\vec{K}$ are vectors defined as

$$\vec{q} = \begin{bmatrix} \rho \\ \rho u \\ \rho v \\ \rho e_t \\ \rho_k \end{bmatrix}, \quad \vec{E} = \begin{bmatrix} \rho u \\ \rho u^2 + P \\ \rho uv \\ (\rho e_t + P)u \\ \rho_k u \end{bmatrix}, \quad \vec{F} = \begin{bmatrix} \rho v \\ \rho uv \\ \rho v^2 + P \\ (\rho e_t + P)v \\ \rho_k v \end{bmatrix},$$

$$\vec{R} = \begin{bmatrix} 0 \\ \tau_{xx} \\ \tau_{xy} \\ -q_x + u\tau_{xx} + v\tau_{xy} \\ -\rho_k U_k \end{bmatrix}, \quad \vec{S} = \begin{bmatrix} 0 \\ \tau_{xy} \\ \tau_{yy} \\ -q_y + u\tau_{xy} + v\tau_{yy} \\ -\rho_k V_k \end{bmatrix}, \tag{2}$$

$$\vec{K} = \begin{bmatrix} 0 \\ \sum_{k=1}^{N} \rho_k f_{x,k} \\ \sum_{k=1}^{N} \rho_k f_{y,k} \\ \sum_{k=1}^{N} \rho_k (u + U_k) f_{x,k} + \sum_{k=1}^{N} \rho_k (v + V_k) f_{y,k} \\ \dot{\omega}_k \end{bmatrix}.$$

Here ρ and ρ_k are the total mass density and the individual species density; u and v are the bulk fluid velocity components in the x and y direction, respectively, and e_t is the total energy per unit mass. $f_{x,k}$ and $f_{y,k}$ are the body forces per unit mass acting on the kth species in x and y directions, respectively. The viscous stress terms τ_{xx}, τ_{xy}, and τ_{yy} appearing in the

conservation equations are given by

$$\tau_{xx} = \left(\kappa - \frac{2}{3}\mu\right)\left(\frac{\partial u}{\partial x} + \frac{\partial v}{\partial y}\right) + 2\mu\frac{\partial u}{\partial x},$$

$$\tau_{xy} = \mu\left(\frac{\partial u}{\partial y} + \frac{\partial v}{\partial x}\right),$$

$$\tau_{yy} = \left(\kappa - \frac{2}{3}\mu\right)\left(\frac{\partial u}{\partial x} + \frac{\partial v}{\partial y}\right) + 2\mu\frac{\partial v}{\partial y}. \quad (3)$$

The terms q_x and q_y appearing in the total energy equation are the net rate of heat flux in the two coordinate directions and can be expressed as

$$q_x = -\lambda\frac{\partial T}{\partial x} + \sum_{k=1}^{N} \rho_k h_k U_k,$$

$$q_y = -\lambda\frac{\partial T}{\partial y} + \sum_{k=1}^{N} \rho_k h_k V_k. \quad (4)$$

The thermodynamic pressure is defined as

$$P = R^{\circ}T\sum_{k=1}^{N}\frac{\rho_k}{W_k}, \quad (5)$$

where W_k is the molecular weight of the kth species, and R° is the universal gas constant. The caloric equation of state is used to define the enthalpy of the individual species, which in turn is used to define the total energy as follows:

$$\rho e_t = \rho e + \frac{\rho}{2}(u^2 + v^2),$$

$$= \sum_{k=1}^{N}\rho_k\left(h_k^{\circ} + \int_{T^{\circ}}^{T} C_{p,k}\,dT\right) - P + \frac{\rho}{2}(u^2 + v^2). \quad (6)$$

The specific heat for each species is obtained by using a sixth-order polynomial in temperature.

$$C_{p,k} = a_{1,k} + a_{2,k}T + a_{3,k}T^2 + a_{4,k}T^3 + a_{5,k}T^4 + a_{6,k}T^5 + a_{7,k}T^6, \quad k = 1,\ldots,N. \quad (7)$$

The various specific heat coefficients and the heat of formations for the various species are obtained from the JANNAF thermochemical tables. The various diffusion coefficients such as thermal conductivity, binary diffusion coefficients, viscosity, and thermal diffusion coefficient are obtained from a rigorous treatment of kinetic theory [18]. A Lennard Jones potential is constructed to model the intermolecular potential function based on which the collision integrals are evaluated. The various diffusion coefficients are then obtained using detailed kinetic theory and are functions of the temperature, pressure, and the various species properties.

Diffusion Velocity Model

The diffusion velocities in a multicomponent reacting flow mixture may arise because of concentrations gradients, pressure gradients, differential body forces, and due to the Soret effect. The diffusion velocities for each of the N species in both the x and y direction are obtained by solving the exact diffusion equation given by

$$\frac{\partial X_k}{\partial x} = \sum_{j=1}^{N}\left(\frac{X_k X_j}{\mathscr{D}_{kj}}(U_j + U_k)\right) + \frac{(Y_k - X_k)}{P}\frac{\partial P}{\partial x} + \frac{\rho}{P}\sum_{j=1}^{N} Y_k Y_j (f_{k,x} - f_{j,x}),$$

$$\frac{\partial X_k}{\partial y} = \sum_{j=1}^{N}\left(\frac{X_k X_j}{\mathscr{D}_{kj}}(V_j - V_k)\right) + \frac{(Y_k - X_k)}{P}\frac{\partial P}{\partial y} + \frac{\rho}{P}\sum_{j=1}^{N} Y_k Y_j (f_{k,y} - f_{j,y})$$

$$k = 1,\ldots,N. \quad (8)$$

Here X_k and Y_k are the mole and mass fraction of the kth species, respectively. Since only $N-1$ equations of the above N equations are independent of each other, the above equa-

tions are solved subject to the constraint that the diffusion velocities introduce no net momentum to the fluid flow, that is,

$$\sum_{k=1}^{N} \rho_k U_k = \sum_{k=1}^{N} \rho_k V_k = 0. \tag{9}$$

Reaction Kinetic Model

The types of reactions of importance in combustion include unimolecular decomposition reactions, bimolecular exchange, and dissociation reactions, and three-body recombination reactions. The following seven types of chemical reactions have been considered:

1. Unimolecular decomposition $AB \rightleftharpoons A + B$.
2. Bimolecular dissociation $AB + M \rightleftharpoons A + B + M$.
3. Bimolecular $A + B \rightleftharpoons C + D$.
4. Bimolecular exchange/dissociation $AB_2 + C \rightleftharpoons AC + B + B$.
5. Recombination reaction $A + B + B \rightleftharpoons AB + B$.
6. Two-body recombination $C + D \rightleftharpoons CD$.
7. Three-body recombination $C + D + M \rightleftharpoons CD + M$.

Here M is a third-body molecule, and A, B, C, and D are representative species.

For a system containing N species undergoing a set of M elementary chemical reaction, the general ith reaction can be expressed as

$$\sum_{k=1}^{N} \nu'_{k,i} S_k \rightleftharpoons \sum_{k=1}^{N} \nu''_{k,i} S_k, \quad i = 1, \ldots, M. \tag{10}$$

The rate of production of the kth species due to the ith reaction is given by

$$\dot{\omega}_{i,k} = (\nu''_{k,i} - \nu'_{k,i}) \times \left[k_{f,i} \prod_{j=1}^{N} (C_j)^{\nu'_{j,i}} - k_{b,i} \prod_{j=1}^{N} (C_j)^{\nu''_{j,i}} \right], \quad k = 1, \ldots, N, i = 1, \ldots, M \tag{11}$$

and the total rate of production of the kth species is obtained by using

$$\dot{\omega}_k = \sum_{i=1}^{M} \dot{\omega}_{i,k}, \quad k = 1, \ldots, N. \tag{12}$$

The $k_{f,i}$ and $k_{b,i}$ are the forward and reverse reaction rate constants. Each $k_{f,i}$ is a function of temperature usually given by the modified Arrhenius expression

$$k_{f,i} = A_i T^{n_i} \exp\left(\frac{-E_i}{RT}\right), \quad i = 1, \ldots, M. \tag{13}$$

The reverse reaction rate constant $k_{b,i}$ is calculated from $k_{f,i}$ and the equilibrium constant (in concentration units) $K_{c,i}$ by the laws of microscopic reversibility.

$$k_{b,i} = \frac{k_{f,i}}{K_{c,i}}, \quad i = 1, \ldots, M. \tag{14}$$

The equilibrium constant $K_{p,i}$ for the ith general reaction is defined by using the standard change in Gibb's free energy as follows:

$$R \ln K_{p,i} = -\frac{\Delta G_i^{\circ}}{T}, \quad i = 1, \ldots, M. \tag{15}$$

The equilibrium constant $K_{c,i}$ in terms of concentrations is then obtained from

$$K_{c,i} = K_{p,i} (RT) \sum_{k=1}^{N} (\nu''_{k,i} - \nu'_{k,i}), \quad i = 1, \ldots, M. \tag{16}$$

Computations were performed using 42 elementary reactions and 15 species to model methane–air kinetics as shown in Table 1.

Governing Equations in the Transformed Plane

The physical domain (x, y) is highly compressed in both the x, y directions in the region where fuel and oxidizer mix. The grid is required to be uniform in the computational domain to maintain a required order of accuracy. The governing equations 1, written in the physical domain (x, y), must therefore be transformed to an appropriate computational domain (ξ, η) for solution. Let the general transformation be given by

$$\tau = t; \quad \xi = \xi(x, y, t); \quad \eta = \eta(x, y, t), \tag{17}$$

then the governing equations 1 can be written as

$$\partial_\tau q + \partial_\xi E + \partial_\eta F = \partial_\xi R + \partial_\eta S + K, \tag{18}$$

TABLE I

Methane Reaction Scheme

	Reaction Scheme			A	n	E
1	$CH_4 + M$	⇌	$CH_3 + H + M$	0.100E18	0.00	86000.0
2	$CH_4 + O_2$	⇌	$CH_3 + HO_2$	0.790E14	0.00	56000.0
3	$CH_4 + H$	⇌	$CH_3 + H_2$	0.220E05	3.00	8750.0
4	$CH_4 + O$	⇌	$CH_3 + HO$	0.160E07	2.36	7400.0
5	$CH_4 + HO$	⇌	$CH_3 + H_2O$	0.160E07	2.10	2460.0
6	$CH_2O + OH$	⇌	$CHO + H_2O$	0.753E13	0.00	167.0
7	$CH_2O + H$	⇌	$CHO + H_2$	0.331E15	0.00	10500.0
8	$CH_2O + M$	⇌	$CHO + H + M$	0.331E17	0.00	81000.0
9	$CH_2O + O$	⇌	$CHO + OH$	0.181E14	0.00	3082.0
10	$CHO + OH$	⇌	$CO + H_2O$	0.500E13	0.00	0.0
11	$CHO + M$	⇌	$H + CO + M$	0.160E15	0.00	14700.0
12	$CHO + H$	⇌	$CO + H_2$	0.400E14	0.00	0.0
13	$CHO + O$	⇌	$HO + CO$	0.100E14	0.00	0.0
14	$CHO + O_2$	⇌	$HO_2 + CO$	0.300E13	0.00	0.0
15	$CO + O + M$	⇌	$CO_2 + M$	0.320E14	0.00	−4200.0
16	$CO + OH$	⇌	$CO_2 + H$	0.151E08	1.30	−758.0
17	$CO + O_2$	⇌	$CO_2 + O$	0.160E14	0.00	41000.0
18	$CH_3 + O_2$	⇌	$CH_3O + O$	0.700E13	0.00	25652.0
19	$CH_3O + M$	⇌	$CH_2O + H + M$	0.240E14	0.00	28812.0
20	$CH_3O + H$	⇌	$CH_2O + H_2$	0.200E14	0.00	0.0
21	$CH_3O + OH$	⇌	$CH_2O + H_2O$	0.100E14	0.00	0.0
22	$CH_3O + O$	⇌	$CH_2O + OH$	0.100E14	0.00	0.0
23	$CH_3O + O_2$	⇌	$CH_2O + HO_2$	0.630E11	0.00	2600.0
24	$CH_3 + O_2$	⇌	$CH_2O + OH$	0.520E14	0.00	34574.0
25	$CH_3 + O$	⇌	$CH_2O + H$	0.680E14	0.00	0.0
26	$CH_3 + OH$	⇌	$CH_2O + H_2$	0.750E13	0.00	0.0
27	$HO_2 + CO$	⇌	$CO_2 + OH$	0.580E14	0.00	22934.0
28	$H_2 + O_2$	⇌	$OH + OH$	0.170E14	0.00	47780.0
29	$HO + H_2$	⇌	$H_2O + H$	0.117E10	1.30	3626.0
30	$H + O_2$	⇌	$OH + O$	0.513E17	−0.82	16507.0
31	$O + H_2$	⇌	$OH + H$	0.180E11	1.00	8826.0
32	$H + O_2 + M$	⇌	$HO_2 + M$	0.210E19	−1.00	0.0
33	$H + O_2 + O_2$	⇌	$HO_2 + O_2$	0.670E20	−1.42	0.0
34	$H + O_2 + N_2$	⇌	$HO_2 + N_2$	0.670E20	−1.42	0.0
35	$HO + HO_2$	⇌	$H_2O + O_2$	0.500E14	0.00	1000.0
36	$H + HO_2$	⇌	$OH + OH$	0.250E15	0.00	1900.0
37	$O + HO_2$	⇌	$O_2 + OH$	0.480E14	0.00	1000.0
38	$OH + OH$	⇌	$O + H_2O$	0.600E09	1.30	0.0
39	$H_2 + M$	⇌	$H + H + M$	0.223E13	0.50	92600.0
40	$O_2 + M$	⇌	$O + O + M$	0.185E12	0.50	95560.0
41	$H + OH$	⇌	$H_2O + M$	0.750E24	−2.60	0.0
42	$H + HO_2$	⇌	$O_2 + H_2$	0.250E14	0.00	700.0

where

$$q = \vec{q}/J,$$

$$E = \left(\xi_t \vec{q} + \xi_x \vec{E} + \xi_y \vec{F}\right)/J,$$

$$F = \left(\eta_t \vec{q} + \eta_x \vec{E} + \eta_y \vec{F}\right)/J,$$

$$R = \left(\xi_x \vec{R} + \xi_y \vec{S}\right)/J,$$

$$S = \left(\eta_x \vec{R} + \eta_y \vec{S}\right)/J,$$

$$K = \vec{K}/J. \tag{19}$$

Here J is the transformation Jacobian:

$$J = \xi_x \eta_y - \xi_y \eta_x = (x_\xi y_\eta - x_\eta y_\xi)^{-1}. \tag{20}$$

The derivatives ξ_x, η_x, and so on can be easily obtained from the derivatives x_ξ, y_η, and so on

by using the following transformation relations:

$$\xi_x = Jy_\eta;\ \xi_y = -Jx_\eta.$$
$$\eta_x = -Jy_\xi;\ \eta_y = Jx_\xi. \tag{21}$$

NUMERICAL FORMULATION

The governing equations for a chemically reacting viscous fluid flow are parabolic in time. Assuming that the flow quantities are known in the flow field at time level t^n, the purpose of the numerical procedure is to advance the solution to a new level t^{n+1} using a large enough time step, Δt.

The major problem in solving Eq. 18 stems from the presence of widely separated fast and slow kinetic rates, which results in a system of stiff governing equations, along with unstable reaction rate equations. The presence of stiffness and unstable behavior is embedded in the reaction rate equations. This usually dictates intolerably small time steps for time-dependent solutions.

The approach used in the present computations to couple the fluid dynamic equations with the reaction rate terms is known as the time step splitting approach [19]. In this approach the individual processes are solved independently and the changes resulting from the separate partial calculations are coupled (added) together. The qualitative criteria for its validity is that the values of the physical variables must not change too quickly over a time step from any of the individual processes. Since the reaction rate terms are chiefly responsible for the stiffness and unstable behavior, they are decoupled from the fluid dynamics over the smallest fluid dynamic time marching step. The reaction rate equations at each grid point are then subcycled over each fluid dynamic time marching step.

The numerical scheme used in the present work for integrating the fluid dynamic equations is a predictor corrector explicit time marching procedure [20, 21]. The model is second-order accurate in both time and space. The complete set of Navier Stokes equations 18 are considered in the transformed plane:

Predictor

$$\begin{aligned} q_{I,K}^{\overline{n+1}} = q_{I,K}^{n} &- \Delta t(E_{I+1,K}^{n} - E_{I,K}^{n}) \\ &- \Delta t(F_{I,K+1}^{n} - F_{I,K}^{n}) \\ &+ \Delta t(R_{I+1,K}^{n} - R_{I,K}^{n}) \\ &+ \Delta t(S_{I,K+1}^{n} - S_{I,K}^{n}) \end{aligned} \tag{22}$$

Corrector

$$\begin{aligned} q_{I,K}^{n+1} = \tfrac{1}{2}\Big[& q_{I,K}^{n} + q_{I,K}^{\overline{n-1}} \\ &- \Delta t\left(E_{I,K}^{\overline{n+1}} - E_{I-1,K}^{\overline{n+1}}\right) \\ &- \Delta t\left(F_{I,K}^{\overline{n-1}} - F_{I,K-1}^{\overline{n+1}}\right) \\ &+ \Delta t\left(R_{I,K}^{\overline{n+1}} - R_{I-1,K}^{\overline{n+1}}\right) \\ &+ \Delta t\left(S_{I,K}^{\overline{n+1}} - S_{I,K-1}^{\overline{n+1}}\right)\Big]. \end{aligned} \tag{23}$$

Here subscripts I and K are the indices of the grid point location in the x and y direction, respectively, and superscript n represents the nth time step. The above explicit scheme is second-order accurate in both space and time. The forward and backward differences are alternated between the predictor and corrector steps as well as between the two spatial derivatives in a sequential fashion.

The derivatives appearing in the viscous terms R and S are differenced so as to maintain second-order accuracy. This is accomplished by differencing the ξ derivative term in R in the opposite direction to that used for $\partial E/\partial \xi$. The coefficient of the ξ derivative term in R was averaged over the grid locations over which the differencing was done. The η derivative term in R was approximated with a central difference. The coefficients of the cross-derivative term were evaluated at the grid location where the central differencing was performed.

Computations involving the compressible Navier Stokes equations exhibit numerical oscillations because of inadequate mesh refinement in regions of large gradients. A set of fourth-order dissipation terms are explicitly added in the manner suggested by Jameson et al. [22]. These artificial dissipation terms are formally of the same order to or smaller than the truncation error involved in the spatial and time difference formulas used to represent the

derivatives. These artificial dissipation terms therefore do not affect the formal accuracy of the present formulation.

Initial and Boundary Conditions

A specific solution of the reactive flow equations is determined by the initial conditions and the boundary conditions that describe the geometry of the system and exchange of mass, momentum and energy occurring between the system and the rest of the physical world. The total density, u, and v momentum and the various species densities are prescribed at both the inner and outer portion of the inflow boundary. The pressure gradients normal to the burner surface are assumed to be zero. At the outflow boundary, the normal gradients of total density, momentum and of all species densities was assumed to be zero. The pressure at large distances from the burner surface is assumed to be equal to the ambient pressure. The pressure at the outflow boundary was then interpolated using

$$P_{(IMAX,K)} = P_{(IMAX-1,K)} + \frac{(P_{atm} - P_{(IMAX-1,K)}) * (X_{(IMAX,K)} - X_{(IMAX-1,K)})}{X_{(IMAX,K)}} \tag{24}$$

where $IMAX$ is the total number of grid points in the "x" direction. A symmetric boundary condition was employed at the center line of the computational domain by use of the anti-symmetric reflection of tangential velocity v, and symmetric reflection of all other variables. A slip wall boundary condition is employed at the lateral boundary by assuming that the flux of all transported properties across the wall is zero.

For a diffusion flame computation, the initial conditions at each point in the domain were the same as inlet conditions. Single step finite rate chemistry computations were used to raise the temperature of the gases to a temperature close to the adiabatic flame temperature. The output of these computations was used as initial conditions for the complete two-dimensional Navier Stokes solver with realistic kinetics.

Integration of the Reaction Rate Equations

The kinetic integrator used for integration of the reaction rate equations

$$\frac{d\rho_k}{dt} = \dot{\omega}_k \tag{25}$$

consists of an exponentially fitted trapezoidal rule [23–25]

$$\rho_k^{n+1} = \rho_k^n + h\left[U_k \dot{\omega}_k^{n+1} + (1 - U_k)\dot{\omega}_k^n\right], \quad k = 1, \ldots, N, \tag{26}$$

where ρ_k^n is the approximation to the exact solution to Eq. 25 at the current time, t^n, h is the time steplength ($= t^{n+1} - t^n$), $\dot{\omega}_k^n = \dot{\omega}_k(\rho_i^n, T^n)$ is the net rate of production of kth species evaluated at time level t^n, T^n, the temperature at time t^n and U_k is a degree of implicitness or "tuning" factor.

The kinetic integrator attempts to identify three distinct regimes referred to as the induction, heat release, and equilibration regimes. These three regimes are not only physically different but also exhibit mathematical characteristics [26, 27]. During the induction regime the concentration of intermediate species increase by many orders of magnitude from very small initial concentrations to values sufficient to initiate exothermic chemical reactions. In this regime the coupling with the energy equation is weak and reactions are essentially isothermal. The full chemical mechanism is active during the heat release regime and is exhibited by sharply defined changes in temperature and molar concentrations. The equilibration regime is characterized by monotonic approach of all species and temperature towards their chemical equilibrium values. During induction and early heat release, the species

equations are dominated by positive time constants, and the temperature also exhibits a positive time constant. The associated ODEs are unstable and are mathematically nonstiff. Since very small steps are required for integrating unstable equations, a simple predictor-corrector scheme with Jacobi-Newton point iteration is used. However, during late heat release and equilibration when the temperature and species equations exhibit negative time constants, large stepsizes can be used, so Newton-Raphson iteration with calculation of the full Jacobian matrix is the optimal convergence method. The governing ordinary differential equations are stable during late heat release and equilibration, but are characterized by widely differing time constants resulting in a system of mathematically stiff equations.

Solution of the Diffusion Equation

Exact evaluation of the diffusion velocities is extremely important while computing flames that are limited by the diffusion of fuel into the oxidizer and vice versa. The diffusion velocities are mainly responsible for the observed flame shape and the height of the stoichiometric tip obtained above the burner surface.

Calculating the diffusion velocities requires solution of Eq. 8 subject to the constraint equation 9. Solution of the diffusion equations 8 requires inversion of a matrix of size $(N \times N)$ where N is the number of species present in the system. The costs of a reactive flow calculation are therefore compounded when there are many reacting species present in the system, since the operation count and hence the computational cost scales as N^3 for each cell. In the present approach the method of Lagrange multipliers was used to incorporate the constraint equation. A least squares approach was then used to minimize the residual and the resulting matrix system of equations are solved by Gaussian elimination to obtain the diffusion velocities. Since the matrices formed at the various grid locations were independent of each other, the procedure of constructing the matrices and inverting them was vectorized over the various grid points. It should be noted that replacing any one of the diffusion equations with the constraint equation did not produce good results.

RESULTS AND DISCUSSION

The results of this study show that it is possible to obtain relatively rigorous solutions to two-dimensional laminar diffusion flame problems when the reaction kinetics are known. The solutions provide the concentration fields of reactants and the spatial distribution of thermodynamic and kinematic variables. From the solution one can trace the progress of reactions along streamlines, identify the sites of maximum heat release rate, and characterize the flow of heat upstream that heats, pyrolyzes, and ignites reactant mixtures.

A schematic diagram of the two-dimensional diffusion flame burner is shown in Fig. 1. Using the numerical model and the finite difference scheme given in the previous sections, an unsteady two-dimensional flame propagation model was formulated for predicting the characteristics of methane-air diffusion flame. The inner and outer duct half thickness were 0.9 mm and 6.0 mm, respectively. The velocity of the gases flowing through both ducts was kept at 10 cm/s, and the temperature of the gases flowing into the computational domain was taken as 298 K. The inner duct contains a mixture of 60% methane and 40% nitrogen. The outer duct contains 80% oxygen and 20% nitrogen. The divider between the fuel and oxidizer ducts is assumed to be infinitesimally thin. The adiabatic flame temperature obtained using the NASA thermochemical equilibrium package was approximately 2800 K. The computational domain consisted of a stretched $64 \cdot 32$ grid, concentrated near the contact point of the fuel and the oxidizer. Validation of the various numerical procedures was done for the case of premixed flames [28].

The fuel and oxidizer flow in stoichiometric proportion at the diffusion flame. Because of the high temperatures established in the diffusion flame, and due to the Arrhenius dependence of reactions on temperature, the reaction rates are much larger than the rate of flow of fuel and oxidizer into the diffusion flame. In most of the diffusion flame there is sufficient heat to assure reactions as fast as molecular

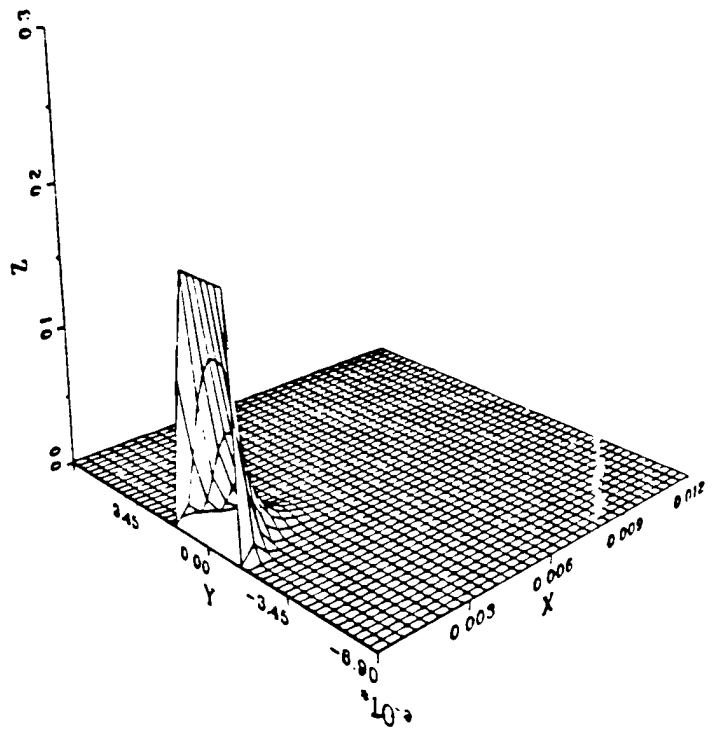

Fig. 2. Surface plot of major reactants CH_4.

scale mixing occurs. It is therefore believed that the diffusion flames are mostly limited by the diffusion process between the fuel and the oxidizer.

However, there is a region very close to the initial point of fuel–oxidizer contact where the temperatures are lower than the ignition temperatures of the mixture. This region is domi-

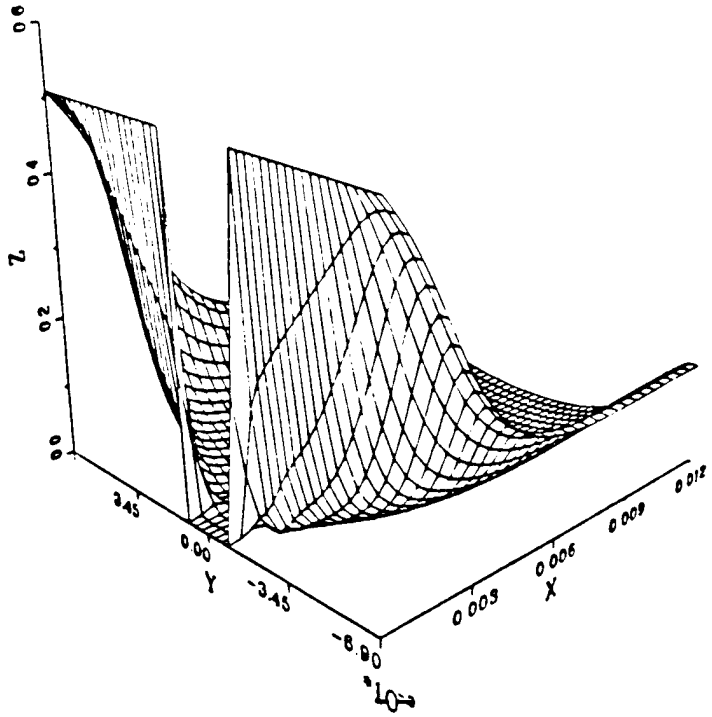

Fig. 3. Surface plot of major reactants O_2.

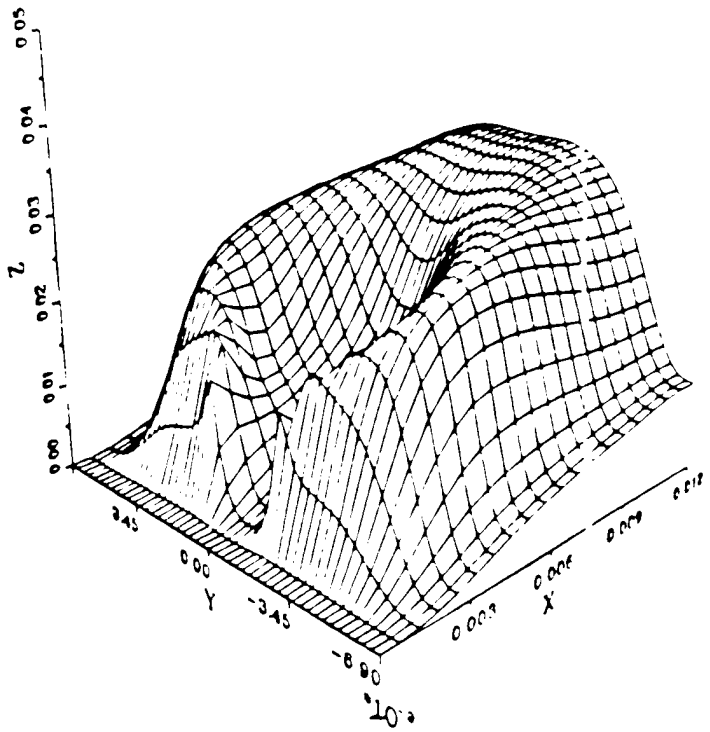

Fig. 4 Surface plot of major products CO_2

nated by the quenching effects of the burner surface. The rate of chemical reactions in this region is extremely small. In this region the interdiffusion will occur faster than rate at which chemical reactions can take place. The interdiffusion process and the lack of appreciable chemical reactions gives rise to a near premixed flow in the region close to the initial

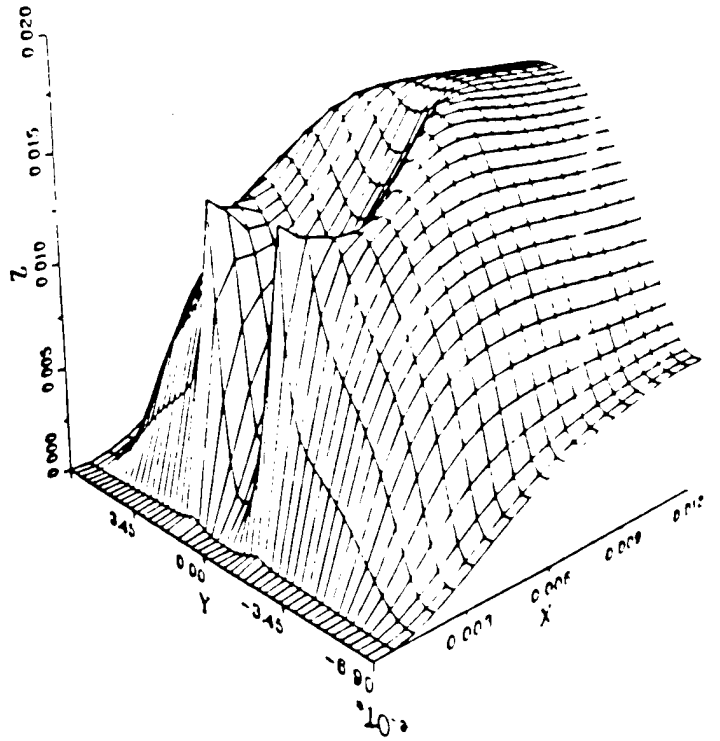

Fig. 5 Surface plot of major products H_2O

point of fuel–oxidizer contact. This region of premixed flow, as it convects away from the burner surface continuously absorbs heat from the diffusion flame. The temperature of this premixed mixture continuously increases as it approaches the diffusion flame. A point is reached where the temperature of this mixture is higher than the ignition temperature. At this point observable ignition along with rapid heat release occurs. The height above the burner surface of the point where rapid heat release occurs is called as flame stand off distance (FSOD). The region where the premixed flow ignites and releases heat is referred to as the leading edge flame (LEF).

The concentration (mol/m^3) profiles for major product species CH_4 and O_2 have been shown in Figs. 2 and 3, respectively. It is observed that methane is consumed almost completely within 3 mm above the burner surface. The flame height (height of the stoichiometric tip) is approximately 6 mm. The flow being considered is a fuel lean flow and there is a significant outflow of excess oxygen through the computational domain. The concentration of major product species such as CO_2, H_2O,

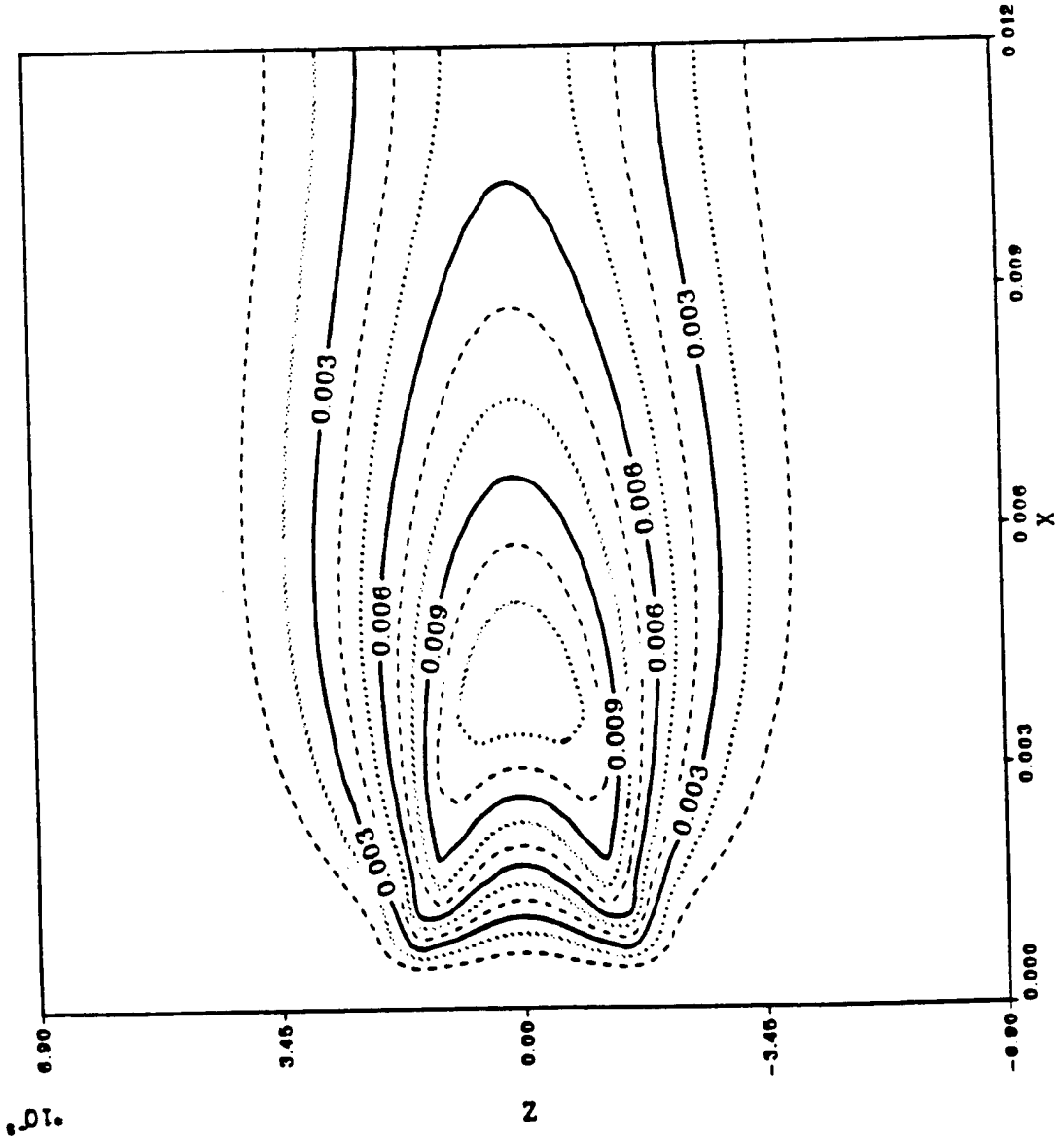

Fig. 6. Contour plot of major products CO.

and CO seem to show a high concentration in the leading edge flame and the diffusion flame. It is believed that the conversion of CO to CO_2 is responsible for much of the heat released in a diffusion flame. The heat release rate profiles seem to support that result. Concentration profiles for major products have been shown in Figs. 4–6. In all surface plots the x axis is a direction perpendicular to the burner surface (distance from the burner surface), the y axis is parallel to the burner surface and the z axis contains the concentrations of the various species and other dependent variables. All dimensions are in SI units.

Figure 7 provides surface plots for heat release rates (J/m^3) per unit volume in the computational domain above a two-dimensional burner. The results show a leading edge portion of the diffusion flame with a definable standoff distance from the burner surface. This portion of the flame consumes the reactants that have mixed in the standoff space, yielding a very high volumetric heat release rate typical of kinetically limited premixed flames. The rapid heat release in the leading edge flame region increases the temperature of the gases downstream of the LEF, to a point where reaction rates are at least as large as the rate at which diffusion occurs. The flame after the LEF is therefore again limited by the diffusion process between the fuel and the oxidizer. The LEF therefore serves as a flame holding site for the rest of the diffusion flame. The upstream heat flow is dominated by this leading edge flame, which, however, stands isolated in a relatively cold reactant flow field and does not reach adiabatic stoichiometric flame temperatures.

The LEF unlike the rest of the diffusion flame is in a region of high heat losses and lower temperature. As a result, its characteristics are substantially dependent on kinetic rates. The development of an appreciable premixed volume, followed by very large reaction rates in the LEF region results in relatively high concentrations of intermediate species in the LEF. Figures 8 and 9 provide contour and surface plots of intermediate species CHO in the region above the two-dimensional burner. Similar behavior was observed for all the intermediate species used in this simulation. The diffusion flame on the other hand showed a relatively small concentration of most intermediate species.

The surface plots for pressure (N/m^2), temperature (K) and magnitude of total tempera-

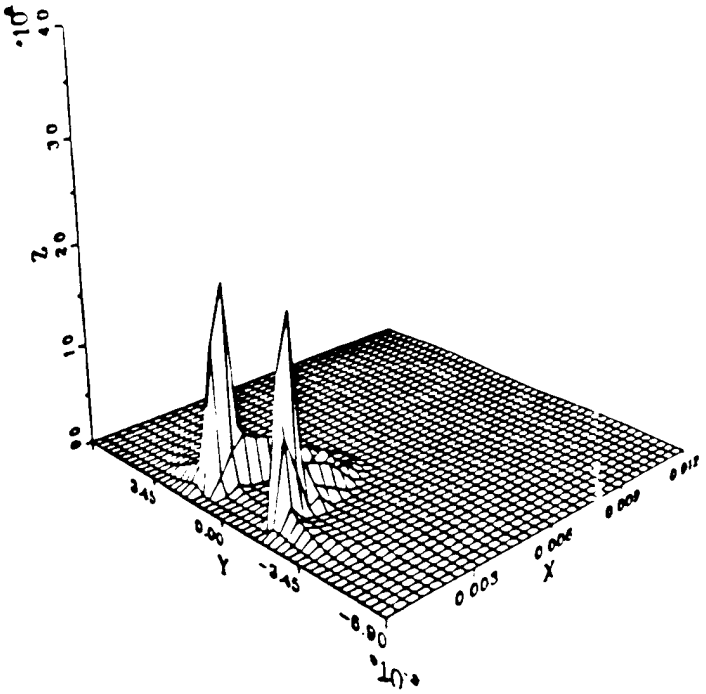

Fig. 7. Surface plot of heat release rate per unit volume

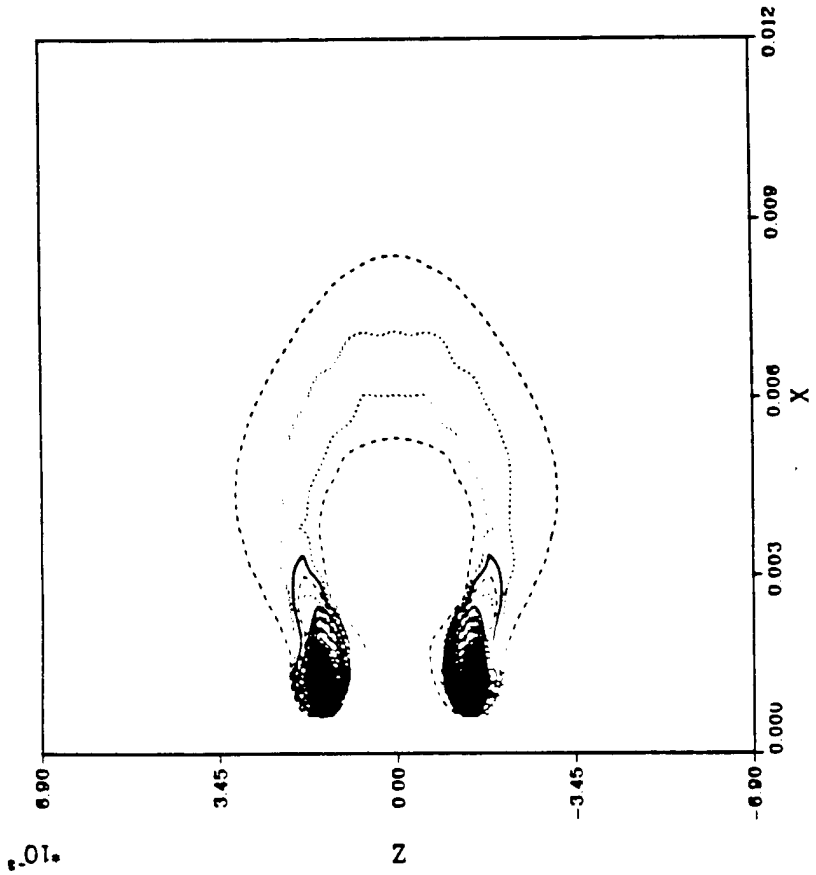

Fig. 8. Contour plot of intermediate species CHO.

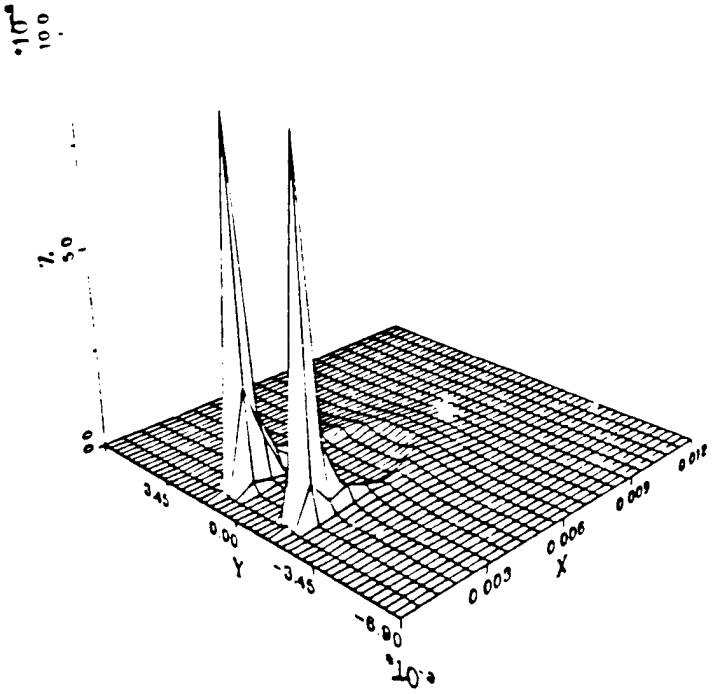

Fig. 9. Surface plot of intermediate species CHO.

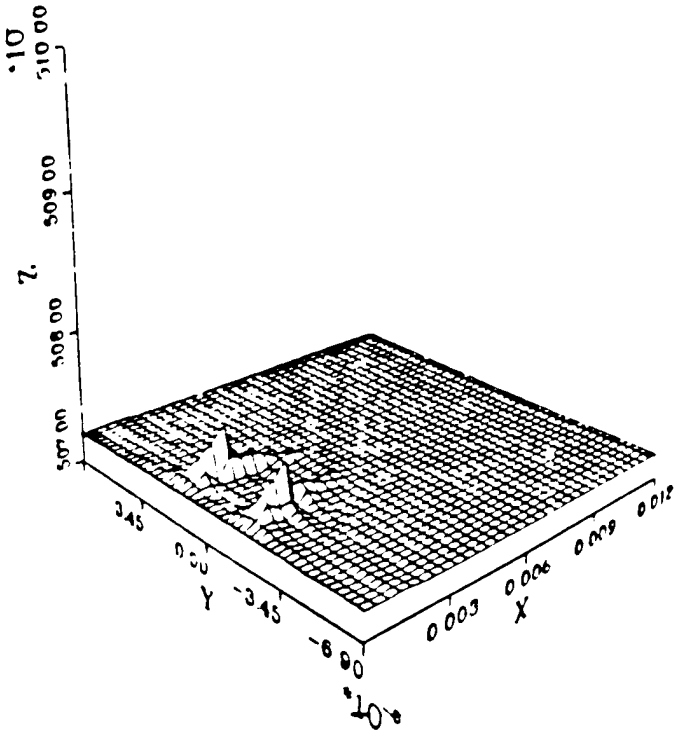

Fig. 10 Surface plot of pressure

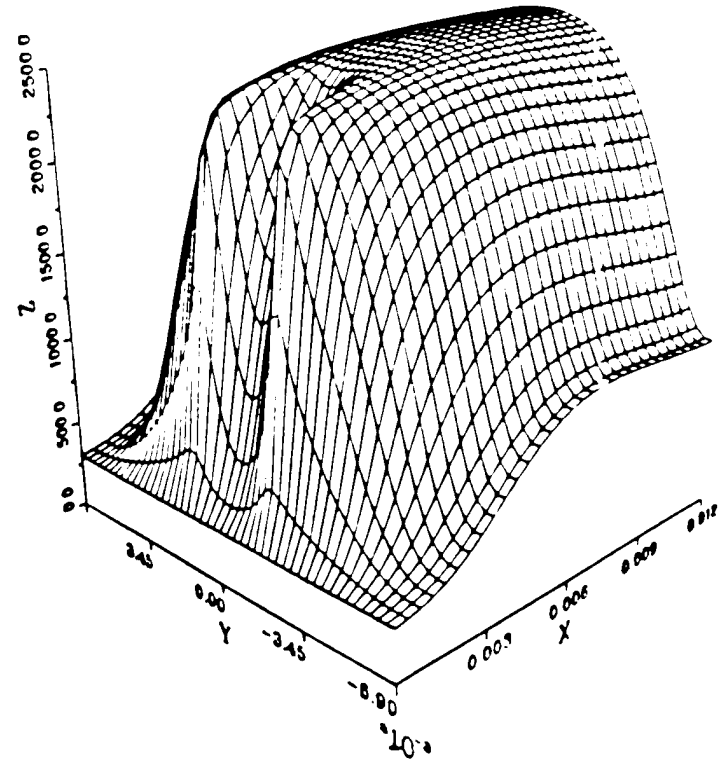

Fig. 11 Surface plot of temperature.

ture gradient (K/m) are shown in Figs. 10–12, respectively. The temperature profiles indicate that the diffusion flame is located in a region where the temperatures are extremely high. However, the temperature gradient plots indicate that the region of the diffusion flame is also nearly adiabatic. The heat release rate profiles indicate that as compared with the leading edge flame, the heat release rate in the rest of the diffusion flame is relatively low, as seen from Fig. 7. The low heat release rate in the diffusion flame can be explained by the small conductive and convective heat losses in the diffusion flame.

The LEF flame region, on the other hand, is located in a region where large conductive heat losses are taking place (Fig. 12). The LEF is mainly responsible for heating the incoming gases to a temperature great enough for near infinite rate reactions to occur. As indicated by the temperature profiles, the LEF is located in a region where temperatures in a given mass element are changing rapidly. Under steady-state conditions a great quantity of heat must be released in this region to balance the conductive and convective heat losses. Due to the large temperature gradients observed in the LEF region, the LEF is mainly responsible for providing heat transfer to any upstream boundary surface.

The large heat release rates in the leading edge flame region results in a rapid increase in temperature. In order to satisfy the equation of state the densities in this region must decrease. The flow under consideration is an incompressible flow, since the Mach numbers are essentially zero. The pressures must therefore essentially stay constant. However, it was observed that the leading edge flame region showed a slight increase in pressure. Surface plots for pressure (N/m^2) have been shown in Fig. 10. Although the pressure gradients are small, the momentum of the gases flowing out of the burner is also small. The pressure gradients are therefore responsible for slowing the incoming gases and turning these gases around the leading edge flame region as shown by the pattern of the particle path lines and by the velocity plots. This indirectly helps in expanding the flow and in reducing the density of the gases in the leading edge flame region. The velocity plots (m/s) for a two-dimensional diffusion flame calculation have been presented in Fig. 13. The particle path lines have been shown in Fig. 14. The decrease in flow velocity into the LEF has the effect of an apparent

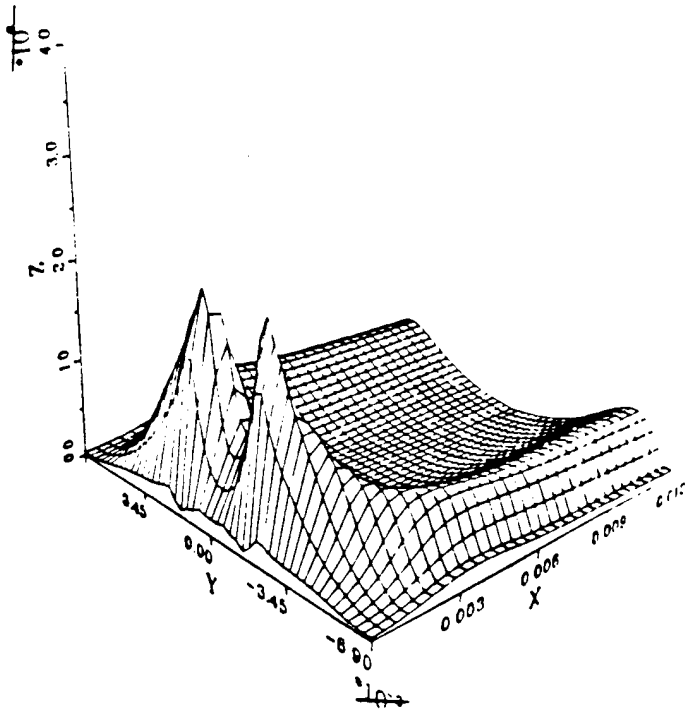

Fig. 12. Surface plot of temperature gradient.

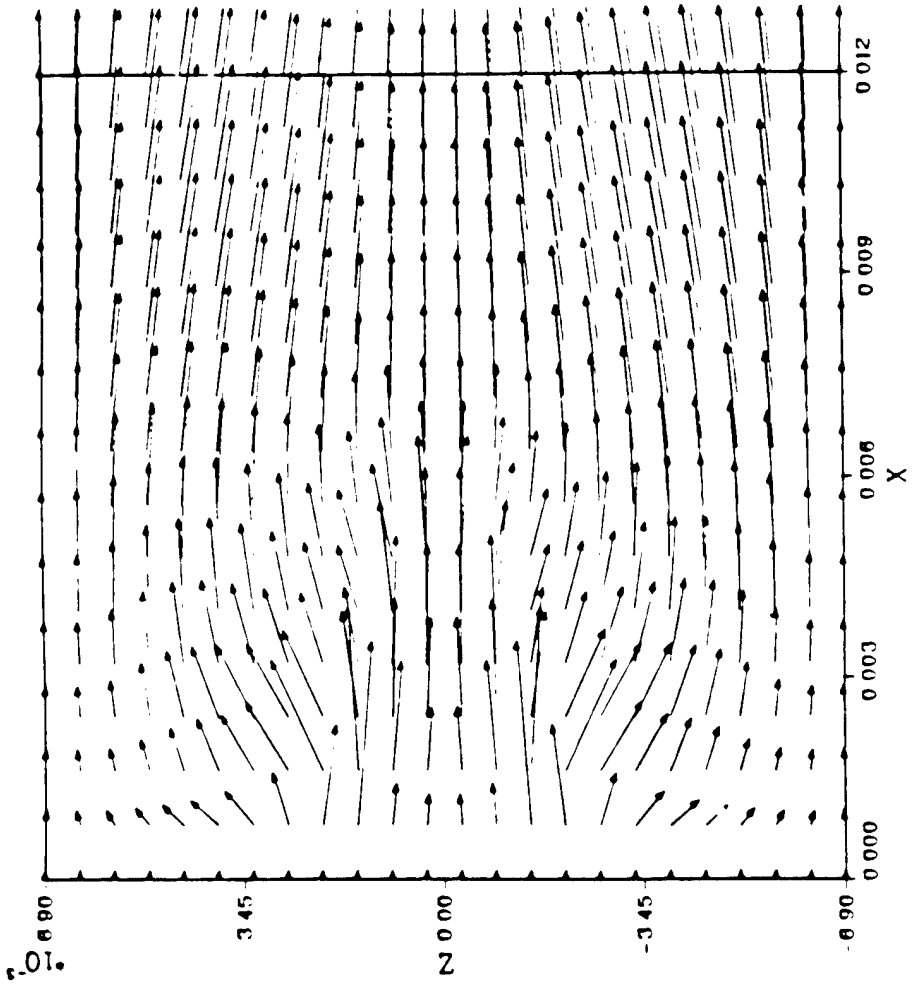

Fig. 13. Velocity vector plots above two-dimensional burner

increase in LEF flame speed, insofar as that flame speed determines the stable position of the flame (flame standoff distance). The stabilization of the LEF is attributed to the balance between flow divergence effects and the heat loss effects, such that the flame will position itself in the mixing flow at a location where its effective flame speed matches the flow speed. This is important in typical combustion situations where progress of a flame depends on the upstream heat flow, and explains the high propagation speeds reported for flames propagating along the stoichiometric surfaces of stratified oxidizer–fuel systems [2], and the high apparent flame speeds in a diffusion flame burner [29]. The particle path lines (Fig. 14) indicate two large recirculation cells that are established between the hot surface of the flame and the cooler shield. The presence of these recirculation cells reduces the total area available for the flow of the combustion gases and hence the velocities are increased due to the combined effects of natural convection and a reduced flow area. The leading edge flame region gives rise to large velocity gradients, which results in viscous stresses and generation of vorticity. The expansion of the gases and the large increase in the velocity of the gases tends to increase the velocities of the gases further away from the leading edge flame due to the viscous stresses.

CONCLUSION

A detailed numerical model has been constructed for the study of the leading edge of laminar diffusion flames. The complete set of Navier Stokes equations for a multicomponent

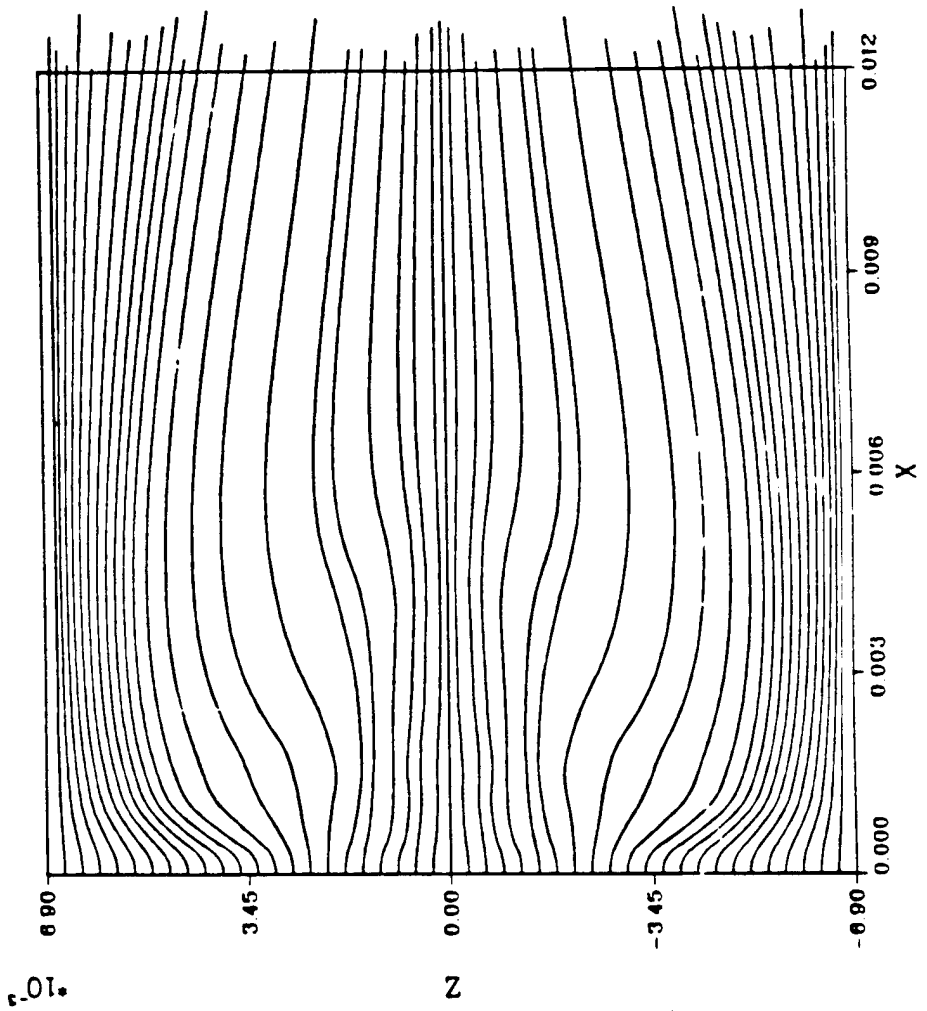

Fig. 14. Streamline profiles above two-dimensional burner.

chemically reacting fluid flow are solved. Chemical reactions are described using detailed kinetics. A real gas thermodynamic model is used and allowances are made for variable transport properties. The following conclusions can be drawn regarding the nature of the leading edge of laminar diffusion flames.

1. The leading edge flame shows the largest rate of heat release per unit volume. This large heat release rate rapidly increases the temperature of the gases to a point where near infinite rate kinetics can take place in the rest of the diffusion flame. The leading edge flame serves as a flame holding cite for the rest of the diffusion flame.
2. Most intermediate species show a very large concentration in the leading edge flame region and very small concentration in the rest of the diffusion flame. The leading edge flame is therefore thought to be dominated by the kinetic aspects of the fuel and the oxidizer species.
3. The leading edge flame shows the presence of small pressure gradients, which are mainly responsible for diverging the flow around the leading edge flame, thereby reducing the density of the gases. The pressure gradients also reduce the momentum of the gases flowing through the leading edge flame so as to match the adiabatic flame speed.

This research was sponsored by Thiokol Corporation and the Office of Naval Research. Computer resources were provided by NSF at the Pittsburgh Supercomputing Center.

REFERENCES

1. Phillips, H., *Tenth Symposium (International) on Combustion*, 1965, pp. 1277–1283.
2. Liebman, I., Corry, J., and Perlee, H. E., *Combust. Sci. Technol.* 1:257 (1970).
3. Ishikawa, N., *Combust. Sci. Technol.* 31:185 (1983).
4. Price, E. W., Sambamurthi, J. K., Sigman, R. K., Panyam, R. R., *Combust. Flame* 63:381–413 (1986).
5. Wichman, I. S., *Combust. Sci. Technol.* 64:295–313 (1989).
6. Dold, J. W., *Combust. Flame* 76:71–88 (1989).
7. Margolis, S. B., *J. Comp. Phys.* 27:410 (1978).
8. Sato, J., and Tsuji, H., *Combust. Sci. Technol.* 33:193 (1982).
9. Dixon-Lewis, G., Davi, T., Haskell, P. H., Fukutani, S., Jinnon, H., Miller, J. A., Kee, R. J., Smooke, M. D., Peters, N., Effelsber, E., Warnatz, J. and Behrendt, F., *Twentieth Symposium (International) on Combustion*, The Combustion Institute, Pittsburgh, 1982, p. 1893.
10. Oran, E. S., and Boris, J. P., *Numerical Simulation of Reactive Flow*, Elsevier, New York, 1987.
11. Oran, E., and Boris, J. P., *Prog. Astronaut. Aeronaut.* 76:154–171 (1981).
12. McMurtry, P. A., Jou, W. H., Riley, J. J., and Metcalfe, R. W., AIAA 85-0143, (1985).
13. Drummond, J. P., and Hussaini, M. Y., AIAA 86-1427 (1987).
14. Bussing, T. R. A., and Murman, E. M., AIAA 85-0331 (1985).
15. Eklund, D. R., Drummond, J. P., and Hassan, H. A., J. AIAA 25:6 (1987).
16. Smooke, M. D., Turnbull, A. A., Mitchell, R. E., and Keyes, D. E., in *Mathematical Modeling in Combustion and Related Topics*, (C. M. Brauner and C. Schmidt-Laine, Eds.), Martinus Nijhoff Publishers, Dordrecht, 1988, pp. 261–300.
17. Williams, F. A., *Combustion Theory: The Fundamental Theory of Chemically Reacting Flow Systems*, Addison-Wesley, Reading, MA, 1985.
18. Chapman, S., and Cowling, T. G., *The Mathematical Theory of Nonuniform Gases*, Cambridge University Press, Cambridge, England.
19. Yanenko, N. N., *The Method of Fractional Steps*, Springer, New York.
20. MacCormack, R. W., and Paullay, A. J., AIAA 72-154 (1972).
21. MacCormack, R. W., and Baldwin, B. S., AIAA 75-1 (1975).
22. Jameson, A., Schmit, W., and Turkel, E., AIAA 81-1259 (1981).
23. Miranker, W. L., *Numerical Methods for Stiff Equations and Singular Perturbation Problems*, D. Reidel, 1981.
24. Shampine, L. F., *Math. Comput.* 39:159 (1982).
25. Babcock, P. D., Stutzman, L. F., and Brandon, D. M., *Simulation* 33:1 (1979).
26. Radhakrishnan, K., and Pratt, D. T., *Combust. Sci. Technol.* 58:155–176 (1988).
27. Radhakrishnan, K., NASA-TP-2372 (1984).
28. Prasad, K., Ph.D. thesis, Georgia Institute of Technology, June 1991.
29. Chiang, H. J., Ph.D. thesis, Georgia Institute of Technology, November 1990.

Received 30 July 1991, revised 30 March 1992

Appendix F

An Experimental Investigation of the Leading Edge of Diffusion Flames

Ph.D. Thesis by Heu-Jei Chaing

School of Aerospace Engineering
Georgia Institute of Technology

November 1990

AN EXPERIMENTAL INVESTIGATION OF THE LEADING EDGE OF DIFFUSION FLAMES

A THESIS
Presented to
The Faculty of the Division of Graduate Studies

By

Hau-Jei Chiang

In Partial Fulfillment
of the Requirements for the Degree
Doctor of Philosophy in Aerospace Engineering

Georgia Institute of Technology
November 1990

TABLE OF CONTENTS

LIST OF TABLES

LIST OF ILLUSTRATIONS

NOMENCLATURE

F/O	Fuel and Oxidizer
FSOD	Flame Stand-Off Distance
L	optical path length of the test object
LEF	Leading Edge Flame
M-Z	Mach-Zehnder
n_0	index of refraction for air at STD condition
N_r	the molar refractivity of the gas in the reference beam
R_0	the universal gas constant
P_0	the ambient pressure
S(x,y)	the fringe shift at location (x,y)
T(x,y)	the absolute temperature at location (x,y)
T/C	thermocouple
Tr	the temperature in the reference beam
$\sum_i X_i N_i$	molar refractivity of a homogeneous mixture
λ	the wavelength of the light source
δ	the fraction change in light velocity; $n=1+\delta$

SUMMARY

This research is devoted to clarifying the nature and behavior of the Leading Edge portion of diffusion flames by experimental observations and the development of a phenomenological model. The motivation of the research originates from the need to better understand combustion of composite solid propellant in rocket motors, especially the role played by the leading edge part of the oxidizer-fuel diffusion flame. Since experimental investigation of actual solid propellant flames is presently not possible in detail because of the microscopic scale of the combustion zone, this research has used an atmospheric gas burner to investigate the characteristics and controlling processes in the leading edge flame zone. Specifically, tests using combustion photography and CH flame radiation measurement were conducted to examine the heat release rate of the LEF region and the subsequent diffusion flame. Systematic variations of measurable parameters such as gas velocities and dilution levels were studied by the help from a Schlieren system, an M-Z interferometer and thermocouple measurement to understand the characteristics of the LEF. The results indicate that the leading edge flame zone has a heat release rate significantly higher than the rest of the diffusion flame. The value of this maximum varies with the change of control variables and the flame adjusts its position accordingly. The heat release rate results suggest that the LEF will contribute the most to the upstream heat transfer from the oxidizer-fuel flows, and the presence, stability, and velocity of the flame as a whole will be heavily dependent on the LEF behavior. Other results from the parametric studies indicate the increase of mixing time necessary for a stable flame to sustain itself against higher gas velocity or higher dilution level. Current studies also suggest that the

stabilization of the LEF could be argued through the balance between the flow divergence effect (lowering velocity) and the heat loss effect (measured flame temperature at the stoichiometric point reflecting the level of lateral heat loss) in a 2-D mixing region. In the case for higher dilution at a given flow velocity, the increase of the flow divergence effect seems to compensate for the needed reduction of the heat loss effect (stays about the same level) On the other hand, flame accommodation to increased flow velocity involves both reduced heat losses and increased divergence factor.

CHAPTER I

INTRODUCTION

1.1 General

The concept of a diffusion flame refers to a flame sustained in the mixing region between otherwise separated volumes of oxidizer and fuel gases. Examples are:

a) a flame in a stagnant buoyantly stratified mixture of fuel and oxidizer in a horizontal corridor as studied by Phillips, Liebman, and Feng [27, 28, 33] (Figure 1-1)

b) a flame burning over a solid or liquid fuel in a stagnant or flowing oxidizing atmosphere, where evaporation or heat from the flame sustains a fuel vapor flow from the condensed fuel (examples are works of Price, Wichman and Hirano [15, 23, 32] (Figure 1-2)

c) a flame in the mixing layer between confluent oxidizer and fuel gas flows [1] (examples are the familiar Burke-Schumann flames; see Figure 1-3)

In a more restrictive sense, a diffusion flame (or part of one) may be called a diffusion limited flame, which means that the rate of reaction is determined purely by the rate at which the oxidizer and fuel diffuse together. Such flames are relatively easy to describe analytically because chemical reaction rate equations need not be included in the analysis [1-6].

Most practical diffusion flames have a small region where accurate description cannot be made without consideration of chemical reactions and reaction rates. This region, which will

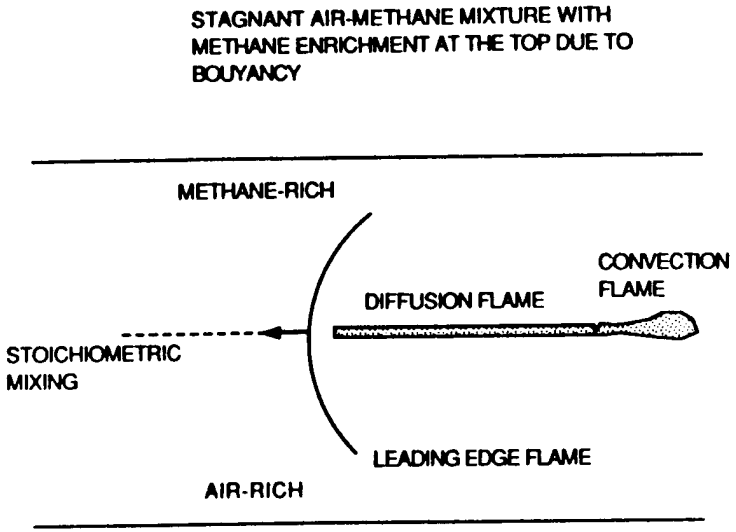

Figure 1.1
Observation of Leading Edge Flame, Diffusion Flame, and Convection Flame Combination in a Simulated Mine Corridor (Sketched from Phillips [27])

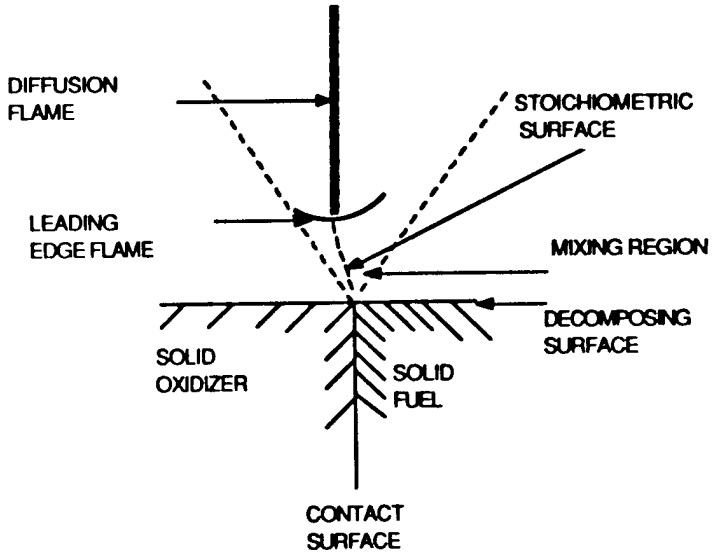

Figure 1.2
Flow-Flame Situation for Flow Originating in Mixing Vapor Flows from Solid Reactants.

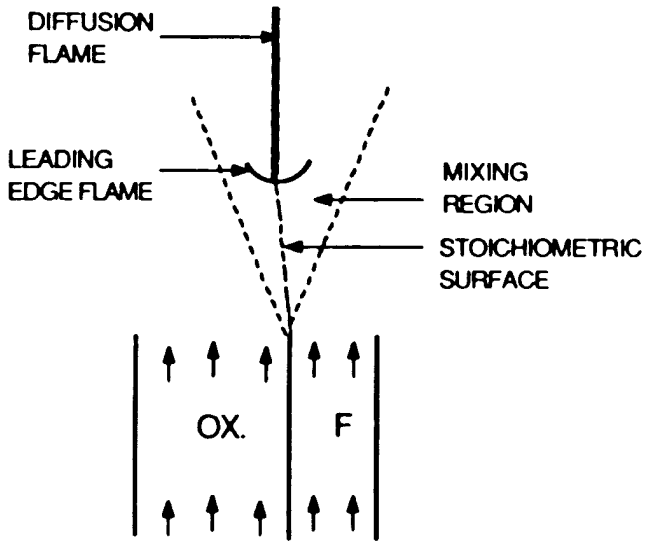

Figure 1.3
Flame in the Mixing Region of an Oxidizer and Fuel
Suggesting the Presence of a Leading Edge Flame

be referred to here as the "leading edge flame" (LEF), is located in a region of the flame where heat flow is distinctly multidimensional and the flame temperatures are correspondingly low, with correspondingly reduced reaction rates. This situation typically arises at an "upstream edge" of the mixing region (Figure 1-3) (in category (a) above, the mixing process is equilibrated, and the leading edge is "upstream" in the sense that it is the leading front of a reactive region moving into the stratified gas field). While the leading edge region is often a minor part of the overall diffusion flame, it dominates the most critical aspects of the overall flame. For example

a) The LEF is the flame holder for the rest of the flame, and hence determines whether there will be any flame.

b) In the stratified mixture problem the LEF determines the propagation speed.

c) In problems where the gaseous fuel supply is determined by flame heating of a condensed fuel, the leading edge controls flame spread over the surface, ignition, and quenching.

d) In confluent flows the LEF determines the location, dynamic stability, and limits of flammability of the flame.

e) In the problem that stimulated this study (combustion of heterogeneous solid rocket propellants), the LEF dominates the heat flow to solid reactants that are the source of the oxidizer and fuel flow, hence dominating burning rate,ignition, quenching, and oscillatory combustion. Because of the microscopic dimensions of fuel and oxidizer flows in propellant combustion, the diffusion regions are short, and the leading edge portion may be a major part of the diffusion flame.

The leading edge portion of the diffusion flame, for all its importance, has been poorly elucidated to date because a) it is so small that detailed observations are extraordinarily

difficult, and b) analytical modeling is extraordinarily difficult because of its inherent multidimensionality, and the necessity to include fairly complete chemical reaction rate equations, temperature dependent transport properties, and viscous effects in a realistic model.

1.2 Literature Survey

1.2.1 Solid Fuel Diffusion Flames

In order to overcome the difficulties in observing details of solid rocket propellant combustion (the motivation which leads to this research program), researchers often look into alternatives and resort to some simple experiments which can aid understanding, or concept building. Ramohalli et al [7-8] have developed a model for composite propellant combustion using a perforated porous plate burner where vapour evolution from the continuous binder is simulated by gaseous fuel transpiration through the porous plate and vapour evolution from the scattered oxidizer particles is simulated by gaseous oxidizer passing through perforations in the porous plate. Their experiments have the convenience that the vapour phase dimensions are expanded sufficiently and can be decoupled from the condensed phase. Also the high pressure and oscillatory behavior of the vapour phase flame zone can be studied in a pressure chamber. It is seen in these studies that the flame stand-off distance from the rugged combustion zone oscillates with the flow oscillations, but the features of the diffusion flamelets were not resolved. Since no individual leading edge flame of the diffusion flamelet can be observed, the LEF behavior certainly can not be revealed by their 1-D model. Recently Chen [9] has constructed a rectangular diffusion flame burner which consists of more than a thousand hyperdermic tubes (0.762 mm inner diameter) to investigate the effect of flow turning upon axial instabilities in solid propellant rocket motors. The oxidizer (air) is supplied through these tubes while the fuel (methane) is supplied through the spaces surrounding the oxidizer supply tubes. His results suggest that the combustion zone affects the absorption of the acoustic energy imposed by the flow turning process. Again the significance of the LEF behavior is not mentioned and no single LEF behavior can be characterized by this study either.

Other researchers have adopted different experimental methods. Of these, the sandwich burning studies are well developed and the concept of a leading edge flame has been extensively used to interpret the results. By edge burning oxidizer-binder sandwiches the combustion zone conforms to a two-dimensional steady state configuration which makes the interpretation of the burning mechanism easier. One series of investigations concerning AP-binder sandwich has been performed by Price et al. In 1980, Price, Panyam and Sigman[10], and in 1981, Price, Handley, Panyam, Sigman and Ghosh [11] reported experiments on sandwiches with tapered binder laminae showing conspicuous difference in features of quenched surfaces along the tapered binder lamina. They developed a theory in which a more complete flame structure was proposed for the sandwich combustion. It consisted of a leading edge that was a kinetically limited (premixed) flame, with a transition to a trailing diffusion-controlled flame further from the interface (Figure 1.2). They interpreted the experimental observations and derived mechanistic arguments from the sandwich combustion and applied these arguments to composite solid propellant combustion theory. Later Price [12] proposed that the region of the flame near the burning surface involved a complex of interactive flames :

a) An AP flame,

b) Kinetically Limited Premixed Flames between binder and AP vapors in the mixing fan, and

c) Trailing diffusion-limited flames.

From experimental observations and physical arguments, they concluded that there was a region, called the "propagation velocity controlling" region which was very important for the combustion behavior. That region included the kinetically limited leading edge of the oxidizer/fuel flame (KLLEF) and supplied most of the heat to pyrolyze the binder. This model for the combustion zone microstructure was further improved later (Figure 1-4) and was successfully applied to interpret the effect of pressure dependence for various binder thicknesses (sandwiches) and AP particle size distributions (propellants) [13-15].

In addition to these experimental efforts addressing the importance of the KLLEF region, there are some solid propellant modellers who also have adopted the concept of a Leading Edge Flame (LEF). For example, Fenn[16] called it the "phalanx" flame, Beckstead [17] called it the "primary" flame zone and Ermolaev [18] called it the "flame root". However, none of them has yet provided a detailed model of the LEF.

The concept of a LEF is also introduced in studies of the prevention and control of flame spread on combustible materials such as the burning of a PMMA surface in a convective air flow. Researchers have the same kind of difficulties with this problem and still fail to demonstrate the existence of the premixed leading edge flame. Fernandez-Pello et al[19,20] have tried to measure the fuel gas concentration ahead of the pyrolysis front on a PMMA surface and have failed to determine the species concentration profiles upstream of the LEF zone. However, the LEF concept has been recognized [21-23] by recent modellers. Ray and Glassman [24] argued the possibility that the fuel vapour generated downstream of the flame leading edge could diffuse through the quenching layer ahead of the pyrolysis front. The fuel diffusion process would be the result of the large concentration gradients and low gas velocities present at the pyrolysis front near the fuel surface. Wichman [25,26] recently developed a model where a premixed flame formed by the upstream diffusion of fuel anchors

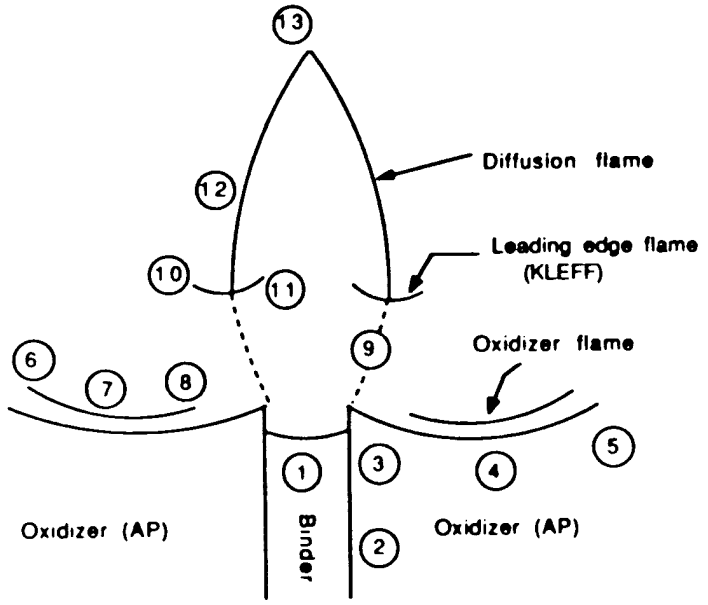

Figure 1.4 Principal Features of the Combustion Zone Microstructure and Processes as Suggested by Price et. al

1) Binder lamina
2) Interface plane between binder and lamina
3) Oxidizer surface adjoining binder smooth band
4) Leading edge of oxidizer burning front
5) Oxidizer region that regresses at the normal AP self deflagration rate
6) AP flame
7) Leading Edge of AP flame
8) Oxidizer flame, modified by the anomalous decomposition in the smooth band
9) Oxidizer fuel diffusion flame region
10-11) Kinetically limited leading edge flame
12) Diffusion flame
13) Tip of diffusion flame

a diffusion flame generated over the burning surface. His model defines a semi-circular premixed flame shape, and the temperature and concentration fields are all of circular symmetry (Figure 1-5).

1.2.2 Gaseous/Liquid Fuel Diffusion Flames

1.2.2.1 Experimental Work

An experiment in which the leading edge flame is clearly visible was described by Phillips [27] for the flame propagation problem along the interface between layered mixtures. Phillips was concerned with explosions in horizontal mine corridors caused by the burning of the methane layer near the corridor roof with the ambient air. He designed an experiment which consists of a horizontal gallery, open at the base, containing a layer of methane introduced uniformly into the top of the gallery. This simulates the mine condition where methane stays on top due to its lighter molecular weight and mixing takes place by molecular diffusion only. A static rig in which methane and air are flowing was also developed to perform the same tests. The flame moving along the stoichiometric surface in the mixed layer between layers of methane and air has a characteristic U-shape front consuming mixtures within the 5%-15% inflammable range (the fuel lean and fuel rich flammability limits for methane). This flame is known as the premixed flame and serves as a "pilot" for the follow-up diffusion flame and the further downstream convection flame. Phillips noted that the speed of the layer flame was much higher than the burning velocity of a stoichiometric methane/air mixture. Through the studies from a particle tracking method, he concluded that the mixture along the stoichiometric streamline (i.e. the streamline which intercepts the stoichiometric point of the flame front) slows down in the approach to the LEF, until the speed is the same as the premixed flame speed for a stoichiometric mixture. Between 1968 and 1970, Liebman et al [28], using a similar setup, confirmed Phillips finding. From the

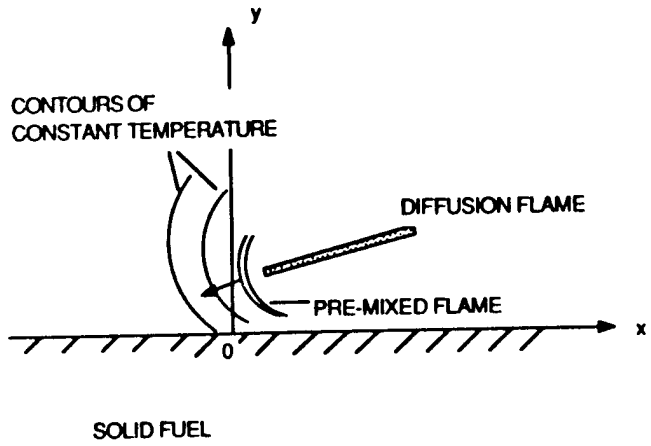

Figure 1.5
The Assumed Physical Configuration of the Premixed-Flame Model of Flame Downward Spread over PMMA in Air (from Wichman [26]).

correlation of the experimental data, they conclude that the interfacial flame speed can be governed by the premixed stoichiometric flame velocity, unburned to burned density ratio of the gases, flammable zone width, and the size of the gallery pertaining to the experiment. Similar flame propagation phenomena were also observed over a liquid fuel surface at a superflash temperature [29]. Roberts [30] in the study of propanol with superimposing air current show that, for either supporting or opposing air current, the flame spread rate increases appreciably as compared to stagnant air, but the flame failed to spread against counter air flow of velocity greater than 200 cm/sec. Between 1973 and 1974, Hirano et al [31,32] examined the aerodynamic and thermal structures across a laminar boundary layer with a diffusion flame stabilizing over a liquid methanol or ethanol surface where the free stream of air is flowing parallel to the surface (flame stabilizes in counter air flow). They noted that, as the free stream velocity is increased, the blue flame zone approaches the liquid-fuel surface, the temperature in the flame increases slightly at a given station, the heat flux to the liquid fuel and the consequent fuel consumption rate also increase. Feng and Glassman [33] were motivated by the phenomenon that a stratified, unconfined combustible mixture over a liquid fuel surface can support a flame propagation velocity of 4 to 5 times the laminar flame speed of the stoichiometric mixture of fuel and air. In 1975, they developed a model using a 1-D stream-tube concept to formulate this horizontal flame propagation problem. Conservation laws were applied at any station in the stream-tube including the station before and after the premixed flame front. Basically the gas ahead of the flame can be displaced laterally by the pressure rise due to the gas expansion in the flame front and this flow divergence effect yields the high propagation speed which is predicted in the model. They conducted experiments on horizontal buoyancy-stratified fuel-air mixture to confirm the prediction of the theories and found that the flame propagation speed is close to those observed by Liebman [28] (180 cm/sec) with the same combustible methane/air layer thickness. The Feng model shows that the increased flame propagation speed (with respect

to the laminar premixed flame speed) is due primarily to a fluid dynamic interaction resulting from the combustion of the leading edge flame. Kaptein and Hermance [34] in 1976 improved Feng's horizontal flame propagation model by including a potential energy term (i.e. work against gravity in this case) and came up with an non-dimensional velocity expression which states that the flame propagation speed is a function of the inverse square of a Froude number, density expansion ratio for an adiabatic flame, and the unburned density ratio between the combustible mixtures and the surrounding gases. This expression predicted the experimental results well providing the fuel type and the thickness of the combustible layer are known. Generally they show that the flame propagation speed increases as the combustible layer thickness increases. Their approach to the problem once again indicates that purely gas dynamic interactions between the propagating front and the external, unburned gases (including the mixture to be traversed by the flame) provides the necessary explanation for the higher propagation velocities (i.e. a divergence of the stream tubes in the approach flow to the LEF slows the flow in which the leading edge flame burns, allowing a high apparent flame propagation speed). Later in the same year, Hirano and Suzuki [35] explored the horizontal flame propagation characteristics in the field of lateral (vertical) concentration gradient of fuel and/or oxygen. Their experiment used a cylindrical combustion chamber with a known methane concentration distribution established over a liquid fuel. Their results show that a flame propagating through a mixture with a concentration gradient will behave very differently from that of a flame propagating through a homogeneous mixture and the leading edge flame will propagate through a layer where the mixture composition in terms of the local equivalence ratio is closer to that for the maximum flame velocity in a homogeneous mixture. The interesting conclusion is that the propagation velocity of the leading flame front decreased as the product of the height of the combustion chamber and the absolute value of the concentration gradient increased. Propagation velocity

can be inferred to approach about 180 cm/sec [28] when extrapolating the data for large values of this parameter.

In 1983, Ishikawa [36] performed an experimental study to simulate secondary combustion mechanisms of a rocket/ramjet in which a hot combustible rocket exhaust and relatively cold ram air mix, ignite, and burn [37]. Of particular interests were ignition processes subject to severe concentration gradients. He developed a diffusion combustor in which concentration gradient fields involving no liquid and no convection can be established. Ishikawa discovered that no other flames appear behind the premixed flame front through a 5 cm travelling distances. His results indicate that the flame with a larger concentration gradient yields a smaller propagation speed, and the ignition energy, local equivalence ratio and concentration gradient in the form of equivalence ratio gradient play an important role in flame quenching, or ignitability. Ishikawa [38] later improved his combustor by elongating the combustor length to 10 cm so that steady flame propagation could be obtained. In this experiment, the premixed flame, the diffusion flame, and the convection flame appear in the limited combustor space, but one after another with some time lag in between (80 msec). This suggests that the diffusion flame and subsequent convection flames are anchored by a premixed leading edge flame. Also he performed some tests to clarify effects of inert gases on flame propagation. As expected, the flame speed is primarily retarded by carbon dioxide, next by nitrogen, and then by argon, and the flame speeds vary almost exponentially with inert gas concentration. Melvin, Moss, and Clarke [39] studied vertical diffusion flames stabilized on a Wolfhard-Parker burner surrounded by an outer jacket flowing with nitrogen. Their original concern was to study the laminar diffusion flame structure using a modified Burke-Schumann equation. Both an Oseen approximation and a boundary layer model are applied to the species conservation equation incorporating a realistic chemical kinetic scheme. However, they realized later that this model can not account for the phenomena at the flame base on the Wolfhard-Parker burner. They measured the variation of temperature and species concentration with distance above the interface of a 2-D burner for the hydrogen and oxygen diffusion flame, and have found that the premixed structure at the flame base is different from that of the conventional Burke-Schumann mixing. Their particle tracking results have illustrated that some of the oxidant streamlines pass through the unburnt premixed leading edge region to the hydrogen side of the flame under an underventilated case and vice versa for an overventilated case.

1.2.2.2 Analytical Work

Theoretical development on diffusion flames has been particularly slow, even though considerable improvements have been made on the Burke-Schumann flame model [1] over the years. In Burke and Schumann's original work, only the species conservation equations were solved for the flame shape. With subsequent advances in diffusion flame modeling by Williams [2], it has become a straightforward matter to simultaneously solve for the temperature distribution, provided the Lewis number (Le) is assumed to be unity. Later the model was further improved by Law et al [3-6] to include the effects of both streamwise and preferential diffusion involving non-unity Lewis number, yet a closed form solution is still obtained. Those improvements have helped the understanding of soot formation, but the major constraints of ignoring the kinetics and the assumption that the fuel/oxidant streams are everywhere separated by a flame sheet still ignores the leading edge flame studies. There have also been several theoretical works focusing on the study of the asymptotic structure, ignition and extinction of diffusion flames [40-45]; and the first Damkohler Similarity group D, the ratio of a time characterizing the flow to a time characterizing the chemical activity, has been introduced to characterize and distinguish the flame structure. Unfortunately those developments are in the field of counterflow diffusion flames. This configuration does not

produce a true leading edge flame and is potentially unstable, especially in the stagnation region, and is, therefore, not suitable for our studies.

Ohki and Tsuge [46] in 1985 published a theoretical study on the problem of horizontal flame propagation through a fuel-oxidizer layered medium with varying equivalence ratio. They adopted the conclusion from Ishikawa [36,38] that the propagation velocity of the flame wave train is governed by the "pilot" premixed flame, independent of the second (diffusion) flame and the third (convection) flame trailing behind (Figure 1-6). No lateral convection was considered, and the propagation velocity was determined as an eigenvalue in the limit of high activation energy. They were able to demonstrate that fuel concentration gradients will affect the flame propagation in the form of the mass burning rate. Their results also show that the higher the concentration gradient at the point of unit equivalence ratio, the smaller the combustible layer thickness would be. As a result, the curvature of the flame front increases, generating larger transverse heat losses; eventually no steady flame propagation is possible. Their result does seem to predict the trend qualitatively [36,38]. However, their model fails to acknowledge the fact that the apparent flame propagation speed (mass burning rate) in this configuration is much higher than the laminar flame speed of a stoichiometric mixture. Wichman [47] in 1989 presented a complex theoretical model to solve a multidimensional, nonlinear boundary value problem in the vicinity of the so-called "triple point", where the two premixed flames and the trailing diffusion flame meet. The physical configuration is sketched in Figure 1-7. Based on the one-step irreversible reaction F+ νO-->P near cold wall, the temperature field in the pure diffusion flame region, in the pure premixed flame region, in the pure quenching region, and in the "triple point" region are analyzed and a formula for the flame quenching distance is obtained which indicates that the multidimensional heat losses increase the quenching radius. Nevertheless, his model also

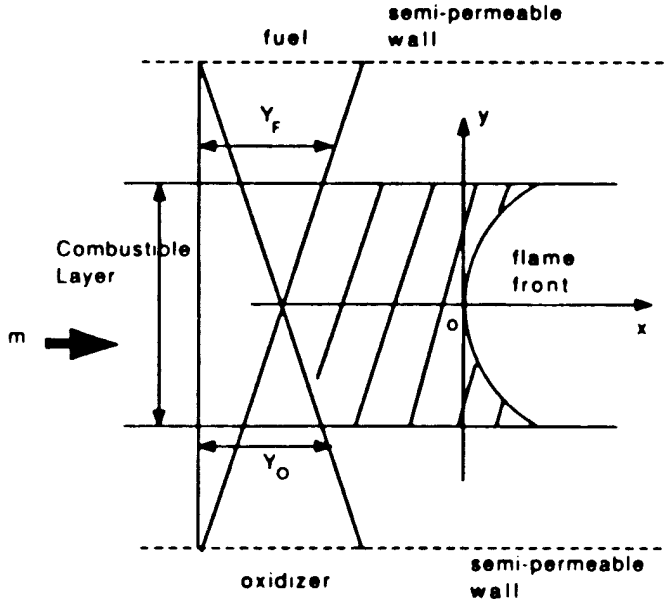

Figure 1.6
Flame Propagation through a Layer with Varying Equivalence Ratio.

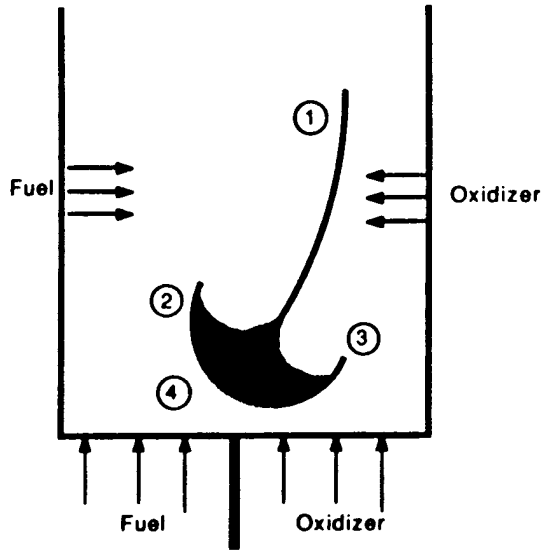

Figure 1.7 Quenching of a Diffusion Flame near a Cold Wall. The Four Flame Regions as Proposed by Wichman are 1) Pure Diffusion Flame, 2) and 3) Premixed Flame, and 4) Triple Point.

disregards the fluid-dynamic influence by assuming a very small mass flux, hence the effect of divergence of the approach flow can not be discussed.

1.2.2.3 Numerical Work

Currently, numerical methods have advanced to a stage where two-dimensional laminar diffusion flames can be simulated by a detailed chemistry, complex transport (full sets of equations for calculating transport properties) combustion model. Smooke et al [48] have had recent success in their development on axisymmetric methane diffusion flames. A complete solution of the diffusion flame flow field has been calculated including the leading edge flame portion. Their results regarding the leading edge flame can be concluded as : (1) extremely high temperature gradients are noted directly above the burner inlet, and (2) most of the methane disappears within 1.0 cm of the fuel jet and the resulting heat release produces an extremely rapid rise in the temperature. Except for these results, no special attention was directed to the leading edge flame. The only other numerical studies of leading edge flames were those of Mao and Fernandez-Pello [49] in a study for flame spread on PMMA surfaces. Mao et al in 1983 numerically solved the two-dimensional, elliptic, gas phase momentum, energy and species equations with a one-step chemical reaction and finite rate Arrhenius kinetics. In this configuration upstream diffusion of fuel is predicted in this analysis. It is seen that because of the no-slip condition at the surface, the low velocity present near the surface permits the considerable upstream diffusion of heat and mass through this region. The results of the influence of the flow velocity (air) indicate that as the free stream velocity increases, the general structure of the flame moves closer to the fuel surface and the upstream diffusion of heat decreases.

It can be seen from the literature that no one has come fully to grips with the LEF problem yet. The streamtube model [33] only addresses the aerodynamic effect. Other theoretical

models [46,47] pertaining to flame structure studies could account for the multidimensional heat loss effect, but then the flow divergence (aerodynamic) effect is neglected. Rigorous description of the flame problem leads to a set of equations that is so unwieldy that the cost of numerical solutions becomes an important barrier. Numerical modelers are even now devoting much of their effort to finding physio-chemical approximations that give satisfactory solutions at lower cost.

In summary, the general concepts obtained from the literature for horizontally propagating LEF between a layer of fuel and oxidizer are from a condition that an infinite free contact surface has always been maintained ahead of the propagation front. These concepts include conformation to premixed flame inflammable range, high propagation speed, decouplement from the diffusion flame, and the effect of combustible layer thickness, concentration gradient, etc. The resulting distinct size of the LEF in those experiment suggests that the assumption of an adiabatic flame temperature applied by the simple streamtube model [33] should be valid. Our research will have to deal with a mixing condition simulating the propellant geometry in which the LEF of the diffusion flame will advance upstream to the root of the mixing region where the flame stabilizes in a high heat loss condition (very nonadiabatic) How well those earlier concepts apply to our configuration remain to be seen and a detailed discussion will be given in Chapter V.

There are some situations where the flame stands close to a physical source of the reactant flow (a burner surface, or a vaporizing or pyrolyzing liquid or solid), heat flow to the physical source becomes an issue. With the burner, the heat flow to the burner becomes a function of burner design. Where the flow originates from one or more condensed reactants, heat flow to the surface is necessary, and the mass flow rate depends on the heat flow rate. In such problems the process of interest is the coupled LEF-reactant pyrolysis problem, as illustrated by pool fires, fire spread over polymer surfaces, and burning of solid rocket propellants. The latter of these examples is the one that motivated the present studies, but a gas burner approach was chosen to minimize the complexity of control and measurement of the combustion zone processes.

1.3 Objective of the Research

A quantitative description of the horizontally propagating LEF phenomenon has been accomplished with varying degrees of physical rigor [27-38]. In the present study, the objective is to clarify the nature and behavior of the confluent flow LEFs by experimental observations and develop a phenomenological model. Specifically, tests using combustion photography and CH flame radiation measurement were performed to examine the heat release rate of the LEF region and the subsequent diffusion flame. Systematic variations of measurable parameters such as gas velocities and dilution levels were studied using a Schlieren system, an M-Z interferometer and thermocouple measurement to clarify the controlling processes in the leading edge flame zone. It is intended from the parametric studies that the nature and characteristic of the LEFs will be summarized and flame stabilization mechanisms will be established. We are fortunate to have access to results of an ongoing analytical-computational study of LEFs in gas burner flames, and will use those results to help in the formulation of the phenomenological model.

CHAPTER II

EXPERIMENTAL SETUP

2.1 Burner System

2.1.1 Design of the 2-D Burner

Our motivation for this study is the behavior of the leading edge flame (LEF) in heterogeneous propellant combustion, The physical situation is pictured in Figure 1.2 where the mixing oxidizer (O) and fuel (F) gas flows originate at the adjoining surface of the decomposing solid oxidizer and fuel. With this configuration in mind a literature search for appropriate burner designs indicated that a suitable choice for the burner geometry for this application is the Wolfhard-Parker diffusion flame burner [50].

In addition to the general considerations such as attempting to provide a uniform flow at the burner exit and stabilizing of the flame, the burner will be required to generate a flame which can respond to the variation of gas velocity such that it can stand away from the surface allowing easier observation on the leading edge portion and study of its position and characteristics as a function of flow and reactant variables.

A modified gas burner of the Wolfhard-Parker type, similar to burners used to study soot formation [51-53] was developed to generate stable two-dimensional flames (Figure 2.1). It consists of three rectangular channels held together with the middle channel being the fuel supply and two outer ones as oxidant supplies. The fuel channel has a dimension of 1.13 cm by 1.13 cm and adjoining oxidizer channels have dimensions of 2.23 cm by 1.13 cm. All the channels have a wall thickness of 0.03 cm, and the interfaces between the

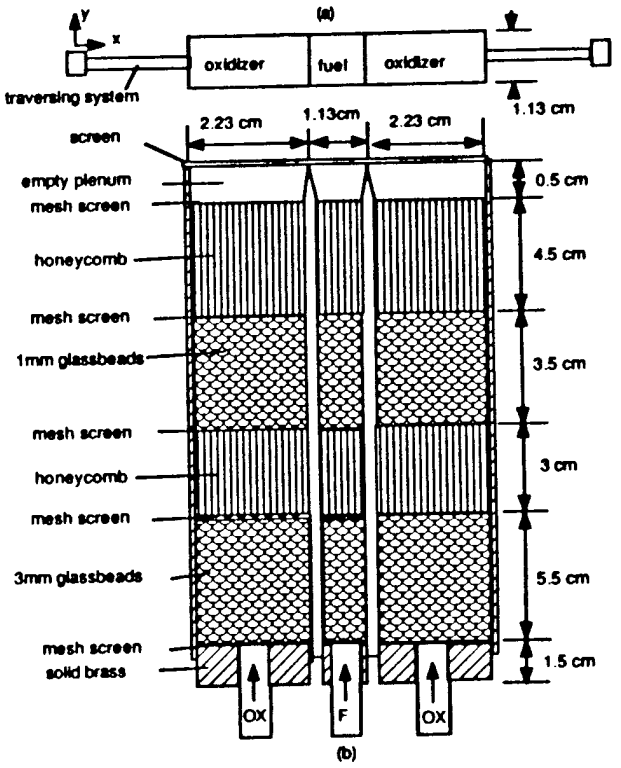

Figure 2.1
2-D Gas Burner (a)Top View
(b) Details Inside the Burner

adjoined F/O channels are tapered to reduce the partition gap. Each channel is 17 cm in length such that proper treatment to the gas flow can be conducted. Inside each channel there are flow straightening materials which consist of five mesh screens, two layers of glassbeads (diameters of 1 mm and 3 mm), and two layers of honeycombs (1/32" in diameter). The glassbeads are used for relieving flow gradients to obtain a uniform flow (the inlet gas must go through transition from 1/4" tube to rectangular channels), and the honeycombs are for straightening the flow. The mesh screens separate the beads and honeycombs. These flow modification devices are commonly adopted by other researchers in their burner to produce uniformity of flow [54-57]. An empty plenum of 0.8 cm in distance is kept below the top of the burner to allow laminar (molecular) mixing to smooth out any boundary layer effects induced by the last layer of honeycomb before the burner exit. Finally a fine mesh screen was fitted on the top of the burner.

2.1.2 The Effect of the Final Screen on the 2-D Burner

The particular form of a stabilizing device can influence the shape of a flame. If a premixed flame is held on a flat screen, it assumes a flat flame shape (in a certain velocity range). This stabilization of the flame is caused by interaction with, and heat loss to, the screen, but it is also because the screen tends to remove transverse gradients which were induced by internal burner surfaces and generates a more uniform flow normal to the surface of the screen. Since our goal is to study the initial mixing of two flows with a uniform velocity, the velocity deficit effect caused by boundary layer adjacent to the splitter plate must be eliminated or reduced to a minimum, and ideally mixing should be due to diffusion alone. Thus, the effect of the screen on the velocity profile above the burner must be examined more closely.

A TSI hot-wire (model 1212-T1.5) was chosen to conduct the velocity measurements across the burner with a fine screen on top. The hot-wire was calibrated between the range of 0 to 120 cm/sec and has sufficient sensitivity to detect any flow disturbance. The probe was mounted on a transversing system allowing 3-D translational movements within 1mm accuracy (See Figure 2.2). The power supply and signal conditioning are all contained in a TSI model 1051-6 anemometer, and the DC output was read from a Fluke digital voltmeter with an accuracy of $\pm$ 0.001 volt. Tests were conducted covering the optimum operation range for producing a stable 2-D flame. In view of burner symmetry, measurements were made over only 1/2 of the burner surface. The results were plotted in Figure 2.4 for two different heights above the burner surface(1 mm and 3 mm) and two gas velocities (15 cm/sec and 45 cm/sec). It can be seen that the velocity deficit smooths out when the height is changed from 1mm to 3mm. Even in the worst case (Ug=45 cm/sec and 1mm height), the maximum velocity variation was less than 7% of the nominal value. In addition, the flame usually stabilizes slightly on the oxidizer side of the channel where the local velocity is even closer to the nominal value. For observation with an M-Z interferometer the optimum operation conditions for a 2-D flame are where the flame stand-off distance (FSOD) is between 1-4 mm, and gas velocity varies between 15-45 cm/sec, Figure 2.3 shows that the velocity remains fairly uniform above the burner screen in this operation range. An additional concern is that the "ordered" porosity of a screen might influence the flow near the splitter plate. Hypothetically, a better choice would be a porous sintered plate since the medium has a random and smaller pore size. Furthermore, the micro porosity creates a large pressure drop which is effective in eliminating transverse gradients and producing a uniform flow. Unfortunately, sintered porous plates are manufactured for use as a filtering medium and the uniformity of porosity in all samples tried has been unsatisfactory to meet the uniform flow requirement. Consultations with the manufacturer confirmed the conclusion that no attempt is made to maintain uniformity of porosity. Furthermore, machining of the thin samples crushes the porous material and adds to the nonuniformity. In any event,

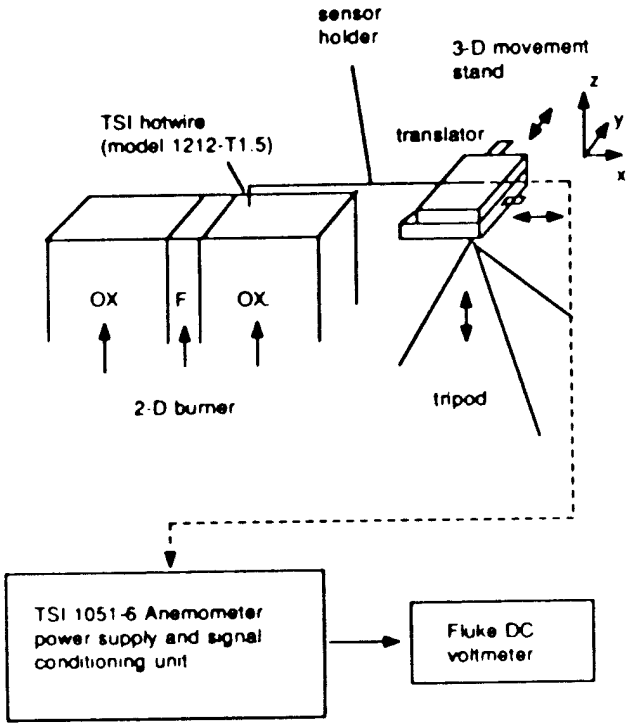

Figure 2.2
Hotwire Setup for Velocity Measurement (Cold Flow)

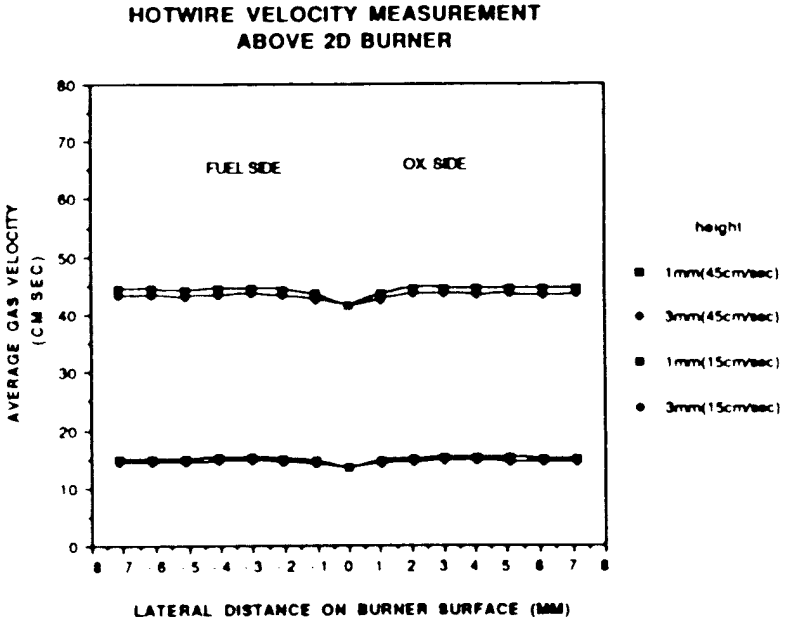

Figure 2.3
Gas Velocity Distribution on 2D Burner

numerous PSS (porous sintered steel) plates were carefully fitted to the burner and hot wire probes were used to measure the velocity across the face of the burner. In all cases, random jets were formed across the burner especially near the critical splitter plate at the edges of the "cut" PSS plates.

As a alternative, two grades of fine wire screens (see Table 2.1) were fitted over the burner. In order to test the effect of the ordered porosity near the splitter plate, a flame was established over the burner and viewed in an M-Z interferometer (see later discussion). The screen was moved laterally one half a mesh cycle and no changes were observed in the M-Z interferometer. The tests were repeated at a different flow velocity (see Table 2.2). A finer wire screen was substituted and the results were repeated. The flames were compared for general shape and flame stand-off distance. As shown in Figure 2.4 and 2.5, the flame stand-off distance is independent of screen location and mesh size. No changes in flame shape were observed.

The results presented here suggest that, when judging from the flame shape and the flame stand-off distances, the flame near the base is insensitive to the screen mesh size and the location of the mesh with regard to the splitter plate of the burner. Since the thickness of the fuel/oxidizer dividing plate in the burner (0.6 mm) is several times larger than the wire diameter and the opening of the screen, it was concluded that the screens used here had grids fine enough to be a good substitute for the porous plate (i.e., the screen arrangement on the burner will not cause any inconsistency of the test results while maintaining a reasonable uniform velocity profile across the burner as well).

The screen of Mesh #60 was used in subsequent experiments.

2.1.3 Flow System Arrangement

Because the burner contains three channels, it is desirable to develop a flow system providing three separate, adjustable gas supplies. Each channel has a flow control system

Table 1 Plain Square Weaves-(SS 304)

Mesh #	Wire Diameter inches	mm	Width of Opening inches	mm	% Open Area
60	.0075	.19	.0092	.23	30
80	.0055	.14	.0070	.18	31

Table 2 Flow Variables and Gas Compositions

Ug \ composition	Fuel	Oxidizer
45 cm/sec	CH4 : 51% N2 : 49%	O2 : 42.4% CO2 : 57.6%
30 cm/sec	CH4 : 56% N2 : 44%	O2 : 38.3% CO2 : 61.7%

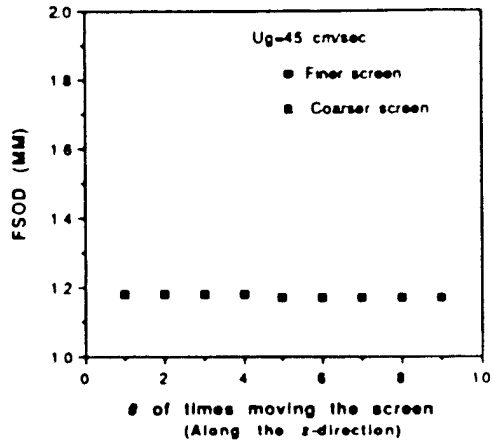

Figure 2-4 2-D Flame at Ug=45 cm/sec

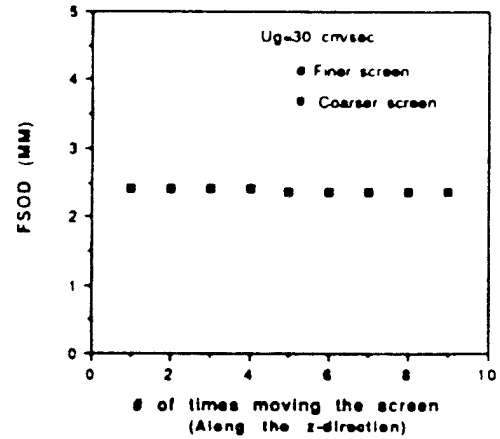

Figure 2-5 2-D Flame at Ug=30 cm/sec

so that a premixed supply of up to three gases can be supplied independently of the other channels. Figure 2-6 provides the schematic of the system. A control rack was designed for this purpose containing three panels for each of the three channels. Each panel contains three sets of flow meters (on the front side) and two mixing chambers (on the back side). Each of the flow meters (rotameters) was calibrated independently. The gases for each panel are mixed in two 20 cm plexiglass mixing chambers filled with 3 mm and 5 mm glass beads. Final "molecular" scale mixing is assured by using a 50 cm supply tube to each chamber. A flame arrester was added on the fuel line near the entrance of the burner to prevent flashback and one way valves prevent contamination of the gas bottles. At the burner exit, the fuel stream and two oxidant streams were shielded by nitrogen flowing through a jacket at the sides of the burner. The flow rate for the shield nitrogen in the jacket was set to approximate the velocity in the F/O streams. The resultant free boundary between the shield nitrogen flow and the F/O flow (Figure 2.6) allow a relatively unrestricted expansion of the hot gases toward the side nitrogen zone. Since the burner width in the direction of edge-on flame viewing is only 1.13 cm, this end expansion can not be neglected. This effect is noted later in determining the temperature field for the downstream diffusion flame when the burner is placed inside a Mach-Zehnder interferometer, and some correction has to be made to account for this effect.

As in other investigations [51,52], it was found that stability of the diffusion flame against flickering was greatly enhanced by contracting the downstream vortex-shedding region on a wire gauze heat sink "nozzle". In the present series of experiments, this heat sink was positioned at about 20 cm from the top of the burner, and it was observed that the presence of the gauze, although reducing the flickering of the downstream diffusion flame, does not appear to have any influence over the leading edge portion of the flame.

It is worth commenting on the Reynold's number of the flow at this point. To simulate composite propellants in which the oxidizer particles are typically 100 microns, the gas

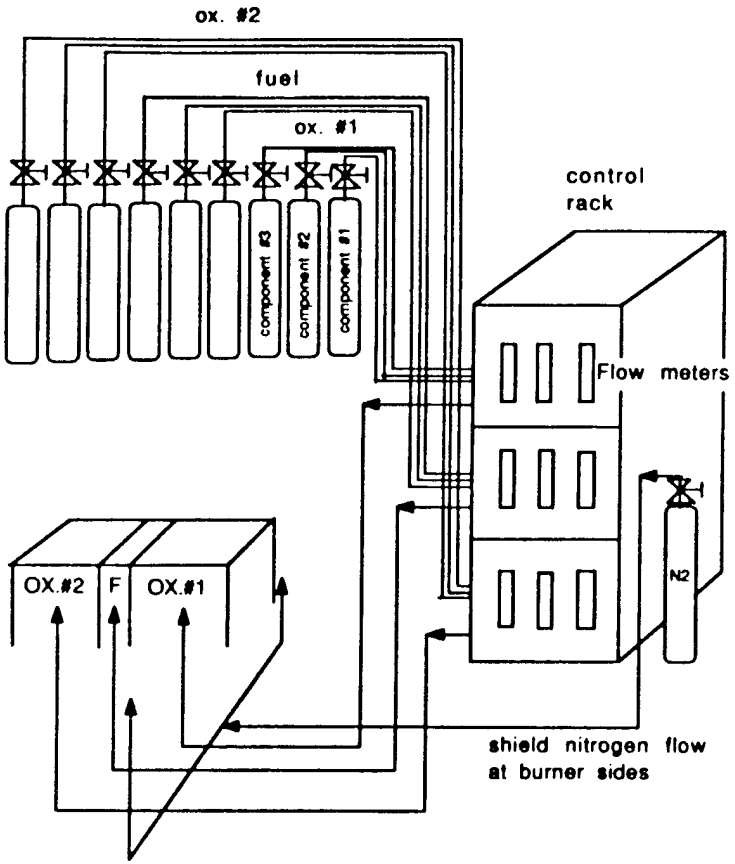

Figure 2.6
Schematic of the Flow System

leaving the burner should be laminar. In order to provide a stable flame, the gas burner velocity usually operates below 50 cm/sec. The Reynolds number corresponding to this velocity in the channel would be below 500. This value is much lower than the experimental critical value (Re=2200) for a laminar pipe flow going through transition [58]. In addition, the shear flow disturbance is further minimized due to the equal velocity setting in the F/O streams. Therefore, we conclude that the flow conditions in our operations are within the laminar flow range with only molecular mixing in the region of the fuel and oxidizer streams of interest near the burner surface.

2.2 Optical Methods

2.2.1 Overview

The temperature profile of a flame is perhaps its most useful single characteristic. Many methods are available for measuring flame temperature but the traditional methods such as probe methods, are intrusive and change the nature of the flow. Furthermore, such probes are usually larger than the regions of interest. Optical methods which obtain instantaneous photographic records of complete temperature fields are eminently suitable for making measurements of this kind. Many optical flow visualization methods (shadowgraph, schlieren, and interferometry) are based on the fact that the speed of light varies with the density of the medium through which it is passing. Shadowgraphs are the simplest to photograph and the most complex to interpret. The contrast of the picture for this method is proportional to the second derivative of density. A Schlieren system is sensitive to the density gradient. Specially, the light rays will be refracted (usually downward) when light passes through the part of the test region with high density gradients, and that part of the deflected light is intercepted by a knife edge at a lens focusing point before it reaches the viewing screen. When the knife edge is facing up, it produces a bright background and dark test region; when the knife edge is facing down, it

yields a dark background and bright test region. These horizontal knife edge settings (facing up or down) are very sensitive to the density gradient in the vertical direction, and hence will provide a good Schlieren image to study the variation of the LEF region with a change in the test conditions. The Schlieren images of the diffusion flame under this kind of setup reveal only the LEF regions on the viewing screen (the subsequent diffusion flames do not appear on the screen because of low gradients in the vertical direction). More details of the shadowgraph and Schlieren methods can be found in many references [59-61]. Both the shadowgraph and Schlieren system were applied to this research, and good qualitative results were obtained by the Schlieren system which will be discussed in section 4.3. The setup of the Schlieren system is given in Figure 2.7.

The other method, interferometry, deals with density distribution directly and is by far the best optical method among the three for the present study. The ability of interferometer to obtain almost continuous temperature profiles nearly up to the burner surface, makes it a good tool for study of the LEF region which is the portion of a 2-D diffusion flame near the burner surface. On the negative side, an interferometer, in general, has inherent problems such as end effects, and refraction errors. Basically these difficulties create an uncertainty in defining the actual optical path length. Other problems include vibration, insensitivity of the fringe shift at high temperatures, and the need to know the refraction index of product gases (details are discussed in next chapter). Nevertheless, with sufficient care and precaution, these problems can be either resolved or minimized and reasonable precision can be obtained.

2.2.2 Mach-Zehnder Interferometer

2.2.2.1 Background

The M-Z interferometer is the oldest, but the most versatile interferometric method yet developed for flow visualization. Originally used in 1891, it is still frequently applied to

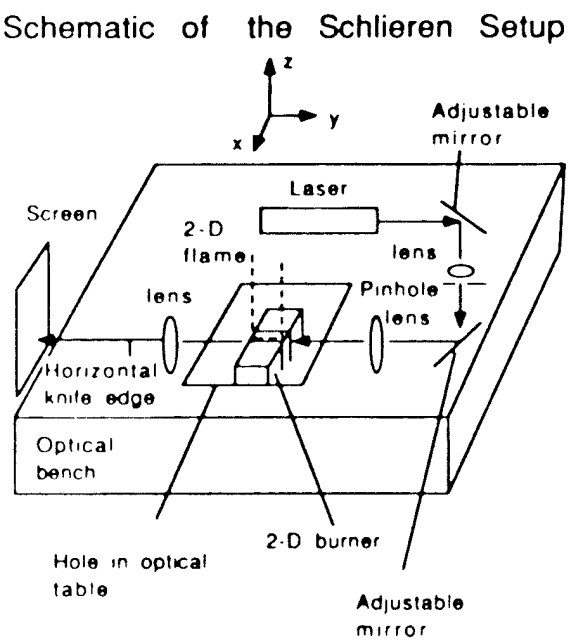

Figure 2-7
The Schlieren System

compressible flow and heat transfer studies [60,62]. However, there are only sporadic applications in combustion studies especially involving mixing gases. Addressing the difficulty in determining both the temperature and gas concentration, Olsen [63] in 1963 has proposed to use interferometry to determine temperature and composition of a j-constituent mixture from interferograms taken at j different wavelengths. He demonstrates this method for a two-component mixture at about 90^0 C. However, the small dispersion of gases together with the loss of sensitivity at higher temperature, make it unlikely that more complex high temperature systems could be analyzed with any accuracy. Schulz-Grunow and Wortenberg [64] have adopted this method to the study of premixed laminar flame structure. Roepor [65] has used a simpler interferometer for the analysis of a counterflow diffusion flame. El-Wakil [66] has applied the M-Z interferometer to measure the temperature contour in a droplet burning situation. Tsuji and Yamaoka [67,68] have also applied the M-Z interferometer to examine the flame structure of the laminar counterflow diffusion flame established in the forward stagnation region of a porous cylinder, and South [69] has used a different laser interferometry technique to study conical flames.

The typical components of an M-Z interferometer, are a light source, two beam splitters, two plane mirrors and a screen or camera (Figure 2.8). The concept of the M-Z interferometer can be envisioned by adopting the wave nature of light. If two monochromatic wave trains, initially from the same source but traversing different paths, are reunited, then dark and bright regions will, appear on the record, corresponding to local crest-trough and crest-crest superposition of the wave caused by variation in phase difference across the photographic record. These bands of illumination are termed interference fringes and they are subject to shift locally depending on the corresponding path difference between the reference beam and the test beam passing through a point (x,y) in the test field. The basic principles and detailed derivation for temperature evaluation with this technique (Weinberg [60], Willcie [62]) are given in Appendix A.

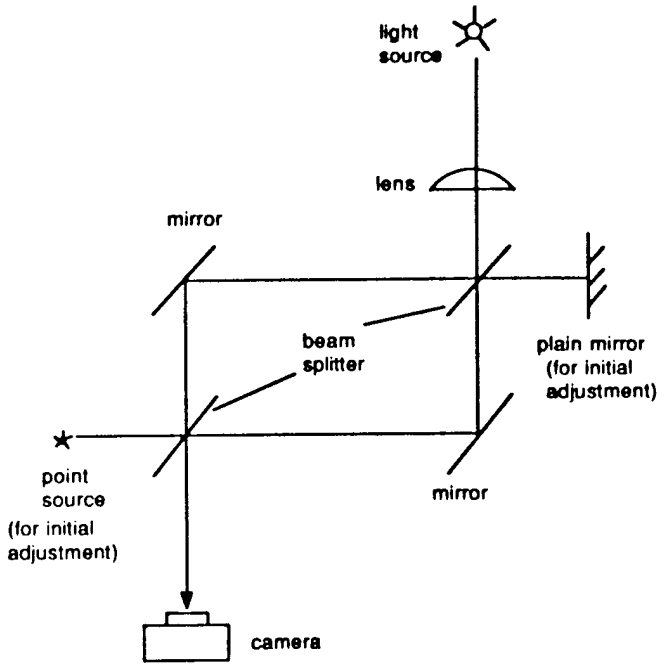

Figure 2.8
Ray Diagram for a Mach-Zehnder Interferometer

2.2.2.2 System Setup

Significant efforts were devoted to build a new M-Z Interferometer in this laboratory prior to the start of this project. A Newport MST46, 4'x6' standard table top, 8" thick with a Ferromagnetic stainless steel working surface 3/16" thick, tapped with 1/4"-20 holes-1" spacing was chosen. An 8"x16" hole was cut through the table to accommodate the burner system and a compromise choice based on reasonable cost was made which adopted Newport NN4-28 non vibration isolation legs (28" long) to support the table top instead of a system with vibration isolations. In order to reduce the transmission of surrounding low frequency vibration to the optical bench, each leg of the bench was mounted on a 12"x12" sandwich consisting of 1.5" of neoprene foam between two steel plates. The necessary optical plates (2 beam splitters and 2 plane mirrors of 2" diameter) and rotators had been obtained. During this project the mirrors were properly mounted on the translators and rotators and arranged on the optical table according to desired dimensions based on a 2:1 spacing ratio to set up the corners of a rectangle with each plate rotating to a 45^0 angle.

This new system exhibited unacceptable fringe vibrations associated with low frequency building vibrations and by room air motions. In addition, the diameter of the viewwindow of this interferometer was partially blocked by the thick beam splitter supporting frame due to the 45^0 inclination of the plates. Furthermore, commercially available optical positioning equipment consists of assembled components which are not capable of producing single axis motion (i.e. rotation without translation) and this assembly usually aggravates the vibration situation. Thus the required adjustment of the instrument was extremely difficult.

As a result, we reactivated an M-Z Interferometer system which was acquired from the Naval Weapons Center. This interferometer has rectangular mirror/beam splitters sandwiched between two thick cover plates which make the system a rigid stand-alone unit. A hole was cut through both plates for the burner installation. All rotators, translators and beamsplitters were built specifically for this unit so that single axis motion can be achieved without image cutoff. It was found that, by following the initial adjustment procedures developed by Price [70], the originally time-consuming adjustment becomes relatively easy. This unit does not yield the vibration and adjustment problems as mentioned earlier because of the excellent rigidity and mounting arrangement of the system. The schematic of this system as well as the general test setup are shown in Figure 2.9. This interferometer was mounted on the Newport optical bench with the burner. A sodium lamp was used as the light source. For recording the interferograms, a Nikon camera equipped with a Nikon 200 mm f4 micro internal focusing lens was chosen for its minimum focus distance (0.71 m) so that all the fine-tune control knobs on the interferometer could be within reach for adjustments while looking through the camera to take pictures. The optical bench also provides the surface for mounting all other diagnostic systems.

2.3 Thermocouple Measurement

In order to validate the results of interferometric determination of temperatures, a platinum vs. platinum-10% Rhodium Thermocouple (T/C) was used to measure the flame temperature. Several miniature thermocouples were purchased from Paul Beckman company. The measuring bead is a 0.003" diameter disk at the end of a 0.003" quartz sheath. To prevent catalytic reactions reported for the hydrocarbon flames [71,72], the thermocouple bead was coated with a thin layer of colloidal silicon oxide. This configuration provides the smallest sheath diameter available for a thermocouple probe. This probe not only has a minimum intrusion effect, but also has minimized the conduction and radiation losses due to the extremely small thermal mass. Also, the response time of the T/C is extremely short because of the exposed bead and minimum mass.

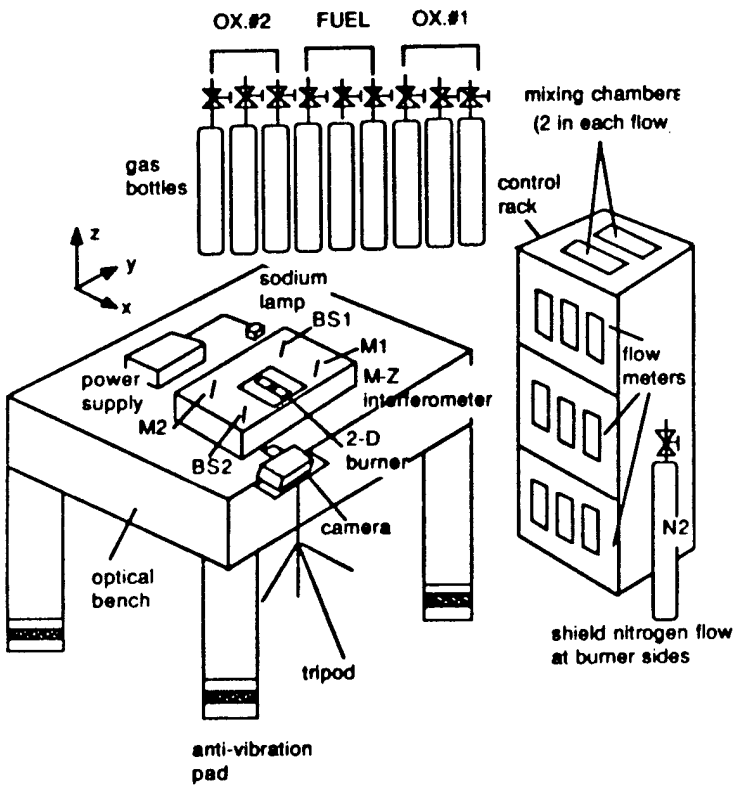

Figure 2.9
General Arrangement of the Test Setup

The T/C is mounted on 3-D translators with dial gauges so that the position can be recorded (See Figure 2.10). The accuracy of the system will be discussed in next chapter.

2.4 CH Flame Radiation Measurement

As a part of this research program, a system to measure the CH radiation intensity was set up in this laboratory. Figure 2.11 provides the schematic of the system. A Hamamatsu R-268 photomultiplier with a narrow-band spectrum filter collecting the (0,0) CH emission band at 431.0um $\pm$ 10um (10% peak transmittance) was used to receive the narrow bandwidth radiation from the flame and convert it to a voltage signal. Since this signal is usually very weak, a Neff 122 DC amplifier was used to amplify the signal. A set of double slits with a dimension 0.015 cm by 0.5 cm was placed in front of the photomultiplier. The slit surfaces are parallel to the invariable y-direction of the 2-D flame so that the radiation from the flame entering these slits is restricted to a narrow width at a measured distance above the burner surface. The photomultiplier was fixed on a traversing stand which allows vertical movement during the tests. The accuracy analysis will be given in next chapter.

Thermocouple (T/C) probe and the adjacent wire are in the direction of isotherms

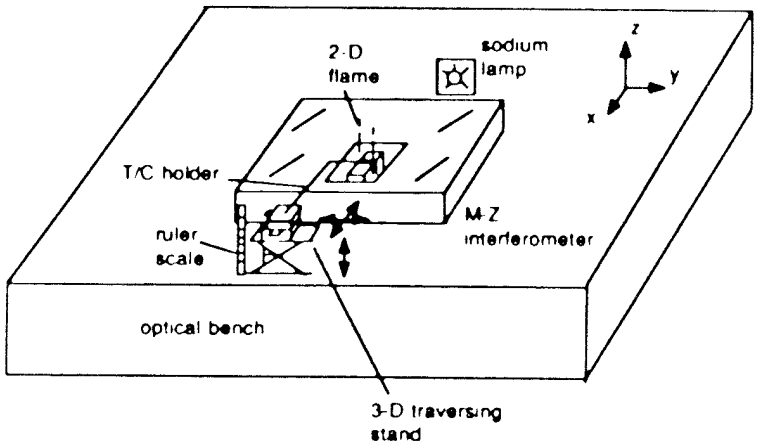

Figure 2.10
Setup for the Miniature Thermocouple (T/C) Probe (0.003")

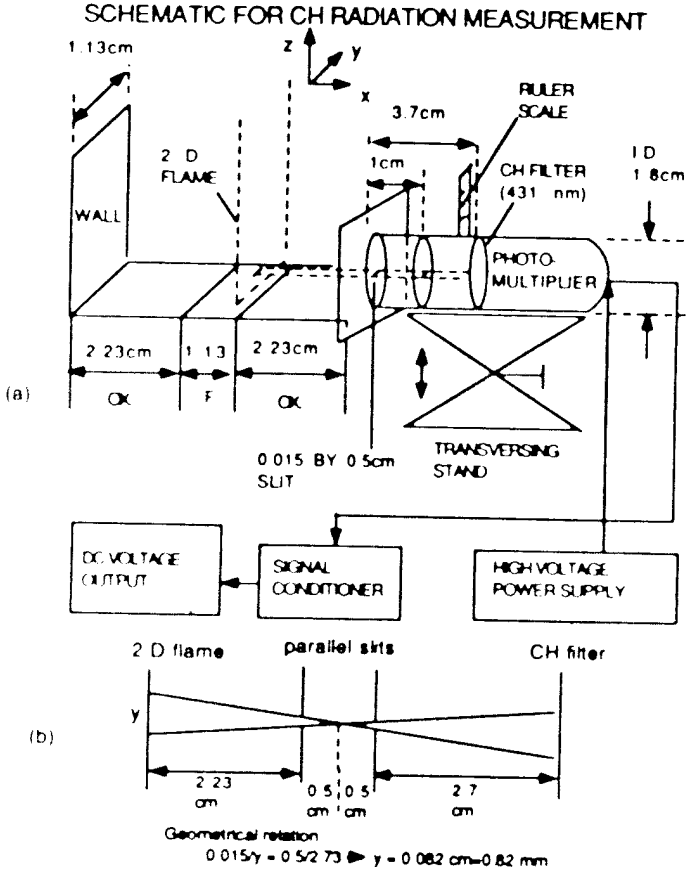

Figure 2.11 (a) System Setup for CH Radiation Measurement
(b) Estimation of the Height of the Integrated Light Collected by the CH Filter

CHAPTER III

PROCEDURE AND ERROR ANALYSIS

Since the experimental apparatus involved here were used for the first time in this laboratory during this project, the operation strategies and error analyses associated with each of the systems had to be evaluated carefully.

Figure 3-1(a) is a photograph of symmetric diffusion flames stabilized on the 2-D burner. Figure 3-1(b) and 3-1(c) compare pictures of interferograms from one of a symmetric pair of flames and a single flame (one outer oxidizer channel was replaced by nitrogen flow) at U_g=30 cm/sec. It can be seen from Figure 3-1(b) that the elevated temperature fields around two flame bases do not interact with each other. Comparison of Figures 3-1(b) and 3-1(c) indicate that the removal of one side of the symmetric diffusion flames does not affect the leading edge portion on the other side of the diffusion flame. Apparently, the fuel slot was too wide for two leading edge flames to "see" each other and the presence of one flame or two flames does not make any impact to the investigation on leading edge flame behavior. Thus, for simplicity, the subsequent experiments are all conducted under a single diffusion flame condition with nitrogen flow introduced to the other oxidizer channel to prevent the onset of unwanted flames.

3.1 Interferometer Error

3.1.1 Cold Flow Checkout

Eq.(12) was obtained at the end of the Appendix (A) as an explicit expression to convert the index of refraction field to a temperature distribution in a 2-D flow field. The equation is rewritten here as

$$T(x,y) = \frac{\sum_i X_i N_i}{\left(\frac{2S(x,y)R_0\lambda}{3P_0L} + \frac{N_r}{T_r}\right)} \qquad (3.1)$$

where $T(x,y)$ = the absolute temperature at location (x,y)

$\sum_i X_i N_i$ = molar refractivity of a homogeneous mixture

$S(x,y)$ = the fringe shift at location (x,y)

R_0 = the universal gas constant

P_0 = the ambient pressure

L = optical path length in the test object

λ = the wavelength of the light source

N_r = the molar refractivity of the gas in the reference beam

T_r = the temperature in the reference beam

A cold flow test was performed to check the applicability of the above equation to the present burner system. First, a cold flow interferogram regarding methane/air diffusion field above the 2-D burner (see Figure 3.1(d)) was examined to obtain actual fringe shift value near the burner surface. Eq. (3.1) is then used inversely for back calculation of an effective optical path length, L, under given conditions at T_r=298^{0}K, p=1 atm, λ=5893A, $\sum X_i N_i = N_{CH4}$=6.597, $N_{r,(air)}$=4.38, and S=2.625 (measured fringe shift near surface), the path length so obtained has the value, L=1.137 cm, only 0.6% higher than the burner width (L=1.13 cm) in the neighborhood of the burner surface. This result indicates that the

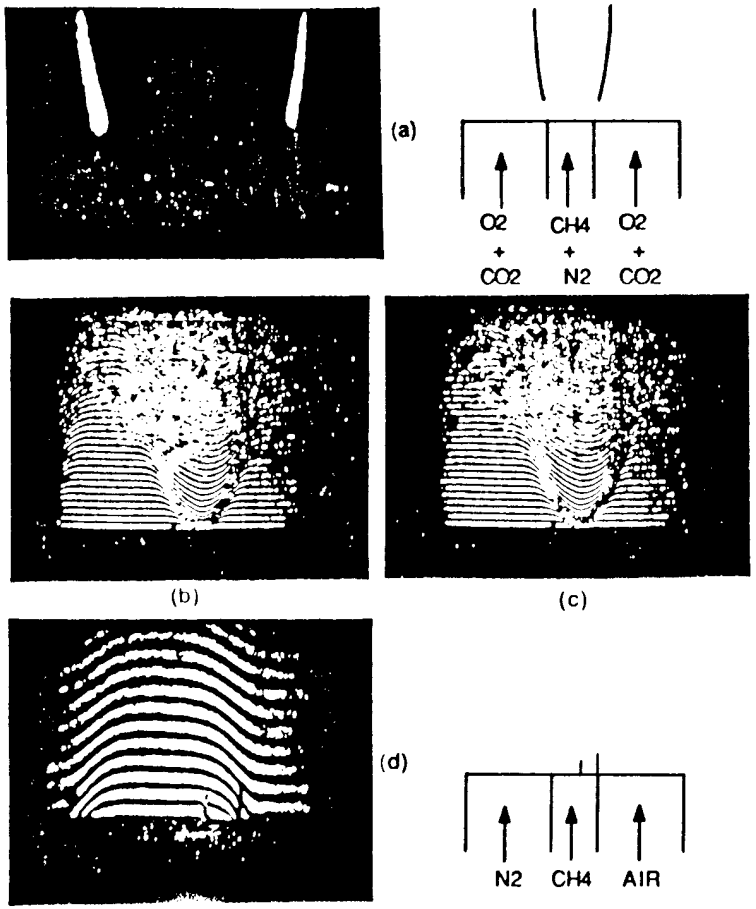

Figure 3.1 (a) photograph of symmetric diffusion flames. (b) fringe pattern on one of a symmetric pair of flames. (c) fringe pattern of a single flame. (d) cold flow mixing with N2/CH4/AIR streams above the 2-D burner

simple optical theory can apply to the present burner system and proper optical constants have been adopted for the associated calculations.

3.1.2 Sensitivity of Fringe Shift

Determination of the temperature field from the interferogram involves magnification of the picture by projection on a screen and measurement of the location (shift) of the fringes. For satisfactory measurements under the present experimental conditions, the distance between adjacent fringes is divided up for interpolation. The accuracy of temperature measurements by this system was examined by Weinberg [60], who used the following equation for the minimum resolvable temperature change

$$dT = -\frac{T^2 \lambda dS}{T_0 L(n_0 - 1)} \qquad (3.2)$$

where T = 1500°K (temperature near the flame base)

λ = 5893 A (wavelength for the sodium D-line)

dS = 1/40 (distinguishable measured fringe shift)

T_0 = 298°K (ambient temperature)

L = 1.13 cm (physical path length of the burner)

n_0 = 1.0002686 (index of refraction for air at STD condition)

Although the formula indicates that the accuracy falls off as the square of the temperature at which measurements are carried out, the smallest variation in temperature detectable in our system is just T=36°K around the flame base. It appears that this kind of accuracy is better than what a normal thermocouple (T/C) can accomplish (however the main virtues of the

interferometer method are nonintrusiveness, and ease of acquisition of complete temperature fields).

3.1.3 Refraction Error

The prime reason to choose a small path length for our burner is to avoid the refraction error. The refraction error involves the deflection of light caused by steep index of refraction gradient. This error can become serious when the path length is long. Weinberg [60] has also pointed out that errors due to refraction can be approximately corrected for by a method of successive approximations. Without refraction error, the optical path is $\int_0^L n dx$. However, the actual path is, in fact $\int_0^S n ds$, where S=total length along s, the coordinate measured along the ray path, which deviates from the x coordinate.

$$\int_0^S n ds = \int_0^L n \sqrt{1 + (\frac{dy}{dx})^2}\, dx = \int_0^L n\left[1 + \frac{1}{2}(\frac{dy}{dx})^2\right]dx \qquad (3.3)$$

From the approximation for gases, $n = 1 + \delta$, where δ is the fractional change in light velocity ($\delta << 1$), the following equation holds

$$\frac{dy}{dx} = -\int_1^2 (\frac{1}{n})(\frac{dn}{dy})dx = -\int_0^s (\frac{\partial \delta}{\partial y})dx \qquad (3.4)$$

After substitution, the error (the difference) in the optical path can be estimated to be

$$(\frac{L^3}{6})(\frac{d\delta}{dy})^2 \qquad (3.5)$$

provided the refractive index gradient is constant. For a case of maximum error where the maximum refractive index gradient occurs at $T_s = 3T_0/2$, the path difference due to heat release only is $(n_0 - 1)L/3$. The fractional error, $E_{(fraction)}$, in the relevant zone is

$$E_{(fraction)} = \frac{(L^3/6)(d\delta/dy)^2}{((n_0 - 1)L/3)} = \frac{L^2(d\delta/dy)^2}{2(n_0 - 1)} \qquad (3.6)$$

For a methane premixed flame, $(d\delta/dy)_{max}$ approaches 10^{-3}/cm, $(n_0 - 1)$ for air is approximately 2.7×10^{-4}, so that the error in optical path is approximately $(L^2/5.4)$ per cent. For the case of our burner, L = 1.13 cm, the maximum error due to refraction would be $E_{fraction} = (1.2/5.4)\% = 0.2\%$. This confirms the preliminary expectation that no appreciable deflection of light can occur within such a short path, and refraction errors are negligible.

3.1.4 End Effect

The "end effect" refers to the fact that the flame and resulting temperature field are not completely two dimensional because the burner is truncated in the third dimension. Thus the test light beam traverses regions in front and back of the flame that contain nitrogen flow with both thermal and molecular diffusion from the "ends" of the flame. The test light beam traverses both the flame region and these front and back regions. It was anticipated that the effect of this end condition would be small in the LEF region because time for diffusion is small. Further up in the flame, the effect may be larger, affecting temperature measurements by interferometry.

On first thought, end effects are less damaging in deducing refractive index gradients than refraction error. The reason is that, although heat transfer in the gas always raises the temperature of the adjacent atmosphere, it also ensures that the steep temperature gradients

which exists in a flame do not extend far beyond their edges. Direct observation shows that the flame tends to expand in the direction of the light path into the shield nitrogen flow right after the leading edge flame where the temperature is approximately 1500^{0}K. Even though this expansion of the flame is small, the effect is still not negligible compared to the dimensions of the system; thus some unwanted fringe shift is present which seriously biases the downstream flame temperature calculation due to the increase of the light path, and the corresponding temperature and temperature gradient at the downstream region of the leading edge flame will be higher than the true value. Calculated results from the interferograms are in support of this observation. An attempt to examine the effective optical path length of the burner was failed because the limited size of the access hole in the interferometer prevents free turning of the burner to 90^0 which is needed to perform the check. Since this research is focusing on the investigations of flame formation at the leading edge of a diffusion flame where the characteristics of the flame such as Flame Stand-Off Distance (FSOD) and maximum temperature gradient are not strongly influenced by this end effect, a correction scheme has been employed for determining the temperature field in the downstream diffusion flame instead of pursuing major hardware or instrumentation changes. For convenience, a thermocouple is chosen to perform the work (See Figure 2.10). The accuracy discussion of the T/C data will be given later (section 3.3). In general, the maximum flame temperature is determined by the T/C measurement with the radiation correction. It is noted that the y-direction temperature variations (i.e. temperature slope) obtained from the interferogram studies approximately match the T/C measurements when the temperatures are below 1500^{0}K. Hence the correction made to those data points on interferogram located in the flame zone is to follow the T/C slope when the temperature reaches above 1500^{0}K.

3.2 Data Reduction of Interferogram

It can be seen from Eq. (3.1) that, generally, temperature is determined from apparent fringe shifts, composition, optical path length, and wavelength of the test beam assuming the state of the gases in the reference section of the M-Z interferometer is known. Since a sodium lamp is used for the light source in the experiment, the sodium D-line, λ= 5893 A, will be the standard wavelength here. Assuming suitable end effect corrections are made, the optical length is known, and only composition and fringe shift due to temperature require further attention.

3.2.1 Composition Effect

In Eq.(3.1) the effect of composition changes is indicated by the total molar refractivities of a mixture. As mentioned in Appendix (A), the molar refractivity (unit : cm^3/mole) is an approximate measure of the actual total volume (without free space) of the molecules in one gram mole, and a variation of molar refractivity, just like a change in index of refraction, will induce some fringe shifts in a interferogram. A listing of molar refractivities for major species is shown in Table 3.1 (See p.59). Cubic spline fitting has been applied to interpolate the best possible data from Gardiner et al [73] at the conditions λ_D = 5893 A, P= 1 atm, and T= 298^0 K. In order to quantify the temperature rise from interferometric data, it is necessary, therefore, to separate the change in refractivity associated with temperature rise from that associated with the accompanying composition changes.

The difficulty involved here can be shown by examination of the following figures. First, photographs of the interferogram pattern regarding CH4/AIR cold flow mixing are presented in Figure 3.2 for three different gas velocities (20, 30 and 40 cm/sec). There are three constant concentration lines (X_{CH4}=1.0, X_{CH4}=0.62, and X_{CH4}=0.24) directly appearing on each of the pictures and the dimension scales set between the two markers in the pictures are 3 minimeter. These lines are obtained by using the infinite fringe setting of an M-Z interferometer. In this adjustment, the reunited beams are coincident and the order of

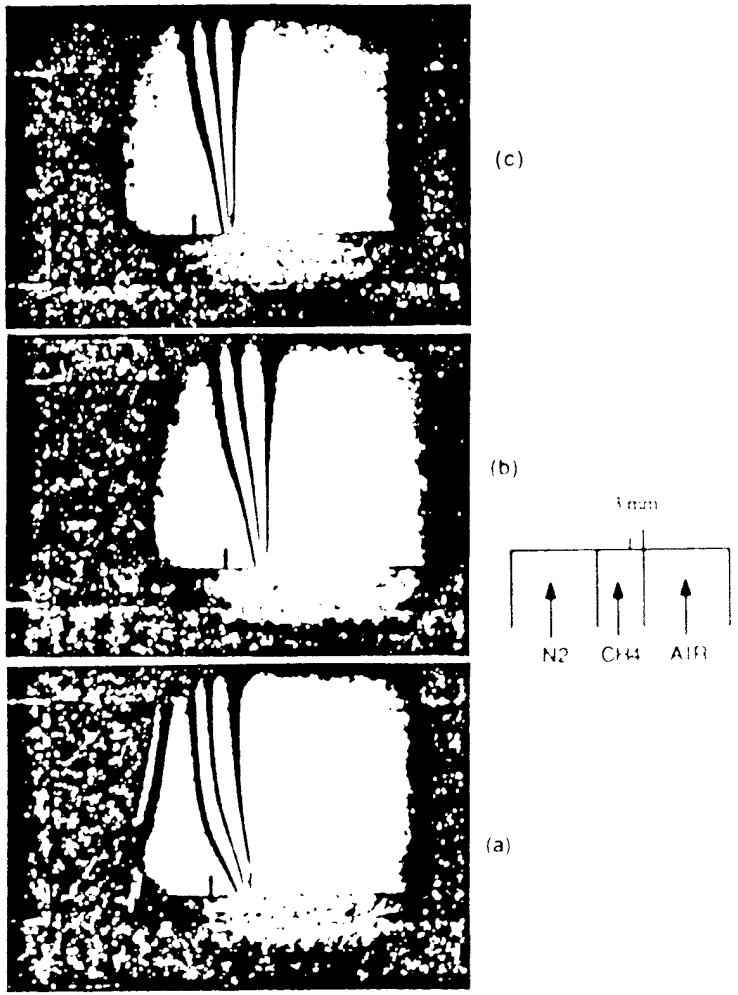

Figure 3.2 CH4/AIR Cold Flow Mixing at Various Velocities
(a) 20 cm/sec (b) 30 cm/sec (c) 40 cm/sec

interference is the same everywhere in the field. Without disturbance the screen will appear uniformly bright or dark. When a disturbance is introduced, the screen will show a succession of dark and bright contours where the disturbance occurs. Each of these contours is a locus of constant path difference (i.e. constant fringe shift). In this test with methane on the left and air on the right, the molar refractivity of the methane is higher than that of air, so the contours (constant path difference lines) become the constant concentration lines in an uniform temperature field. The results from this figure will be used later (section 5.2) to demonstrate the effects of the diffusion and convection on the cold flow mixing of two gases.

When a diffusion flame is present, the change of the fringe pattern occurs. Figure 3.3(a) gives a typical fringe pattern with flame using the same infinite fringe setting. These resulting interference pattern would constitute a family of isotherm curves if the molar refractivity is uniform in the field. Instead, the fringe lines show an asymmetric pattern about the flame (the flame is revealed in this picture by using a second exposure of the film imaging the self luminosity of the flame). There are more fringes on the methane side of the flame because of an overall gradient in molar refractivity across the mixing region. Figure 3.3(b) and 3.3(c) are double exposure pictures of interferograms obtained from the same test condition as that in Figure 3.3(a), but 3.3(b) illustrates a horizontal fringe setting and 3.3(c) is a superposition of (a) and (b). Since the horizontal fringe setting interferogram was chosen to carry out the data reduction, 3.3(b) and 3.3(c) will be used later to facilitate the understanding of the data reduction procedure (section 3.3.2).

In order to obtain the temperature distribution from those fringe curves (constant path difference lines), One may attempt to calculate molar refractivity field, and make correction for this in compensation of the temperature field. However, another strategy was used to resolves this problem.

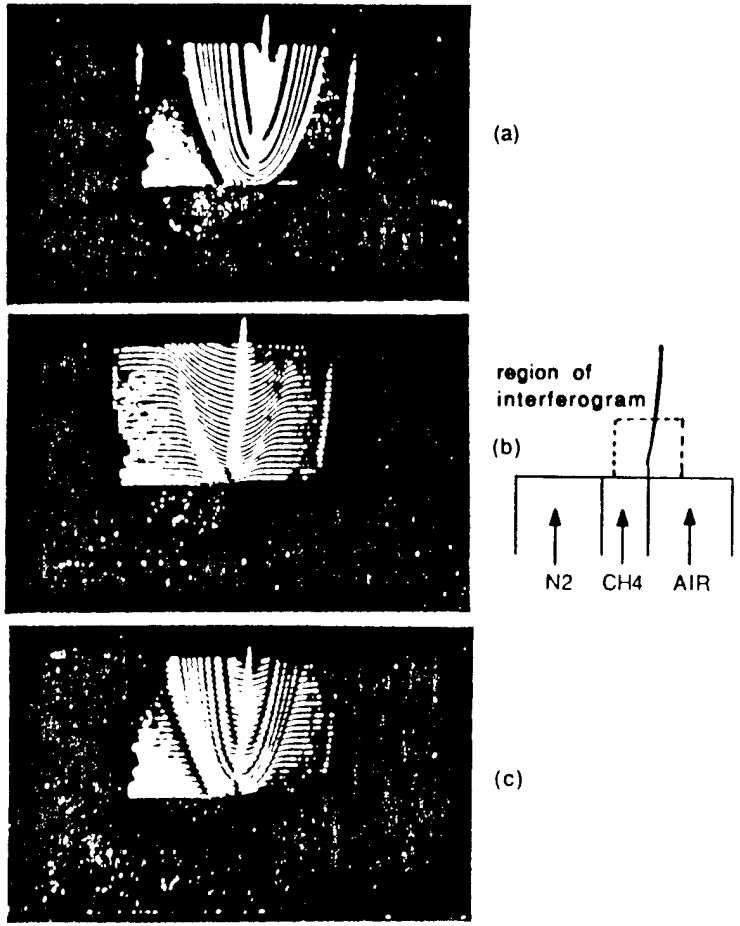

Figure 3.3 (a) a double exposure photograph of CH4/AIR self luminosity flame with an infinite fringe setting of the M-Z interferometer (b) a double exposure photograph of CH4/AIR self luminosity flame with a horizontal fringe setting of the interferometer (c) a photograph of the superposition of (a) and (b)

One method for avoiding fringe shift due to composition changes is to mix CO_2 with O_2 for the oxidizer stream and use CH_4 and N_2 in the fuel stream. CO_2 has a molar refractivity value close to that of CH_4 and O_2 has a similar molar refractivity value to that of N_2, so it is possible to keep the molar refractivity uniform in the mixing field by proper adjustment of diluent gases. Stable flames could be obtained over a wide range of reactant concentrations while keeping matched molar refractivities. Consequently, this scheme is good for parametric studies.

Since this scheme eliminates the fringe shift effect caused by the composition induced refraction index changes in the premixed region ahead of the flame, the fringe shift in this region is due completely to the temperature rise. Another advantage of this scheme is that the molar refractivity of a mixture remains virtually unchanged when going from the unburned reactant states to the burned product states and throughout the mixing/interaction processes. An example is given here to estimate the variation of the molar refractivity in a diffusion flame field. At λ=5893A, P=1 atm, and T=298 K, the complete combustion of the diluted methane with the diluted oxygen is written as

$$(CH_4+0.4888N_2) + 2(O_2+2.4253CO_2) \longrightarrow 2H_2O+0.4888N_2+5.8505CO_2$$

In the above case, both the reactants in the fuel stream and in the oxidizer stream carry the same molar refractivity value, $\sum$ XiNi=5.898, the fringe pattern remains uniformly spaced throughout the field of mixing in the cold flow diffusion case, indicating no fringe shift due to the diffusion induced composition changes, and the presence of large dilutions everywhere will give the final products a molar refractivity value of $\sum$ XiNi=5.838, a total difference of 1% with respect to the unburned condition. Thus, we should be able to neglect the composition related index of refraction changes throughout the mixing/combustion field. Figure 3.4 demonstrates a combustion/diffusion field from the

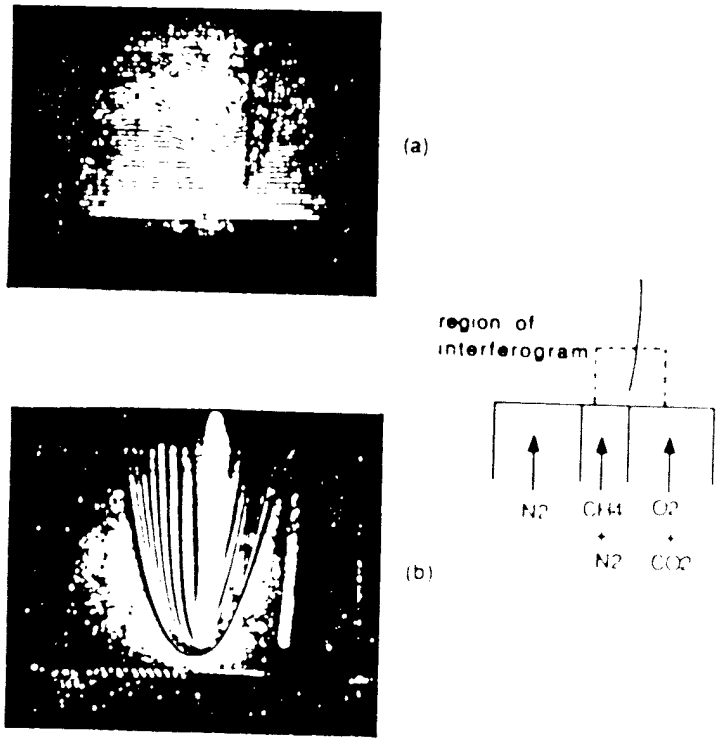

Figure 3.4 (a) diffusion flame in a equal molar refractivity field through a horizontal fringe setting of an M-Z interferometer (b) a double exposure photograph of diffusion flame in an equal molar refractivity field

equal molar refractivity flow with both horizontal and infinite fringe setting of the M-Z interferometer. Figure 3.4(a) is a typical picture used for the data reduction purpose. Figure 3.4(b) is a double exposure picture containing equal numbers of fringe lines on both sides of the diffusion flame. Unlike the asymmetric fringe pattern (more fringe lines on the fuel side of the flame) in Figure 3.3(a), an uniform bright field appearing in the flame upstream region in Figure 3.4(b) is a result of the equal molar refractivity flow.

Furthermore, CO_2 is a stable product. Reaction of CO_2 requires high temperature and can only take place at post-burning stage of methane flame [74,93]. Hence, CO_2 may be considered as an inert gas in the premixed region and up to the leading edge flame region where the temperature is considerably below the adiabatic flame temperature due to heat losses.

3.2.2 Fringe Counting Procedure

After previous discussions, the last quantity in Eq. (3.1) to be determined from the interferogram studies is the fringe shift. In an uniform molar refractivity field, the lines of constant fringe shifts correspond to the isotherms through the simple conversion of Eq. (3.1), and isotherms have been chosen to present the data here. The reason is that the heat flux vector is always in the direction normal to the isotherms, so the temperature gradient taken at that direction represents the overall gradient, not the component of it. Since the gradient study plays a crucial role in our experiments for justifying the presence and the location of the leading edge flame, the use of isotherms will facilitate the interpretation of our results.

There is a direct way to obtain constant fringe shift contours. As mentioned in section 3.2.1, the M-Z interferometer can produce instantaneous constant fringe shift contours (i.e. isotherms in an equal molar refractivity field) by a method called infinite fringe setting. Unfortunately, the isotherms generated by this method are separated by one fringe shift and

do not have enough resolution for the temperature gradient studies. i.e., there are not enough isotherms directly visible in the field of interest to produce enough data points for gradient analysis. It can be seen from Figure 3.3(a) and 3.4(b) that the infinite fringe setting interferograms produce too thick a fringe width to give accurate temperature evaluation and the numbers of isotherms available are also limited. In order to get narrow fringes with correspondingly more points for describing the temperature profile, a horizontal finite fringe interferogram was adopted to perform the data reduction.

There are two methods of counting the fringes, one method is to superimpose disturbed and undisturbed patterns and the loci of the intersections of dark and bright fringes can be seen as grey lines in the field, these are lines of constant fringe shift, having shifts 1/2, 3/2, 5/2, etc. and are therefore isotherms. If the undisturbed pattern can be moved by 1/10 of a fringe spacing, isotherms for S=0.6, 1.6, 2.6, etc. can be obtained, and similarly for other fractions of a fringe width. This method will induce some uncertainty when trying to move the undisturbed pattern and superimpose with the disturbed pattern. Another method can be used when the disturbed fringe pattern contains some undisturbed fringes (i.e. the outer cold flow; see the horizontally parallel fringes in Figure 3.3(b) on the air side and Figure 3.4(a) on the oxidizer side). In this case, there is no need to record the undisturbed pattern but only to extrapolate the straight fringes and count the fringe shift at any point of intersection with a disturbed fringe. Thus at any point (x,y) the fringe shift S from the cold flow can be measured and the temperature can be calculated. It can also be seen from Figure 3.3(b) and 3.3(c) that the maximum fringe shift points of the disturbed fringe with respect to its undisturbed part are located in the flame zone.

Since we are interested in isotherms, the procedure is to determine at which locations, (x,y), the constant fringe shift changes occur. This procedure is implemented as follows (see Figure 3.5):

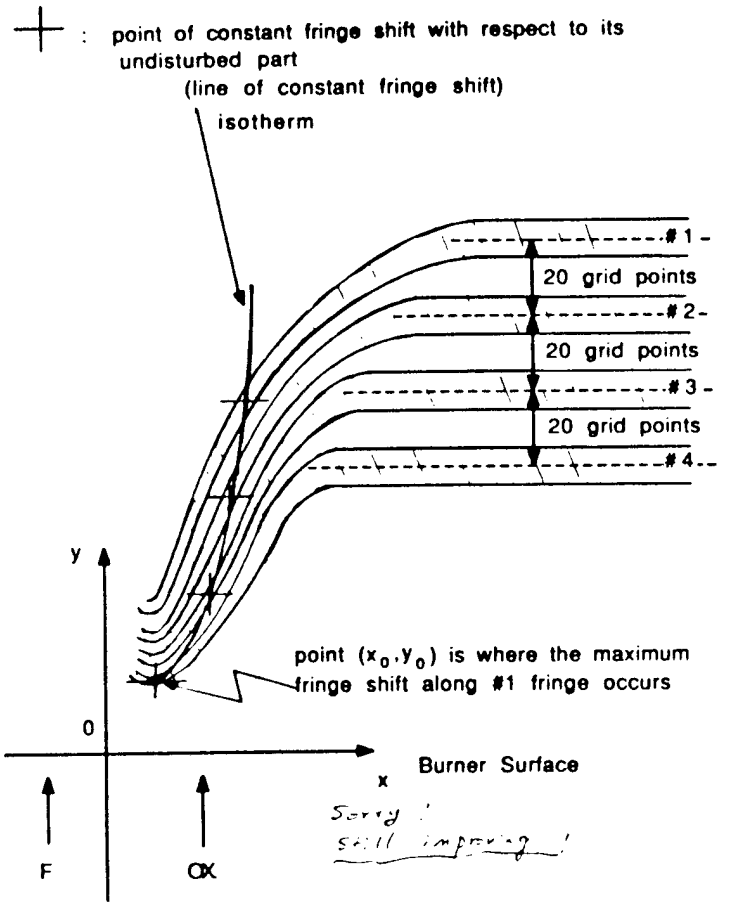

Figure 3.5 Fringe Counting Procedure for Isotherm Studies

1) Project the test interferogram with horizontal fringe setting onto a screen of uniform grid system

2) Define the coordinates above the burner surface in the grid system. Align, number and record the centerline y-coordinates of the reference fringes in the undisturbed part of the field such that there will be 20 grid points located between two reference fringes

3) Start from the undisturbed part of the field. Follow through each fringe which has a detectable fringe shift. Record the coordinates at the locations where the maximum fringe shifts occur (e.g. (x_0, y_0) in Figure 3.5 is the maximum fringe shift location for #1 fringe). These maximum fringe shift values will be used to draw the constant fringe shift contours. (Usually the maximum happens in the flame zone or directly upstream of a flame in the preheating zone.)

4) Use a cross cursor system to locate the (x,y) coordinates for a constant fringe shift value on each fringe.

5) Interpolate one set of constant fringe shift coordinates with a least square method to fit through a 5th order polynomial. Establish the contour lines of different fringe shift values across the test field.

6) Convert those loci of constant fringe shifts to isotherms by Eq. (3.1) and the method described in section 3.2.4 for downstream correction.

3.3 Miscellaneous Systems

Thermocouple Errors

Two kinds of procedures are developed for the T/C measurements. First, we travel the T/C micro-probe in the direction perpendicular to the optical path of the 2-D flame to check the effective path length in the downstream diffusion flame zone (the y-direction in Figure 2.10). This path length is determined between the locations where high temperatures (above 1250°K) are recorded by the T/C. When this effective path length obtained from T/C measurement is used as the input to the temperature conversion formula Eq.(3.1), the calculated temperature generally shows reasonable agreement (± 50°K) with the T/C temperature measurement. Next, efforts are exercised to achieve the optimum measurement accuracy. For a T/C to give optimum results, it needs to be placed into a reaction zone with a configuration in which the immediate leads to the thermojunction lies in an isothermal plane in the flame (Dixon-Lewis [75]). This is to avoid heat conduction down the wire. A system of 3-D translators was assembled on the bench and used to insert the T/C probe into the flame zone in the direction parallel to the optical path and move it along the vertical distance above burner surface (the z direction in Figure 2.10). This configuration can eliminate the heat conduction losses imposed on the head. Although the radiation losses still exist, they are more predictable, hence they can be corrected good accuracy. The details of radiation corrections are given in Appendix (B) and Table 3.2 lists the calculated results after corrections.

CH Radiation Measurement Error

CH radiation measurement is used as a complementary tool to check the heat release rate from the interferometry results. Therefore, these two measurements are conducted together during one test run. The geometrical relation between the set of double slits (0.15x5 mm) and the test region (Figure 2.11) is such that only the radiation from less than 1 mm of flame height will be able to penetrate through these slits. The output DC voltage is very stable in general with a fluctuation less than ± 1%, allowing a direct readout from voltmeter.

Table 3.1
Collection of major refractivities for major species [73]

Major species	Molar refractivities at 589.3 nm (cm**3/mole)
CH4	6.597
O2	4.046
N2	4.468
CO2	6.662
H2O	3.761
H2	2.076
CO	5.007
NO	4.400

Table 3.2

Radiation Corrections for the Thermocouple Measurements Assuming a Spherical Bead Geometry

Thermocouple Temperature(K)	Radiation Correction(K)	Corrected Temperature(K)
1300	22	1322
1400	28	1428
1500	35	1535
1600	42	1642
1700	52	1752
1800	61	1861
1900	72	1972
2000	84	2084

CHAPTER IV

EXPERIMENTAL RESULTS

The Leading Edge Flame (LEF) behavior of a single methane diffusion flame stabilizing on a modified Wolfhard-Parker burner at atmospheric pressure has been studied in this research program through an experimental approach. First, combustion photography and CH flame radiation measurement were conducted to examine the heat release rate at the LEF region. Then, Schlieren system, M-Z interferometer, and thermocouple temperature measurement were applied to study the controlling processes of the LEF region in a systematic way (i.e., varying gas velocities and dilution levels). The results were used to assist the development of a phenomenological model which will be discussed in next chapter.

4.1 Combustion Photography

It is believed that the LEF anchors the whole diffusion flame and dominates the heat transfer back to the upstream boundaries (burner surface, propellant surface, etc.). In order to justify this argument, we begin with a simple qualitative investigation using combustion photography methods. First, photographs are taken using infrared film to detect the location of the "hot" spot. Besides being infrared sensitive, this film is also documented by Kodak to be sensitive to the blue light which is the radiation emission from CH radical. This intermediate species is believed to be a measurement of heat release rate (See next section for details). An infrared photograph of the flame is shown in Figure 4.1, where it is

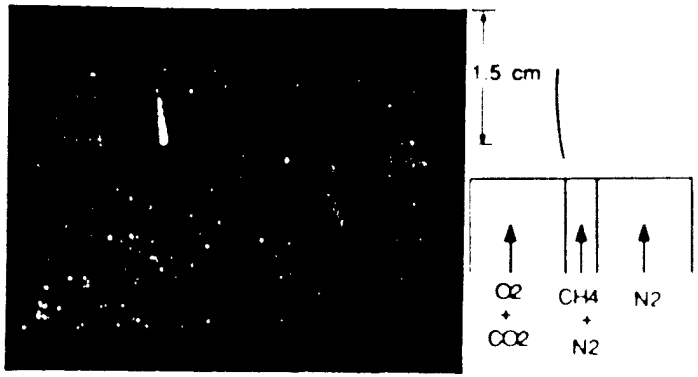

Figure 4.1 Photograph of a Diffusion Flame from an Infrared Film

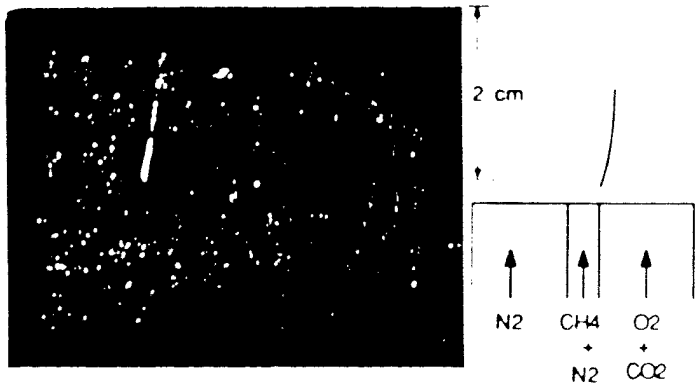

Figure 4.2 Photograph of a Diffusion Flame through a CH Filter

seen that the brightest part is in the LEF, and the intensity gradually decreases as the diffusion flame trails off downstream. Next, based on the argument that CH flame radiation intensity is proportional to the heat release rate [82], pictures are taken with a CH filter in front of the camera lens. Figure 4.2 provides a typical picture of such a flame. The variation of the flame luminosity is very similar to that of the infrared picture obtained in Figure 4.1 (i.e., the LEF region is the brightest part of the flame).

4.2 CH Flame Radiation Intensity Measurements

In order to obtain quantitative results to distinguish the heat release rate distribution between the LEF and subsequent diffusion flame, experiments were conducted in a systematic way using an indirect approach. Earlier researchers [77-81] have shown that C$_2$ and CH are among the most prominent transient species observed spectroscopically in all hydrocarbon-oxygen flames. It has been established that, for both the premixed flame and diffusion flames [82-84], the emission from these radicals in the visible spectral region is confined almost exclusively to the reaction zone, hence the intensities of radiation from radicals C$_2$ and CH provide a measure of the reaction rate and thus, the heat release rate of flames.

Both CH and C$_2$ filters were tested for the experiment, the results indicated that the CH blue band has a much stronger radiation detectable intensity level than the C$_2$ green band, hence the following tests were all conducted by using the CH filter.

Observations using aligned double pin holes in front of the radiation receiver (photomultiplier) to collect the parallel light from a point in the flame was not successful because the radiation intensity passing through these two pinholes was too weak to be detected. The current setup using aligned slits (Figure 2.11) was found to have adequate

sensitivity and accuracy (see section 2.4). The arrangement permits CH intensity be recorded as a function of height above the burner surface.

Test conditions for CH flame radiation measurements included variation of flow velocities for known compositions (Figure 4.3-4.4), and variation of mixture compositions at given velocities (Figure 4.5-4.7).

Profiles of normalized heat release rate vs height above the burner surface (positive y-direction) at 6 different velocities are plotted in Figure 4.3 for the CH4/AIR diffusion flames. In the figure, the heat release rate is normalized by a reference value (1.39 volt) which is the maximum value of the CH radiation intensity at a velocity of 15 cm/sec. In each case, the heat release rate first rises abruptly to a maximum value at the leading edge flame zone, then drops off after the LEF into the downstream diffusion flame. It is observed that, for different velocities, the heat release rates all have maximum values at the LEF region and the peak values increase with the increase of gas velocity.

A similar plot of the heat release rate data vs y-location at different gas velocities is provided in Figure 4.4 for a different primary mixture (Fuel: CH4/N2=0.54/0.46, OX.: O2/CO2=O.383/0.617). For this mixture, the molar refractivities (an optical property related to the index of refraction) are set equal in both the fuel and oxidizer flows - an optical condition suitable for the temperature evaluations from an interferogram. The results show a trend similar to Figure 4.3, but the maximum intensity level detected in Figure 4.4 at a given velocity is higher than that in Figure 4.3 for the same gas velocity and the LEF is stabilized at a location closer to the burner surface. Thus the results suggest that the CO_2 flame (N_2 was replaced by CO_2 in the oxidizer flow) for the current compositions has a higher flame temperature than the CH4/AIR flame at the same velocities. The CO_2 flame has more oxygen concentration (mole fraction=0.383) in the oxidizer flow as compared to air (oxygen mole fraction=0.21) and the adiabatic stoichiometric flame temperature

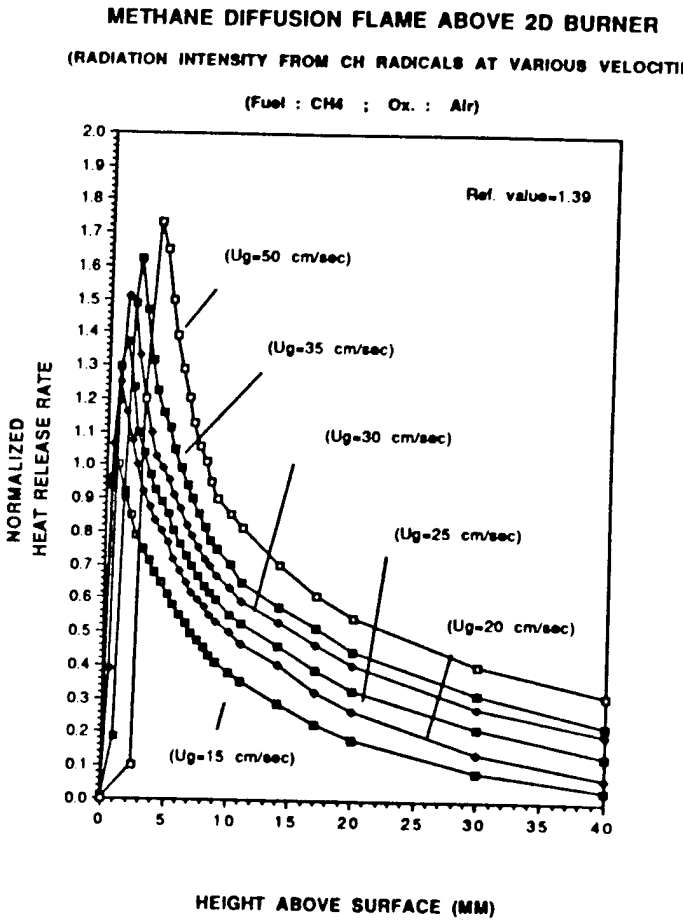

Figure 4.3 CH Radiation Measurement for CH4/AIR Diffusion Flames at Various Velocities

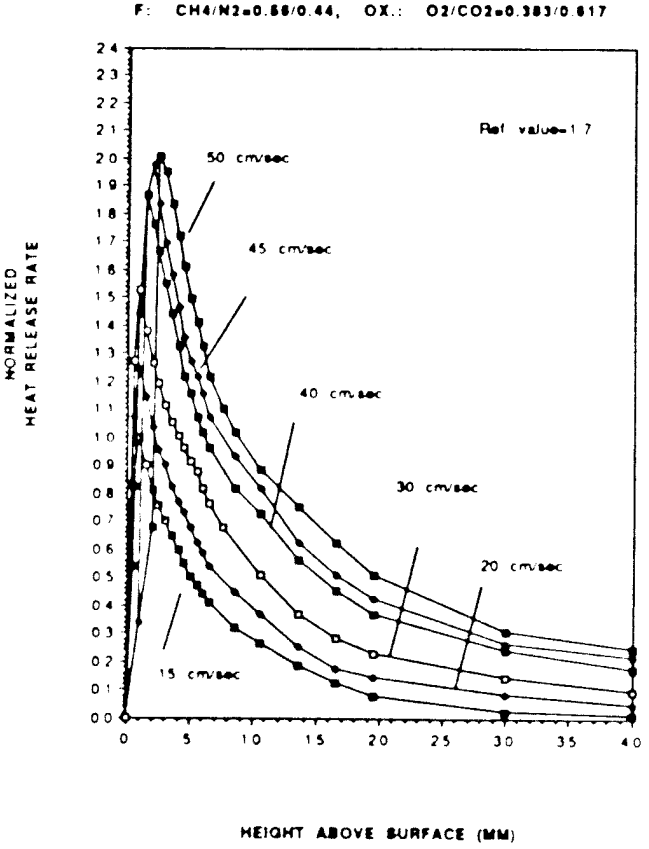

Figure 4.4 CH Radiation Measurement at Various Velocities (R=0.617)

calculated from the chemical equilibrium codes [85] for the CO_2 flame has a value of 2280°K compared to 2180°K for the CH4/AIR flame, explaining the higher reaction rate in Figure 4.4.

The next plot, Figure 4.5, gives the normalized heat release rate vs height for 5 cases of different molar refractivities. In each case, the condition of equal molar refractivity is maintained in the fuel/oxidizer (F/O) streams (See Table 4.1). The gas velocity is set at a constant value of 30 cm/sec for these cases. The heat release rate in each case again yields a maximum value indication of the leading edge flame zone with a rapid decrease on both sides. The leading edge moves further out in the mixing region with higher dilution. In addition, the peak values of the heat release rate decrease with the increase of the CO_2 mole fraction in the oxidizer flow, hence this CO_2 mole fraction will be used as an index to describe the dilution level in the mixing region of the equal molar refractivity flows. Additional tests for the same mixture compositions, but at a different gas velocity (45 cm/sec) are plotted in Figure 4.6, the main difference in the results at 30 and 45 cm/sec is that the peak heat release rates are higher at LEF zone at higher gas velocities, consistent with the higher reactant mass rates into the flames at higher velocity.

A different set of dilution tests (dilution of the fuel stream while keeping the composition in the oxidizer stream constant) is plotted in Figure 4.7. Unlike the notation in previous plots, R, in this figure, refers to the CH_4 mole fraction in the fuel flow. This plot will be used later as a cross check to assist with the interferogram studies.

During this sequence of tests, it was also learned that, at a low velocity (15 cm/sec) the LEF stays close to the burner surface, and the variations of the Flame Stand-Off Distance (FSOD) are rather insensitive to the changes of the mixture compositions at this velocity. This indicates that the heat transfer back to the burner surface exerts more influence on the stabilization of the flame than that from the 2-D heat balance in the gas mixing region. Since

Table 4.1
Equal Molar Refractivities Between the Fuel and Oxidizer Flows.

channel \ molar refractivity		5.554 or R=.576	5.607 or R=.597	5.660 or R=.617	5.701 or R=.633	5.742 or R=.648
Ox. Flow (Mole Fraction)	O2	0.424	0.403	0.383	0.367	0.352
	CO2	0.576	0.597	0.617	0.633	0.648
Fuel Flow (Mole fraction)	CH4	0.51	0.535	0.56	0.579	0.598
	N2	0.49	0.465	0.44	0.421	0.402

(R=CO2 mole fraction in the ox. flow)

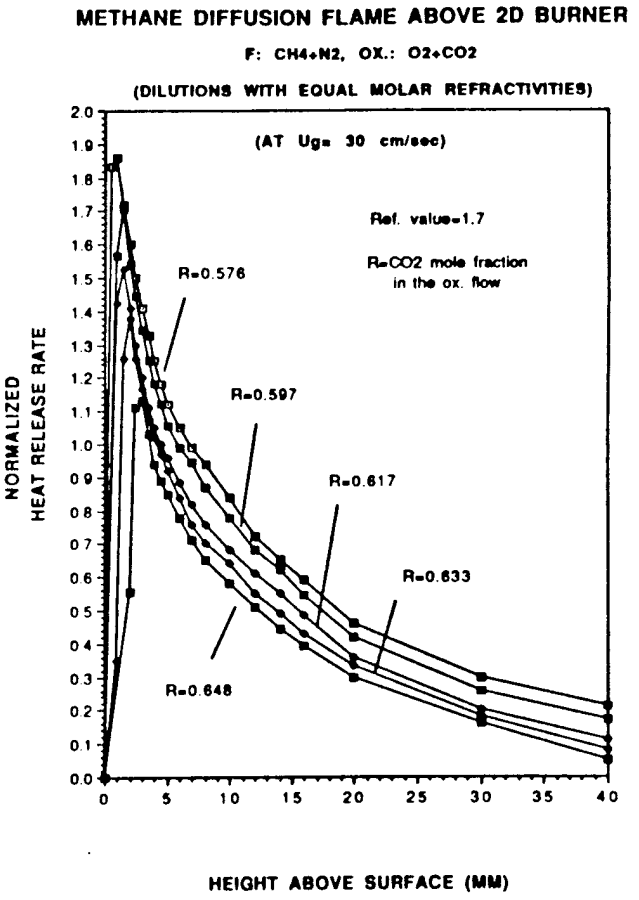

Figure 4.5 CH Radiation Measurement at Various Dilutions (Ug=30 cm/sec)

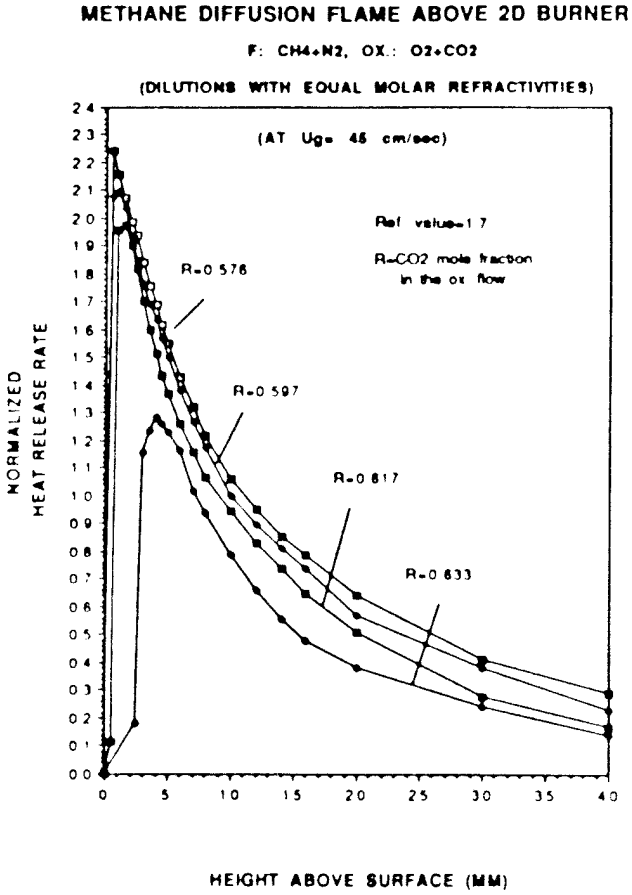

Figure 4.6 CH Radiation Measurement at Various Dilutions (Ug=45 cm/sec)

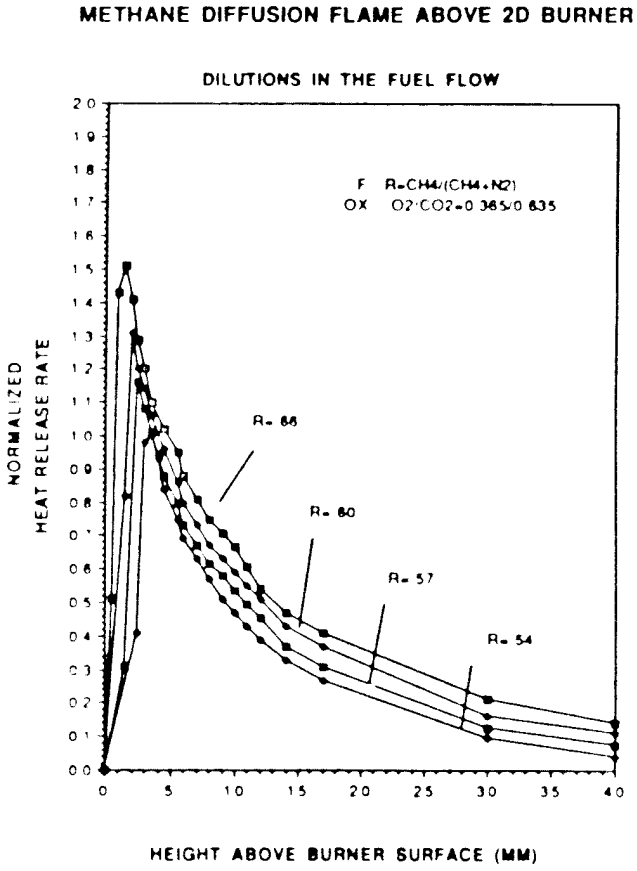

Figure 4.7 CH Radiation Measurement for Dilution in the Fuel Flow (Ug=30 cm/sec)

we have no control of the heat transfer back to the burner surface, this flow velocity (15 cm/sec) will be used as the low operation limit of gas velocity.

4.3 Schlieren Studies

A better qualitative perspective of the total LEF is given by the Schlieren photography (figure 2.7). Tests were conducted on methane diffusion flames with equal optical properties between the fuel and oxidizer streams (F: CH_4+N_2, OX.: O_2+CO_2), as illustrated in Figure 4.8. These images were all taken with the same schlieren sensitivity setting, and show the location and size of the steep temperature gradient region for flame at different velocities (30,40 and 45 cm/sec) and oxidizer dilution levels (R=0.597, 0.617, 0.633 and 0.648; where R is CO_2 mole fraction in the oxidizer flow).The results indicate that the dark region (approximately at the region where the LEF occurs) is clearly distinguishable from the rest of the diffusion flame (not appearing on the screen). It can be seen that, as the gas velocity increases, this dark region (LEF region) moves away from the burner surface and increases in size (i.e. area) by trailing off further downstream on both sides of the centered unseen diffusion flame. The same trend is observed in the cases of increasing dilutions. As the dilution level increases, this LEF region retreats downstream while becoming bigger. The Flame Stand-Off Distance (FSOD) in the case for R=0.633 and Ug=45 cm/sec is about 4.5 mm and all the pictures are under the same kind of magnification ratio (i.e. same dimensional scale).

4.4 Interferogram Studies

An M-Z interferometer has been used to study the temperature distributions around the leading edge portion of a diffusion flame. An investigation adopting parametric studies can

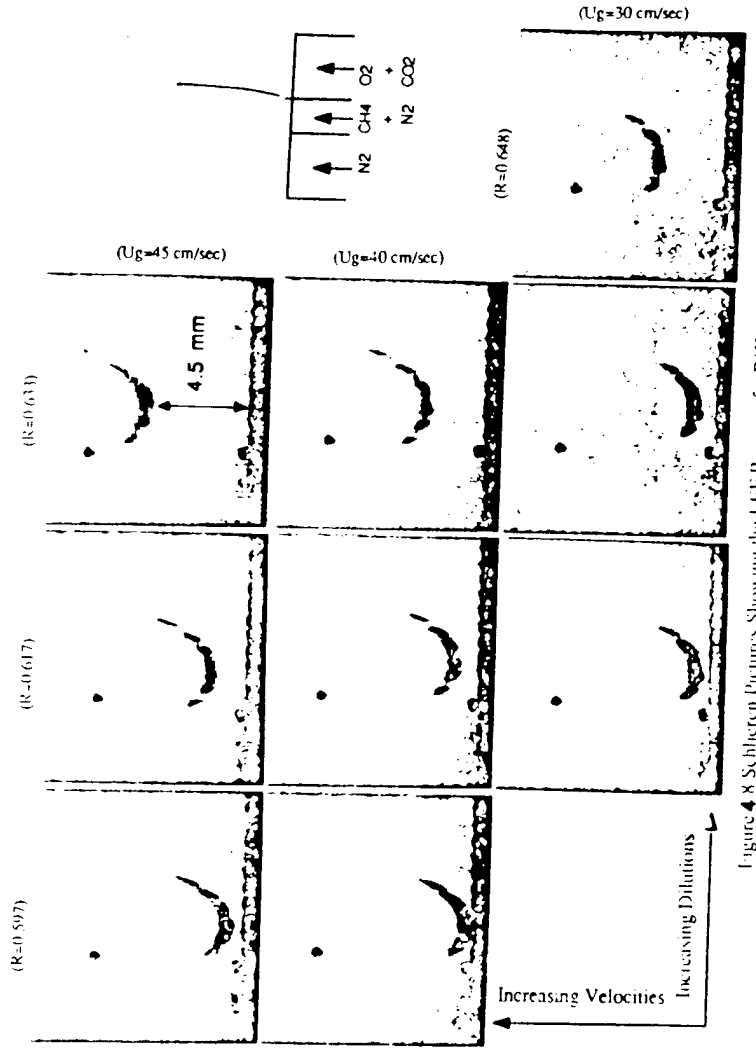

Figure 4.8 Schlieren Pictures Showing the LEF Region of a Diffusion Flame (R=CO2 Mole Fraction in the Ox. Flow)

provide the physical evidence needed to understand the flame structure of the LEF and, in turn, to support the phenomenological analyses regarding the characteristic of the LEFs

4.4.1 Effect of Gas Velocity

Systematic studies of varying flow and reactant variables with the LEF stabilizing on the burner have been performed. The effect of the gas velocity is investigated by comparing five cases of different velocities (20, 30, 40, 45, 50 cm/sec). In each case, the compositions in the fuel flow are set to be 56% CH_4 and 44% N_2 and the mixtures in the oxidizer flow have the compositions of 38.3% O_2 and 61.7% CO_2. For these mixtures, the condition of equal molar refractivity between the fuel and oxidizer flow is satisfied, a condition suitable for temperature evaluation from interferograms.

Because of the importance of heat flow from the LEF upstream into the "cold" reactant source, there is particular interest in the conditions along that path in the temperature field corresponding to the maximum vertical temperature gradient. In principle, this should be somewhere near a vertical line below the point of stoichiometric mixture ratio on the LEF (intersection of the LEF and the stoichiometric surface in the mixing flow). Since the burner operates with a dilute oxidizer, the stoichiometric surface is inclined in the side of the oxidizer flow (as indicated by the curved lines in pictures such as Figure 4.1 and 4.2). The temperature field was obtained from the interferogram using the data reduction procedure described in section 3.2.2. Temperature contours (isotherms) near the LEF region for gas velocity of 30, 40 and 45 cm/sec are presented in Figure 4.9 to 4.11. The apexes of these isotherm curves (where the flame is located) all appear in the oxidizer side of flow. In addition, the lateral temperature gradient on the fuel side is consistently lower than that on the oxidizer side. This is attributed to the ease of chemical reaction on the oxidizer side of flame simply because in this region, only small amount of fuel is needed to

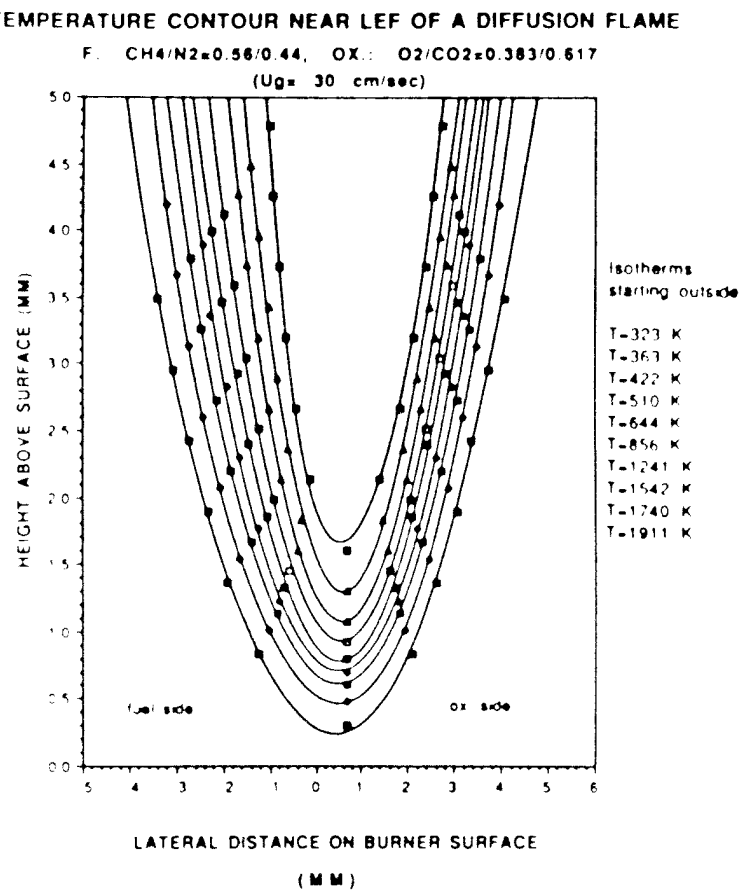

Figure 4.9 LEF Temperature Contours at 30 cm/sec

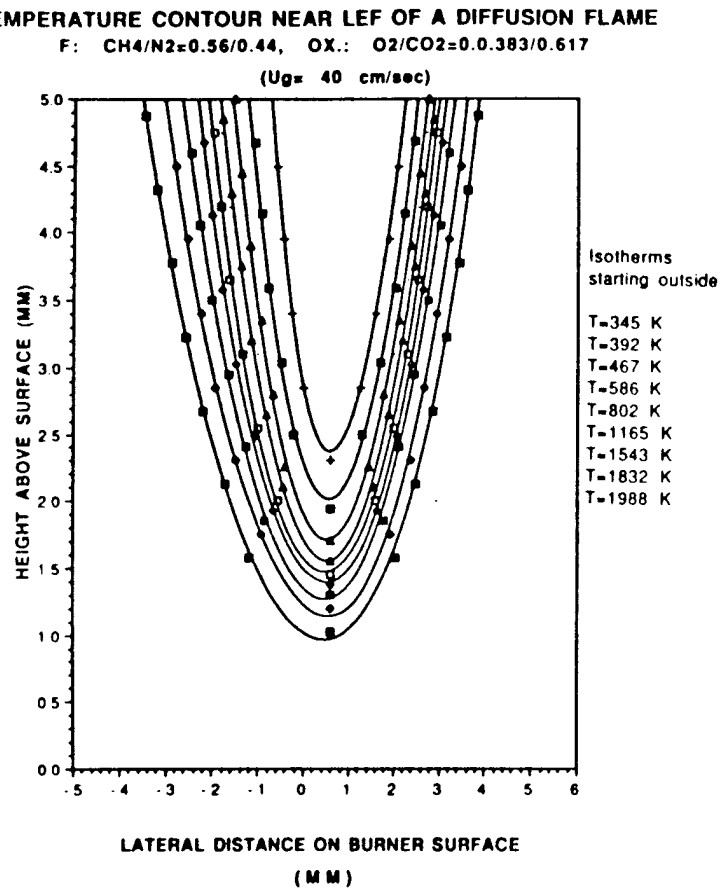

Figure 4.10 LEF Temperature Contours at 40 cm/sec

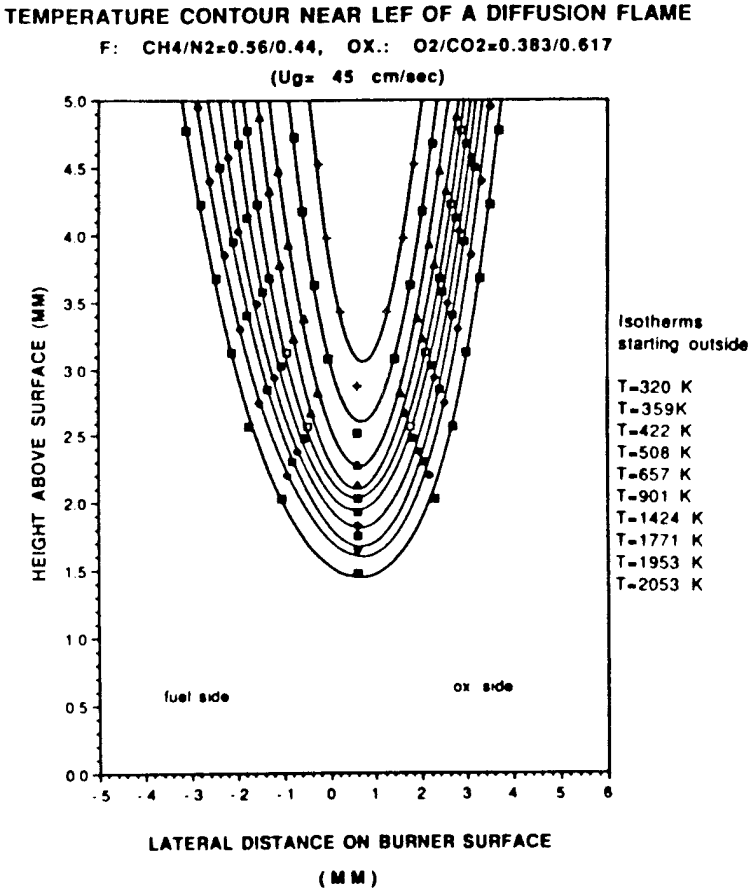

Figure 4.11 LEF Temperature Contours at 45 cm/sec

burn with the dilute oxidizer. Other trend indicates that the isotherms in a 2-D temperature field start to pack together when the convective gas velocity increases (i.e. the lateral derivative increases when the gas velocity is increased).

In order to acquire the desired maximum vertical temperature gradient and compare the interferometry results with the T/C results, the data for the temperature variation vs height above the burner surface was obtained and the results for 5 velocities are presented in Figure 4.12 for easy comparison. Data points represent the maximum fringe shift points (as referred to their undisturbed reference values) in the interferograms with the diffusion flame present (See Figure 3.3(b) and (c) for example). These points each represents the location which would yield the maximum measured temperature at a given height above the burner surface and corresponds to the apex of isotherm. In principle, these points should follow the stoichiometric surface between the fuel and oxidizer flows. As far as the lateral positions of these data points are concerned, they start from a lateral position in the oxidizer flow and remain unchanged in the y-direction prior to the flame, then follow through the reaction zone in the y-direction (the deviation in lateral distance is within 0.2 mm for the range of investigation, so the data points in each case are almost located on a constant vertical line). The initial lateral position of these data points is about 0.7 mm from the dividing plate into the ox. side of flow.

Due to the lateral expansion of the flame in the direction of the optical path, interferometer temperature evaluations in the flame zone were biased, hence the maximum equilibrium flame temperatures were determined with the help from the thermocouple (T/C) measurements incorporating radiation corrections (Appendix B). Generally, these y-direction temperature variations obtained from the interferogram studies approximately match the T/C measurements when the temperatures are below 1500°K. Therefore, the slopes of the temperature variations in Figure 4.12 follow the T/C slopes when the

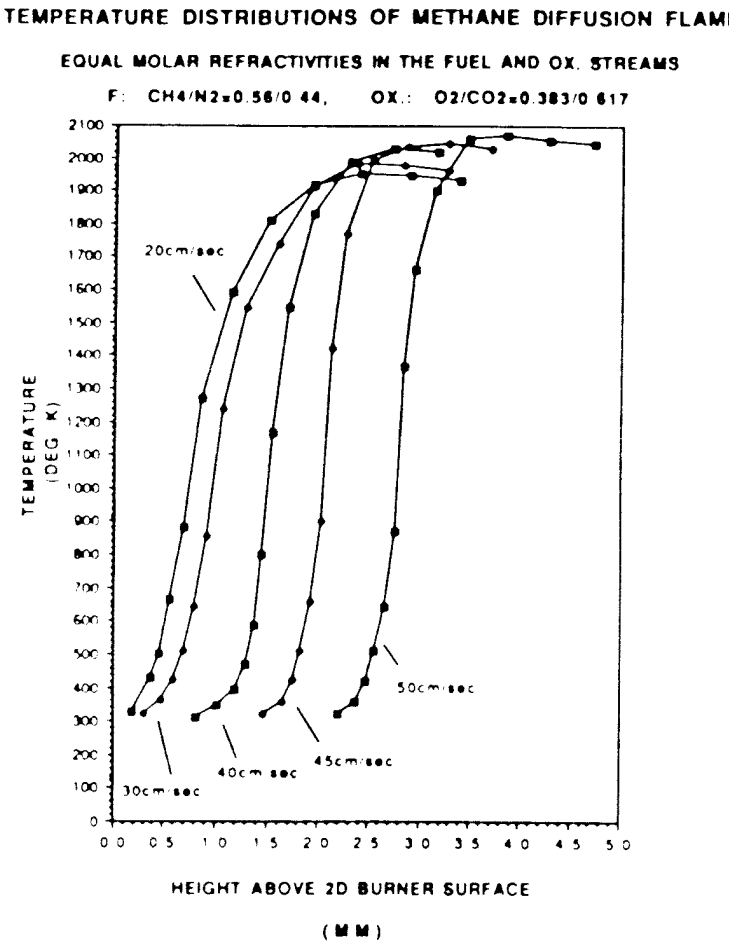

Figure 4.12 Effect of Gas Velocity on Temperature Distribution

temperature reaches above 1500^{0}K. Since emphasis is on diffusion/convection region leading to the formation of the LEF where both of the temperature measurements (either from interferogram studies or from T/C measurements) match, and the correction is limited to a region less than 1mm in height, this correction is not critical to the conclusions. It can be seen that, as the flow velocity is increased the FSOD increases, the temperature gradient in the flame increases, and the equilibrium flame temperature reaches a higher value. As would be expected, the observed temperatures are lower than the theoretical temperatures for adiabatic stoichiometric reaction to equilibrium (2180^{0}K for methane-air and 2280^{0}K for the CO_2 diluted combustion used here). Comparisons of the measured temperatures (including both CO_2 and AIR flames) and the temperatures obtained from the literature for methane-air diffusion flame [90] show a reasonable match in values and trend. Systematic studies indicate that the choice of using the primary mixture composition as the input to calculate the adiabatic flame temperature along the stoichiometric surface between the fuel and oxidizer flow seems reasonable because the trend goes as expected.

Figure 4.13 plots the needed temperature gradients against heights (positive y-direction with origin at burner surface) along these maximum fringe shift points on the interferograms. They are computed from the data presented in Figure 4.12 using a forward difference procedure. All the gradient plots indicate a rapid increase of temperature gradient before the LEF and a rapid decrease in temperature gradient after the LEF zone where the equilibrium condition is quickly obtained. This figure also provides the location of the Flame Stand-Off Distance (FSOD) which is defined here as the y-position where the maximum temperature gradient occurs at a test condition. The values of the maximum temperature gradient values are higher for flames at higher flow velocities, consistent with the requirement that the flame heats up a higher flux of reactants to remain stationary in the higher flow velocity.

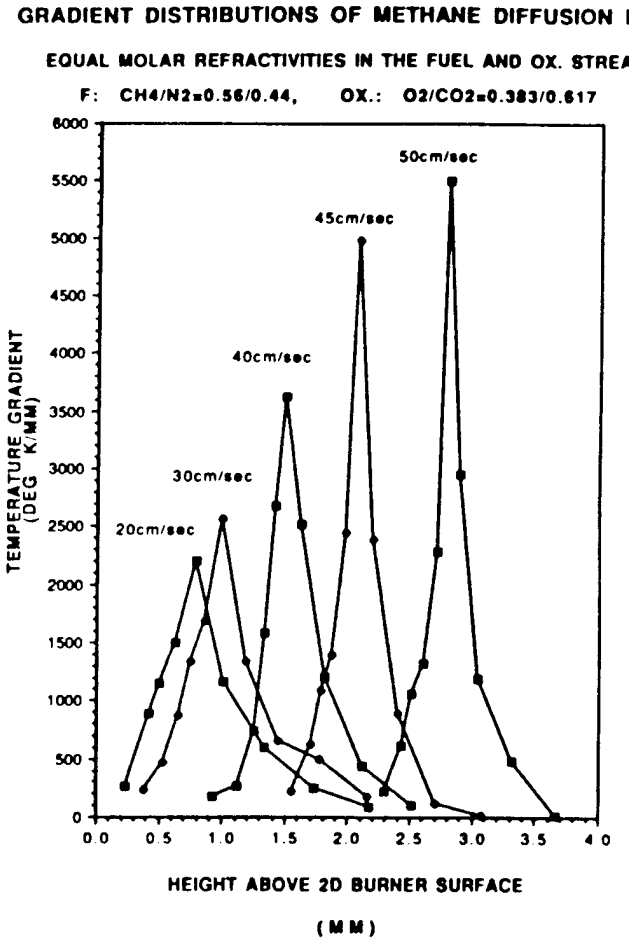

Figure 4.13 Effect of Gas Velocity on Gradient Distribution

Three important parameters; FSOD (determined from peak temperature gradient point), maximum temperature gradient and normalized Heat Release Rate (HRR, obtained from the CH radiation measurement) are plotted against gas velocity in Figure 4.14. The general trend from the three plots are consistent, i.e., the LEF stabilizes further out at a higher gas velocity with a higher heat release rate and a correspondingly higher maximum temperature gradient in that region.

4.4.2 Effect of Dilutions

As previously described, the condition of equal molar refractivity between the fuel and oxidizer streams is maintained at each case so that the effects from composition induced fringe shifts are completely eliminated in the cold flow region (see section 3.3.2 and Figure 3.3 for details) and an accurate temperature distribution can be computed from interferograms. For example, if a certain amount of CO_2 is used to replace O_2 in the diluted oxidizer flow (O_2+CO_2), a corresponding amount of CH_4 must be added to the diluted fuel stream (CH_4+N_2) to replace N_2 in order to maintain equal molar refractivity. The two substitutions usually have opposing influences on the LEF behavior if applied individually to the burner (i.e., oxidizer dilution corresponds to concurrent fuel enrichment).

Figure 4.15 presents some test results (temperature distribution vs height above burner surface) for dilution in one stream only. All these tests were conducted with the gas velocity set at 30 cm/sec. It can be seen that, the temperature rise induced by the 4% CO_2 change in the oxidizer flow (case 1 and 5) is significantly higher than that induced by the 12% N_2 change in the fuel flow (case 2,3,4,5) while keeping the composition in the other flow unchanged. It is obvious that the need for relatively large quantity of oxygen and small quantity of methane to complete the stoichiometric burning of diluted CH_4/O_2 mixtures make the system very dependent on oxidizer composition change. Therefore,

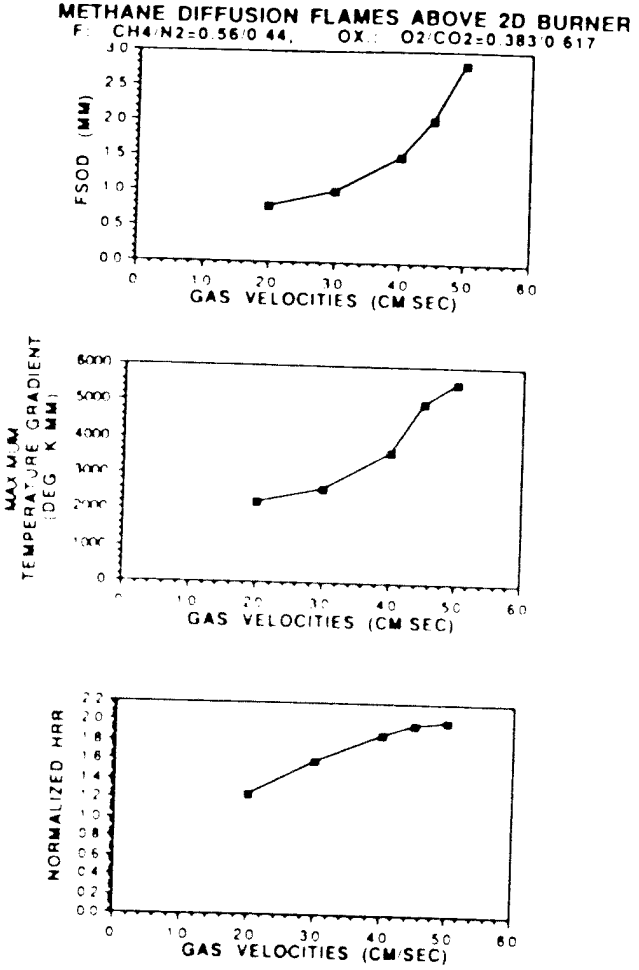

Figure 4.14 Effect of Gas Velocity on Heat Release Rate

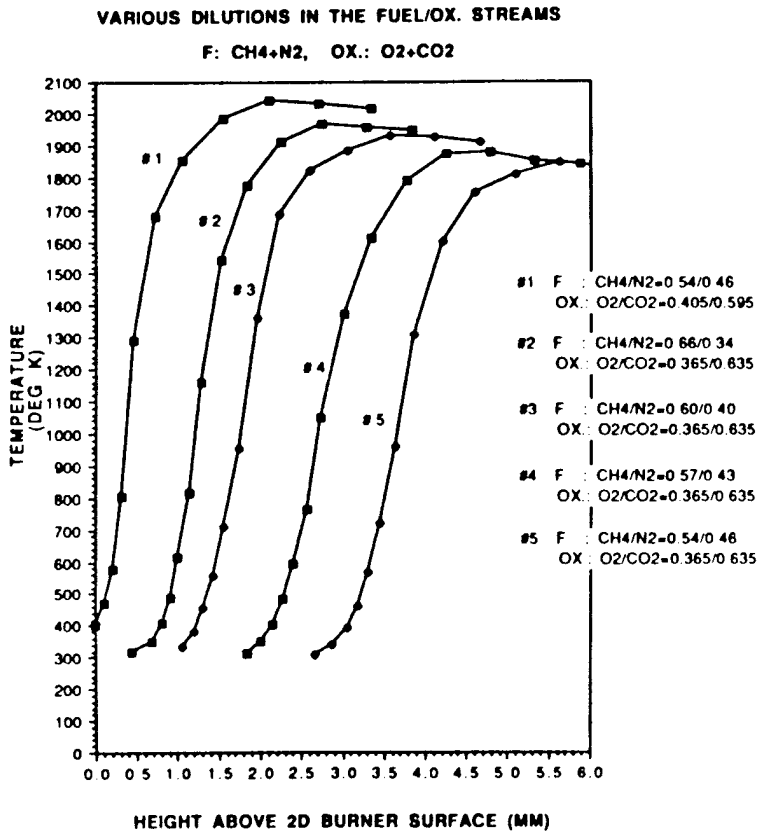

Figure 4.15 Effect of Dilution on Temperature Distribution (One Channel)

when both concentration changes are applied to the system simultaneously (to preserve uniform molar refractivity), the overall effect will be following the variation of the CO_2 content (i.e. the diluent) in the oxidizer flow.

A sequence of plots regarding the dilutions are now considered. First, five cases (See Table 4.1) were studied with a gas velocity of 30 cm/sec. The temperature contours around the LEF region are plotted here for comparison (See Figure 4.16, 4.9, and 4.17 for R=0.597, 0.617, and 0.648, where R=CO_2 mole fraction of in the oxidizer flow). More temperature variation vs y-location along the maximum fringe shift points on the interferograms are given in Figure 4.18. It is observed that the equilibrium flame temperature decreases with the increase of CO_2 mole fraction in the oxidizer flow. Corresponding plots of temperature gradient vs height above burner surface are provided in Figure 4.19. The results indicate that the flame temperature and maximum temperature gradient are decreased with an increase of CO_2 content. It can be seen from the figures that, as the dilution level increases, the LEF will retreat from the surface, and the isotherms begin to spread out in both vertical and lateral directions. Although this CO_2 flame imposes a complicated dilution, it was found from Fristrom [74] that CH_4 and N_2 in the fuel flow have about the same level of diffusion coefficients vs O_2 or CO_2 in the oxidizer flow [74]. Thus, the use of the primary mixture composition as the input to compute the adiabatic flame temperature along the stoichiometric surface (the leading part of the LEF) between the fuel and oxidizer flow should be close to the actual values. Thermochemical equilibrium calculations are made based on the 2 to 1 mixing ratio between the primary F/O compositions for these 5 cases. Consistent results are obtained in which the adiabatic stoichiometric flame temperature increases as the CO_2 mole fraction in the oxidizer flow decreases.

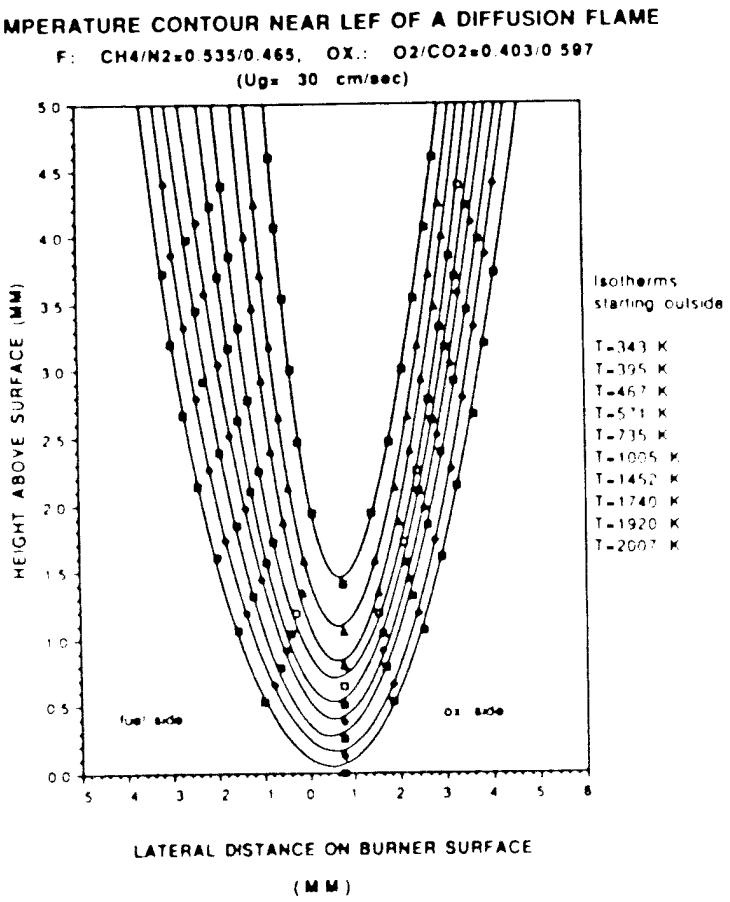

Figure 4.16 LEF Temperature Contours (R=0.597)

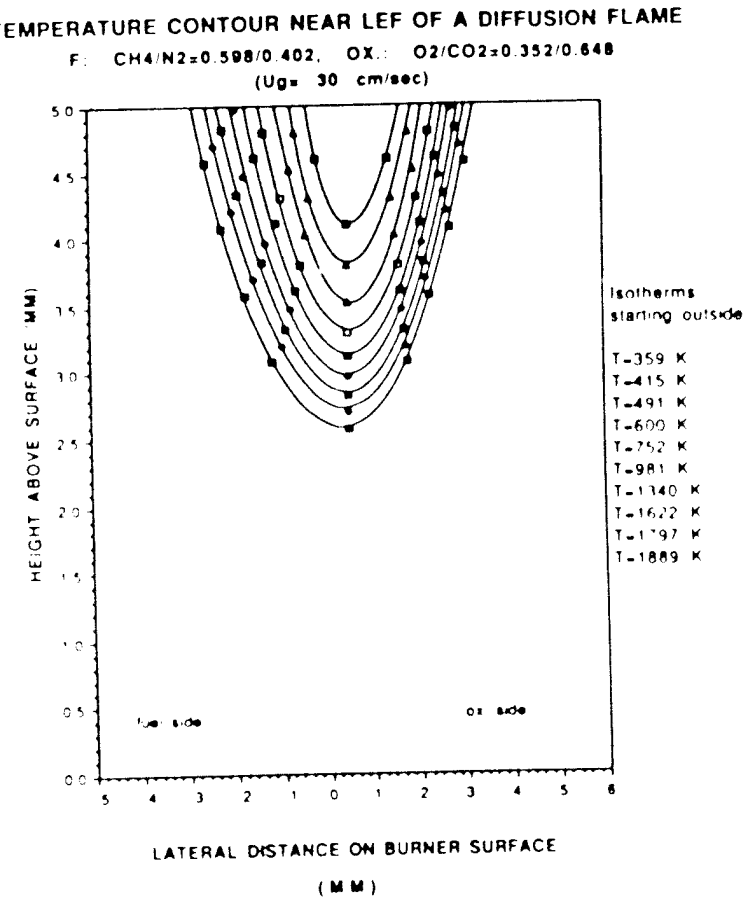

Figure 4.17 LEF Temperature Contours (R=0.648)

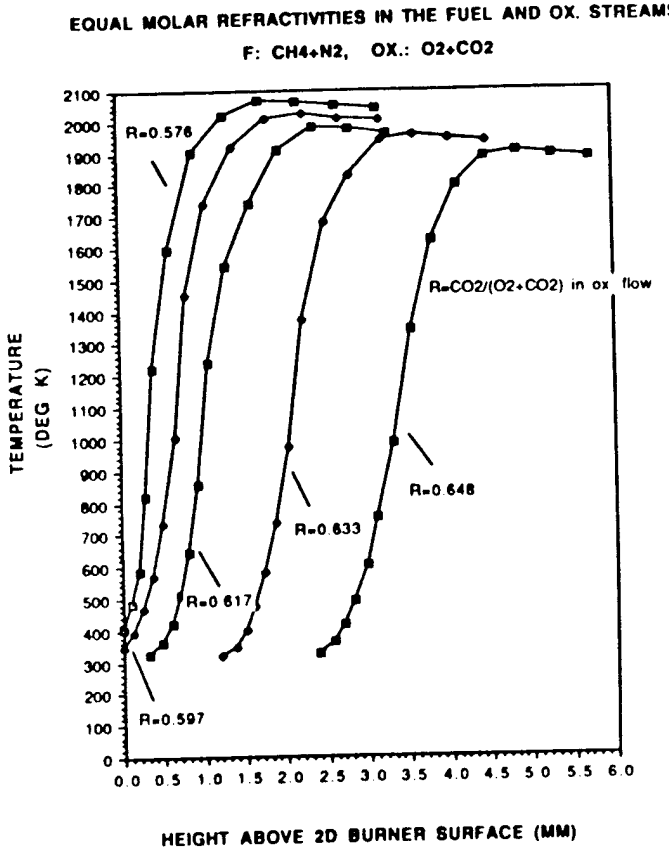

Figure 4.18 Effect of Dilution on Temperature Distribution (Equal Molar Refractivity Flow)

The physical concept of an "ignition" temperature has also been checked. For a methane flame, T=1250^{0}K is generally recognized as the ignition temperature [77,86] which divides the preheating zone from the reaction zone. A plot of FSOD (at locations of maximum dT/dy) vs FSOD (at locations of T=1250^{0}K) is presented in Figure 4.20. The result indicates that use of the point of maximum temperature gradient as the flame location is consistent with the idea that ignition occurs at 1250^{0}K.

4.4.3 Systematic Parametric Evaluation

In this section the systematic data regarding the leading edge flame behavior are presented with a complete test matrix which included 4 different settings of the molar refractivity values (R=0.597, 0.617, 0.633) in an operating range of gas velocities from 15 to 50 cm/sec. Figure 4.21 plots the results of FSOD vs gas velocity under these conditions. Each curve represents test conditions for various velocities at given compositions. The results indicate that, when the velocity increases, the LEF stabilizes at a location further out than would result from convective stretching of the mixing zone alone, and it moves out much further at higher dilutions. Figure 4.21 is also used for the definition of the mixing time. Since the scale of the mixing time usually is proportional to the scale of the mixing region developed between the fuel and oxidizer streams, it would be very helpful to evaluate this parameter. The mixing time is estimated here as the ratio between measured FSOD and gas velocities. Figure 4.22 illustrates the mixing time vs dilution level for the test matrix in Figure 4.21. It is clear from the figure that the increase of mixing time (measured FSOD/U_g) is necessary for a LEF to stabilize in a higher velocity or more dilute flow.

The systematic measurements of temperature by the thermocouple method (as illustrated earlier in Figure 4.12 and 4.18) are summarized in Figure 4.23 (against U_g) and 4.24

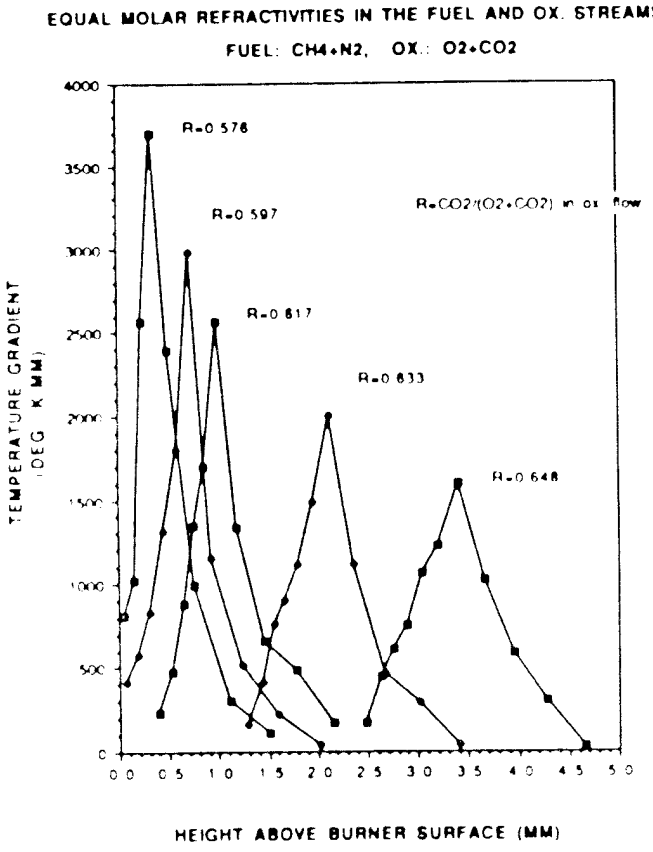

Figure 4.19 Effect of Dilution on Gradient Distribution (Equal Molar Refractivity Flow)

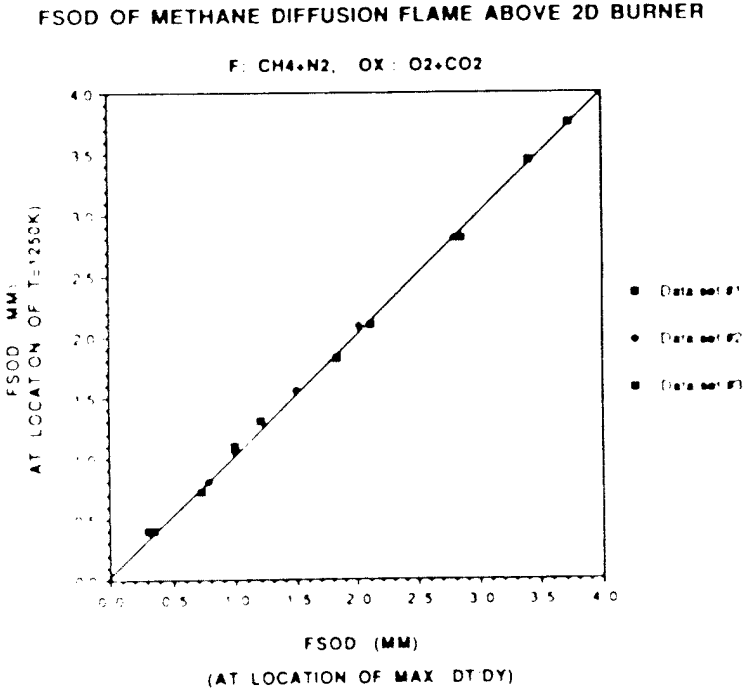

Figure 4.20 FSOD at Ignition Temperature

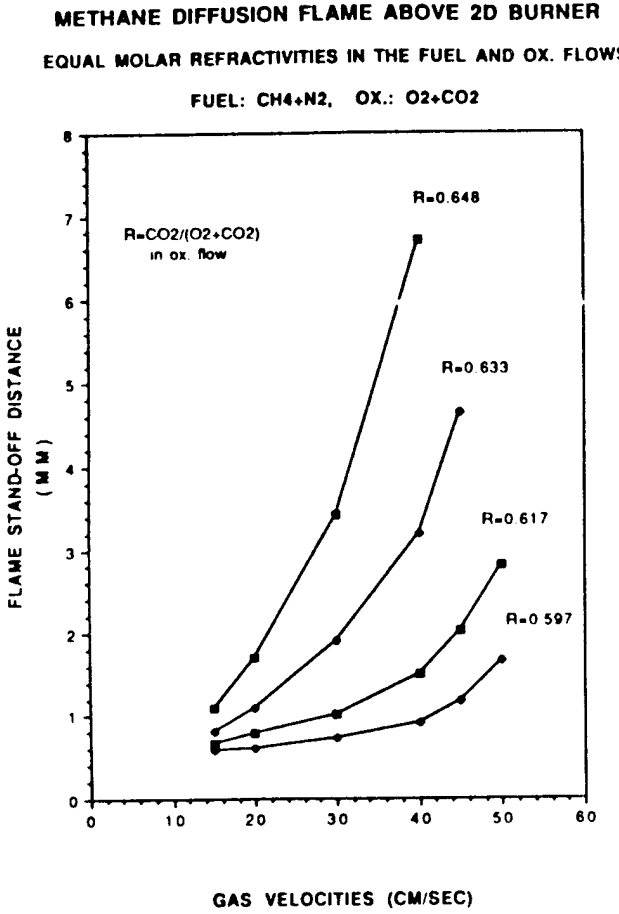

Figure 4.21 Gas Velocity Effect on Flame Stand-Off Distance

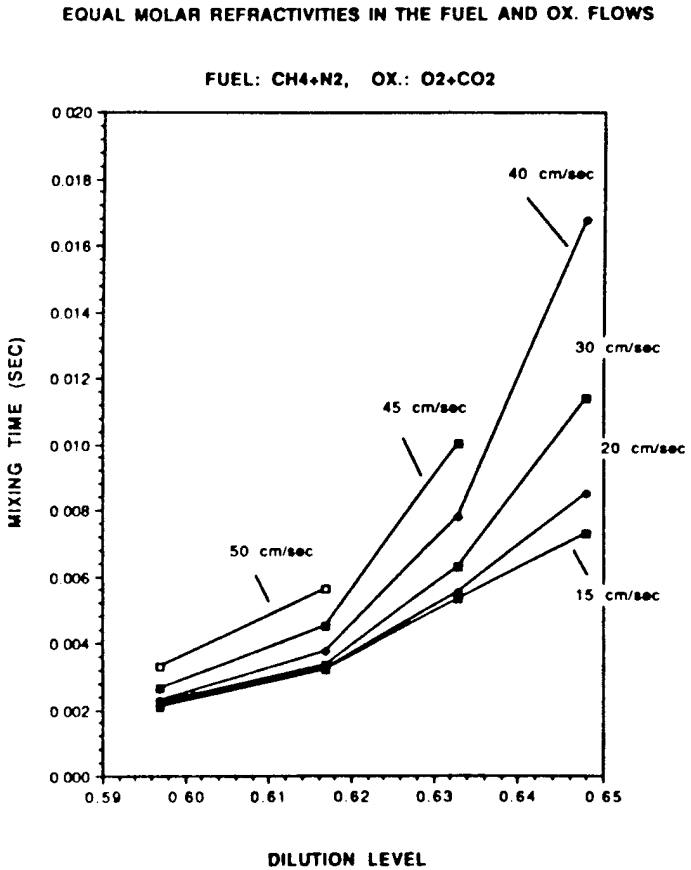

Figure 4.22 Dilution Level Effect on Mixing Time

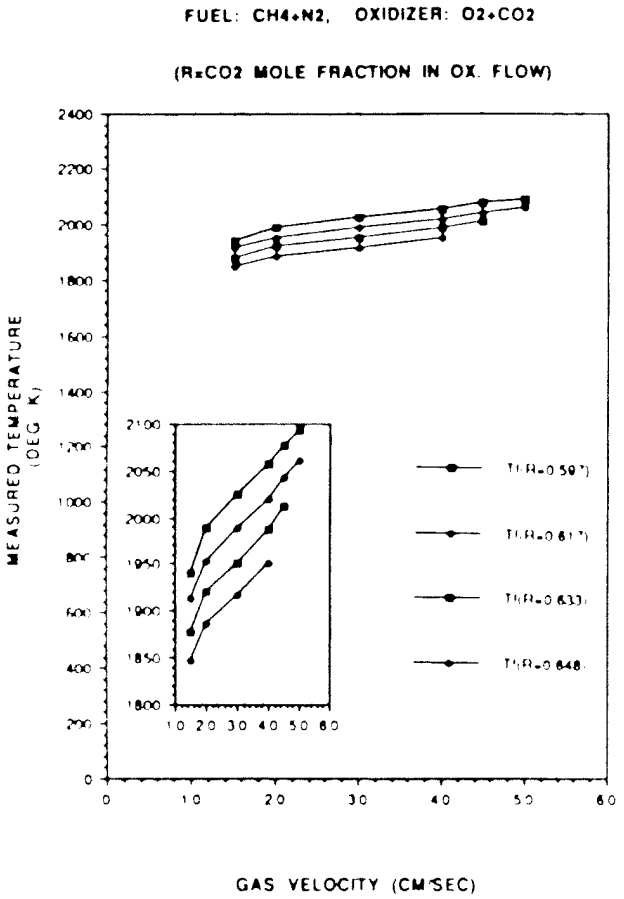

Figure 4.23 The Effect of Gas Velocity on Measured Temperature

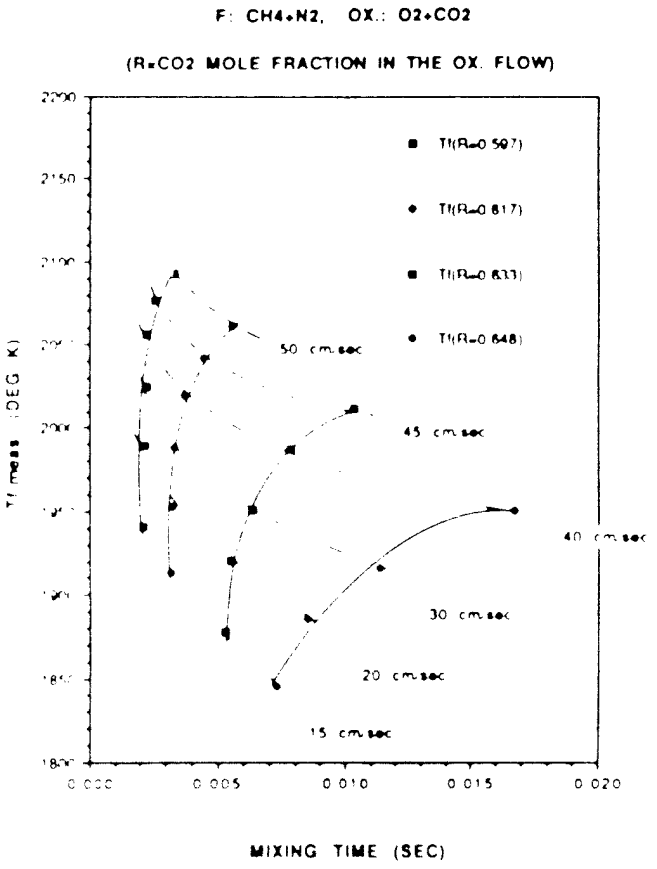

Figure 4.24 The Effect of Mixing Time on Measured Temperature

(against mixing time). In Figure 4.23, each curve again represents test conditions for various velocities at given compositions. For a stable flame, an increase in temperature with increasing velocity is observed (as would be expected in order to give the higher reaction rate needed to match the higher reactant flow). a decrease in temperature with increasing dilution level is also recorded. From Figure 4.24, it is clear that the increase in temperature with increasing velocity is achieved by moving the flame to a location of larger mixing time where lower proportional heat loss from the flame prevails. However, the outcome from increasing mixing time for a diluted mixture apparently does not provide enough reduction in heat loss to compensate for all the heat forfeited by dilution and a decrease of flame temperature is seen (dash line in Figure 4.24) with the increase of mixing time.

Note that while the use of a mixing time is physically important, the use of the gas velocity as a single factor is somewhat simplified. Numerical computations of flames indicate a modification of the approach flow to the flame which may influence the actual mixing time. Actual measurement of the velocity is beyond the scope of this thesis.

CHAPTER V

DISCUSSION

Most of the experimental results regarding the LEF studies were presented in the previous chapter. In this chapter, discussion starts from describing the important features and differences between a confluent flow LEF and a horizontally propagating LEF between layered mixtures. Then an attempt will be made to explain the trends of the experimental results. Finally a qualitatively phenomenological model will be developed to describe the controlling processes involved for a LEF stabilizing in the 2-D mixing region. Some definitions will have to be introduced and additional experimental results will be brought in to support and test the theory.

5.1 Comparison with previous studies

In the studies by Phillips and others (Ref. 27-38) for the horizontally propagating LEF between layered mixtures, the size of the LEF is significantly larger than the trailing diffusion flame and the flame is observed to propagate 4 to 5 times faster than the velocity of a stoichiometric premixed planar flame of the same gases. Investigations of these stratified mixture flames show a curved LEF (Figure 1-1) with its lead point located at the stoichiometric point in the stratified mixture. The flame extends outward on the fuel-rich and oxidizer-rich sides as far as the mixture will sustain the flame. The LEF differs from a 1-D, premixed flame in that the gas ahead of the flame can be displaced laterally by the local pressure excess due to the gas expansion in the flame. Viewed in a coordinate framework

fixed in the flame, the gas is flowing toward the LEF and is deflected by the pressure peak in the flame, which effectively diverges the oncoming stream tubes. The divergence causes the flow that is entering the flame to have a lower velocity than it would have if the flame were one dimensional. It is this flow divergence effect (the so-called aerodynamic effect in the literature) which permits the flame to have such a high propagation velocity. In effect, at some distance ahead of the center of the leading edge flame, the stagnant gas is set in motion away from the oncoming flame. Everywhere in the reactants entering the flame the velocity of the gas relative to the reaction wave is lower than would be the case for a one dimensional wave of the same flame temperature, this effect being due to the divergence of the stream tubes.

The stratified layer LEF (Figure 1-1) has an important difference from the LEF stabilized in the mixing region of confluent oxidizer fuel flows (the configuration of this research as illustrated in Figure 1-3). In the stratified layer the mixing is in equilibrium and the concentration profiles in the mixing layer are determined by the opposing effects of diffusive mixing and buoyant "unmixing". The flame establishes a configuration consistent with the resulting composition field, and the resulting flame is significantly wider in size as compared to the trailing diffusion flame with only moderate curvature at the leading edge. Since the scale of the divergent flow ahead of the flame is determined by the size of the flame, in the stratified layer LEF, the corresponding retardation of flow along the streamlines entering the center of the stratified layer LEF will start well upstream, where the temperature has not risen yet. With a smaller LEF close to the burner surface as observed in the confluent flow cases, the region of divergent flow may be in the heat-up region from the flame. From the view of one-dimensional flow, the approach flow becomes diverging stream tubes with heat addition. In the wide flame the deceleration of the flow prior to the heat up region is actually seen in experiments, while with small flames close to the burner surface it may be unresolvable because the divergence region is superimposed on the heat up region. This does not mean that there is not a divergence-caused deficit in flow velocity entering the flame, only that it is not resolvable without detailed comparison with the velocity field ahead of the a 1-D flame. The LEF will still show an excess propagation velocity.

5.2 Mechanism for the Mixing Region

In the LEF mixing region of confluent flows, the mixing field is one that develops as the gas moves downstream along the flow field. As the two gas flows with equal upward velocities leave the burner surface, the concentration gradients at the interface of the two flows are initially very steep, and mixing proceeds very rapidly by molecular diffusion as the gases flow away from the surface. Under the condition of laminar flow, it may be assumed for simplicity that near the plate surface diffusive mixing will proceed primarily in the lateral direction, at a rate that is independent of mean convective velocity in the vertical direction. The concentration profiles will smooth out with time or distance as in Figure 5.1(a). The details will depend on the relative diffusion constants, heat capacities, and molecular weights of the gases involved and the effects of heat-up from the flame, but these effects will be neglected at this point, or at least assumed to be independent of convective velocity. The reason for developing the cold flow mixing concept is simply because the size(width) of the mixing region increases upon the increase of mixing time with or without the presence of the flame. When the gas velocity is increased, a specific concentration profile which corresponds to a given flow diffusion time (Figure 5.1(a)) will occur at a distance out from the surface that is proportional to the flow velocity (Figure 5.1(b)). In other words, the location of those concentration profiles is stretched out in the "y" direction when the convection velocity is increased. The experimental results shown in Figure 3.2 are designed to check this argument

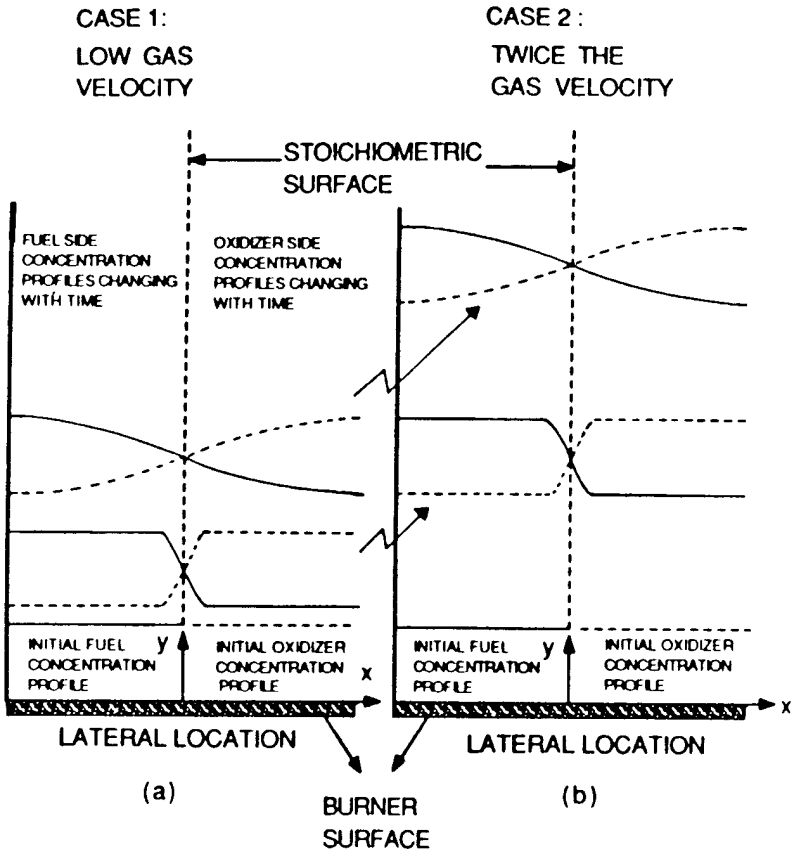

FIGURE 5.1
Sketch of Concentration Profiles vs Height from the Burner Surface for Two Primary Flow Velocities

which indicate approximately linear stretching of the constant concentration lines in the "y" direction upon increasing flow velocity. The results suggest that the axial diffusion which will complicate the stretching of the mixing region is small compared to lateral diffusion and the assumption that lateral diffusion as the primary effect responsible for the development of the mixing layer in the LEF region is reasonable.

5.3 Mechanism for Heat Release Rate

There is very little experimental data in the literature on the detailed shape of the leading edge of diffusion flames, and the configuration suggested here (e.g., Figure 1.1) was based on the idea that a thin, partially premixed flame stands in the mixing fan as observed in the case of LEFs in stratified O/F fields. Combustion photography (Figure 4.1 and 4.2) of the diffusion flame in confluent flows indicates that the LEF is not conspicuously distinct from the rest of the diffusion flame, but it is the brightest part of the flame. The reason can be attributed to the different mixing situation at the LEF compared to the subsequent diffusion flame. The heat release rate is dependent on the state of "premixedness" of the reactants and on kinetics of the reaction and temperature reached in the (nonadiabatic) flame. When the temperature in the mixing region is below the so-called "ignition" temperature which is about 1250^{0}K (obtained from Figure 4.20 in this studies), no appreciable reaction will take place and rapid "accumulation" of the partially premixed reactants due to high concentration gradients will occur. This should make the LEF a premixed-like flame when it forms. The heat release rate (per unit volume) in premixed flames like the LEF should be very high. The subsequent diffusion flame is controlled by the relatively low rate of diffusion of oxidizer and fuel to the flame through a layer of reaction products, hence the heat release rate (per unit volume) is significantly lower in the outer diffusion flame than that at the leading edge portion and is not strongly dependent on reaction kinetics. The experimental results given

from Figure 4.3 to 4.7 all indicate that the LEF regions have maximum values of heat release rates in the whole diffusion flames, hence it is reasonable to say that the heat flux situation at the LEF contributes the most for the heat transfer back to the upstream boundaries such as the burner surface or composite propellant surface. Therefore, from the view point of heat release rate, the LEF region actually "anchors" the follow-up diffusion flame, and the presence, stability, and velocity of the flame as a whole will be heavily dependent on the LEF behavior.

5.4 Phenomenological Theory on Flame Stabilization

5.4.1 General

Considering the premixed-like nature of the LEF, it will be very helpful to view this reaction region as a curved flame sheet like that observed in Phillips and others [27,38] for horizontally propagating LEF, because one can then apply the many concepts and properties established in laminar premixed flame theory. Thus, each point on the flame surface has a propagation velocity, which is determined primarily by local reactant and diluent concentrations and corresponding flame temperature. The maximum flame temperature and flame velocity presumably occur at or near the point along the curved flame sheet where the mixture ratio is stoichiometric, and this will correspond to the leading point in the curved flame front. The flame trails off on either side due to lower flame velocities associated with the stratification of the mixture ratio, and the outer extremities correspond to flammability limits in the oxidizer rich and fuel rich regions (Figure 5.2). When the LEF is in upstream locations, the lateral concentration gradients are large, and the amount of flammable mixture is small. Further downstream the concentration gradients are lower and the amount of flammable mixture is larger. If ignition is produced in a downstream location, a relatively

Figure 5.2 Qualitative Features of the LEF-Diffusion Flame in a Mixing Fan (Shown with the LEF at Two Possible Locations in the Mixing Fan)

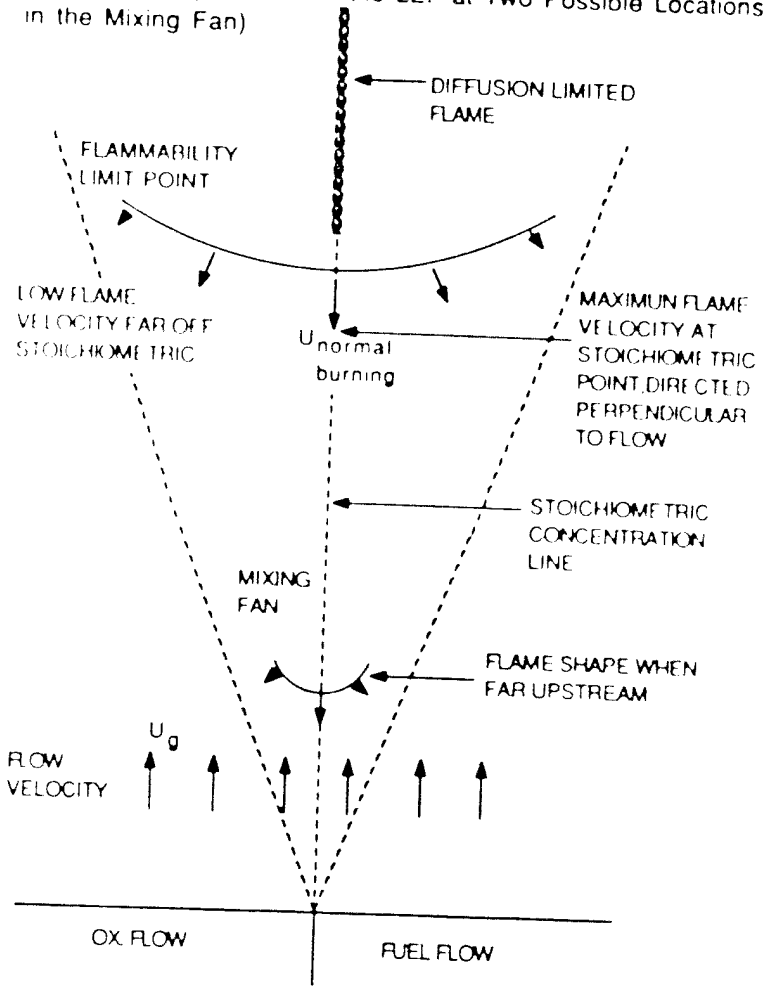

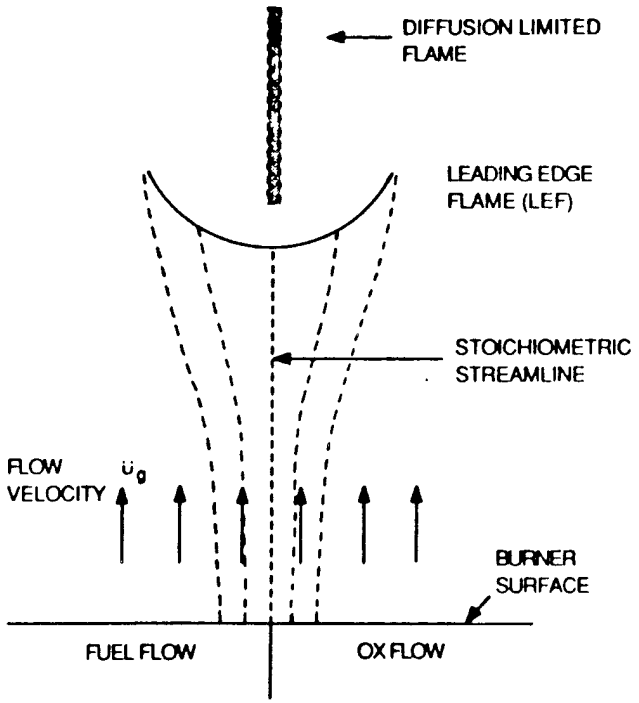

Figure 5.3 Flow Divergence Effect In the Approach to the LEF

velocity/temperature relationship is achieved by dilution of the reactant flow (Figure 5.4 provides such a relationship obtained from the literature[93, 94]). In addition, this 1-D definition for flame speed in the leading portion of the LEF (where the temperature measurement were made) will provide the desired separation between the heat loss and flow divergence effect because most of the heat loss and "stretch" effects are accommodated by use of the measured temperature.

In general, the flame speed obtained from the above calculation will be lower than the gas velocity in the cold reactant approach flow because the flame is stabilized in a "diverged" approach flow. For the stationary flame, the difference between the defined 1-D speed and gas velocity is attributed to reduction in speed of the approach flow into the flame due to the necessity to "flow around" the pressure spike produced by the LEF. This effect will be defined here as

$$\text{Divergence Factor} = \left|\frac{U_{f,\text{eff}}}{U_f}\right| = \left|\frac{U_g}{U_f}\right| \qquad (5.1)$$

where $U_{f,\text{eff}}$ is the effective flame speed that is equal to the approach flow speed, U_g, from the burner. This factor is a multidimensional fluid dynamic effect, caused by the gas expansion in the flame, and can be viewed as either a "correction" factor for U_f, or its reciprocal can be viewed as a correction factor for U_g.

It is well understood that the size of the LEF region would impose large influence on divergence effect. If the size of the flame becomes larger, then more total heat release and more flow divergence would be expected. In addition, if a LEF is present at a larger FSOD, then more upstream free distance is available and less change in flow direction is required to make the necessary flow divergence transition. This would also be in favor of the flow

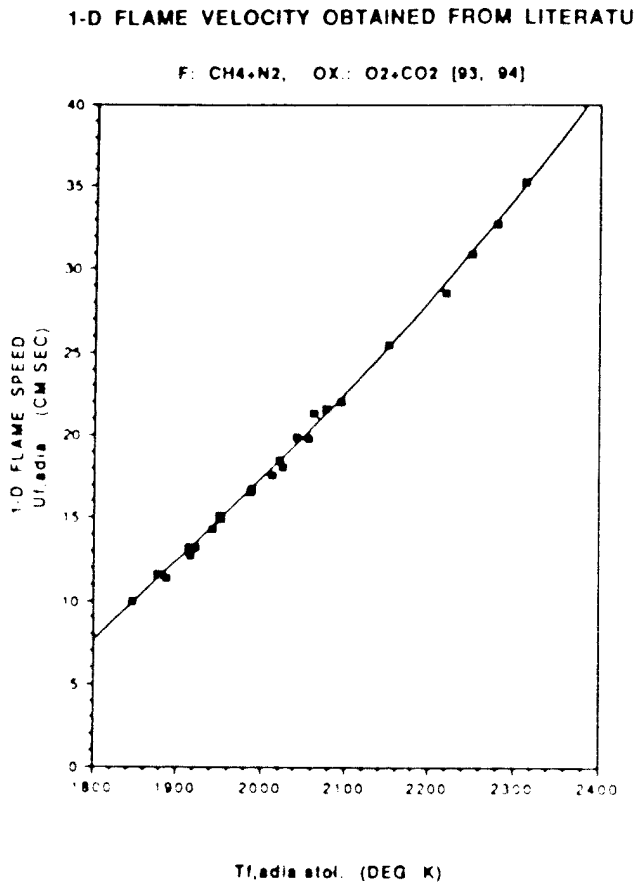

Figure 5.4 Flame Temperature/Velocity Relationship from Dilution of Stoichiometric Mixture

divergence effect. However these are two dimensional processes, not amenable to simple quantitative rationalization. The present study does not address the subject of total heat release. The definition of divergence effect in the present study is more concerned with the leading part of the LEF which has the highest temperature. Because of the strong dependence of flame speed on temperature, the flame speed at this part of the flame would be the most important velocity to balance against the oncoming gas velocity for a stationary flame. Therefore it is expected that the above definition will give a good qualitative representation to reflect the presence of a divergence effect.

5.4.4 Flame Stabilization Mechanism

From the concept we have developed so far, the Leading Edge Flame (LEF) is known as a distinctly multidimensional, nonadiabatic flame that positions itself in the mixing fan at the point where its upstream propagation speed matches the initial flow velocity. The stabilization of the LEF is seemingly influenced by both the lateral heat loss effect and flow divergence effect. In the following, how these two effects go with position in the mixing fan is examined.

5.4.4.1 Interpretation of Heat Loss Studies

Two major domains of test conditions (varying flow velocities and varying dilution levels) are discussed here. First, the effect of increasing flow velocity of a given mixture on the stabilization of the LEF is considered. In response to the increase of gas velocity, the LEF moves out to a site corresponding to larger mixing time (Figure 4.22) when the flow speed is increased. The longer mixing time prepares a broader mixing region, hence the leading part of the LEF is more nearly one dimensional with higher flame temperature possible due to lower lateral heat loss. This argument is complicated by the effect of convection on the flame,

the difference in flame speed along the LEF causes more curvature of the flame when the gas velocity is higher (the isotherm plots in Figure 4.9 - 4.11 indicate this trend), and hence more deviation in lateral heat flow from one dimensional. Theoretical prediction of the outcome of these opposing effects on lateral heat loss from the leading part of the flame would be difficult without a currently unavailable rigorous model for the LEF, hence experimental results from temperature measurement will be used later for further discussion.

The other major domain to be considered is the variation of dilution levels at a given gas velocity. The primary effect imposed by the dilution is to decrease the heat of reaction of the mixture. A second effect is a reduction in diffusion rate of fuel into oxidizer due to lower concentration gradients. A third effect is a reduced O-F collision frequency because of ineffective collision involving diluent molecules. As the dilution level increases,a rapid increase of mixing time is needed for realization of a stationary flame. The LEF retreats from the burner surface to locations of reduced lateral heat loss that will permit the same flame temperature as before dilution. As a result, a wider flame will be formed in a larger part of the mixing region. If the convective velocity is kept constant while increasing the dilution, the wider LEF region means less (lateral) temperature gradient, hence the (lateral) heat loss is reduced. Prediction of the importance of this reduction of lateral heat loss as compensation for the decrease of heat generation rate due to dilution would be difficult without a rigorous model. Again experimental results from temperature measurements will be used for further discussion.

Temperature measurements at the stoichiometric point of stable LEFs are given in Figure 4.23(vs gas velocity) and 4.24 (vs mixing time). An increase in temperature with increasing velocity (Figure 4.23) results through flame stabilization at a location of larger mixing time (Figure 4.24) so that a larger partially premixed region and more net heat are available there. The rather modest increase in temperature with mixing time (Figure 4.24) as gas velocity is increased (over a large range) is a reflection of the strong dependence of reaction rate on temperatures, which allow large increases in reactant consumption rate in the flame (necessary at higher gas velocity) with only modest temperature increases. If the view is adopted that the flame speed depends primarily on the highest temperature along the LEF, then the flame temperature at the stoichiometric point of the LEF is the most important temperature and that temperature is limited to values below the adiabatic stoichiometric flame temperature due to lateral heat losses. At higher velocity, the flame stabilizes in a low loss location (broad flame with higher flame temperature) where high reaction rate is achieved to consume high mass rate.

In the case of dilution of the reactants, it is reasonable to expect that the flame temperature would be lowered, as it is (Figure 4.24). However one might anticipate that the flame would position itself far enough out in the flow so that the enthalpy deficit due to dilution would be compensated for by reduced lateral heat losses, leading to only a small effect of dilution on temperature of stationary flames. This is pictured in Figure 5.5, where the upper horizontal lines #1-4 represent the anticipated adiabatic flame temperature for four levels of dilution. The lower line is the measured flame temperature for the undiluted LEF. The arrows reflect what heat loss would be if the dilute flames all stabilizes at the same LEF temperature as suggested above. The decrease in heat loss just balances the enthalpy loss due to dilution (less heat loss for high dilution). However it is conspicuous that the measured LEF temperature are not all the same, and in fact, decrease with increasing dilution (Figure 5.6). In fact in the example in this figure, the LEF temperature decreases more with dilution than would be expected on the basis of the direct effect of enthalpy lost by dilution alone (i.e., by displacement of reactants). This somewhat surprising result is better shown in Figure 5.7, where the heat loss, $C_p(T_{f,adia.} - T_{f,meas.})$, is shown vs mixing time for all test conditions. Thus it can be seen (dotted curve) that heat loss is roughly

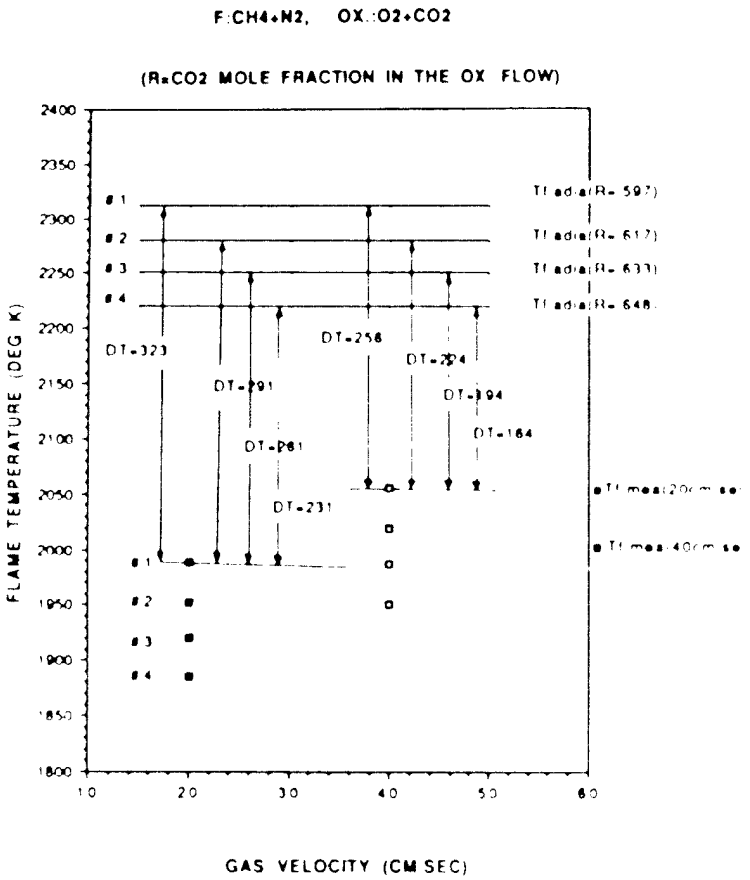

Figure 5.5 Temperature Difference between Adiabatic Flame Temperature and Undiluted measured Temperature

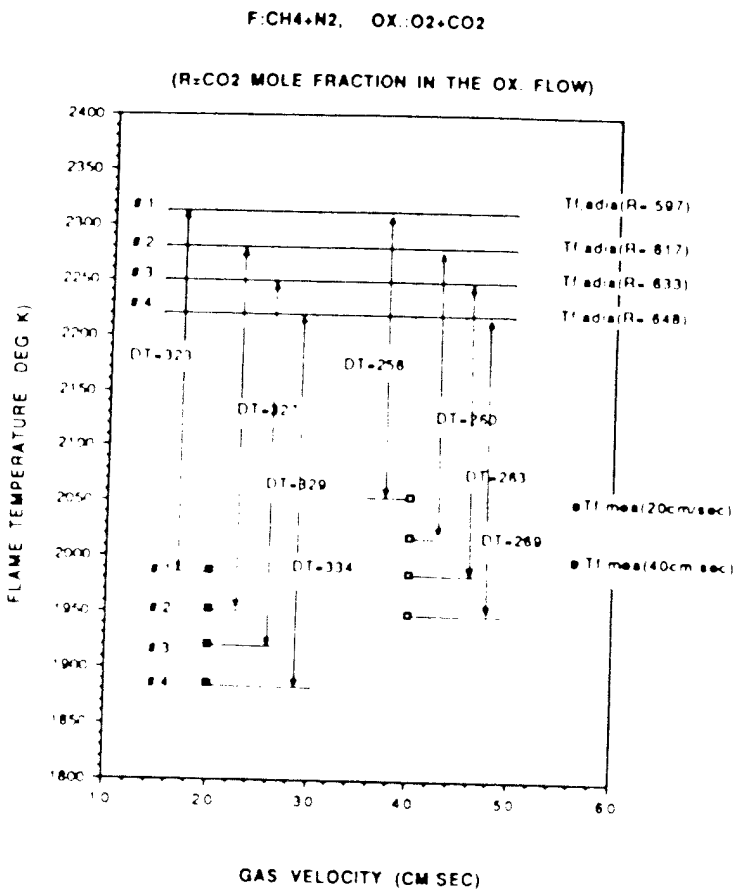

Figure 5.6 Temperature Difference between Adiabatic Flame Temperature and Diluted measured Temperature

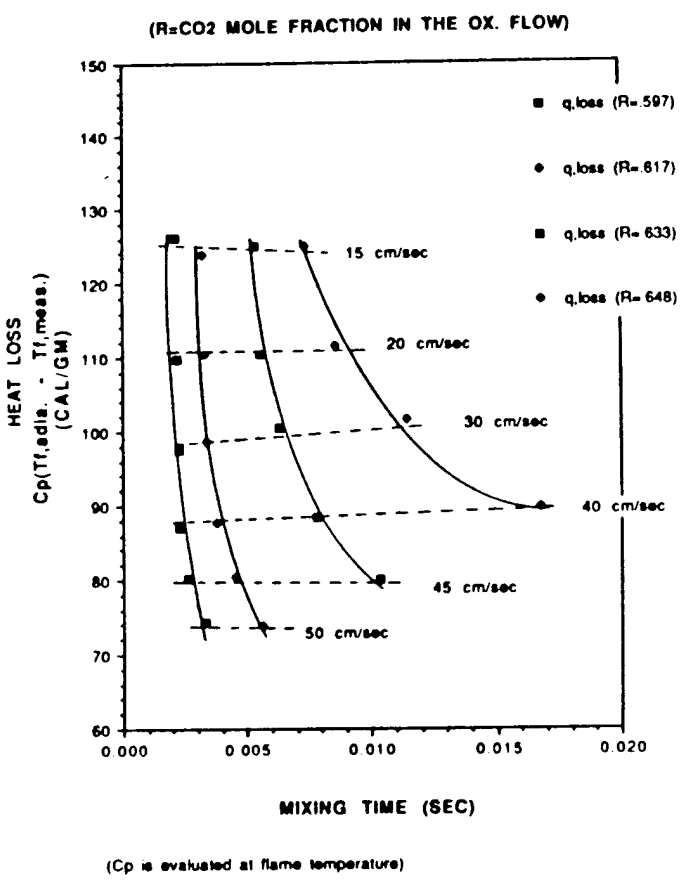

Figure 5.7 Enthalpy Reduction at the Leading Part of the LEF

invariant under dilution, while being strongly dependent on flow velocity as noted earlier. This unexpected result led to a look into the accuracy of this measurement/calculation combination. The uncertainty of the temperature measurement is expected to be small (20^0K). The uncertainties of knowing the dilution concentration at the stoichiometric surface which affects the equilibrium calculation were examined and the effects all seem to be small. There appears to be some mechanism other than energy balance controlling flame position during dilution.

5.4.4.2 Interpretation of Flow Divergence Studies

Based on the previous definition (sec. 5.4.3), the 1-D flame speed evaluated at the measured temperature (obtained from the definition in Figure 5.4) is plotted against Ug in Figure 5.8. It can be seen that this flame speed at the stoichiometric point of the LEF is very low as compared to the oncoming gas velocity. The trend with gas velocity and dilution are necessarily the same as the temperature trend with gas velocity and dilution because of the U_f=U_f(T) (Figure 5.4) relation here.

After defining the 1-D flame speed, the scale of the divergence effect can be studied. The Divergence Factor which is the ratio between the effective flame speed and 1-D flame speed for a stationary flame (Eq.5.1) is plotted vs FSOD and mixing time in Figure 5.9 and 5.10. The trend generally shows that the Divergence Factor increases with the increase of FSOD or mixing time regardless of the test condition (i.e., independent of the parameters chosen to vary). This result is not a surprise because large FSOD or mixing time tends to go with bigger mixing region (i.e. LEF region) which increases the scale of the divergence effect and less flow turning change is required to accommodate the streamtube expansion of a large FSOD flame. The range of values of Divergence Factor obtained here is within the range extremities from literature for horizontally stratified layer LEF [27-38].

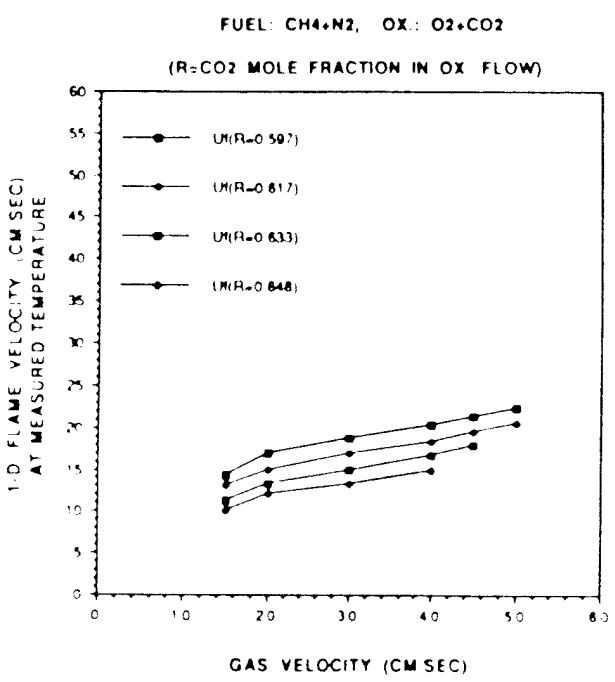

Figure 5.8 Definition of 1-D Flame Speed

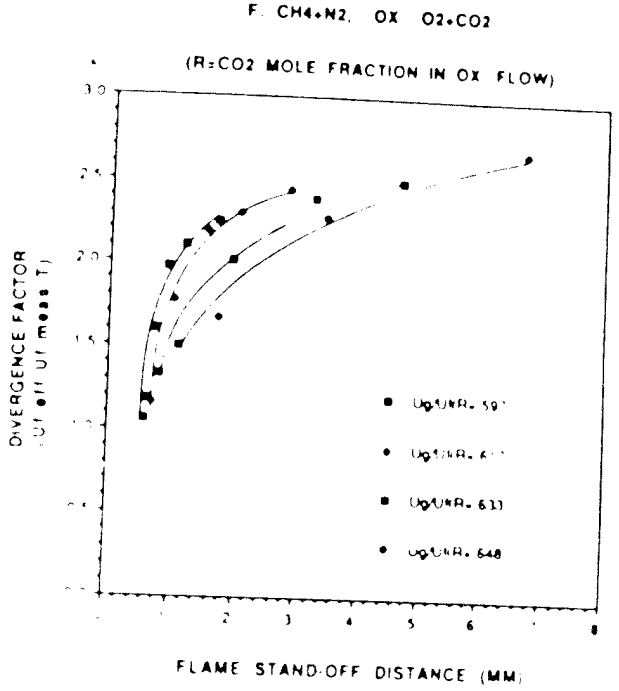

Figure 5.9 Scale of Flow Divergence Factor at Various FSOD

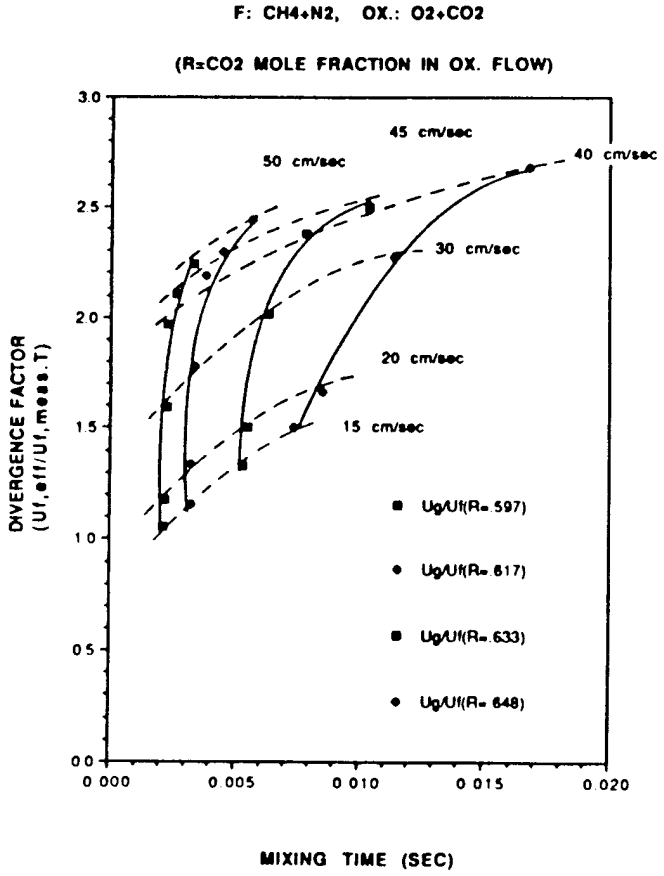

Figure 5.10 Scale of Flow Divergence Factor at Various Mixing Time

Thus on the basis of these argument it appears that the main factor determining establishment of a new stable location for a dilute flame is not from an establishment of a less lossy flame, but instead one with a larger flow divergence factor. In other words, the increase of flow divergence effect in a dilute flame can make up for part of the heat forfeited by dilution and gives the needed balance for a low temperature flame to support itself against the same gas velocity.

On the other hand, flame accommodation to increased flow velocity involves both reduced losses and increased divergence factor.

CHAPTER VI

CONCLUSIONS AND RECOMMENDATIONS

The role of the leading edge of a single methane diffusion flame, stabilized on a modified Wolfhard-Parker burner at atmospheric pressure has been investigated experimentally in this research program. These studies reveal that the Leading Edge Flame (LEF) is the most important part of the diffusion flame even though it may be only a small portion of the whole diffusion flame. The significance and characteristics of the LEF learned so far have been summarized below.

1. The LEF is a region of very high heat release as compared to the rest of the diffusion flame. This is due to different mixing situations between these two flame regions. A mixing fan containing partially premixed mixtures will have to be developed first until the conditions in this mixing region are favorable for existence of a stable flame. The results of this study indicate that 1250^{0}K can be regarded as the ignition temperature for methane flame. This suggests that the existence of the LEF is strongly dependent on kinetics and on the temperature. High combustion intensity results, typical of a premixed flame. The downstream (classical) diffusion flame is controlled by a low rate of diffusion between the F/O flows through a layer of reaction products. Hence on the basis of per unit volume, the LEF will yield a value of heat release rate much higher than that of the subsequent diffusion flame. Because of the heat release rate behavior at the LEF, it will anchor the diffusion flame and will contribute most for the heat transfer back to any upstream boundary such as composite solid propellant surface; hence the LEF should play a dominant role in the combustion behavior in solid propellants, fire spread, etc.

2. It seems reasonable to regard the lateral diffusion as the primary factor in the development of a mixing region near the burner surface. The "premixedness" of the LEF region depends upon the change of test conditions. In general, the increase in mixing time to provide a larger premixed region is necessary for a LEF to sustain itself against higher gas velocity or mixture dilution level, and the flame adjusts its position accordingly.

3. It is observed that the gas velocity on this burner can be set to a value higher than the adiabatic stoichiometric flame velocity suggesting the presence of the flow divergence effect at the LEF. i.e., the high effective speed is due to divergence of the approach flow to the flame induced by the local pressure rise in the intense reaction region.

4. Unlike the stratified layered LEF which is significantly larger in size than the trailing diffusion flame, the size for the confluent flow LEF is very small. The measured flame temperatures at the stoichiometric point of the confluent flow LEF indicate a trend of increasing temperature upon the increase of gas velocity and a trend of decreasing temperature upon the increase of dilution level. However, all these values are much lower than the attainable adiabatic stoichiometric flame temperature. This reduction of flame temperature is attributed to the heat losses due to lateral heat conduction.

5. The stabilization of the LEF is attributed to the balance between the flow divergence effect and the heat loss effect and the flame will position itself in the mixing flow at a location where its effective flame speed matches the flow speed from the gas source. Determinations of the scale of these effects from the variation of burner out-flow speed, and as a function of flame enthalpy (controlled by dilution) are successfully achieved by choosing the proper definition of a 1-D flame speed to minimize the interactions between these two effects. The

results reveal that flame accommodation to increased flow velocity involves both reduced heat losses and increased divergence factor. However, the main factor determining establishment of a new stable location for a dilute flame is not from an establishment of a less lossy flame (i.e., the adjustment in flame position to reactant dilution does not involve much change in heat loss), but one with a larger flow divergence factor obtained during the process of moving out.

In the future one might hope to improve the phenomenological model for the fundamental contributing mechanisms involved in the present scenario. Some of the detailed studies that would be useful are recommended as follows:

1. To obtain accurate flame temperature distribution measurements along the stoichiometric surface between the F/O flows by an M-Z interferometer alone (without an assist from thermocouple measurement) would be desirable. This can be achieved by rebuilding a 2-D burner with 5 cm width in the direction of optical path and enlarging the access hole in the M-Z interferometer unit. Past research [64] has successfully applied the M-Z interferometer to a premixed flat flame study of this dimension (i.e., the so-called "end effect" as discussed in section 3.1.4 is negligible).

2. Apply other hydrocarbon fuels such as propane to examine the similarity and difference between the characteristics and stabilization of the LEF in response to the change of flow velocity and dilution levels in the flow.

3. The enrichment of the partially premixed region prior to the LEF can be achieved by adding fuel to the oxidizer flow or oxidizer to the fuel flow. This study has the advantage in that the addition of fuel to the oxidizer flow actually simulates the combustion behavior for the heterogeneous solid propellant better simply because the oxidizer particles, ammonium perchlorate, in the propellant is a monopropellant. This operation will generate another premixed flame at the LEF region, hence will significantly affect the stabilization of the LEF in the mixing region.

Appendix A

Derivation of Temperature Evaluation in an M-Z Interferometer

A.1 General

Interferometry is the optical method which directly uses the property of index of refraction. When the local velocity of light encounters a flow disturbance in the light path, it slows down and changes the index of refraction which is defined as

$$n = \frac{\text{velocity of light in vacuum}}{\text{velocity of light in the medium}}$$

Thomas Young in 1802 showed that rays of light would be represented to a first approximation by a wave train of the form

$$y = a \cdot \sin \frac{2\pi}{\lambda}(x - vt)$$

where y is the displacement, a the amplitude, λ the wavelength and v the phase velocity of a sinusoidal wave form, moving in a direction x in a time t. The intensity of illumination is proportional to the square of the amplitude.

When beams of light intersect, they continue beyond the region of intersection undisturbed. Within this region, they obey the "principle of superposition" and, based on this wave nature part of light, may add up to give patterns of varying intensity of illumination known as interference fringes.

If the distribution of the index of refraction in the flow field is known, the density distribution can be deduced which, then, leads to the distribution of temperature when ideal gas law $P = \rho RT$ is applied.

A.2 The Fringe Shift and Interferogram

When an M-Z interferometer is set up to produce wedge fringes, e.g., at the horizontal fringe setting, for a uniform temperature and composition field, the fringes are straight and equally spaced. These lines represent a constant path difference with two adjacent fringes separated by one wavelength of the beam and they keep either monotonically increasing or decreasing one wavelength in the direction normal to the uniform fringes. When disturbances are introduced into the test beam, the corresponding variations in density change refractive index and consequently change the optical path length of the beam. This causes the initially straight fringes to shift in position to conform to the new pattern of path difference distributions. The change from bright to dark to bright again is said to have a shift of one, and the apparent fringe shifts at a point can be defined as:

$$S = \frac{L}{\lambda} \qquad (1)$$

where L is the change in path length and λ is the wavelength.

A picture which stores the density distribution information this way is called an interferogram.(e.g. Fig.3.2)

A.3 Gladstone-Dale Law and Lorenz-Lorentz Law

There are two well-known equations that relate the density to the index of refraction explicitly, the Gladstone-Dale law and the Lorenz-Lorentz law.

Gladstone-Dale equation

$$N_G = \frac{n - 1}{\rho} \qquad (2)$$

Lorenz-Lorentz equation

$$N_L = \frac{n^2 - 1}{n^2 + 1} \quad \frac{1}{\rho} \qquad (3)$$

where N molar refractivity (cm^3/mole), i=G,L

n index of refraction

ρ molar density (mol/cm^3)

Molar refractivity is, to a first approximation, independent of temperature or physical state, and it provides an approximate measure of the actual total volume(without free space) of the molecules in one gram mole. Since, for gases, the value of the index of refraction is close to unity, we can see that $N_G \approx 3N_L/2$ gives a good approximation, hence, Eqs. (2) and (3) are basically the same equations with only different constants being inserted to each of the equations. Experimental data provided by Gardiner[73] shows that molar refractivities are additive molecule properties, that is, the average molar refractivity of a gas mixture, $N_{mixture}$ can be computed from adding up the proportion of molar refractivities of the major species in the mixture.

$$N_{L,mixture} = \sum_{i=1}^{n} N_{L,i} X_i \qquad (4)$$

Where X_i is the mole fraction of species i, and subscript L means data is for the Lorenz-Lorentz equation.

A.4 Evaluation of Temperature Distribution

Fig 2.2 illustrates how the coordinate system is defined on the burner surface when the burner is placed into the test section of an M-Z interferometer. Light rays travel in the positive z direction and the interferogram will be recorded only when the fringes are sharply focused on the object plane (the x-y plane). The object plane is selected in such a way that the refraction error, often accompanying the high density gradient in the light path, can be minimized (Wilkie [62]). Since the magnitude of the fringe shift at any one point in the x-y plane is directly proportional to the change in the optical path length of light ray passing through that point in the test section, the expression for the change in optical path length $\Delta D(x,y)$ caused by a disturbance of length L in the test section is (Goulard [66])

$$\Delta D(x,y) = \int_0^L [n(x,y,z) - n_r] \, dZ \qquad (5)$$

where $n(x,y,z)$ = the index of refraction of the test medium at any point

n_r = the index of refraction of the reference medium

When precaution is taken so that the properties of the gases remain unchanged in the z direction, e.g., when two-dimensionality is achieved in the system, the integral can be removed,and Eq. (5) can be simplified to

$$\Delta D(x,y) = [n(x,y) - n_r] \, L \qquad (6)$$

Substituting Eq. (6) back into Eq. (1), the fringe shift s(x,y) at the same point is known to be

$$S(x,y) = \frac{L}{\lambda}[n(x,y) - n_r] \qquad (7)$$

When the test field involves mixture of gases, the Lorenz-Lorentz law will change to the following form by incorporating Eq. (3)

$$(n-1) = \frac{(n^2+2)}{(n+1)}\rho\sum_i X_i N_i \qquad (8)$$

Based on the fact that the indices of refraction for gases are very close to unity(e.g., n_{air} =1.000289 at STD condition,etc), Eq. (8) can be reduced quite accurately to

$$(n-1) = \frac{3}{2}\rho\sum_i X_i N_i \qquad (8A)$$

When hydrocarbon fuel is burned with diluted oxygen in an open atmosphere,the reactants and the products will be considered still to obey the ideal gas law, $P=\rho RT$, Eq. (8A) can now be rewritten as

$$(n(x,y)-1) = \frac{3}{2R_0}\frac{P}{T}\sum_i X_i N_i \qquad (9)$$

where P is the total absolute pressure in atm, T, the absolute temperature in deg K, R_0, the universal gas constant, and $\sum X_i N_i$, the molar refractivity of a mixture with i species. Obviously, the index of refraction in the reference beam would have to obey the same equation

$$(n_r-1) = \frac{3}{2R_0}\frac{P_0}{T_0}N_r \qquad (10)$$

By combining Eqs. (6), (9), and (10), we can, now, write the final form for the fringe shift in the general system as

$$S(x,y) = \frac{3}{2R_0}\frac{P_0 L}{\lambda}\left[\frac{1}{T(x,y)}\sum_i X_i N_i - \frac{N_r}{T_r}\right] \qquad (11)$$

or rewrite it for the temperature expression

$$T(x,y) = \frac{\sum_i X_i N_i}{\left(\frac{2S(x,y)R_0\lambda}{3PL} + \frac{N_r}{T_r}\right)} \qquad (12)$$

Appendix B

Radiation Corrections for the Thermocouple

The usual radiation corrections consider the balance between radiation losses from the thermocouple to the wall and heat transfer by forced convection from the gas phase to a bead lying normally across the flow. For a quatz-coated Thermocouple (T/C), different investigators have adopted different procedures to evaluate parameters and their corrections for radiation losses ranging from negligible to 82^{0}K [75, 87-90]. The correction relationship employed here is from Symth et al [53]

$$\Delta T = \frac{\sigma \cdot E \cdot d}{N_u \cdot K}(T_{tc}^4 - T_b^4)$$

where

σ = the Stefan-Boltzmann constant ($5.6688X10^{-8}$ w/m^2-k^4)

E = the T/C emissivity (E = 0.3 obtained from kastan [91])

d = T/C bead diameter (d = 0.003" = $7.62X10^{-5}$ m)

Nu = the Nusselt number (Nu=2.0 for a spherical bead)

K = the gas thermal conductivity (from Eckert [92] for air)

T_{tc}= the T/C temperature

T_b = the background temperature (T_b=298^{0}K)

BIBLIOGRAPHY

1. Burke, S. P. and Schumann, T. E. W., " Diffusion Flames," Indust. Eng. Chem., Vol. 29, 1928, p.998.
2. Williams, F. A., "Combustion Theory," Addison-Wesley, Reading, Mass., 1965.
3. Law, C. K. and Chung, S. H., "Steady State Diffusion Flame Structure With Lewis Number Variations," Combust. Sci. Tech., Vol. 29, 1982, p.129.
4. Law, C. K. and Chung, S. H., "On the Flame-Sheet Assumption and Flame Temperature Determination in Combustion Modeling," Combust. Sci. Tech., Vol. 36, 1983.
5. Law, C. K. and Chung, S. H., "Structure and Extinction of Convective Diffusion Flames With General Lewis Numbers," Combust. Flame, Vol.52, 1983, p.59.
6. Law, C. K. and Chung, S. H., "Burke-Schumann Flame with Streamwise and Preferential diffusion," Combust. Sci. Tech., Vol.37, 1984, p.21.
7. Ramohalli, K. and Magiawala, K., "Perforated Porous Plate Burner to Model Composite Propellant Combustion," AIAA Journal, Vol. 19, No.1,1979, p.92.
8. Ramohalli, K., "Vapor Phase Details in the Oscillatory Combustion of Propellants- A Porous Plate Analogue," AIAA paper 79-1174, 1979.
9. Chen, T., Y., "Driving of Axial Acoustic Fields by Sidewall Stabilized Diffusion Flames," Ph.D thesis, Georgia Institute of Technology, 1990
10. Price, E. W., Panyam, R. R. and Sigman, R. K., "Mocrostructure of the Combustion Zone : Thin-Binder AP-Polymer Sandwiches," CPIA No. 329, Vol. 1, 1980.
11. Price, E. W., Handley, J. C., Panyam, R. R., Sigman, R. K. and Ghosh, A., "Combustion of Ammonium Perchlorate - Polymer Sandwiches," AIAA Journal, Vol. 19, No.3, 1981.
12. Price, E. W., Panyam, R. R., Sambamurthi, J. K. and Sigman, R. K., "Combustion of Ammonium Perchlorate-Polymer Sandwiches," CPIA No. 366, Vol.I, 1982.
13. Price, E. W., and Sambamurthi, J. K., "Dependence of Burning Rate of AP-Polymer Sandwiches on Thickness of the Binder Laminae," CPIA No. 383, Vol. 1, 1983.
14. Price, E. W., Sambamurthi, J. K., Panyam, R. R. and Sigman, R. K.," Combustion of Ammonium Perchlorate - Polymer Sandwiches," Annual Contract Report to Office of Naval research, Georgia Institute of Technology, 1984.
15. Price, E. w., Sambamurthi, J. K., Sigman, R. K. and Panyam, R. R.,"Combustion of Ammonium Perchlorate - Polymer Sandwiches," Combust. and Flame, Vol. 63, 1986.

16. Fernandez-Pello, A. C. and Williams, F. A., "Experimental Technique in the Study of Laminar Flame Spread over Solid Combustibles," Combust. Sci. Tech., Vol. 14, 1976, p 155.

17. Fernandez-Pello, A. C. and Hirano, T., "Controlling Mechanisms of Flame Spread," Combust. Sci. Tech., Vol.32, 1983, p 1.

18 Williams, F. A., "Theory of Combustion in Laminar Flows," Annual Review of Fluid Mechanics, Vol 3, 1971, p.171.

19 Glassman, I., "Fire Spread over Solid," Fifth Annual Conference on Fire Research, National Bureau of Standards, Washington, DC, August 1981

20) Fernandez Pello, A. C., "Flame Spread Modeling," Combust. Sci Tech., Vol 39, 1984, p 119

21 Ray, S. R and Glassman, I., "The Detailed Processes Involved in Flame Spread over Solid fuels," combust. Sci Tech., Vol 32, 1983, p 33

22 Wichman, I.s., "Flame Spread in an Opposed Flow with a Linear Velocity Gradient," Combust and Flame, Vol 50, 1983, p.287

23 Wichman, I. S., "A Model Describing the Influences of Finite Rate Gas Phase Chemistry on Rates of Flow Spread Over Solid combustions," combust. Sci. Tech., Vol 40, 1984, p 233

24 Fenn, J. B., "A Phalanx Model for the Combustion of Solid Propellants," Combust. and Flame, Vol 12, 1968, p 201

25 Beckstead, M. W., Derr, R. L. and Price, C. F., "A Model of Solid Propellant Combustion Based on Multiple Flames," AIAA Journal, Vol 8, No 12, 1970, p 2200

26 Bakhman, N. N and Librovich, V. B., "Flame Propagation along Solid Fuel - Solid Oxidizer Interface," Combust. and Flame, Vol 15, 1970, p 143

27 Phillips, H., "Flame in a Buoyant Methane Layer," Tenth Symposium (Int.) on Combustion, The Combustion Institute, 1965, p 1277

28 Liebman, I., Corry, J. and Perlee, H. E., "Flame Propagation in Layered Methane Air Systems," Combust. Sci. Tech., Vol. 1, 1970, p 257

29 Glassman, I. and Hansel, J. G., "Some Thoughts and Experiments on Liquid Fuel Spreading, Steady Burning and Ignitability on quiescent Atmospheres," Fire Res. Abst Reviews, Vol 10, 1968, p.217.

30 Roberts, A. F. and Burgoyne, J. H., "The Spread of Flame Across a Liquid surface II Steady State conditions," Proc. Roy. Soc. A308, 1968, p 55

31 Hirano T. and Kanno Y., "Aerodynamic and Thermal Structures of the Laminar Boundary Layer over a Flat Plate with a Diffusion flame," Fourteenth symposium (Int.) on Combustion, Combustion Institute, 1973, p.391.

32 Hirano T. and Kinoshita, M., "Gas Velocity and Temperature Profiles of a diffusion Flame Stabilized in the Stream over Liquid Fuels," Fifteenth symposium (Int.) on Combustion, Combustion Institute, 1974, p 379.

33 Feng, C. C., Lam, S. H. and Glassman, I., "Flame Propagation through Layered Fuel-Air Mixtures," Combust. Sci Tech., Vol. 10, 1975, p 59

34 Kaptein, M. and Hermance, C. E., "Horizontal Propagation of Laminar Flames Through Vertically Diffusing Mixtures above a Ground Plane," Sixteenth symposium (Int.) on Combustion, Combustion Institute, 1977, p 1295

35 Hirano, T., Suzuki, T. and Mashiko, I., "Flame Propagation Through Mixtures with Concentration Gradient," Sixteenth Symposium (Int.) on Combustion, Combustion Institute, 1977, p 1307

36 Ishikawa, N., "A Diffusion Combustor and Methane Air Flame Propagation in Concentration gradient fields," Combust. Sci. Tech., Vol 30, p 185

37 Glassman, I. and Charyk, J. V., "The Ram Rocket, Jet Propulsion Engines, Vol XII, High Speed Aerodynamics and Jet Propulsion," Princeton University Press, 1959, p 625

38 Ishikawa, N., "Flame Structure and Propagation Through an Interface of Layered Gases," Combust. Sci. Tech., Vol 31, 1983, p 109

39 Melvin, A., Moss, J. B. and Clarke, J. F., "The Structure of a Reaction Broadened Diffusion Flame," Combust. Sci. Tech., Vol 4, 1971, p 17

40 Fendell, F. E., "Ignition and Extinction in Combustion of Initially Unmixed Reactants," J. Fluid Mech., Vol 21, Part 2, 1965, p 281

41 Linan, A., "The Asymptotic Structure of Counterflow diffusion Flames for Large Activation Energies," Acta Astronautica, Vol 1, 1974, p 1007

42 Peters, N., "Effects of Chemical Equilibrium on the Structure and Extinction of Laminar Diffusion Flames," Progress in Astronautic and aeronautics, Vol 95, 1984, p 37

43 Puri, I. K. and Seshadri, K., "Extinction of Diffusion Flame Burning Detailed Methane and Diluted Propane in diluted Air," Combust. and Flame, Vol 65, 1986, p 137

44 Peters, N. and Kee, R. J., "The Computation of Stretched Laminar Methane-Air Diffusion Flame Using a Reduced Four-Step Mechanism," Combust. and Flame, Vol 68, 1987, p 17.

45. Seshadri, K. and Peters, N., "Asymptotic Structure and Extinction of Methane-Air Diffusion Flames," Combust. and Flame, Vol. 73, 1988, p.23.

46 Tsuge, S. and Ohki, Y., "Flame Propagation Through a Layer with Varying Equivalence Ratio," Progress in Astronautics and Aeronautics, Vol. 105, 1985, p.233

47. Wichman, I. S., "On the Quenching of a Diffusion Flame Near a Cold Wall," Combust. Sci. Tech., Vol.64, 1989, p.295.

48. Smooke, M. D., Mitchell, R. E. and Keyes, D. E.," Numerical Solution of Two-Dimensional Axisymmetric Laminar diffusion flames," Comb. Sci. Tech., Vol.

49. Mao, C. P., Kodama, H. and fernandez-Pello A. C., "Convective Structure of a Diffusion Flame over a Flat Combustible Surface," Combust. and flame, Vol. 57, 1984, p.209.

50. Parker, W. G. and Wolfhard, H. G., "A Spectroscopic Investigation into the Structure of diffusion flames," Proc. Phys. Soc., A65, 1952, p.2.

51. Kent, J. H., Jander, H. and Wagner, H. G., "Soot formation in a Laminar diffusion Flame," Eighteenth Symposium (Int.) on Combustion, Combustion Institute, 1981, p.1117.

52. Miller, J. H., Mallard W. G. and Smyth, K. C., "The Observation of Laser-Induced Visible Fluorescence in Sooting diffusion flames," combust. and Flame, Vol. 47, 1982, p.205.

53. Smyth, K. C., Miller, J. H., Dorfman, R. C., Mallard, W. G. and Santoro, R. J., "Soot Inception in a Methane/Air Diffusion Flame as Characterized by Detailed Species Profiles," Combust. and Flame, Vol. 62, 1985, p.157.

54. Powling, J., "The Flat Flame Burner, Experimental Methods in combustion Research," Pergamon Press, New York, 1961.

55. Beidler, w. T. and Hoelscher, H. E., "Studies in a New Type of Flat Flame Burner," Jet Propulsion, Vol. 27, 1957, p.1257.

56. Pandya, T. P. and Weinberg, F., "The Study of the Structure of Laminar Diffusion Flames by Optical Methods," Ninth Symposium (Int.) on combustion, Academic Press Inc., 1963, p.587.

57. Chung, S. L. and Katz, J. L.,"The Counterflow Diffusion Flame Burner: A New Tool for The Study of The Nucleation of Refractory Compounds," Combust. and Flame, Vol. 61, 1985, p.271.

58. White, F. M., "Fluid Mechanics," McGraw-Hill Book Company, New York, 1979.

59. Liepmann, H. W., Roshko, A., "Elements of Gasdynamics," Wiley, New York, 1957.

60. Weinberg, F. J., "Optics of Flames," Butterworth and Co. Ltd., 1963.

61. Merzkirch, W.,"Flow Visualization," academic Press, Inc., New York, 1987.

62. Wilkie, D. and Fisher, S. A., "Measurement of Temperature by Mach-Zehnder Interferometry," Proc. Instn. Mech. Engrs., Vol. 178, Pt 1, No. 17, p.461.

63. Olsen, H. L., "An Interferometric Method of Gas Analysis," Third Symposium on Combustion, Academic Press Inc., 1943.

64. Schultz-Grunow, F. and Wortberg, G., "Interferometrische Messungen an Einer Ebenen Laminaren Flamme," Int. J. Heat Mass Transfer, Vol. 2, 1961, p.56.

65. Roepor, E., "Eine Neue Schlierenblende," Optic, Stuttgart 12, 1955, p.283.

66. Goulard, R., "combustion Measurements : Modern Techniques and Instrumentations," Section 7, Academic Press, New York, 1976.

67. Tsuji, H. and Yamaoka, I., "The Counterflow Diffusion Flame in the Forward Stagnation Region of a Porous Cylinder," Eleventh Symposium (Int.) on Combustion, Combustion Institute, 1967, p.979.

68. Tsuji, H. and Yamaoka, I., "The Structure of Counterflow Diffusion Flames in the Forward Stagnation Region of a Porous cylinder," Twelfth Symposium (Int.) on Combustion, Combustion Institute, 1969, p.997.

69. South, R. and Hayward, B. M., "Temperature Measurement in Conical Flames by Laser Interferometry," Combust. Sci. and Tech., Vol. 12, 1976, p.183.

70. Price, E. W., "Initial Adjustment of The Mach-Zehnder Interferometer," Vol. 23, No. 4, The Review of Scientific Instruments, 1952, p.162.

71. Friedman, R., "Measurement of The Temperature Profile in a Laminar Flame," Fourth Symposium on Combustion, The williams and Wilkens Co., Baltimore, 1953, p.68.

72. Leah, A. S. and Carpenter, N., "The Estimation of Atomic Oxygen in Open Flames and The Measurement of Temperature," Fourth Symposium on combustion, The williams and Wilkens Co., Baltimore, 1953, p.68.

73. Gardiner, W. C., Hidaka, Y. and Tanzawa, T., "Refractivity of Combustion Gases," Combust. and Flame, Vol. 40, 1981, p.213.

74. Fristrom, R. M. and Westenberg, A. A., "Flame Structure," MaGraw-Hill Book Company, New York, 1965.

75. Dixon-Lewis, G. and Isles, G. L., "Flame Structure and Flame Reaction Kinetics III," Proc. Roy. Soc., A308, 1969, p.517.

76. Kanury, A. M., "Introduction to Combustion Phenomena," Gordon and Breach Science Pub., New York, 1977.

77. Gaydon, A. G. and Wolfhard, H. G.,"Flames; Their Structure, Radiation and Temperature," Chapman and Hall Ltd., 1970.

78. Gaydon, A. G. and Wolfhard, H. G.,"Spectroscopic Studies of Low-Pressure Flames II. Effective Translational and Rotational Temperatures From CH Bands," Proc. Phys. Soc., A199, 1949, p.89.

79. Gaydon, A. G. and Wolfhard, H. G.,"Spectroscopic Studies of Low-Pressure Flames III Effective Rotational Temperatures and Excitation Mechanism for C_2 Bands," Proc. Phys. Soc., A201, 1950, p.561.

80 Porter, R. P., Clark, A. H., Kaskan, W. E. and Browne, W. E., "A Study of Hydrocarbon Flames," Eleventh Symposium (Int.) on Combustion, Combustion Institute, 1967, p 907.

81 Jessen, P. F. and Gaydon, A. G., "Estimation of Carbon Radical Concentrations in Fuel-Rich Acetylene-Oxygen Flames by Absorption Spectroscopy," Twelfth Symposium (Int.) on Combustion, 1969, p.481.

82 Hurle, I. R., Price, R. B., Sugden, T. M. and Thomas, A., "Sound Emmision From Open Turbulent Premixed Flames," Proc. Phys. Soc., A303, 1968, p 409

83 Price, R. B., Hurle, I. R. and Sugden, T. M., "Optical Studies of The Generation of Noise in Turbulent flames," Twelfth (Int.) Symposium on Combustion, The Combustion Institute, 1969, p 1093

84 Shivashankara, B. N., Strahle, W. C. and Handley, J. C., "Combustion Noice Radiation by Open Turbulent Flames," Progress in Astronautics and Aeronautics, Vol 37, 1975, p 287

85 Computer Code for Thermochemical Equilibrium Calculations acquired from Naval Weapons Center

86 Rosser, W. A., Inami, S. H. and Wise, H., "The Effect of Metal Salts on Premixed Hydrocarbon-Air Flames," Combust. and Flame, Vol. 7, 1963, p 107

87 Fishenden, M. and Saunders, O. A., "The Errors in Gas Temperature Measurement and Their Calculation," J. Inst. Fuel, No. 64, Vol. 12, 1939, S5

88 Cooksen, R. A., Dunham, P. G. and Kilham, J. K., Combust. and Flame, Vol. 8, 1964, p 168

89 Kremer, H., "Mixing In a Phase Free-Turbulent-Jet diffusion Flame," Eleventh Symposium on Combustion, 1966, p 799

90 Aham, DPS, "Methane Combustion in Laminar diffusion Flames," Proc. Instn. Mech. Engrs., Vol. 203, 1989, p 65

91 Kaskan, W. E., "The Dependence of Flame Temperature on Mass Burning Velocity," Sixth Symposium (Int.) on Combustion, 1956, p 134

92 Eckert, E. R. G. and Drake, R. M. Jr., "Analysis of Heat and Mass Transfer," Mcgraw-Hill, New York, 1972.

93 Zhu, D. L., Egolfopoulos, F. N. and Law, C. K., "Experimental and Numerical Determination of Laminar Flame Speeds of Methane/(Ar, N_2, CO_2)-Air Mixtures as Function of Stoichiometry, Pressure, and Flame Temperature," Twenty-second Symposium (Int.) on Combustion, 1988, p 1537.

94 Lewis, R. and Von Elbe, G., "Combustion, Flames and Explosions of Gases," Second Edition, Academic Press, New York, 1961.

Appendix G

Combustion Characteristics of Sandwiches with New Ingredients

Proceedings of the 32nd JANNAF Combustion Meeting, Huntsville, AL, October 1995.

COMBUSTION CHARACTERISTICS OF SANDWICHES WITH NEW ENERGETIC INGREDIENTS*

E. W. Price, S. R. Chakravarthy, and R. K. Sigman
Georgia Institute of Technology, Atlanta, GA.

ABSTRACT

The paper concerns combustion characteristics of solid propellant formulations with new energetic oxidizers -- ammonium dinitramide (ADN) and hexanitrohexazaisowurtzitane (HNIW) -- and conventional hydrocarbon binders. The sandwich burning methodology is employed in the experiments. The results are compared with previous results with ammonium perchlorate (AP). Results for ADN indicate importance of the leading edge of the diffusion flames attached to the lamina interface of sandwiches in controlling the burning rate. Evidence is also obtained that points to complicated multiphase processes in a microscopically thin surface layer that may dictate the structure of the gas phase flame complex. The results for HNIW suggest that the exothermic decomposition of fine oxidizer particles (and possibly reaction with binder) in the surface layer strongly controls the burning rate. Burning rates of formulations based on both the oxidizers are not sensitive to addition of ferric oxide.

INTRODUCTION

The controlling mechanisms of combustion of heterogeneous solid propellants are resistant to quantitative and analytical evaluation because of the complexity of the propellant, three dimensional geometry and microscale of the flame complexes, and problems of realistic modeling of reaction chemistry superimposed on the diverse multicomponent reacting flows. Almost nothing about these processes can be observed directly during combustion at rocket motor pressures, and a variety of strategies are used to lead to more tractable experiments and models. The present study extends studies in which the micro geometry of the propellant is simplified by edge-burning of "sandwiches," laminates of a binder between two laminates of oxidizer. To the extent that this leads to two dimensional behavior, it leads to

(a) easier observation and description of combustion;
(b) easier and less ambiguous description and control of propellant microstructure;
(c) relative ease and safety of preparation of test samples, with minimal amounts of sometimes scarce ingredient materials;
(d) an extensive back log of experience with and interpretation of test results.

While such methods may help elucidate some important aspects of propellant combustion, it is always wise to remember that there are aspects of propellant combustion that are not revealed, aspects that relate to three dimensional and statistical features of a propellant and with granular ingredients.

Most of the past studies have used sandwiches consisting of AP and polybutadiene binders. In the present report, the sandwich method was used to evaluate the combustion behavior of systems using several different oxidizers, ferric oxide catalyst, and aluminum. Because of limited availability of some oxidizers, the sandwiches mostly incorporated the "new" oxidizers in the binder lamina, with the two pure oxidizer laminae being dry-pressed AP. This use of AP for the oxidizer laminae was motivated by practical considerations, i.e., limited supplies of the other oxidizers and uncertain safety of dry-pressing them. The relatively advanced understanding of burning of AP sandwiches is a help in interpretation of results, but of course does not fully reveal how the sandwiches would burn with oxidizer laminae of different materials.

It is useful to take a brief look at the limited literature on thermal decomposition (and combustion) of the new oxidizers. Brill et al. [1] have performed thermal decomposition of ADN, and have studied the temporal evolution of final products such as NH_3, HNO_3, NO_2, H_2O, etc. using T-Jump/FTIR Spectroscopy. ADN first decomposes into $NH_3 + HN(NO_2)_2$; subsequent decomposition yields NO_2 in considerable quantity, whose reaction

* This work was performed under ONR grant N00014-89-J-1293 with Dr. R. S. Miller as technical monitor. Dr. Robert Wardle of Thiokol Corporation supplied the principal ingredients used in this study.

with NH_3 results in a pronounced overall exothermicity even at atmospheric pressure. Parr and Hanson-Parr [2] have performed CO_2 laser assisted burning of ADN/binder/ADN sandwiches with relatively thick binder laminae (~300 μm), in the pressure range 1-14 atm, using both energetic (GAP, BAMO/NMMO) and non-energetic (wax, HTPB) binders. Their diagnostics include CN, NO and OH PLIF imaging, chemiluminescence and Mie scattering techniques. They report that ADN begins to burn by itself at 2-3 atm. As such, the O/F diffusion flame rapidly diminishes in significance as compared to the self-deflagration of ADN at elevated pressures, even with energetic binders; the binder lamina remains virtually unburned. They also report appearance of a spray of large liquid droplets above the ADN laminae. Pak [3] reported that the burning rate of ADN-based propellants increases with ADN particle size (an effect that is reverse of that in AP propellants). Parr et al. speculate that such an effect is understandable in view of their observations.

Pesce-Rodriguez et al. [4] have performed thermal decomposition tests on HNIW, and HNIW/TPE unplasticized and plasticized with nitrate esters, using a variety of modern techniques such as P-GC-FTIR spectroscopy, etc. They find that the pyrolysis products are in many ways similar to those of RDX and HMX, but certainly different to some extent. TPE binders and, or plasticizers (or their decomposition products) do seem to react with HNIW products. Patil and Brill [5] have performed slow TGA and fast-heat-and-hold/FTIR spectroscopy on HNIW decomposition, and have concluded that the $N\text{-}NO_2$ homolysis is the dominant step in the slow decomposition of HNIW. Unlike RDX and HMX, where the $N\text{-}NO_2$ homolysis lowers the barrier to C-N fission, in the case of HNIW, the liberated NO_2 oxidizes radical sites in the condensed residue, resulting in NO production. The global kinetics of HNIW decomposition fits first order and second order mechanisms equally well. All the gas products appear just after a sharp exotherm, indicating that HNIW does not undergo autocatalysis. The same workers [6] have proceeded to characterize the residue by T-Jump/FTIR spectroscopy. The residue is thermally stable up to 700°C. The presence of HNCO, HCN, CO_2 and NO_2 is detected. NO_2 indicates that the functional group $-NO_2$ is still retained by HNIW during dissociation.

EXPERIMENTAL

TECHNIQUES

The two major combustion experiments employed in this study were: (i) Combustion photography and burning rate measurements, and (ii) Quenching by depressurization, followed by examination in the scanning electron microscope (SEM). These experiments are rather routine, and details of the setups are outlined elsewhere [7]. The present results would be better understood in the light of observations of ingredient thermal response and interaction on a hot stage microscope. These observations have been reported previously [8,9], and are briefly mentioned at the beginning of next section.

INGREDIENTS AND SAMPLES

ADN, HNIW and HMX were provided by R. Wardle of Thiokol Corporation. The particle sizes these materials were 40, 10 and 10 μm respectively. The particle sizes of fine AP (used for comparison) are 10 and 33 μm. These are nominal size values obtained by viewing a sample of the particles in the optical and scanning electron microscope. No attempt was made to quantitatively characterize the particle size distribution of these particles beyond what is mentioned above.

Approximately 1.6 g of ADN or AP was pressed at 25000 lb for 2 hours to make pressed pellets for the oxidizer laminae in the sandwiches. (Fabrication on sandwiches is detailed elsewhere [7].)

The proportions of the binders used in this study are as follows: (i) PBAN - 64.14%, DOA - 15% and ECA - 20.86%; (ii) HTPB - 75.73%, DOA - 18.39% and IPDI - 5.88%. The ferric oxide used in this study is "Pyrocat," supplied by MACH I (particle size - 0.003 μm, specific surface area - 270 m^2/g, density - 0.05 g/cm^3).

RESULTS

HOT STAGE MICROSCOPIC OBSERVATIONS

At the outset, it is useful to look at the hot stage microscopic observations of a few pertinent ingredients and combinations of ingredients. Typical values for temperatures of melting and decomposition of individual ingredients are listed in Table 1. Interaction between two or more ingredients is described briefly here.

ADN WITH PBAN: At 90 °C, ADN melts inside the binder. Above 140 °C, ADN begins to decompose inside the still solid binder; the binder turns dark and the ADN gas products seem to rupture through the binder and emanate suddenly at 200 °C. The binder melts and vaporizes above 480 °C, but a considerable amount of residue suggestive of ADN-binder reactions remains after binder decomposition is complete.

ADN WITH HTPB (CURED BY IPDI): The above sequence of events is followed up to ADN decomposition, but the gases do not escape as dramatically; instead, they cause the binder to soften and melt earlier than usual. Some charred residue is left behind. Above 470 °C, the binder begins to vaporize; the residue is found floating amidst the bubbling, and remains after binder vaporization.

ADN WITH UNCURED HTPB: In this particular test, the heating stage was heated just up to the melting temperature of ADN and cooled down. The melted ADN migrated together within the uncured (liquid) HTPB prepolymer and recrystallized into a single large disk-like particle of size ~1000 μm back at room temperature.

HNIW (200 MM) WITH PBAN: A crystal phase change is observed for HNIW at around 150 °C. Above 190 °C, HNIW begins to decompose, and this is reflected in a mild agitation on the binder surface. Just above 200 °C, the agitation rapidly intensifies, and a local explosion occurs. The little remains of the binder melts and vaporizes at 470-500 °C.

SCANNING ELECTRON MICROSCOPIC OBSERVATIONS

1. SANDWICHES WITH ADN PARTICLES IN THE MATRIX: Surface features of sandwiches with ADN (40 μm)/PBAN and HTPB = 7/3 are shown in Fig. 1 (a) and (b) respectively. Since ADN melts and decomposes at temperatures much lower than those for these binder (HSM), no ADN particles can be readily identified on these surfaces. For the PBAN sandwiches, one can see a crater whose size is of the order of the matrix lamina thickness; this is typical of quench samples at various pressures. As for the HTPB sandwiches, there are sharp as well as smooth ups and downs in the region corresponding to the matrix lamina. These observations can be understood in the light of the hot stage observations of interactions of the above combinations.

2. HNIW/PBAN SANDWICHES: Fig. 2 shows surface features of a sandwich with AP laminae on either side of a matrix of HNIW/PBAN = 7/3 matrix of lamina thickness ~375-400 μm, quenched at 500 psi. Unlike the corresponding AP sandwiches where the oxidizer particles were seen as mounds covered by the binder [7], the matrix surface here is practically flat, with some cuts and pores, and larger holes. A sketch of the surface profile of HNIW/PBAN sandwiches is shown in Fig. 3. The AP laminae in the immediate vicinity of the matrix lamina are unprotruded and exhibit a dry quality, as opposed to a protruded region of smooth surface quality for AP-filled PBAN sandwiches.

BURNING RATE MEASUREMENTS

1. DEFLAGRATION OF PRESSED ADN: Unlike AP which has a low pressure deflagration limit of about 280 psi, ADN sustains deflagration at much lower pressures. Fig. 4 shows the deflagration rate of pressed ADN compared to AP rate in the pressure range 100-2000 psi. In general, ADN burning rates are 2-3 times higher than AP burning rates. The ADN burning rate curve as a plateau in the low pressure range 100-300 psi. The reason for this feature is not clear.

2. ADN/PBAN/ADN SANDWICHES: Sandwiches with two pressed pellets of ADN sandwiching a lamina of pure PBAN binder of thickness ~70 μm were burned at different pressures. The binder lamina thickness corresponds to maximum burning rates (in the intermediate pressure range 300-1000 psi) based on AP/PBAN sandwiches. More elaborate studies with variation of the binder lamina thickness at different pressures were obviated by limited availability of ADN. The pressure dependence of the ADN/PBAN sandwich burning rate is shown in Fig. 5 along with the ADN self-deflagration rate, AP/PBAN sandwich burning rate, and the AP self-deflagration rate curves. The results clearly show the predominance of the ADN/PBAN flame over the ADN self-deflagration flame, particularly at intermediate pressures, similar to AP/PBAN sandwiches. This is against the results reported by Parr et al. [2], where ADN/binder sandwiches with thick binder laminae were burned with assistance from laser radiation.

3. ADN/PBAN MATRIX SANDWICHES WITH AP LAMINAE: Sandwiches with two AP laminae on either side of a matrix lamina containing ADN particles in PBAN binder of lamina thickness ~375-400 μm were burned at four pressure levels: 100, 300, 500 and 1000 psi. The matrix mixture ratio was varied as ADN/PBAN = 7/3 and 5/5. The burning rate versus pressure plot is shown in Fig. 6a. Similar plot for AP/PBAN is shown in the companion Fig. 6b [7]; the AP particle size is 33.5 μm.

The ADN/PBAN = 5/5 matrix burns at 1000 psi only. (The AP/PBAN = 5/5 matrix does not sustain combustion in the entire test pressure range.) The ADN matrix is seen to be sensitive to the presence of the AP laminae (in the sandwich) on two counts: (a) The burning rate of the ADN 7/3 sandwich is higher than the matrix rate to a greater extent than is the AP 7/3 sandwich compared to its matrix. (b) The burning rate of ADN sandwiches is mostly insensitive to the matrix mixture ratio, whereas there is a big difference between the burning rates of the ADN 7/3 matrix and the 5/5 matrix, when it burns (at 1000 psi). This is against a considerable difference between the 7/3 and 5/5 burning rates for the AP/PBAN sandwiches.

4. ALUMINIZED ADN/PBAN MATRIX SANDWICHES WITH AP LAMINAE: 10% Al (15 μm) was added to the ADN/PBAN = 7/3 matrix, and sandwiches were fabricated with AP laminae on either side. Corresponding sandwiches with AP (10 μm) were also tested for comparison. The burning rate results are shown in Fig. 7. With AP matrix sandwiches, Al increases rate at high pressures and reduces it slightly at low pressures. In the matrix, this effect is reversed; and the pressure dependence of the rate is correspondingly low (plateau at 1000 psi). With ADN matrix sandwiches, Al has an effect similar to that in AP sandwiches. The effect in the ADN matrix is conspicuously different than with the AP matrix. The rate is low at 100 and 300 psi, and high at 500 and 1000 psi, with a jump between 300 and 500 psi. The combustion photography indicates that the low ADN matrix rate at low pressure is associated with very poor Al combustion, and that the high pressure is accompanied by a very good aluminum combustion (better than in AP matrix samples).

5. ADN/HTPB MATRIX SANDWICHES WITH AP LAMINAE: Burning rates of sandwiches similar to item 3 above, but with HTPB binder, are shown in Fig. 8. The ADN/HTPB = 5/5 did not burn at all test pressures. Results are otherwise similar to the ADN/PBAN cases (Fig. 8a). That is, the 7/3 sandwich rates are considerably higher than their matrix burning rates, and there is little overall difference between the 7/3 and 5/5 sandwich burning rates.

6. ADN/HTPB MATRIX SANDWICHES WITH ADN LAMINAE: Fig. 9 shows results for sandwiches with an ADN/HTPB = 7/3 matrix sandwiched by ADN laminae. Results for similar sandwiches with AP laminae (part of item 5 above), and the burning rate of the matrix burning alone are shown for comparison. The matrix sandwiches with ADN lamina burn the fastest among the curves shown, at any pressure. The presence of the ADN laminae has an enormous effect over the matrix lamina (comparing sandwich and matrix burning rates). It can be seen in the video pictures that at low pressures (100 psi), the matrix lamina fairly protrudes above the rest of the sandwich surface. Although it may not be exactly appropriate to compare ADN/HTPB matrix sandwiches with ADN/PBAN/ADN pure binder sandwiches (item 2 above), it may be noted that the curves for the two are almost coincidental.

7. HNIW/PBAN AND HMX/PBAN MATRIX SANDWICHES WITH AP LAMINAE: Sandwiches with AP laminae and matrix with HNIW/PBAN = 7/3 and HMX/PBAN = 7/3 were burned at 100, 300, 500 and 1000 psi. Burning rates are shown in Fig. 10. Within limits of experimental error, there is no consistent trend between the HNIW sandwich and matrix burning rates, and they are nearly equal at all test pressures. The rates are higher than for AP/PBAN sandwiches, and the burning rate-pressure curves for HNIW have a higher pressure exponent than for AP/PBAN samples, in general. On the other hand, the HMX/PBAN matrix burning rates are low by an order of magnitude when compared to typical values for other systems. The presence of the AP laminae in the sandwiches increases the HMX/PBAN burning rates to levels comparable to other systems.

8. CATALYZED MATRIX SANDWICHES WITH AP LAMINAE: 1% Pyrocat ferric oxide was included in a matrix of oxidizer/PBAN = 7/3, where the oxidizer was ADN or HNIW. The matrix was sandwiched by AP laminae, with the matrix lamina being approximately 375-400 μm thick. The burning rates of catalyzed samples are compared with the uncatalyzed sample burning rates in Fig. 11. Companion figures are included for AP of nominal sizes 10 μm (comparable to HNIW size) and 33.5 μm (comparable to ADN size). In the case of ADN (Fig. 11a), a mild catalytic effect is seen for the ADN/PBAN sandwich, but marginal effect for the matrix. The effect of the catalyst is negligible in the case of both the sandwich and matrix containing HNIW (Fig. 11b). These non-effects are in contrast to the major effect of ferric oxide on the samples containing fine AP particles.

DISCUSSION OF RESULTS

Research on combustion mechanisms of composite propellants has always had to rely on indirect observations (e.g., SEM of quenched samples) and parametric variation of global results (e.g., mean burning rate). The results themselves may be significant, but the task of reporting them is far from complete if the results are not collectively interpreted in a manner that does not pose any contradictions. In doing so, it is natural to begin by considering a picture of the propellant combustion zone microstructure in such detail as afforded by the current state of knowledge based on past studies. More precisely, it is impossible to ignore the vast body of knowledge developed over several decades for AP-hydrocarbon binder systems while considering the combustion characteristics of formulations based on new ingredients. With particular regard to this paper, interpretation of results of sandwich burning with new ingredients relies on a relatively detailed (in a multidimensional as well as a microscopic sense) picture of the combustion zone developed by systematic studies with AP/PBAN sandwich systems.

There are two aspects of the AP/PBAN combination that are fundamentally pertinent to the present study: (i) The two ingredients decompose within a narrow temperature range, rendering the surface layer very thin and fairly "contiguous"; (ii) The melting and decomposition temperatures of either ingredient are not too far apart, resulting in a fairly "dry" surface (very thin melt layers). These factors offer least obscuration of the surface features (in combustion photography and quenched samples), and have permitted undistracted focus on details of the gas phase combustion zone. On the other hand, the systems considered in the present study, viz., ADN and HNIW with hydrocarbon binders, have ingredients that are markedly different in their decomposition temperatures, causing thicker surface layers and subsurface activity; furthermore, ADN and HTPB melt substantially before decomposition, allowing the possibility of complicated multiphase processes to precede the emergence of vapors that react at the gas phase flames. The task, therefore, is to consider first the details of the gas phase flame complex for AP/PBAN systems, and then examine how the combustion zone may be altered in the presence of the new ingredients. The goal is to apply the scenario of the overall combustion zone thus evolved to reconciliation of the reported global results, and explore those sites and processes in the combustion zone that act as burning rate controlling.

DETAILS OF THE GAS PHASE COMBUSTION ZONE

The burning rate of a AP/PBAN/AP sandwich is controlled by the leading edge portion of the O/F diffusion flame [10], referred to as the "leading edge flame (LEF)." The LEF is intensely hot owing to the premixing gases upstream of its location, and is located at a point on the diffusion flame structure (stoichiometric sheet) that is closest to the burning surface (significant in terms of heat feedback). The sandwich burning rate is further controlled by the extent to which adjacent LEFs "interact," in the sense of optimum consumption of reactants from both the adjacent mixing fans (on which the LEFs are anchored) and maximum two-dimensional gas phase heat feedback to the surface. This interaction is reflected in a maximum in the burning rate at a binder lamina thickness of ~50-75 μm (in the intermediate pressure range 300-1000 psi), as shown in Fig. 12.

When modest amounts of fine AP particles (~10 μm) are included in the binder lamina [11], specifically at AP/PBAN ratios that are too low (e.g., 5/5) to let the AP-filled binder matrix to self-sustain burning, the effect of the AP particles is primarily two-fold: (i) They decrease the concentration of the fuel species in the matrix lamina. This is reflected in a much greater matrix lamina thickness (~250-275 μm) corresponding to maximum burning rate (Fig. 12); the larger thickness enables adequate supply of fuel species to the LEFs and facilitates maximum interaction between them, resulting in maximum burning rate.(ii) The AP particles also supply oxidizer species that can premix with the fuel gases before reaching the hot O/F flames (depending on the particle size). This causes the LEFs to move inward, and more over the matrix lamina, besides increasing the lateral extent of the LEFs on the side of the matrix lamina. The net effect is to increase the heat release of the LEFs to the surface.

For greater amounts of fine AP particles (~10 μm) than considered in the above paragraph (e.g., AP/PBAN = 7/3 [11]), the matrix may sustain burning by itself at intermediate pressures, by means of a premixed flame. When such a matrix is sandwiched between AP laminae, the LEFs are connected by a premixed flame "canopying" the matrix lamina, and may be appropriately designated as "canopy flame." The sandwich burning rate is still, under most conditions, controlled by the LEFs (since the sandwich burning rate is almost always greater than the matrix burning rate), but the canopy flame helps augment the interaction between the adjacent LEFs, as can be seen by the pronounced peak in the burning rate versus matrix lamina thickness curve in Fig. 12.

At higher pressures (>1000 psi), or for larger fine AP particles (33.5 μm) in the matrix, premixing of oxidizer and fuel species may be incomplete before they reach the LEF standoff height, and O/F diffusion flames may be attached to the AP particles (regardless of the mixture ratio in the matrix). The leading edge portions of such O/F flames attached to the fine AP particles may be designated as "particle leading edge flames (PLEFs);" and, the LEFs attached to the lamina interfaces of the sandwich (considered so far) may be designated as "lamina leading edge flames (LLEFs)," in order to distinguish them from the PLEFs.

The canopy flame may stand farther away from the burning surface than the LLEFs because it consumes a typically very fuel rich reactant mixture, whereas the LLEFs are established along the stoichiometric surfaces. For this reason, the PLEFs may be established at more or less the same distance from the burning surface as the LLEFs. However, in the case where significant exothermic heat release occurs in the matrix surface layer, the vapors feeding the PLEFs would be hotter than those arriving at the LLEFs, the PLEFs have an opportunity to stand closer to the burning surface than the LLEFs. This case is pertinent in the present context considering the significantly exothermic decomposition of the new energetic oxidizers, ADN and HNIW.

The purpose of sandwiching matrix laminae containing the new oxidizers with AP laminae is to examine the response of the matrix to the presence of a pair of LLEFs. In order to prevent the sandwich burning rate from being controlled by maximum interaction between the LLEFs, the matrix lamina thickness in the sandwiches was chosen in the thick matrix range (~375–400 μm), based on considerations discussed in the foregoing paragraphs (and presented in Fig. 12).

FORMULATIONS BASED ON ADN

The available results facilitate consideration of the flame structure of ADN-based propellants at two different length scales separately: (i) The O/F flame structure attached to the periphery of coarse ADN particles in a propellant, as simulated by the pure binder (PBAN) sandwiches with ADN laminae, (ii) The flame structure associated with areas of fine ADN/binder matrix in the propellant, as simulated by sandwiches with such matrix sandwiched by AP or ADN laminae.

The high burning rates of ADN lamina (compared to AP, Fig. 4) may cause suspicion that an "inert" binder lamina adjacent to it (in the sandwiches) may primarily act as a heat sink and decrease the burning rate. This idea is supported by the work of Parr and Hanson-Parr [2]. However, Fig. 5 shows burning rates of ADN/PBAN sandwiches to be typically high, and certainly higher than the self-deflagration rate of ADN lamina. This indicates a principal role for the LEFs in controlling the burning rate of ADN sandwiches just as in AP sandwiches. When a thin binder lamina is used in sandwiches and when the samples are burned under nearly adiabatic conditions, the heat loss due to the pyrolysis of the endothermic binder is reduced, and the O/F flamelets are positioned with respect to each other in such a way that the net heat release to the surface is enhanced.

The predominance of the LLEFs with ADN laminae over the matrix flame in the case of sandwiches with the ADN/HTPB matrix is also clear from Fig. 9 (compared to Fig. 5). This result suggests that the burning rate of ADN-based propellants would be controlled by the O/F flamelets attached to the coarse ADN particles. How this could lead to the particle size dependence of burning rate (higher burning rates for larger particles) reported by Pak [3] is not clear.

The significance of the LLEFs in the combustion of ADN-based matrices is also clear from the results of sandwiches with AP laminae. This can be seen from the following features: (i) The difference in the sandwich and matrix rates is greater for ADN-based matrices than for AP-based matrices (Figs. 6 and 8). (ii) The ADN-based matrix sandwich burning rates are insensitive to the matrix composition while the matrix burning rates are sensitive, implying an overwhelming effect of the presence of the LLEFs (in the sandwiches) on the ADN-based matrix

regardless of its composition.(iii) The singular effect of aluminum on the ADN/PBAN matrix is smeared in the presence of LLEFs (Fig. 7). (iv) The catalytic effect of Pyrocat is negligible on the ADN/PBAN matrix, whereas, there is a slight effect on the sandwiches (Fig. 11a). LLEFs are known to be moderately catalyzed by ferric oxide [12].

The flame structure related to the fine ADN particles in the matrix may briefly be considered. At moderate pressures (100-300 psi), fine ADN particles most probably do not support individual PLEFs, but decompose (exothermally [1]) and mix with binder vapors and support a canopy flame downstream of the surface, of course, depending on the mixture ratio of the matrix. It is not clear if PLEFs are attached at higher pressures (500-1000 psi). The burning of ADN/PBAN = 5/5 matrix supports such an idea. The effect of aluminum on the ADN/PBAN matrix may also be considered in this regard. In the AP analog (Fig. 7b), the matrix is expected to support a canopy flame [11] even at 1000 psi, and the presence of the LLEFs is required to support effective Al ignition and combustion, and cause an increase in the burning rate (comparing sandwich and matrix curves). On the other hand, the jump in the burning rate of aluminized ADN/PBAN matrix between 300 and 500 psi (Fig. 7a) implicates a possible change in the flame structure above the matrix from a canopy flame to an array of PLEFs. The exothermic nature of ADN decomposition lends credibility to existence of PLEFs, following the earlier discussion on the effect of surface heat release on the gas phase flame structure.

Certain peculiarities need to be overcome while considering the possibility of PLEFs on ADN particles in the matrix. At 1000 psi, the thermal wave in the solid is thin, and ADN particles may melt closer to the "top" of the surface as opposed to melting "beneath" the surface at lower pressures. Therefore, at high pressures, patches of ADN liquid may migrate from one place to another in the surface layer, gasify, weaken the binder layers around, and jet out into the gas phase. The task of identifying the particle or set of particles to which a PLEF is attached becomes difficult under such circumstances. The PLEFs would also have to be pictured as fluctuating along the direction of overall surface regression depending on the local pressure build-up due to accumulation of gasifying ADN underneath the solid binder, and wandering laterally along with the pools of migrating liquid ADN in the surface layer.

The SEM pictures do not offer any evidence about the possibility of PLEF attachment on ADN particles. This may simply be because of the fact that ADN melts before vaporization, and possibly migrates and collects together, as observed on the hot stage microscope. The perplexing nature of the SEM pictures at best do not provide any evidence against the simplistic picture constructed from the hot stage microscopic observations; they do not provide any additional insight into the processes taking place under real combustion conditions.

FORMULATIONS BASED ON HNIW

The available results for HNIW-based formulations allow consideration of the combustion zone details related to areas in the propellant burning surface covered by a matrix of fine HNIW particles and binder. The possibility of 10 μm HNIW particles deflagrating in the matrix is slim considering the heat loss to adjacent binder layers. It is not clear if the gas phase flame structure above the matrix lamina is a canopy or a PLEF array, but considering that HNIW undergoes rapid exothermic decomposition at ~270 °C, and possibly reaction with the binder, supports the possibility of PLEFs at least at high pressures (1000 psi). In Fig. 2, the matrix surface is relatively flat (devoid of any oxidizer particles), and filled with cuts and pores indicative of subsurface decomposition of HNIW particles.

The heat generated in the matrix appears to control the burning of the HNIW/PBAN sandwiches. This is implied by the following observations: (i) The sandwich and matrix burning rates hardly differ (Fig. 10); and (ii) The region in the AP laminae in the immediate vicinity of the lamina interface are unprotruded and have a dry surface quality (Figs. 2 and 3) indicating little or no lateral heat transfer from the AP laminae to the matrix lamina [10,11]. (iii) While the HNIW/PBAN matrix burning rate is not catalyzed by Pyrocat, neither is the sandwich burning rate (Fig. 11b). This is to say that, even if the LLEFs were catalyzed by Pyrocat [12], the increased heat release from them is still inadequate to surpass the heat ordinarily generated in the matrix and gain control of the sandwich burning rate.

One needs to examine the location of heat generation within the matrix. The following speculation is offered. As opposed to the negligible effect of LLEFs on the HNIW/PBAN matrix (discussed above), the HMX/PBAN matrix burning is extremely sensitive to the LLEFs (Fig. 10). This implies that the heat generated by the HMX/PBAN matrix is certainly not sufficient to control the sandwich burning rate. The gas phase

decomposition products of HNIW and HMX are somewhat similar [4]. One may suspect that their matrices with PBAN would support similar gas phase flame structures, if one disregarded the disparity in their thermochemistry. If the heat release in the gas phase flame above the matrix lamina (canopy flame or PLEFs) is significant, then matrices with both the oxidizers would be equally insensitive to the presence of LLEFs; which is not the case. The difference between HMX and HNIW arises from the fact that HNIW decomposes significantly more exothermally than does HMX [5]. It thus appears that the exothermic decomposition of HNIW (and possibly reaction with the binder) is the main factor that determines the burning rate in HNIW-based matrix formulations. If condensed phase reactions between HNIW and the binder are indeed important (in terms of exothermicity), then the burning rate may be directly dependent on the size of fine HNIW particles.

CONCLUSIONS

The scenario with new energetic ingredients is quite different than with AP. ADN deflagrates considerably faster than AP. However, the leading edges of the O/F diffusion flames still control the burning rate in the case of pure binder sandwiches with ADN laminae, as in the case of sandwiches with AP laminae. But the effect of the O/F flamelets is so intense as to overwhelm any additional heat release due to the addition of fine ADN particles in the propellant. For this reason, the dependence of the burning rate on propellant formulation variables may be slightly-to-considerably different for ADN than for AP.

Rigorous modeling of composite propellant combustion with ADN is made further difficult by the fact that ADN melts and decomposes at temperatures significantly lower than the characteristic temperatures of typical hydrocarbon binders. The exothermicity of ADN decomposition also makes conditions conducive for attachment of LEFs on sites where the fine particles melt, migrate, accumulate and vaporize in the surface layer. Depending on whether the binder can melt or not, such accumulates may result in unsteady micro jets of oxidizer species in the gas phase, or gain "mobility" and vaporize at locations different from their initial locations in the precombustion geometry.

The strong exothermic decomposition of fine HNIW particles in the surface layer of the propellant appears to be the controlling factor for the burning rate of HNIW sandwiches. Again, since the decomposition temperature of HNIW is significantly lower than that of typical hydrocarbon binders, HNIW may decompose "beneath" the binder surface, if the binder does not melt substantially.

Burning rates of formulations based on both of these oxidizers seem to be insensitive to inclusion of conventional burning rate catalysts such as ferric oxide.

The crucial role of complicated (microscopic, multidimensional, multiphase) physical and chemical processes taking place in the thin surface layer of propellants with ADN or HNIW indicates a significant departure from the scenario with AP propellants where the burning is predominantly controlled by details of the gas phase flame complex.

REFERENCES

1. Brill, T. B., Brush, P. J., and Patil, D. G., "Thermal Decomposition of Energetic Materials 58. Chemistry of Ammonium Nitrate and Ammonium Dinitramide Near the Burning Surface Temperature," Combustion and Flame, Vol. 92, 1993, pp. 178-186.

2. Parr, T., and Hanson-Parr, D., "ADN Diffusion Flame Structure at Elevated Pressure," Proceedings of the 30th JANNAF Combustion Meeting, October 1993.

3. Pak, Z. P., "Some Ways to Higher Environmental Safety of Solid Rocket Propellant Application," AIAA Paper 93-1755, 29th AIAA/SAE/ASME/ASEE Joint Propulsion Meeting, June 28-30, 1993.

4. Pesce-Rodriguez, R. A., Fifer, R. A., McNesby, K. L., Morris, J. B., Schroeder, M. A., Miser, C. S., and Liebman, S. A., "Thermal Decomposition of HNIW and HNIW - Based Formulations," Technical Report BRL-TR-3402, Ballistic Research Laboratory, Aberdeen Proving Ground, MD, September 1992.

5. Patil, D. G., and Brill, T. B., "Thermal Decomposition of Energetic Materials 53. Kinetics and Mechanism of Thermolysis of Hexanitrohexaazaisowurtzitane," Combustion and Flame, Vol. 87, 1991, pp. 145-151.

6. Patil, D. G., and Brill, T. B., "Thermal Decomposition of Energetic Materials 59. Characterization of the Residue of Hexanitrohexaazaisowurtzitane," Combustion and Flame, Vol. 92, March 1993, pp. 456-458.

7. Lee, S. -T., "Multidimensional Effects in Composite Propellant Combustion," Ph.D. Thesis, Georgia Institute of Technology, Atlanta, GA, May 1991.

8. Price, E. W., Sigman, R. K., Chakravarthy, S. R., and Paulsen, P. D., "Hot Stage Microscope Studies of Decomposition of Propellant Ingredients," Proceedings of the 30th JANNAF Combustion Meeting, October 1993.

9. Price, E. W., Chakravarthy, S. R., Zachary, E. K., and Sigman, R. K., "Ingredient Response and Interaction during Heating on a Hot Stage Microscope," Proceedings of the 31st JANNAF Combustion Meeting, San Jose, CA, October 1994.

10. Price, E. W., "Effect of Multidimensional Flamelets in Composite Propellant Combustion," Journal of Propulsion and Power, Vol. 11, No. 4, July-August 1995, pp. 717-728.

11. Lee, S. -T., Price, E. W., and Sigman, R. K., "Effect of Multidimensional Flamelets in Composite Propellant Combustion," Journal of Propulsion and Power, Vol. 10, No. 6, November-December 1994, pp. 761-768.

12. Markou, C. P, Effect of Different Binders and Additives on Sandwich Burning," Ph.D. Thesis, Georgia Institute of Technology, Atlanta, GA, May 1988.

Table 1

No.	Ingredient	Melting Temp. [°C]	Decomposition Temp. [°C]	Residue	Remarks
1.	AP	–	> 400[a]		decomposes rapidly
2.	ADN	90	165		
3.	HNIW	–	270	black solid	decomposes abruptly
4.	HMX	255	290		
5.	PBAN	480	500		
6.	HTPB	330-370	500		melts slowly
7.	Aluminum	673	2493		
8.	Ferric oxide	–	not < 1000		turns dark above 200

[a]Does not melt at low heating rates.

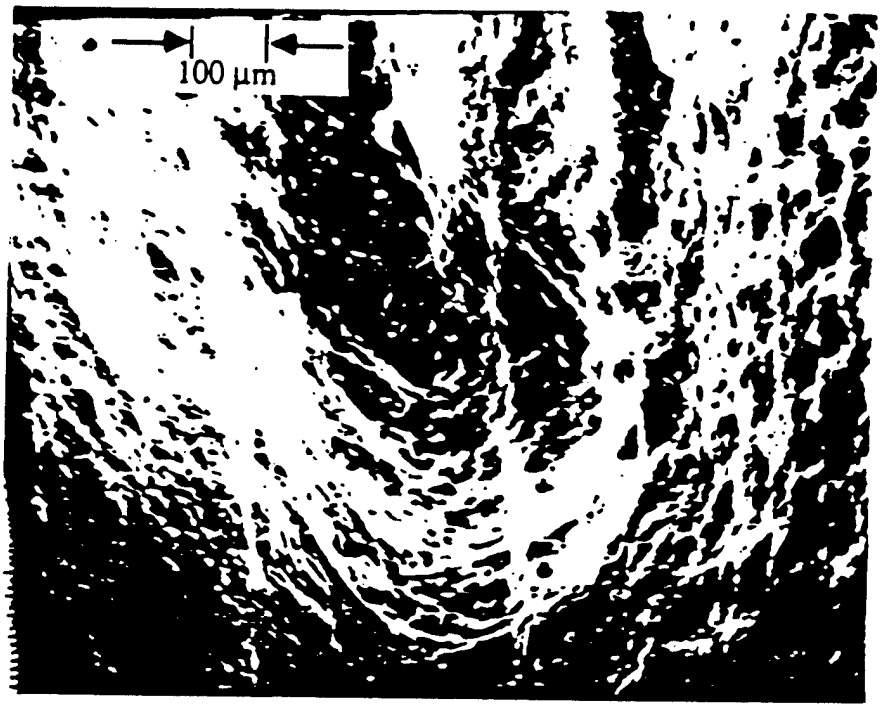

(a)

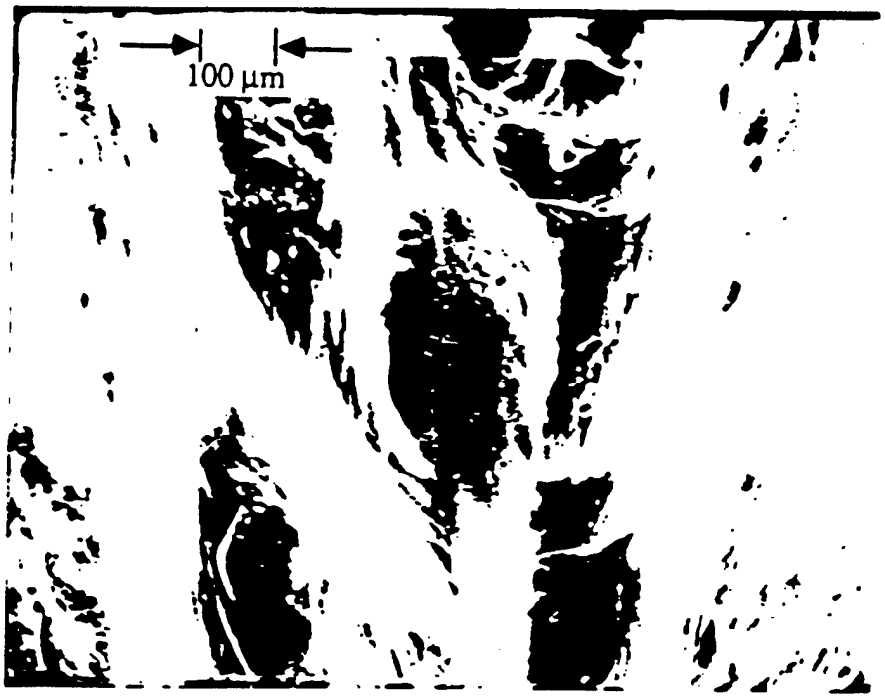

(b)

Fig. 1 Surface features of sandwiches with ADN (40 µm)/ binder = 7/3 matrix lamina (thickness ~375-400 µm). (a) PBAN, (b) HTPB(IPDI).

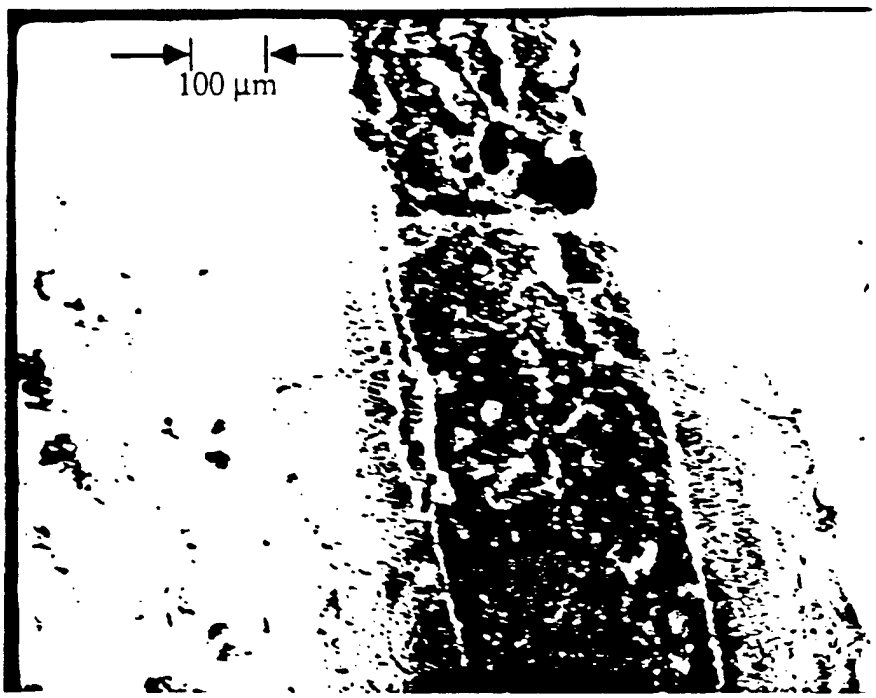

Fig. 2 Surface features of a sandwich with HNIW (10 μm)/ PBAN = 7/3 matrix lamina (thickness ~375-400 μm) quenched at 500 psi.

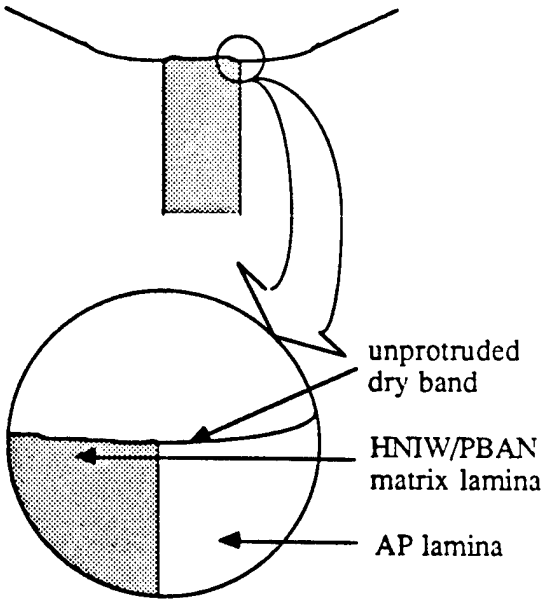

Fig. 3 Surface profile of a sandwich with HNIW (10 μm)/PBAN = 7/3 matrix lamina (thickness ~375-400 μm) at 500 psi.

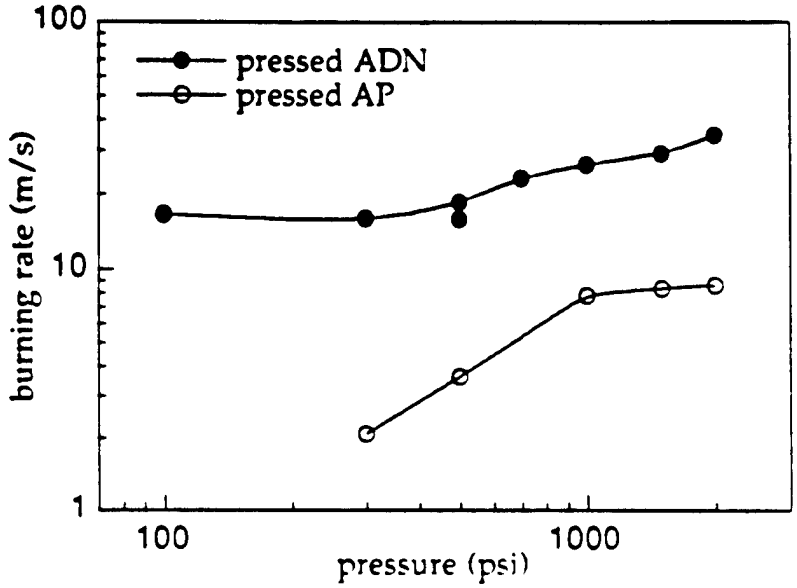

Fig. 4 Pressure dependence of self-deflagration rate of pressed ADN. Rates for pressed AP are shown for comparison

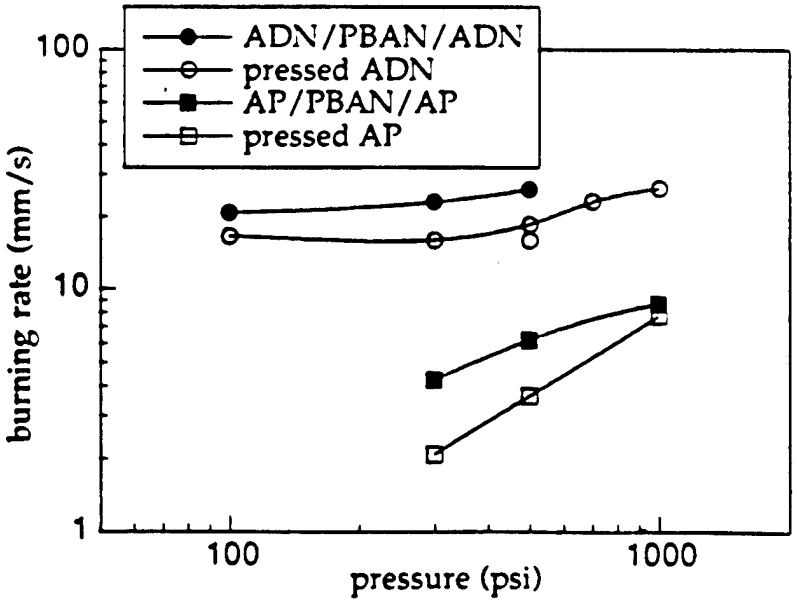

Fig. 5 Pressure dependence of burning rate of ADN/PBAN/ADN sandwiches with binder lamina thickness ~75-100 μm. The burning rates for similar AP/PBAN/AP sandwiches, pressed ADN and AP are shown for comparison.

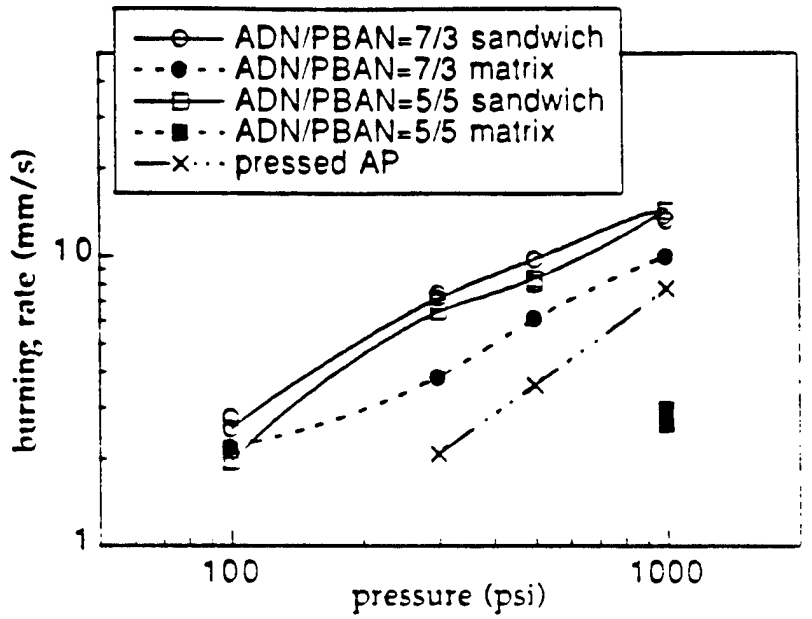

(a)

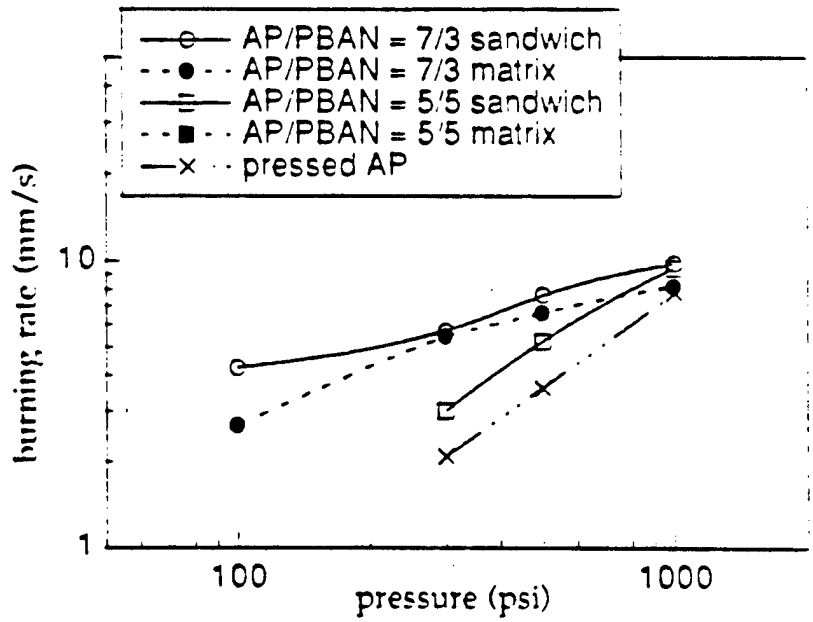

(b)

Fig. 6 Pressure dependence of burning rate of sandwiches with oxidizer/PBAN = 7/3 and 5/5 matrix laminae of thickness ~375-400 μm, for two oxidizers: (a) ADN (40 μm), (b) AP (33.5 μm) [7]. The matrix lamina was sandwiched by AP laminae.

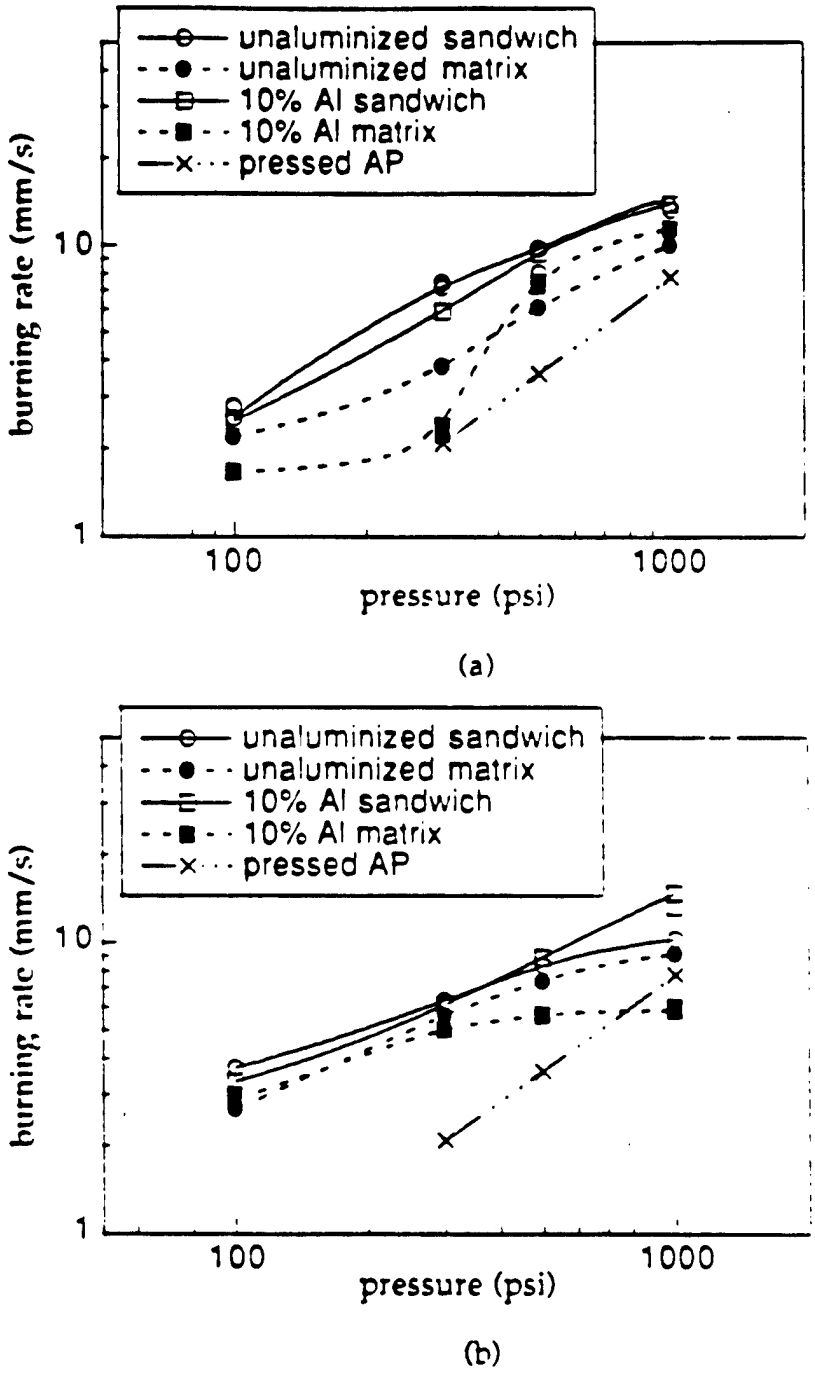

Fig. 7 Pressure dependence of burning rate of sandwiches with an oxidizer/PBAN = 7/3, 10% Al (15 μm) matrix lamina of thickness ~375-400 μm for two oxidizers: (a) ADN (40 μm), (b) AP (10 μm). Corresponding curves for unaluminized samples are included for comparison. The matrix lamina was sandwiched by AP laminae.

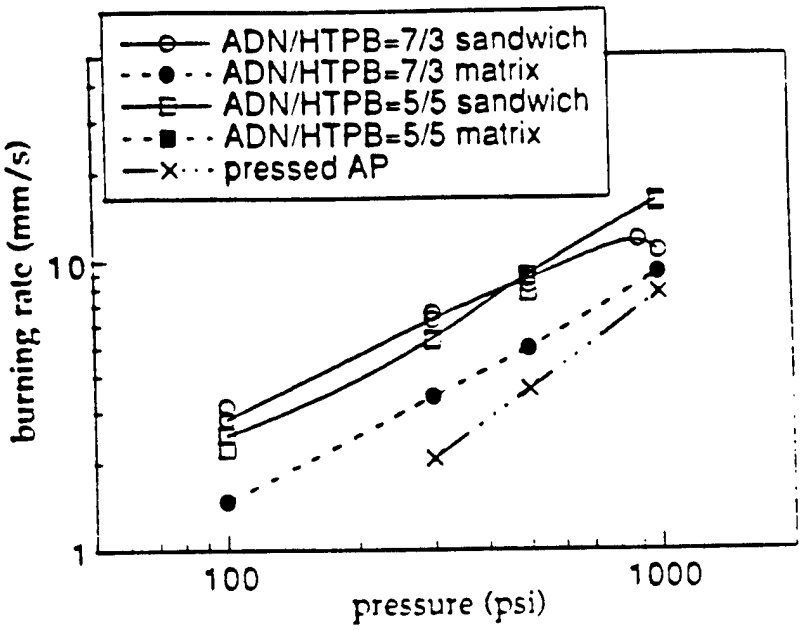

Fig. 8 Pressure dependence of burning rate of sandwiches with ADN (40 μm)/HTPB = 7/3 and 5/5 matrix laminae of thickness ~375-400 μm. The matrix lamina was sandwiched by AP laminae.

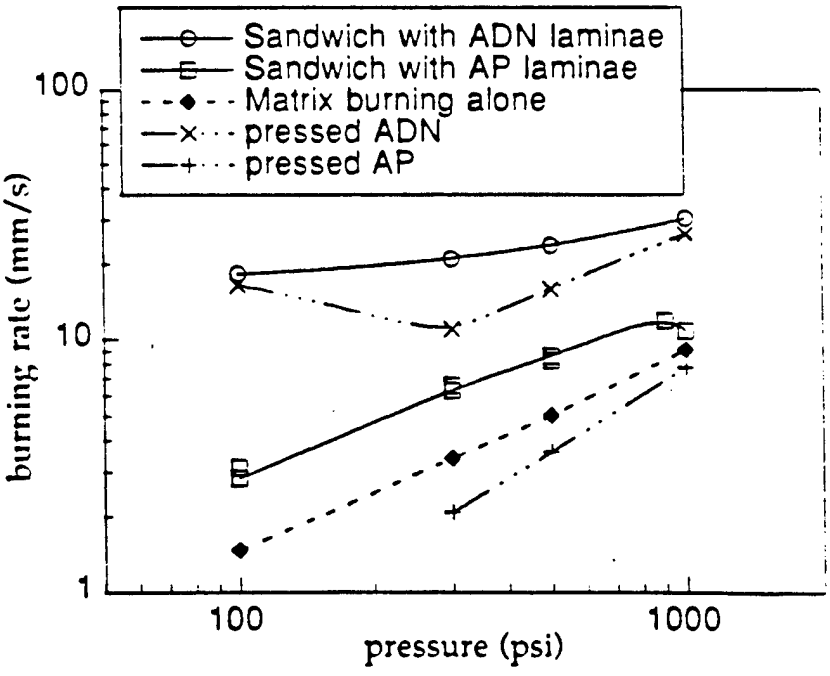

Fig. 9 Pressure dependence of burning rate of sandwiches with ADN (40 μm)/HTPB = 7/3 matrix lamina of thickness ~375-400 μm. The matrix lamina was sandwiched by ADN laminae.

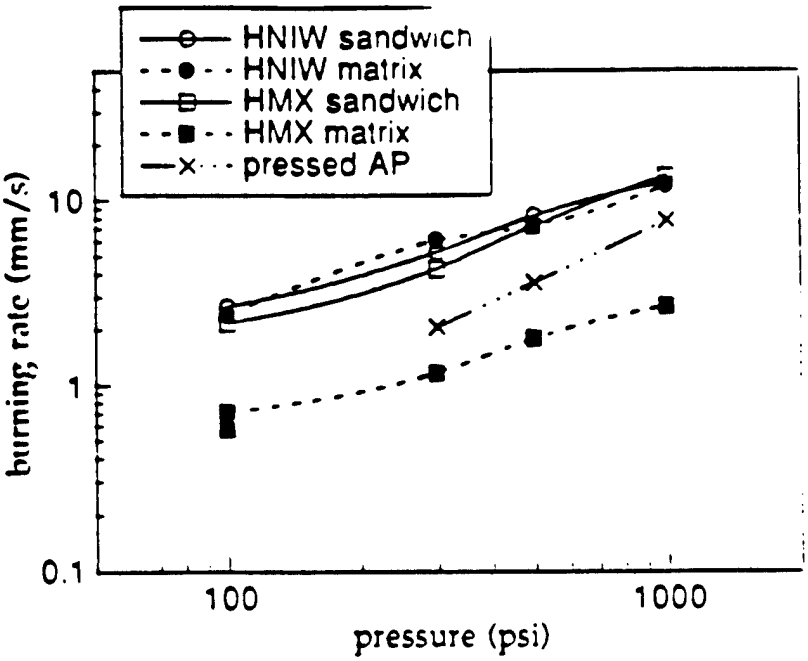

Fig. 10 Pressure dependence of burning rate of sandwiches with oxidizer (10 μm)/PBAN = 7/3 matrix lamina of thickness ~375-400 μm, for two oxidizers. HNIW and HMX. The matrix lamina was sandwiched by AP laminae.

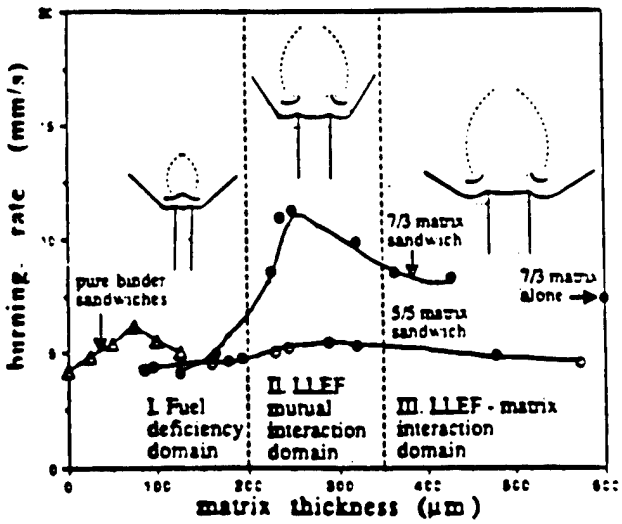

Fig. 12 Typical dependence of sandwich burning behavior on matrix lamina thickness for pure PBAN binder and AP (10 μm)/PBAN = 7/3 matrix. The burning rate of matrix alone is shown on the right ordinate. Circles in the flame structures indicate the zone of influence of the LLEFs.

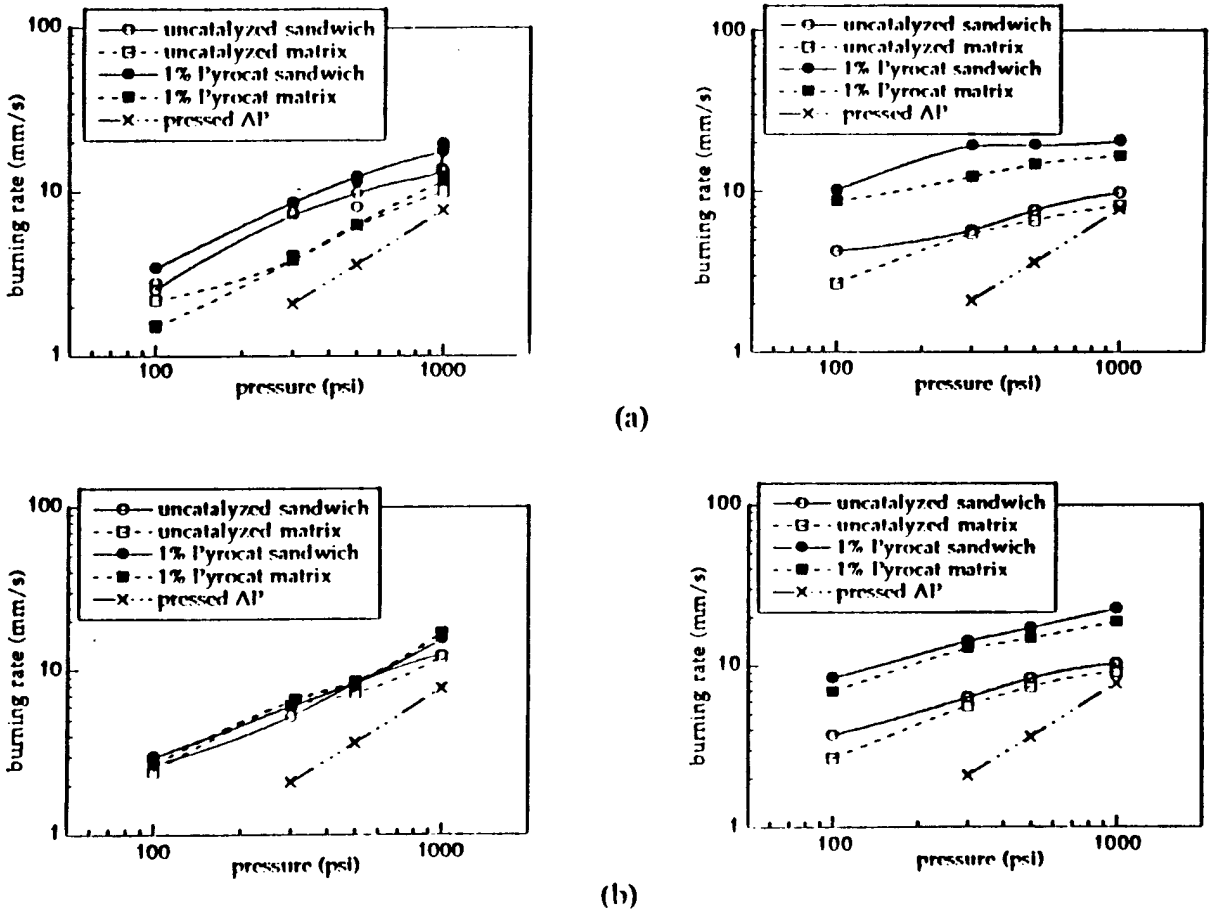

Fig. 11 Comparison of effect of ferric oxide on sandwiches with matrix lamina containing different oxidizers versus AP: (a) ADN (40 μm) vs. AP (33.5 μm), (b) HNIW (10 μm) vs. AP (10 μm). The sandwiches consisted of AP laminae and a matrix lamina of oxidizer/PBAN = 7/3 (with 1% Pyrocat), of lamina thickness ~375-400 μm.

Appendix H

Leading EdgeFlame Detachment:Effect on Pressure Coupled Combustion Response

Journal of Propulsion and Power

Volume 14, Number 2,March-April 1998, pp. 160-165

JOURNAL OF PROPULSION AND POWER
Vol. 14, No. 2, March–April 1998

Leading-Edge Flame Detachment: Effect on Pressure-Coupled Combustion Response

C. A. Beiter* and E. W. Price†
Georgia Institute of Technology, Atlanta, Georgia 30332

An experiment was conducted to establish the critical role of a detailed aspect of the flamelet structure in composite propellants in determining the overall combustion response to pressure oscillations during combustor instability.

Nomenclature

a_b = velocity of sound of gases in T-burner
g_c = units conversion factor
L = length of interior cavity of T-burner
R_p = pressure-coupled response function
r = burning rate
S_b = cross-sectional area of cavity of T-burner
S_c = burning surface area of propellant sample
α_c = combustion amplification
α_d = burner damping during burning
α_1 = exponential growth rate during burning, decay rate in pulse test
α_2 = decay rate after burnout
$\alpha_2(f_1)$ = decay rate corrected to frequency during burning
ρ_s = density of solid propellant

Introduction

THE pressure-coupled response of combustion rate to imposed pressure disturbances is the primary cause of combustion instability in solid rocket motors. This response has been difficult to measure reliably and to model analytically. There is not yet an analytical model that describes the physical phenomenon realistically for heterogeneous propellants. This paper concerns an experiment designed to illustrate the importance of a basic aspect of the flame response that is absent or superficially represented in current models, but that is expected to be important.

To describe this aspect of flame response, it is necessary to describe certain microscopic aspects of the flame complex (described in some detail in Refs. 1–3). The burning surface of a typical heterogeneous propellant consists of areas of burning oxidizer, ammonium perchlorate (AP), interposed in a connected web of hydrocarbon polymer binder that holds the matrix together and supplies the fuel for the oxidizer/fuel (O/F) diffusion flamelets around the AP particles. Those flamelets (Fig. 1) provide the primary source of heat for the pyrolysis of the fuel. The character of a diffusion flamelet is illustrated in Fig. 2. As the nominally parallel flows of oxidizer and binder vapors move outward from the surface, a diffusion layer develops, with a progressively increased O/F mixture as a function of distance outward. Interior to this mixing fan is a stoichiometric surface, which is typically thought of as the site of the diffusion flame. The onset of this flame is located somewhere far enough from the surface for a balance to be maintained between the local heat release and the heat lost to the surface and oncoming flow. At that point, e.g., 50 μm or so from the surface at 3.5 MPa, there is enough flammable mixture to result in an intense sustainable heat release, referred to here as the leading-edge flame (LEF) for the outer diffusion flame. Such a flamelet has been referred to variously as a flame root,[4] a phalanx frame,[5] and a primary flame.[6] The actual location and scope of the LEF are determined by the kinetics of the O/F reaction and by the diffusion process that prepares the mixture upstream of the LEF. As such, the energy of the LEF and its proximity to the surface are dependent on pressure. Further, the heat release may be relatively large because the LEF burns a substantial amount of premixed oxidizer and fuel close to the surface. Thus, the LEF can be a relatively large contributor to the local surface heating along the O/F contact line in the oxidizer–binder surface. Because of its proximity to the heterogeneous surface, the characterization of the individual LEF must be regarded as a three-dimensional process, localized above the outer boundary of the oxidizer particle surface with three-dimensional heat return to the surface. It is important to note that the close three-dimensional coupling between the LEF and the O/F contact line makes it impractical to represent the dynamic response of the combustion by any conventional one-dimensional, surface-averaged model. Put more generally, whereas the combustion response that is important to the combustor instability is a surface-averaged response, this response is determined primarily by the responses of a myriad of microscopically nonsteady, three-dimensional localized processes in the combustion layer.

The present research is based on the postulate that when the LEF retreats from the surface with decreasing pressure it will arrive at the stoichiometric tip (Fig. 3) at some specific pressure (dependent on the size of the AP surface); and upon a further decrease in pressure, the LEF will be quenched, and the O/F flame for that particle will establish itself at some more remote location typical of a fuel-rich premixed flame. In practice, this discontinuous jump in the flame cannot be observed directly because 1) in a practical (rocket-motor-like) environment, the event is too small to be spatially resolved experimentally; and 2) the details of the event depend on the state of neighboring flamelets from AP surfaces of different sizes (from either different sizes of AP particles or different stages in the burning of like particles).

If one could make a propellant consisting of equal-size parallel rods of oxidizer, and burn it endwise with progressively lower pressure, there would presumably be a collective transition from LEF-dominated burning to premixed-flame burning when pressure reached the LEF detachment level. At that point, an observable drop in burning rate would occur. When particulate oxidizer is used, even with uniform particle size, the size of exposed oxidizer surfaces depends on the burning

Received July 24, 1997; revision received Sept. 25, 1997; accepted for publication Oct. 6, 1997.

*Graduate Research Assistant, School of Aerospace Engineering; currently Propellant Analyst, U.S. Army Foreign Science and Technology Center, Attn.: IAFSTC-RMT, 220 Seventh Street, Northeast, Charlottesville, VA 22901-5396. Member AIAA.

†Regent's Professor Emeritus, School of Aerospace Engineering. Fellow AIAA.

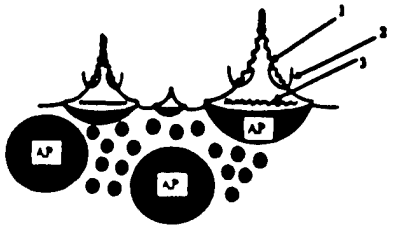

Fig. 1 Microscopic features of the combustion zone of an AP/hydrocarbon binder propellant (typical of 6–8 MPa). 1, diffusion-limited O/F flame; 2, O/F LEF, holds diffusion flame; and 3, AP self-deflagration flame.

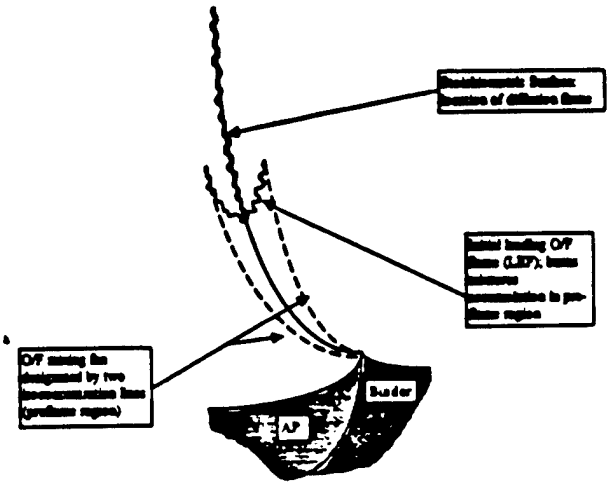

Fig. 2 O/F mixing fan and diffusion flamelets.

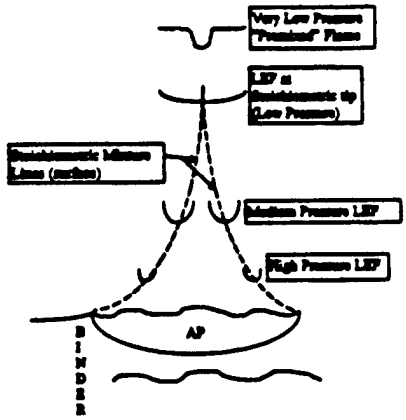

Fig. 3 Outward displacement of the LEF at decreasing pressure, and the singularity when the LEF reaches the stoichiometric tip.

stage of the particles. Thus, the burning rate transition associated with LEF detachment would not be abrupt, as in the case of a rod propellant, but it might be manifested over a narrower pressure range than with a propellant with a wide blend of oxidizer particle sizes. This idea was tested as a way of verifying the presence of an LEF-detachment effect on burning rate.[2] The result (Fig. 4) shows a characteristic, particle-size-dependent pressure range in which the burning rate drops off rapidly with decreasing pressure, supporting the postulate of the LEF-detachment effect on burning rate. In Ref. 2 and Fig. 4, the propellant that was used had a bimodal oxidizer particle size distribution to obtain the high O/F ratio typical of commercial propellants. Such a bimodal propellant burns with a surface consisting of scattered large (400 μm) particles and a surrounding fuel-rich matrix of fine AP particles and hydrocarbon binder. The fine component of AP (in the present study) was chosen to have a narrow size distribution. The LEF-detachment effect involves the fine-particle matrix (at intended test conditions).

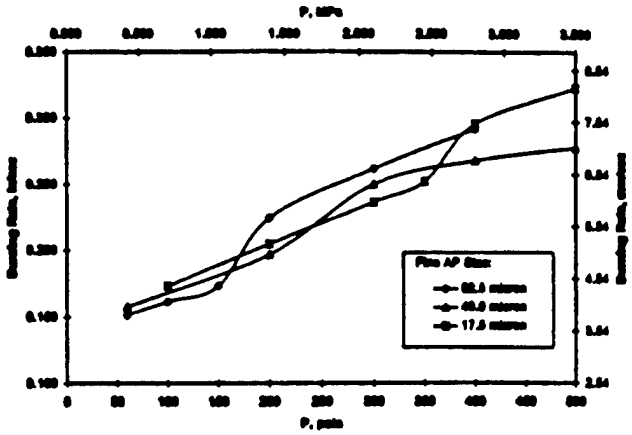

Fig. 4 Burning rate curves of three bimodal propellants,[2] showing the steep-slope regimes corresponding to LEFs at transition condition (AP–polybutadiene acrylonitrile propellant, 87.5% AP, 8:2 ratio of 400 μm, and indicated fine AP).

This study is a test of a postulate that, at the LEF detachment (transition pressure ranges), the LEF will periodically detach and reattach if the pressure oscillates, with the reasonable projection that the dynamic combustion–response function will exhibit a maximum at the corresponding transition pressure interval. This effect on pressure dependence of the response function was tested by a series of T-burner tests on a bimodal AP propellant similar to that used in Ref. 2 for Fig. 4.[3,7,8]

Experiment

Strategy

The initial plan was to prepare three propellants similar to those that led to Fig. 4 and use them to run T-burner tests over the pressure range of those earlier burning rate tests,[3] to determine whether a maximum in the response function (Fig. 5) occurred in the pressure intervals in which the rapid rises in mean burning rate were manifested in Fig. 4. Such a result would be consistent with the interpretation that the pressure-coupled combustion response is sensitive to the condition of LEF detachment. (In Fig. 5 the values of R_p were chosen for convenience; the argument requires only that a maximum occur at the indicated pressures.)

In choosing T-burner tests a choice had to be made as to the frequency of the pressure oscillation, i.e., length of the T-burner. It was presumed that the event of LEF detachment and reattachment during a cycle of pressure oscillation involved no slow processes, in which case the effect of LEF detachment–reattachment on the response would not be strongly dependent on frequency. However, this point was tested by choosing three frequencies, 350, 500, and 800 Hz, that would be near that for the maximum response for typical AP propellants of this burning rate.

Practical considerations caused some deviations in the preceding strategy:

1) Cost limited the number of tests, so that testing of the full range of propellants (three) at all three frequencies proposed was not done (Table 1).

2) Propellant processing problems caused a lower coarse-to-fine AP ratio value than that used for the tests leading to Fig. 4.

3) The initial spread of particle size distribution for the fine AP was larger than intended, sometimes resulting in indecisive T-burner test results, i.e., maxima in the measured R_p vs p curves were not as clearly manifested above the scatter in the T-burner test results as implied in Fig. 5. One extra mix of propellant (mix 1b) was made with a relatively more narrow

Table 1 Propellant information

Ingredient	Percent by mass (volume)
Ammonium perchlorate	87.5 (79.4)
Coarse	61.25 (55.58)
Fine	26.25 (23.82)
Binder	12.5 (20.6)
Prepolymer, polybutadiene acrylonitrile acrylic acid (PBAN) (HB polymer)	8.02
Curative, epoxy curing agent (ECA)	2.61
Plastisizer, dioctyl adipate (DOA)	1.88

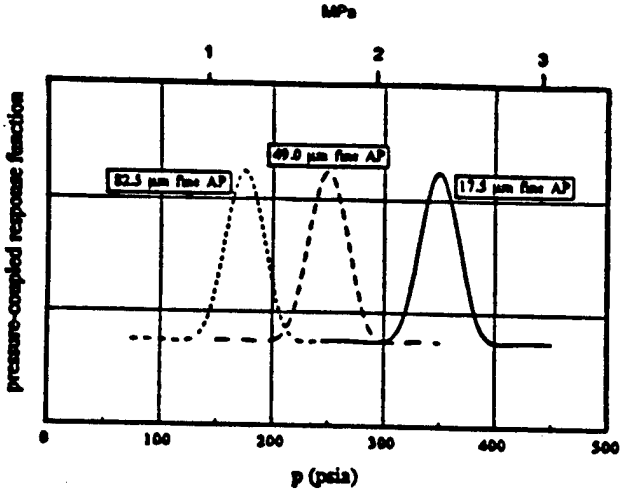

Fig. 5 Expected pressure dependence of the oscillatory combustion response to pressure oscillations for three bimodal propellants (peaks are expected in the pressure ranges of LEF transitions on the fine AP).

size distribution of the fine AP when tests on the 1a mix gave some ambiguous test results.

4) For this family of propellants the T-burners were marginally unstable. Measurements of combustion response were made from spontaneous oscillations when possible; however, there were conditions where spontaneous oscillations did not occur and repeat tests were run with pulsed oscillations.[7,8]

Propellant

Following the lead of Ref. 2 the propellant formulation was chosen to be as shown in Table 1. All mixes used coarse (400 μm) AP with fine AP in a 70:30 ratio. Mix 1a used 17.5-μm-fine AP with a size range of 5.7–53.7 μm (see Ref. 3 for quantitative size distribution). Mix 1b used 19.1-μm-fine AP with a size range of 6.1–36.9 μm. Mix 2 used 43.5-μm-fine AP with a size range of 10–70.1 μm. Mix 3 used 81-μm-fine AP with a size range of 36–120 μm. The propellants were mixed in a 1-gal vacuum mixer and vacuum cast in tubes (somewhat larger in diameter than that of the o.d. for test samples), which were machined to disks of the desired thickness and diameter.[8]

Burning rate vs pressure was determined (Fig. 6) for each mix by video photography of strands burning in a nitrogen-flushed window bomb. It was noted that the r vs p curves did not exhibit the high-slope regions that were identified previously with LEF attachment (Fig. 4). Also, the burning rates were much lower than those in Ref. 2. These large differences from the results with analogous propellants in Ref. 2 were not expected on the basis of the differences in the AP coarse-to-fine ratios (7:3 here, 8:2 in Ref. 2). However, the constraints on the program did not permit further experimentation with the propellant formulation. It was anticipated that the detachment and reattachment of LEFs would be more organized with

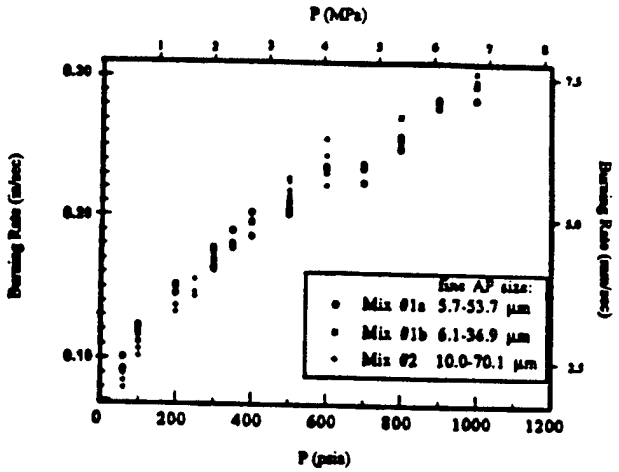

Fig. 6 Burning rate vs pressure for mixes used in this study (for details see Ref. 3).

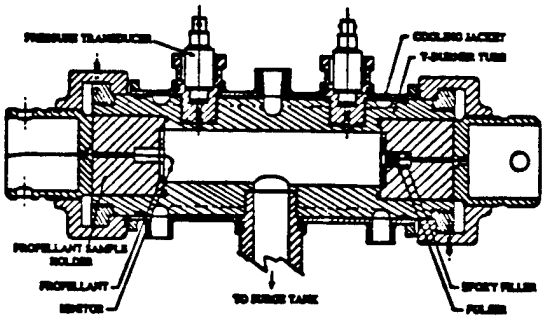

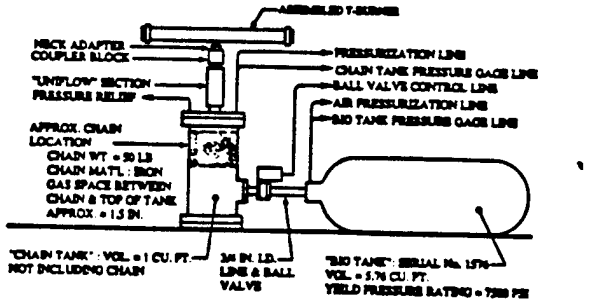

Fig. 7 T-burner test apparatus used in this study.

pressure oscillations than with steady pressure. On this basis, it was judged that the T-burner test program would show the enhanced oscillatory combustion response indicative of coupled LEF response, and so the proposed tests were carried out.

T-Burner

The tests (constant mean pressure) were run in the standard apparatus at the U.S. Naval Air Weapons Center, described in Ref. 8 and in Fig. 7. In this facility the exponential growth rate α_1 of oscillations (or the decay rate of pulses) during burning is computed from the digitized output of the pressure transducer, using a computer code developed at the U.S. Naval Air Weapons Center for this determination. The decay rate α_2 of oscillations (spontaneous or pulsed) after propellant burnout is also measured. The cause of α_1 is the concurrent contribution of α_r and α_d during burning; α_2 is an indication of the damping present during pulse 1, so that the amplification from com-

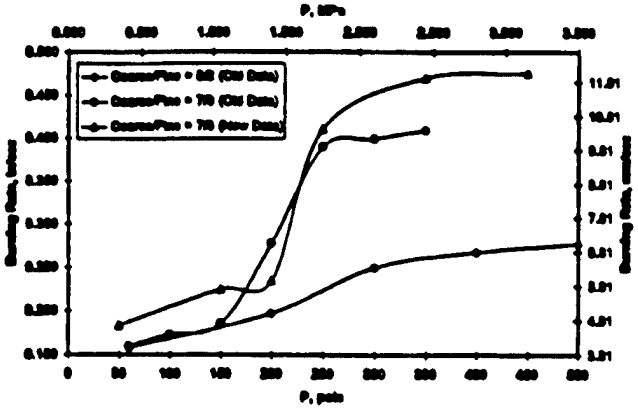

Fig. 8 Burning rates, not previously reported, of propellants analogous to mix 1b, but showing the LEF transition effect reported in Ref. 2 and Fig. 4.

bustion is $\alpha_1 + \alpha_2$. However, a correction to α_2 is usually made because the observed frequency during α_2 is usually lower than during α_1.[8] A dependence of α_2 on frequency is determined from accumulated tests, and an adjusted value of α_2 is used in each test to give α_d corresponding to the measured frequency during α_1

$$\alpha_r = \alpha_1 - \alpha_2(f_1) = \alpha_1 - \alpha_d$$

The in-phase (real) part of the pressure-coupled combustion response is then computed from

$$R_p = \frac{\beta L g_c \alpha_r}{2A\rho_p \bar{a}_b^2 (S_b/S_c)}$$

This expression arises from the one-dimensional stability analysis for the first axial mode of the T-burner.[8,9]

As noted in the preceding text, some tests exhibited spontaneous oscillatory behavior. This is indicative of high α_r and

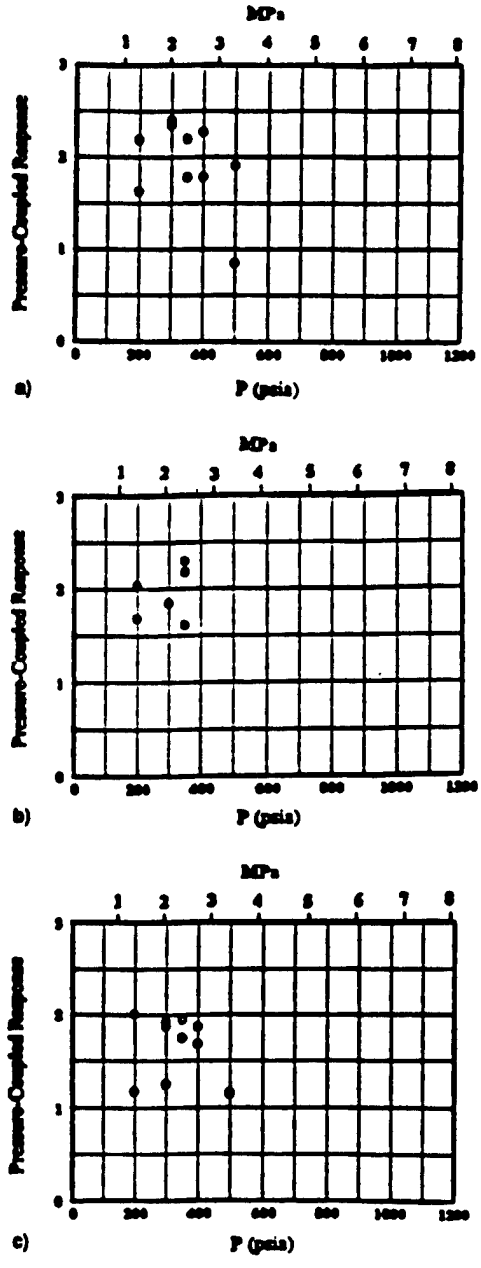

Fig. 9 Response function vs pressure for mix 1a at a) 350, b) 500, and c) 800 Hz. ○ = spontaneous, ● = nonspontaneous.

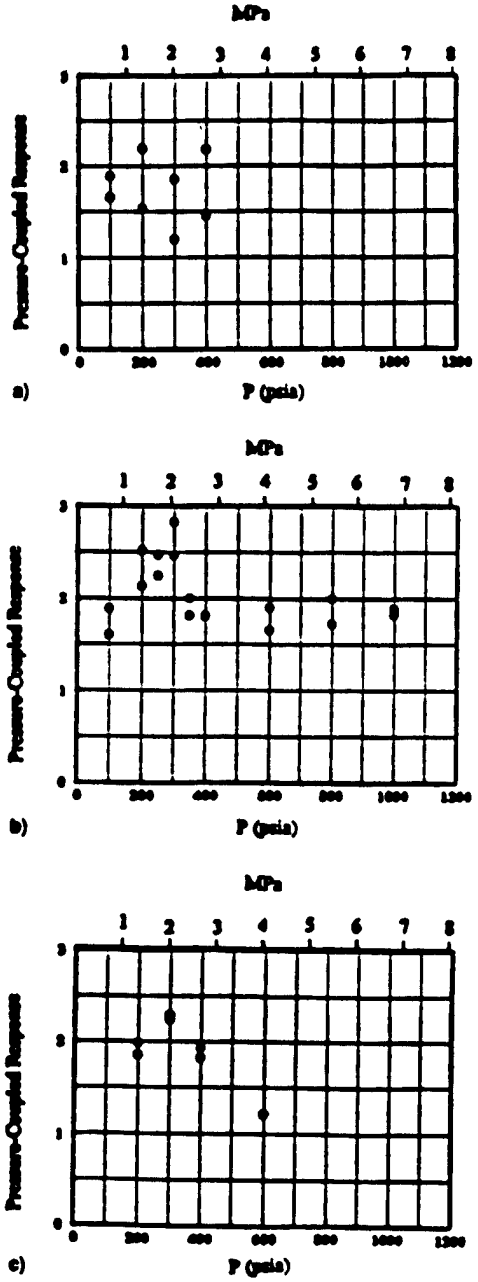

Fig. 10 Response function vs pressure for mix 1b at a) 350, b) 500, and c) 800 Hz. ○ = spontaneous.

R_p under those test conditions, and it generally occurred under test conditions that were expected to (and did) yield high R_p, i.e., propellant mix 1b, and tests with other mixes in the pressure range of postulated LEF detachment instability.

Under some conditions the burners did not oscillate spontaneously, and α_1 and α_2 were determined by the pulsed method.[7,8] This method was required under two different test conditions:

Condition 1: Conduct some tests at pressures above and below the expected LEF transition range.

Condition 2: Repeat tests in a second year on mix 1a at 500 Hz and mix 2 at 800 Hz, i.e., with aged propellants.

The computed values of R_p were low in all of the pulse tests, consistent with the fact that spontaneous oscillations did not occur. Condition 1 is consistent with expected low values of R_p. Condition 2 indicates that the aged propellants behaved differently than they did in first-year tests. (The results of the test on the aged propellants were so different that they were excluded, but are available in Ref. 3 for the record. Discussion with U.S. Naval Air Warfare Center personnel indicated that divergent performance of aged propellants is not unprecedented, but generally unexplained).

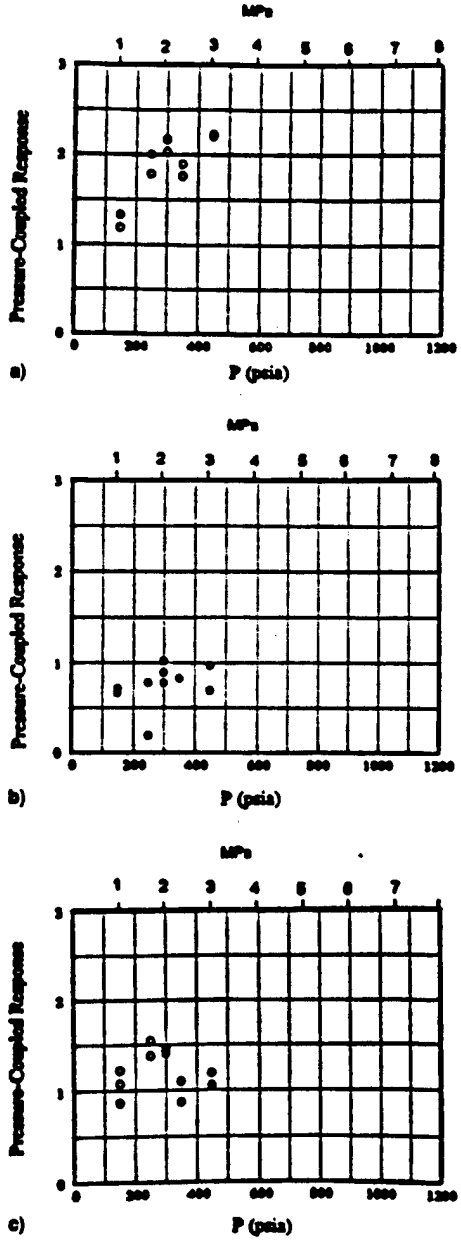

Fig. 11 Response function vs pressure for mix 2 at a) 350, b) 500, and c) 800 Hz. ○ = spontaneous, ● = nonspontaneous.

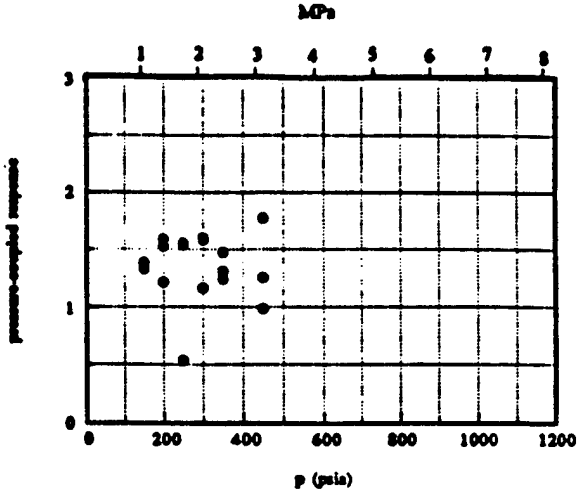

Fig. 12 Response function vs pressure for mix 3 at 500 Hz. ● = nonspontaneous.

Summary of Results

As noted earlier the burning rate vs pressure curves for the present propellants (Fig. 6) did not show the transitions that were reported in Ref. 2 and Fig. 4. This difference was initially attributed to the difference in ratio of coarse-to-fine AP in the propellants. However, a later review of the work leading to Ref. 2 revealed that a 7:3 formulation had been tested then (Fig. 8). The tests of that earlier investigation have recently been repeated and the results are similar to the early study and to Fig. 2 (the new results for the 7:3 formulation are included in Fig. 8). The low rate and absence of transitions in the $r(p)$ curves for the mixes used in the T-burner tests remain unexplained.

The results of the T-burner tests are shown in Figs. 9–12 and are described in the following text.

Mix 1a: Tests were spontaneously unstable in the pressure range expected for LEF transition. Maxima appear to be indicated, but data scatter is bad and measurements at higher and lower pressure are minimal.

Mix 1b: All tests were spontaneously unstable. At 500 and 800 Hz, R_p indicates a clear peak (~2.4 compared to about 1.7 outside an LEF transition pressure range centered on 2.3 MPa. At 350 Hz, the data were too scattered to identify a maximum.

Mix 2: At 350 Hz, all tests were spontaneously unstable and a maximum of about 2.2 is indicated at 2.3–2.8 MPa. Measurements on the high-pressure side of the maximum are lacking. At 500 Hz, all tests required pulsing, resulting in low values of R_p (around 0.8) with no sign of a maximum. At 800 Hz a modest peak in R_p (1.5) is indicated at 1.9 MPa.

Mix 3: This mix was tested only at 500 Hz. All pressures required pulsing, giving an R_p around 1.4, with large data scatter and no systematic pressure dependence.

Taken collectively, the T-burner results show relatively high values of R_p in the postulated LEF transition range of pressure, and lower R_p at higher and lower pressure. Tests under some conditions gave unambiguous evidence of R_p maxima in the LEF transition range. Such results were not extensive enough to establish the postulated dependence of pressure for $(R_p)_{max}$ on the size of the fine AP particles. There were some test sets, notably mix 3 at 500 Hz and mix 1b at 350 Hz, for which the expected R_p maxima were either absent or lost in the data scatter.

Discussion

With all of the adversities of the reported results (anomalous steady-state burning, change in behavior with propellant aging,

and failure to show the expected elevated R_p under some test conditions), it could easily be concluded that the results do not demonstrate LEF transition enhancement of oscillatory combustion response. Certainly it would be desirable to repeat the T-burner tests with propellants that showed LEF transition effects in the steady-state burning rate (and to know why mixes 1a, 1b, 2, and 3 did not show such behavior in steady-state burning). However, there is no doubt that these mixes had bimodal oxidizer size distributions that would be conducive to organized LEF transition behavior, and such behavior is evident in much of the response function data (most clearly in Fig. 9b) and at the expected LEF transition pressures. Such selective behavior is unprecedented in tests on conventional propellants, and demonstrates, in accordance with the strategy for the investigation, that oscillatory LEF transition is strongly pressure coupled, so much so that it was manifested even for bimodal propellants that did not exhibit organized LEF transition in the steady-state burning rate. Such a demonstration of the role of any detailed aspect of the flame complex in determining combustion response is unprecedented. However, this is just a beginning as far as LEF transition effects are concerned because LEF transition is a very complex dynamic event about which very little is known. The present results simply demonstrate that it is an important contributor to pressure-coupled response. This is presumably true also for more conventional particle-size distribution, but, because the effect is spread out over the whole pressure range, it is not distinguishable from other aspects of flame complex response. In the interest of more realistic modeling of pressure-coupled combustion response, it will be important to learn more about the dynamics of LEF detachment and reattachment, and of other microscopic, three-dimensional nonsteady behavior in the combustion zone.

Acknowledgments

The authors thank the Office of Naval Research (R. S. Miller, Technical Monitor) for financial support of the research. Thanks also go to the U.S. Naval Air Warfare Center, China Lake, for the preparation of propellants and provision of the T-burner facility (Fred Blomshield, James E. Crump, and H. B. Mathes). Thanks also go to R. K. Sigman for guidance in the Combustion Laboratory at Georgia Institute of Technology, and to S. R. Chakravarthy for new data for Fig. 6 verifying the burning-rate data of Sambamurthi[2] in Fig. 4.

References

[1]Price, E. W., "Effect of Multidimensional Flamelets in Composite Propellant Combustion," *Journal of Propulsion and Power*, Vol. 11, No. 4, 1995, pp. 717–728.

[2]Price, E. W., Sambamurthi, J. K., Sigman, R. K., and Panyam, R. R., "Combustion of Ammonium Perchlorate-Polymer Sandwiches," *Combustion and Flame*, Vol. 63, No. 3, 1986, pp. 381–413.

[3]Beiter, C. A., "The Role of Combustion Zone Microstructure on the Pressure-Coupled Response of Composite Propellants," Ph.D. Dissertation, Georgia Inst. of Technology, Atlanta, GA, May 1991.

[4]Ermolaev, B. S., Korotkov, A. I., and Frolov, Y. V., "Laws of Combustion of a Solid Propellant Sandwich," *Fizika Goreniya i Vzryva*, Vol. 6, No. 3, 1970, pp. 277–285.

[5]Fenn, J. B., "A Phalanx Flame Model for the Combustion of Composite Solid Propellants," *Combustion and Flame*, Vol. 12, June 1968, pp. 201–216.

[6]Beckstead, M. W., Derr, R. L., and Price, C. F., "A Model of Composite Solid Propellant Combustion Based on Multiple Flames," *AIAA Journal*, Vol. 8, No. 12, 1970, pp. 2200–2207.

[7]Price, E. W., Mathes, H. B., Madden, O. H., and Brown, B. G., "Pulsed T-Burner Testing of Combustion Dynamics of Aluminized Solid Propellants, *Astronautics and Aeronautics*, Vol. 10, April 1972, pp. 65–69.

[8]Mathes, H. B., "A Facility for Testing the Acoustic Combustion Instability," *Proceedings of the 26th International Symposium, Instrumentation in the Aerospace Industry*, Vol. 26, Instrument Society of America, Research Triangle Park, NC, 1980, pp. 376–378; also *Advances in Test Measurement*, Vol. 17, 1980, pp. 367–378.

[9]Culick, F. E. C., "Report of the Committee on Standardization of Combustion Instability Measurements in the T-Burner," Chemical Propulsion Information Agency, Publication 191, Columbia, MD, Nov. 1969.